Submarining and Abdominal Injury for Rear-Seated Mid-Size Males during Frontal Crashes

Allison Jean Guettler

Dissertation submitted to the faculty of the Virginia Polytechnic Institute and State University in partial fulfillment of the requirements for the degree of

Doctor of Philosophy
In
Biomedical Engineering

Warren N. Hardy, Chair
Andrew R. Kemper
John H. Bolte
Kerry A. Danelson
Jessica S. Jermakian
Costin D. Untaroiu

April 25, 2023
Blacksburg, VA

Keywords: ATD, PMHS, Submarining, Abdominal Injury, Frontal Crash, Rear Seat Safety

Submarining and Abdominal Injury for Rear-Seated Mid-Size Males during Frontal Crashes

Allison Jean Guettler

ABSTRACT

Historically, the rear seat has been considered safer compared to the front seat for all restrained occupants; however, studies have found that the front seat in newer vehicles might be safer for older adults than the rear seat. While adults make up only 19% of rear seat occupants in frontal crashes, they make up 48% of fatalities (Tatem & Gabler, 2019). The rate of rear-seat occupancy by adults is expected to increase due to the use of ride share services and the potential of autonomous vehicles. Minimal research has been done to assess rear-seat occupant protection for a mid-sized adult male. Submarining, in which the lap belt slips off of the pelvis and directly loads the abdomen, is of particular concern as a restraint-based injury mechanism of the abdomen. The objective of this study is to investigate submarining protection and abdominal injury risk for rear-seated mid-sized male occupants in frontal crashes and to assess the biofidelity of two anthropomorphic test devices (ATDs) with respect to submarining response when compared to post-mortem human surrogates (PMHS). Twenty-four frontal crash sled tests were conducted with the THOR-50M and Hybrid III 50th-percentile male ATDs in three crash conditions and seven modern vehicles. The vehicles included a minivan, an SUV, 3 compact SUVs, and 2 sedans from the US vehicle fleet (model years 2017-2018). Four vehicles had conventional restraints (ie. 3-point belt with retractor at the shoulder) in the rear seat and three vehicles had advanced restraints (ie. 3-point belts with a pretensioner and load limiter at the retractor). Two of the crash conditions were vehicle-specific pulses: NCAP85 (ΔV = 56 kph) and Scaled (ΔV = 32 kph). The final pulse was a Generic (ΔV = 32 kph) pulse, created by averaging all seven Scaled pulses. Matched PMHS tests were conducted on four of the vehicles in the NCAP85 condition. Two tests were conducted for each vehicle with 8 PMHS for a total of 8 sled tests. The occurrence of submarining was identified and assessed for severity by: symmetry of lap belt slip, degree of abdominal loading, and forward excursion of the pelvis. Pelvis and lap-belt kinematics were assessed for the matched NCAP85 tests to identify trends with respect to submarining. Damage to the abdomen, pelvis, and lumbar spine of the PMHS was identified during post-test autopsy. The Hybrid III did not submarine in any test, but the THOR submarined in 16/24 tests. Three PMHS underwent submarining in 2/4 vehicles, and the THOR submarined in 3/4 vehicles in the matched NCAP85 tests. Three PMHS did not undergo submarining but sustained pelvis fractures at lap belt loads of 7.4 kN and higher, and damage to the abdominal viscera occurred regardless of submarining occurrence. Pelvis and lap-belt kinematics revealed the complex nature of the interactions of the occupant and the restraints within each vehicle environment, but did not clearly differentiate between submarining and non-submarining tests. The Hybrid III was not able to predict submarining risk for the PMHS in the rear seat environment. While the THOR underwent submarining, it was not perfect in predicting submarining risk. Pelvis geometry, lap belt engagement, and other factors contributed to the differences in submarining between the two ATDs and the PMHS. Restraint type was not indicative of whether or not the THOR or PMHS would submarine. Many other factors in the rear seat environments of these vehicles likely contribute in combination to the effectiveness of submarining prevention and occupant protection in the rear seat. This study provides information regarding submarining and abdominal injury for three surrogate types, two crash severities, and seven modern, real-world vehicle environments. Ultimately, this study found substantive gaps in occupant protection in the rear seats of modern vehicles for mid-sized adult male occupants.

Tatem, W. M., & Gabler, H. C. (2019). Differential fatality risk between rear and front seat passenger vehicle occupants in frontal crashes. In *Proceedings of the 2019 International IRCOBI Conference on the Biomechanics of Injury* (pp. 554–560).

Submarining and Abdominal Injury for Rear-Seated Mid-Size Males during Frontal Crashes

Allison Jean Guettler

GENERAL AUDIENCE ABSTRACT

Historically, the rear seat has been considered safer than the front seat for restrained occupants in frontal crashes. However, with advances in safety systems for the front seat, studies have found that the front seat might be safer for older adult occupants. The objective of this study is to investigate submarining protection and abdominal injury risk for rear-seated mid-sized male occupants in frontal crashes. Submarining occurs when the lap belt slips off of the pelvis and directly loads the abdomen, potentially producing severe abdominal injuries. Twenty-four sled tests were conducted with the THOR-50M and Hybrid III 50th-percentile male anthropomorphic test devices (ATDs) in three crash conditions and seven modern vehicles. The vehicles selected included a minivan, SUVs, compact SUVs, and sedans from the US vehicle fleet. Three of the vehicles had advanced restraints in the rear seat and four had conventional restraints. The three crash conditions were a generic low speed test and a low and high-speed vehicle-specific crash pulse. Eight tests were conducted with eight different post-mortem human surrogates on a subset of four vehicles (2 with advanced restraints, 2 with conventional restraints) using the high-speed crash condition. The Hybrid III never submarined, but the THOR submarined in 16 out of 24 tests (5 out of 7 vehicles). Three out of eight PMHS submarined, in two of the four vehicles. Three heavier PMHS sustained pelvis fractures, and all but one PMHS had sustained damage to the abdominal viscera. Restraint type was not an indicator of submarining risk in the rear seat, suggesting that other seat and vehicle design variables contribute to submarining risk. Comparison of the responses of the ATDs with the PMHS suggests that the THOR is a more reasonable surrogate than the Hybrid III for submarining assessment in the rear seat. Inclusion of data from other body regions is necessary to make a definitive determination of the appropriate ATD for the assessment of occupant protection for a mid-sized male in the rear seat during frontal crashes. Overall, this study suggests that protection against submarining and injury to the pelvis and abdomen for mid-sized male passengers in the rear seat of modern vehicles in the US fleet could be improved.

Acknowledgements

There are many people I would like to thank for their contributions to this work and support throughout the process of this degree. First, I would like to thank my advisor, Warren Hardy, for his guidance, understanding, and support throughout my time in graduate school. It has been an honor to work with him and learn from his wealth of knowledge of impact biomechanics.

Thank you to the members of my committee, Andrew Kemper, John Bolte, Kerry Danelson, Jessica Jermakian, and Costin Untaroiu. I greatly appreciate the time you contributed to helping me obtain this degree, and am indebted to you for your patience and understanding in delays in the process.

I would like to acknowledge the people who made this project possible: Warren Hardy, Andrew Kemper, Devon Albert, Sam Bianco, David Boyle, Dave Mellichamp, and Matt Mason. The teamwork and dedication of everyone on this project are the only reason it was possible. I'd specifically like to acknowledge Sam Bianco, whose dissertation made up the other half of this project, I'm glad we had each other to lean on during all of the chaos. To my labmates, past and present, who pushed me, supported me, and (perhaps most importantly) made me laugh: I thank you from the bottom of my heart.

There are no words to describe my love and appreciation for my family and friends. Mom and dad, you always supported me, never made me question my interests, and never pushed me to do the things that were not for me. Thank you for, well, everything. Midge, you always showed me the same love and support; thank you for accepting me as your bonus daughter. Thank you to my siblings, for your support, love, and understanding. A special thanks to my brother, Andrew, for keeping me grounded. To my cousin, Chelsey, one of my best friends and a major inspiration as a woman in science: your guidance, support, and understanding has bolstered me through my graduate career. To friends who became family, from all phases of my life, thank you for being there during the ups and downs, and being my biggest cheerleaders. Finally, Will, thank you for your love, support, and absolute refusal to accept any of my self-doubt. Your confidence in me (and delicious home-cooked meals) helped me get through countless hard days.

This work was funded by the National Highway Traffic Safety Administration, contract No., DTNH2214D00328L, Task Order, DTNH2217F00177. The PMHS were obtained from informed consent programs. We are thankful for the anatomical donors, who make this work possible.

Contents

List of Figures

List of Tables

Attribution

The ATD portion of this work has been published in the Journal of Transportation Safety

Guettler, A. J., Bianco, S. T., Kemper, A. R., Albert, D. L., & Hardy, W. N. (2022). Submarining protection for 50th-percentile male anthropomorphic test devices in the rear seat during frontal crash sled tests. *SAE International Journal of Transportation Safety*, *10*(09-10-02–0016).

Other publications and reports from this project include:

Bianco, S., Guettler, A. J., Hardy, W. N., Albert, D. L., & Kemper, A. R. (2022). Evaluation and comparison of thoracic injury risk for the Hybrid III and THOR 50th-percentile male anthropomorphic test devices in the rear seat during frontal impacts. *SAE International Journal of Transportation Safety*, *10*(09-10-02–0015).

Rear-Seat Frontal Crash Protection Research with Application to Vehicles with Automated Driving Systems, Volume 1, Warren N Hardy, Andrew R Kemper, Costin Daniel Untaroiu, Devon L Albert, Yunzhu Meng, Keegan M Yates, Allison J Guettler, Samuel T Bianco, David M Boyle, Whitney Tatem, Michelle Chaka, DOT HS 813 269.

Several people contributed to this work:

Warren Hardy, Andrew Kemper, Devon Albert, and Samuel Bianco made significant contributions to the project as a whole.

Devon Albert provided Vicon data for the ATD pelvis angle analysis.

Warren Hardy provided lap belt angle data and contibuted significantly to data processing and manuscript feedback.

Figures 18, 19, 20, 27, 29, 31, 32, 68, 69, 70, 73, 75, and 77 are derivative of figures published in:

Guettler, A. J., Bianco, S. T., Kemper, A. R., Albert, D. L., & Hardy, W. N. (2022). Submarining protection for 50th-percentile male anthropomorphic test devices in the rear seat during frontal crash sled tests. *SAE International Journal of Transportation Safety*, *10*(09-10-02–0016).

Chapter 1: Introduction

Traditionally, the rear seat has provided greater levels of protection against serious injury or death for restrained passengers compared to the front seat (Huelke & Compton, 1995; Padmanaban & Ray, 1992; Kathleen M Smith & Cummings, 2004). However, more recent studies have found that while the rear seat maintains a greater level of protection for younger occupants, restrained older-adult occupants may experience better protective benefits in the front seat than the rear seat during frontal crashes (Bilston, Du, & Brown, 2010; Kent, Forman, Parent, & Kuppa, 2007; Kuppa, Saunders, & Fessahaie, 2005; K.M. Smith & Cummings, 2006; Tatem & Gabler, 2019).

Typically a small percentage of rear-seated occupants are adults, approximately 19% of rear-seated occupants in frontal crashes from 1999-2015 (Tatem & Gabler, 2019). However, adults 20 years and older account for a disproportionate number of fatalities for restrained rear-seat passengers (Tatem & Gabler, 2019). Increased use of ride-sharing services and the potential availability of autonomous vehicles might lead to a shift in rear passenger demographics as more adults self-select to the rear seat. One survey of seating preference in autonomous vehicles suggests that occupants will self-select to the rear seat, in potential face-to-face or conventional seating configurations (Nie, Gan, Chen, & Zhou, 2020). An increase in adult rear-seated passengers could lead to an increase in fatalities during MVCs.

Limited research has been performed to investigate occupant protection for rear-seated adults (Forman, et al., 2009a; Forman, , et al., 2009b; Forman, et al., 2008; Hu, et al., 2015; Hu et al., 2017; Kuppa et al., 2005; Michaelson, et al., 2008; Rouhana, Horsch, & Kroell, 1989; Trosseille et al., 2018; Tylko & Dalmotas, 2005; Uriot, et al., 2015; Zellmer, Lührs, & Brüggemann, 1998). Studies have focused on Anthropomorphic Test Devices (ATDs) and post mortem human surrogates (PMHS), restraint features and design, and many other occupant safety considerations for the rear seat. While some discuss submarining outcomes (Forman, et al., 2009; Forman et al., 2008; Hu et al., 2015, 2017; Michaelson et al., 2008; Rouhana, et al., 1989; Trosseille et al., 2018; Tylko & Dalmotas, Aa2005; Uriot, et al., 2015), most of these studies provide little-to-no detail regarding the methods used for identifying submarining.

Real-world crash data suggest that safety advances for the front seat have outpaced those for the rear seat, providing an increased protective-effect for older adult occupants in the front seating row. Rates of occupancy for adults in the rear seat are expected to increase given changes in transportation trends (e.g. ridesharing) and the potential for autonomous vehicles. Therefore, the limited research that has been conducted for adult rear-seat occupant safety must be built upon. Moreover, more detailed descriptions of

submarining assessment would help to further inform submarining protection for adult rear-seated occupants.

Research Objectives

The overall goal of this study is to investigate the safety of a rear-seated mid-sized male occupant during a frontal crash in newer vehicles with a focus on submarining protection and abdominal injury. Specifically:

1. Determine the submarining responses of the Hybrid III and THOR 50th-percentile male ATDs in the rear seat during frontal crashes using seven vehicles and three crash conditions.
2. Determine the submarining responses of PMHS in the rear seat during frontal crashes using four vehicles and one crash condition for each vehicle, and identify any associated damage to the abdomen, lumbar spine, and pelvis during these tests.
3. Compare the ATD responses to those of the PMHS to determine: a) which ATD better approximates the kinematics and submarining responses of the PMHS, and b) the extent to which either ATD predicts injury risk.
4. Attempt to identify which vehicle seat or restraint characteristics are associated with better occupant protection with respect to submarining, and to gain some understanding of rear seat submarining protection in newer vehicles.

Chapter 2: Background

Anatomy

The following is a review of abdominal anatomy and is derived from Moore's Clinically Oriented Anatomy (7th edition, 2013) and Accidental Injury: Impact and Injury Response of the Abdomen (Hardy, Howes, Kemper, & Rouhana, 2015; Moore, Dalley, & Agur, 2013). The spinal column is made up of 33 vertebrae that are divided into 5 segments. The segments, from superior to inferior, are: cervical (7 vertebrae), thoracic (12 vertebrae), lumbar (5 vertebrae), sacral (5 vertebrae), and coccygeal (4 vertebrae). The sacral and coccygeal vertebrae are fused in adults, making up the sacrum and coccyx. The thoracic vertebrae articulate with the ribs, some of which encompass the more superior sections of the abdomen. The lumbar spine provides anchoring for the abdominal aorta, inferior vena cava, and the mesentery. The sacrum makes up the posterior aspect of the pelvic girdle. The remainder of the pelvic girdle is made up of the hip bones. They are right and left paired bones made up of three fused bones: the ilium, ischium, and pubic bone.

The abdomen is the region of the torso that spans from the diaphragm superiorly to the pelvic inlet inferiorly. At the pelvic inlet, the abdomen is continuous with the pelvic cavity. There are two methods for subdividing the abdomen: abdominal quadrants and nine abdominal regions. The quadrants are divided by the median plane of the torso (right and left sides) and the transumbilical plane, which passes though the umbilicus, dividing the upper and lower halves. The nine regions are created by four planes: the right and left midclavicular planes pass from the midline of the clavicles to the midpoints of the inguinal ligaments, the subcostal plane which passes through the 10th costal cartilage, and the transtubercular plane which passes through the right and left iliac tubercles on the pelvis.

Unlike the thorax, the abdomen has minimal protection from the skeleton. However, due to the location of the diaphragm in the thoracic cavity, the more superior abdominal viscera are protected by the lower half of the rib cage posteriorly and laterally. The inferior-most organs have some lateral protection from the greater pelvis (i.e. the iliac wings). The remaining protection is offered by the muscular abdominal wall and visceral fat.

The diaphragm is a membrane made of muscle and tendon separating the thoracic and abdominal cavities. The diaphragm is the primary muscle in respiration. The diaphragm is domed and has peripheral attachments on the lower ribs, sternum, and lumbar vertebrae. The top and center of the dome is made up of the central tendon and extends to the 5th rib superiorly. The caval opening, esophageal hiatus, and aortic hiatus allow for the passage of the inferior vena cava, esophagus, and thoracic aorta into the abdomen, respectively.

Once it passes through the aortic hiatus of the diaphragm at the level of T12, the thoracic aorta becomes the abdominal aorta. The abdominal aorta is retroperitoneal and travels along the anterior surface of the lumbar spine until it bifurcates into the right and left common iliac arteries at the level of L4. Major bilateral branches from the abdominal aorta include the renal arteries. There are three unpaired branches of the abdominal aorta that supply blood to much of the abdominal viscera. From superior to inferior these branches are the celiac trunk, the superior mesenteric artery, and the inferior mesenteric artery.

The inferior vena cava is formed by the union of the right and left common iliac veins at the level of L5. Also retroperitoneal, the inferior vena cava travels along the right side of the lumbar spine and exits the abdomen at the level of the T8 vertebra.

The alimentary canal, or gastrointestinal tract, is the series of hollow organs from the mouth to the anus. As the first abdominal part of the gastrointestinal tract, the esophagus enters the abdomen through the esophageal hiatus of the diaphragm at the level of T10, anterior to the abdominal aorta. The stomach is located primarily in the upper left quadrant, begins at the cardiac sphincter, and has four parts: the cardia, fundus, body, and pyloric part. At the most distal part of the pyloric region forms another sphincter that controls the movement of material from the stomach to the first part of the small intestine. The fundus of the stomach is in contact with the left side of the inferior surface of the diaphragm.

The subsequent part of the gastrointestinal tract is the small intestine, which has three parts: the duodenum, jejunum, and ileum. The duodenum is somewhat C-shaped and begins at the pyloric opening of the stomach. The descending part of the duodenum is retroperitoneal. The duodenum routes to the peritoneum again and becomes the jejunum at the duodenojejunal flexure. The next part of the small intestine is the jejunum, which makes up approximately 40% of the length of the small intestine. The final section of small intestine is the ileum, which ultimately meets the cecum of the large intestine at the ileocecal junction. The small intestine is tethered to the spine by the mesentery and the superior mesenteric artery, which provides its blood supply. The large intestine has several parts. The cecum is the first segment and lies within the lower right quadrant of the abdomen. It is part of the ascending colon, which runs superiorly until the level of ribs 9 or 10 and turns medially at the right colic flexure. The next section is the transverse colon, which crosses the abdomen before the colon turns inferiorly at the left colic flexure. The descending colon then travels inferiorly until it becomes the S-shaped sigmoid colon, then the rectum, and ends at the anus. The large intestine is also anchored by the mesentery and receives blood supply from the inferior mesenteric artery.

The liver is a large parenchymal (solid) organ that is located in the upper right quadrant of the abdomen, positioned directly inferior to the diaphragm. Oxygenated blood is supplied from the hepatic artery, which stems from the celiac trunk. The portal venous system, which returns nutrient-charged blood from the

digestive organs, also brings blood to the liver. Blood leaving the liver returns to the heart via the inferior vena cava. The gall bladder is attached to the inferior, or visceral, surface of the liver, and stores bile made by the liver.

The spleen is another solid organ, but it is in the upper left quadrant of the abdomen, directly inferior to the diaphragm and posterior to the stomach. The spleen is relatively mobile and protected by the thoracic cage.

The pancreas is a glandular organ that produces insulin, which it secretes into the duodenum via the main and accessory pancreatic ducts, which combine at the hepatopancreatic ampulla. The pancreas is retroperitoneal, with its tail positioned near the spleen and its head meeting the duodenum.

Finally, the kidneys are parenchymal organs of the urinary tract that produce urine. The right and left kidneys are at the level of the 11^{th} and 12^{th} ribs. The kidneys are protected by the ribs as well as retroperitoneal fat. Urine is carried to the bladder via the ureters.

Epidemiology

Rear Seat vs. Front Seat

When considering belted occupants, the rear seat has been considered safer than the front seat for all occupants, historically. Using data from the National Automotive Sampling System (NASS) from 1982-1986, injury rates between front- and rear-seated occupants were compared for vehicles from model years (MY) 1979-1986 (Padmanaban & Ray, 1992). Rear-seated occupants had lower rates of injury at all crash severities, which were categorized by ΔV. Further analysis compared the effectiveness of lap-only belts and lap-shoulder belts using police-reported accident data, and rear-seated occupants were found to have lower rates of injury than front-seat occupants regardless of belt type. A matched-cohort analysis of NASS data from 1980-1991 compared injury risk between front and rear-seated passengers in the same vehicle (Huelke & Compton, 1995). Frontal crashes with restrained and unrestrained passengers were examined. Again, belted occupants in the rear seat had lower risk of injury than belted occupants in the front row, and unbelted occupants had similar injury outcomes regardless of row. The lack of specificity in injury risk for unbelted occupants between seating rows agrees with an earlier NASS study (Padmanaban & Ray, 1992). In 1984, NHTSA mandated frontal air bags in passenger vehicles. The presence of airbags in the driver's seat could have skewed the results of these studies. However, one of the studies excluded vehicles with frontal airbags to remove these effects from their analysis (Huelke & Compton, 1995).

A NASS-CDS (Crashworthiness Data System) study of vehicles MY 1948-2001 involved in crashes from 1993-2000 found reduced risk of death or serious injury for passengers in the rear seat (Smith & Cummings, 2004). The study included occupants of all ages, and 62% of rear-seated passengers were 15 years old or younger. The wide span of vehicle model years might have skewed the analysis as many safety standards

were changed in that time. Later, the same group studied how various occupant and vehicle factors would change their results (Smith & Cummings, 2006). Vehicles were restricted to MY 1975-2001 and were included if there were two or three passengers—one of whom died. Restraint use, occupant age, and presence of front-passenger air bags were analyzed as factors that could alter relative risk between seating rows. When considering all included crash data, the risk of death was 21% lower for front occupants than for rear-seated occupants. In vehicles with airbags, young occupants (<12 years old) had the greatest benefit (reduced risk of death) from sitting in the rear seat. In contrast, restrained occupants who were older than 60 years had a slightly higher risk of death in the rear seat of vehicles with front-passenger air bags.

In 2005, a study using data from the Fatality Analysis Reporting System (FARS) and NASS-CDS found that the rear seat was safer for occupants younger than 50 years of age, but the front seat was safer for occupants older than 50 (Kuppa et al., 2005). Shortly after that study, an analysis of FARS years 2000-2003 was published that showed the rear seat had higher survivability than the front seat regardless of occupant age, vehicle type, impact point, or restraint use (Mayrose & Priya, 2008). However, this study did not control for vehicle age, did not delineate occupant ages above 16 years old, and included all crash types. These factors could have obscured the safety trends found in other studies (Bilston et al., 2010; Kuppa et al., 2005; Mitchell, Bambach, & Toson, 2015; Smith & Cummings, 2006; Tatem & Gabler, 2019).

In 2007, to expand upon the work by Kuppa et al. (2005), a FARS study was conducted to determine how the use of advanced restraints (pretensioners and load limiters) in the front seat changed the relative effectiveness of the rear seat in preventing fatalities when compared to the front seat (Kent et al., 2007).The study included FARS data from 1993-2005, dividing vehicles into two groups: MY 1991-1998 and 1999-2005. The division was based on the rapid increase of advanced restraints in the fleet after MY 1998. In MY 1991-1998 vehicles, the rear seat was more effective at preventing fatalities than the front seat for occupants up to age 50. This held true for vehicles with and without front passenger airbags. However, in vehicles with airbags, the rear seat was less effective for older occupants (greater than 50 years of age). In the newer vehicle group, the front seat tended to be more effective than the rear seat at mitigating fatalities for occupants 25 years and older; however, this was not statistically significant.

In 2010, a study was conducted to investigate how occupant and vehicle age affected relative safety between the front and rear seats (Bilston et al., 2010). The study included NASS-CDS crash data from 1993-2007. To compare the effectiveness of the front passenger airbag, made mandatory in 1997, vehicles were split into two groups: MY 1990-1996 and MY 1997-2007. Occupants were divided into three groups: ages 9-15, 16-50, and 51 years and older. Children younger than 9 years of age were excluded as they require additional restraints. In both vehicle groups, the youngest occupant group had a lower risk of AIS3+ injury in the rear seat than in the front seat. In older vehicles, younger adults had similar protection in both seating

rows, but the front seat was slightly safer in newer vehicles. Older adults (51+) had a larger safety benefit in the front seat than the younger occupant groups — an effect that was greater for the newer vehicle group.

A matched-cohort study analyzed crashes that were police-reported or that resulted in hospitalization in New South Wales between 2001-2011 (Mitchell et al., 2015). The study focused on differences in injury severity between front and rear-seated occupants in the same vehicle. They found that rear occupants had a higher odds ratio of sustaining severe injuries compared to front passengers, especially when airbags deployed. It was also noted that, for all seating positions, the risk of severe injury increased with occupant age and road speed limit.

A combined NASS-CDS and FARS study investigated fatality rates of passenger vehicle occupants from 1999-2015 (Tatem & Gabler, 2019). The study determined the relative risk of death (RR) for occupants in the rear seat compared to the front seat. Adults 20 years of age and older were over-represented in fatalities of rear seat occupants accounting for 48% of fatalities in the rear seat but only 19% of the population. The study found that while occupants up to 39 years old had a safety benefit in the rear seat (RR<1), older occupants had a higher relative risk of fatality (RR>1). The relative risk of fatality was even more pronounced for occupants 75 years and older (RR = 4.07). The cohort of newest vehicles (MY 2007+) had a significantly higher risk of fatality for rear seat passengers compared to front seat passengers. Odds ratios were used to compare the risk of fatality of rear seat occupants in the MY 2003-2006 and 2007+ vehicle groups to the 2000-2002 group. The results showed that the risk of fatality did not increase over time, so the increase in relative risk is driven by improved safety of the front seat.

Seat-belt Related Injury

Many studies have identified that restraint use reduces the risk of death and serious injury at all seating positions (Huelke & Compton, 1995; Padmanaban & Ray, 1992; Parenteau & Viano, 2003; K.M. Smith & Cummings, 2006; Zhu, Cummings, Chu, & Cook, 2007). In fact, unrestrained rear-seated passengers have been found to have the same injury risk as unbelted front seated passengers (Huelke & Compton, 1995; Padmanaban & Ray, 1992). However, rear-seated occupants have continued to be less likely to wear their seat belt compared to front passengers (Bhat, Beck, Bergen, & Kresnow, 2015; Parenteau & Viano, 2003). A survey study in 2015 showed that only 62% of adults reported always wearing a seat belt in the rear seat (Bhat et al., 2015). Seat belt laws were found to be effective at increasing belt use.

Seat belts couple the occupant to the vehicle and therefore prevent injuries due to a freely-moving occupant. However, because seat belts directly load the occupant, there can be injuries associated with their use, identified early-on as the “seatbelt syndrome” (Garrett & Braunstein, 1962). In that 1962 survey study, which had a somewhat limited population, it was determined that in low-severity crashes the seat belt

produced no risk to occupants, and only in severe accidents did the seat belt contribute to occupant injury (Garrett & Braunstein, 1962). Importantly, they concluded that while seat belts did not increase injury risk in occupants, they did alter injury patterns.

For example, in 1991, one study found that 81.3% of occupants with lumbar spine injuries were restrained while 86% of occupants with cervical spine injuries were unrestrained (Anderson, Rivara, Maier, & Drake, 1991). While occupants wearing lap belts did not sustain cervical or thoracic spine injuries, they were more likely to sustain injury to the small intestine as well as lumbar injuries. It is important to note that most of the occupants wearing a lap only belt were in the rear seat. Intestinal injury was found to be more common in belted occupants, who had fewer head injuries, shorter hospital stays, and lower mortality than unbelted occupants (Rutledge et al., 1991).

Abdominal Injuries

Abdominal injuries are not as common as other types of injuries in MVCs, but they make up a high portion of severe injuries. National Crash Severity Study (NCSS) data from 1977-1979 showed that abdominal injuries made up 2.6% of all injuries in MVCs resulting in a tow-away vehicle (Bondy, 1980). However, abdominal injuries made up 14.6% of all AIS3+ injuries. Later, a study found that 13.6% of patients in the emergency room with serious MVC-related injuries had abdominal injuries (Rutledge et al., 1991). The study included patients who were admitted for more than 24 hours or that died while in the emergency department. Patents that had abdominal injuries were more severely injured and had double the risk of mortality (8.7% vs. 4.0%) than patients without abdominal injuries. Several studies have found that many abdominal injuries, especially those to the hollow organs, often show delayed signs or mixed results during diagnosis (Doersch & Dozier, 1968; Kearney, 1989; Rutledge et al., 1991). Many severe abdominal injuries due to seat belt loading do not present signs of internal injury immediately and can often be difficult to identify (Doersch & Dozier, 1968). Seat belt related injuries are often paired with “seat belt sign”, which includes abdominal contusions and abrasions. Injuries included mesenteric and intestinal tears, perforations of the bowel, transected muscles, and thrombosis in major vessels. Difficulty in diagnosing abdominal injuries early leads to delayed treatment and might cause greater declines in health.

In an effort to identify priorities in abdominal injury criteria and to provide rationale for the development of biofidelic, instrumented ATD abdominal inserts, one study surveyed NASS to determine the prevalence and severity of abdominal injuries to the driver and front passenger during frontal crashes (Elhagediab & Rouhana, 1998). The study found that in crashes from 1988-1994, abdominal injuries made up a higher proportion of total injuries as AIS severity increased, with the majority of injuries occurring in unbelted drivers contacting the steering wheel. Steering wheel contact was most commonly associated with damage

to the liver and spleen while injuries to the hollow "digestive organs" were caused by the lap/shoulder belt, mostly in front passengers.

In a survey of NASS from 1993-1997, abdominal injuries made up about 5.2% of the total number of injuries recorded, 15.6% of which were rated AIS 3-6. (Lee & Yang, 2002). Hollow organ injuries were the most common but were infrequently severe (4.2%) and were most frequently caused by contact with the seat belt. While solid organ injuries made up about 35% of abdominal injuries, a relatively high percentage of them (32.0%) were severe. Again, these solid organ injuries were commonly caused by contact with hard vehicle structures (e.g. the steering wheel). Of the eight body regions, the abdomen was seventh in overall number of injuries; however it was the third-most severely injured region behind only the head and thorax.

In 2006, a paper was published discussing abdominal injury patters in frontal crashes that occurred in France from 1970-2005 (Lamielle et al., 2006). The study included non-ejected occupants 12 years of age and older in frontal crashes with Energy Equivalent Speeds (EES) of 40 to 79 kph. Of the included occupants, 6.53% sustained AIS 3+ abdominal injuries. Hollow organ injuries were the most frequently injured in belted occupants where as in unbelted occupants, solid organ injuries were most common. They found that the risk of AIS3+ injury increased significantly as EES increased and rear occupants had the highest abdominal injury risk out of all belted occupants.

The trends in abdominal injury risk and types of affected organs by type of contact were seen again in a recent study of US data (Klinich, et al., 2010). While this study included multiple crash types and focused on drivers and front passengers, they still found that solid organ injuries were associated with contact with vehicle structures while hollow organ injuries were produced by seat belt contact. Additionally, the rate of rib fracture injuries increased with increasing crash severity. The probability of injury to the liver and spleen was much larger with rib fractures than without. Meanwhile, the rate of hollow organ injuries only increased when crash severity exceeded 65 kph. Finally, the study identified a decrease in abdominal injury risk as the vehicle model year increased (decreased risk in newer vehicles). However, it is important to remember that this includes only drivers and front-seated occupants.

In an analysis of 1998-2010 accident data from the UK Cooperative Crash Injury Study (CCIS), differences in abdominal injury types by seating position and restraint type during frontal crashes were identified (Frampton, Lenard, & Compigne, 2012). The study found that the rate of moderate to severe (AIS 2+ and AIS 3+) abdominal injuries was highest for rear seat passengers, and that injuries occurred at lower speeds for rear occupants. Additionally, belt-only restraints, when compared to advanced restraints (pretensioners, load limiters, air bags, and anti-submarining features), were the least effective in preventing abdominal injuries, while being the predominant restraint type in the rear seat. There were also differences in injury

patterns between front and rear seat occupants—the rear seat occupants having higher rates of spleen injuries and much higher rates of intestine (large and small) and mesentery injuries. Similar to Klinich et al. (2010), this study found that liver and spleen injuries were associated with rib fractures, specifically when 2 or more fractures were present, and injuries to the hollow organs were associated with one or no rib fractures.

Submarining Experimental work

Submarining Kinematics

The overall kinematics of the occupant and the kinematics of the pelvis are both important considerations for submarining. Adomeit and Heger determined that limiting vertical downward motion and promoting forward rotation of the torso are important factors for mitigating submarining with seat and restraint design (Adomeit & Heger, 1975). Later, Adomeit defined two types of submarining (Adomeit, 1977). The first, classical submarining, includes excessive forward displacement of the pelvis resulting in rearward rotation of the torso, and belt slip. The second involves large vertical displacement of the pelvis. While the first type leads to low head and neck injury values, the second type can produce higher head accelerations as well as an increased axial loading of the lumbar spine.

Many studies have focused specifically on the pelvis and lap belt kinematics required to initiate submarining. One study found that the HIII would submarine after 28 degrees of rearward rotation from an initial angle of 22-23 degrees from vertical (Rouhana, Horsch, et al., 1989). Lap belt angle in the X-Z plane and distance between lap belt anchors have also been identified as important factors in submarining (Leung, Tarriere, Fayon, Mairesse, & Banzet, 1981).

Historically, lap belt angle, pelvis angle, and the relative angle between the two have been understood to be important factors in predicting submarining for a long time (Adomeit & Heger, 1975; Horsch & Hering, 1989; Leung et al., 1982; Luet, Trosseille, Drazétic, Potier, & Vallancien, 2012; Nilson & Håland, 1995; Rouhana, Horsch, et al., 1989; Uriot, Potier, Baudrit, Trosseille, Richard, et al., 2015). Adomeit & Heger (1975) identified an ideal lap belt angle of 45-50° from horizontal to prevent submarining kinematics and to reduce undesired torso rotation. Several studies identified a critical angle between the belt and pelvis where the tangent of the relative angle must be larger than the coefficient of friction between the belt and pelvis to producing belt slip (Horsch & Hering, 1989; Leung et al., 1982; Nilson & Håland, 1995). In addition to the friction coefficient changing the critical angle, one study determined that lifting of the buckle by the shoulder belt reduced the critical angle (Horsch & Hering, 1989). While these studies focused on the X-Z planar projection of belt and pelvis angles, Leung et al. (1982) determined that the angle of the belt in the X-Y planar projection was also critical for assessing restraint characteristics for submarining risk.

Submarining Differences between Surrogate Types

While occupant surrogates of different sizes will have different interactions with restraints during MVCs, different surrogates representing the same population have also been shown to respond differently.

One study compared the submarining response of the Hybrid II and Hybrid III 50th-percentile male ATDs and 50th-percentile male PMHS during frontal-crash sled tests (Luet et al., 2012). The seat had a fixed back covered in foam and a rigid seat pan. The 3-point restraint was separated into separate shoulder and lap parts, the shoulder part with a retractor at the shoulder and the lap part with retractors on either side of the seat. One test with each of the three test configurations was conducted for each ATD, and three tests with each configuration were conducted with the PMHS (9 PMHS in total). Configuration 1 had $\Delta V = 40$ kph, a horizontal seat pan, and an average belt angle of 37.5 degrees from horizontal. Configurations 2 and 3 both had a $\Delta V = 50$ kph. Configuration 2 had a horizontal seat pan, and an average belt angle of 50 degrees while configuration 3 had a seat pan angle of 5 degrees, and a belt angle of 37.5 degrees. They used reduction in lap belt load and high-speed videos to determine the timing of submarining. The Hybrid II submarined in all three configurations; however, it only submarined during the unloading phase in the second configuration, which is not significant in terms of injury risk. The Hybrid III submarined during two tests, but only during the unloading phases. Finally, seven out of nine PMHS submarined. Only one PMHS and the HII submarined in configuration 3 (steep lap belt angle) while every surrogate submarined in the other configurations.

Later, a similar study compared the submarining responses of the Hybrid II, Hybrid III, and THOR to PMHS in a standard front passenger seat during 50 kph frontal sled tests (Uriot, Potier, Baudrit, Trosseille, Richard, et al., 2015). Tests were conducted with the surrogates in three seating positions: standard position, slouched position, and slouch position with a load-limited lap belt. The Hybrid III never submarined and the Hybrid II and THOR submarined in the slouch position. Additionally, the THOR might have submarined in the condition with the load limiter. All three PMHS submarined during the slouched tests and no PMHS submarined in any other tests. Ultimately, in terms of predicting the PMHS response, the HIII failed to predict submarining, and while both the Hybrid II and THOR submarined, the Hybrid II submarined more easily.

Both of these studies indicate that in these seating conditions: 1) three different 50th-percentile male ATDs have different submarining responses, 2) the Hybrid III is the least sensitive to submarining, and 3) the Hybrid II appears to be the easiest to submarine. Other studies have found that the Hybrid II submarines too easily and over-represents the response of PMHS (Leung et al., 1979).

Submarining in the Rear Seat

ATDs

Rouhana et al. investigated submarining of rear-seated HIII-5F and HIII-50M ATDs during frontal sled tests at increasing speeds (Rouhana, Horsch, et al., 1989). The 3-point restraints had a retractor at the outboard anchor rather than the shoulder. Belt tension was measured for both ATDs and rotational acceleration of the pelvis was measured for the HIII-5F in some tests. The HIII-50M had its full standard instrumentation in addition to an in-line pelvis accelerometer array and load-bolt pelvis (Daniel, 1974). The authors determined submarining independently from: videos, load-bolt data, belt load data, and pelvis rotation data when available. The HIII-5F submarined bilaterally in every test with the baseline restraint system, so no submarining threshold could be determined in the 35-52 kph range. The HIII-50M submarined bilaterally in the two highest tests, on the inboard side only at 44 kph, and did not submarine at 40 kph, so 42 kph was determined to be the threshold for submarining with a basic restraint in the rear seat.

In 2005, Tylko and Dalmotas conducted full rigid barrier crash tests (FMVSS 208, ΔV = 48 kph) comparing the response of the HIII-5F seated in the front passenger and rear passenger seats (Tylko & Dalmotas, 2005). Of the three vehicles used in the study, the rear-seated HIII-5F submarined in a sedan and large SUV, while not submarining in a small SUV. Submarining was identified using video analysis. The resultant lumbar force in the two submarining tests was larger than in the non-submarining test, coincident with direct loading of the abdomen by the lap belt. The authors also noted that the proportion of lap belt force to shoulder belt force was indicative of submarining where a value of less than 0.5, as in the sedan, related to extreme submarining and a value near 1.0 (as in the small SUV) was related to no submarining.

Another study conducted frontal sled tests using two severities (ΔV = 29 and 48 kph), with standard and advanced restraints in a representative rear seat of a 2004 mid-sized sedan, and four ATDS (Forman et al., 2008). Of the ATDs, there were three adults: the HIII-5F, HIII-50M, and THOR-NT. The study found a reduction in most injury measures in all tests with a force limiter-pretensioner restraint (FL-PT). No submarining occurred in any test; however, no information was given as to how that was determined, and the THOR-NT had the kinematics deemed to be most likely to produce submarining as defined by Adomeit and Heger (Adomeit & Heger, 1975).

More recently, a study used a rear-seat buck with a modified seat pan of a mid-sized sedan to assess rear-seat occupant protection based on several factors (Hu et al., 2015). The study used two pulses, both at ΔV = 63 kph, one “soft” and one “severe”, a fully frontal (0°), and a 15° offset for a driver-side impact. The Hybrid III 95th-percentile male (HIII-95M) did not submarine in any test and the HIII-5F submarined in all severe tests and one soft test. Meanwhile, as indicated by the iliac crest load cells, the THOR-NT

submarined in all but one test (soft pulse, 15°). Additionally, the THOR-NT submarining was bilateral in all cases but one. While this study was continued to include a variety of advanced restraint features, no further discussion of submarining was included (Hu et al., 2017).

PMHS

A series of studies was conducted to determine the kinematics and injuries of rear-seated PMHS during frontal crash sled tests (Forman, et al., 2009; Forman, et al., 2009; Michaelson et al., 2008). The studies included 8 PMHS in frontal sled tests with a $\Delta V = 48$ kph. The studies used the rear seat from a 2004 sedan and had two different types of restraints: a standard 3-point belt and a belt with a pretensioner and load limiter at the retractor (labeled as FL+PT). In the first test series, which involved standard restraints, all three PMHS had large forward pelvis excursions and little-to-no forward rotation of the torso (Michaelson et al., 2008). The two approximately mid-sized male PMHS underwent submarining, as confirmed by offboard high-speed video, while submarining could not be confirmed for the larger female PMHS. While all three PMHS sustained many rib fractures, no abdominal injuries were found. Next, tests with three additional mid-sized male PMHS with FL+PT restraints were conducted (Forman, et al., 2009). In these tests, only one PMHS submarined while the other two had much smaller pelvis excursions and larger forward rotations of the torso than the first group. This group sustained fewer injuries, and still no injuries to the abdomen. However, comparison between the responses of the mid-sized male PMHS in these studies is difficult as the two PMHS in the standard belt study were well below the weight range for the 50th-perctile male, while the three in the FL+PT series where much closer to the appropriate weight range. Finally, the last study found that larger male occupants that did not have the benefit of the advanced restraints and had submarining kinematics, ultimately falling off of the seat (Forman, et al. 2009). Again, no abdominal injuries were found.

Proposed Injury Prediction

Over the years, many physical parameters have been proposed as correlates for abdominal injury (Hardy et al., 2015). The source data and target injuries cover a wide array of crash types, impact types, impact locations, and measurement types. Tolerances and injury mechanisms can vary by occupant age, experiment type, initial conditions of specific organs (e.g. stenosis, intestinal contents), and muscle activation.

Crushing or compression injuries are common in the abdomen during direct loading by the lap belt or contact with the vehicle interior. Maximum compression has been found to correlate with injury severity in seat belt loading tests (Miller, 1989). However, these correlations vary by study and by loading scenario (Hardy et al., 2015).

Many studies have investigated rate effects on abdominal injury in that both the rate and magnitude of abdominal loading are important in the determination of injury type and probability. For example, seat belt loading (low velocity and high compression) and airbag impact (high velocity and low compression) both can cause injury (Rouhana, Lau, & Ridella, 1985). Rouhana et al. developed the Abdominal Injury Criterion (AIC) based on lateral impacts to rabbits, which is the product of the maximum impact velocity and the maximum compression, or Vmax*Cmax (Rouhana et al., 1985). Another proposed metric, the Viscous Tolerance Criterion (Viscous Criterion, or VCmax) is the maximum of the product of impact velocity and compression over time (Lau & Viano, 1986; Viano & Lau, 1985, 1988). VCmax has the added benefit of providing the timing that could be associated with injury. Additional studies have found that the maximum loading rate alone is also important with respect to abdominal injury prediction.

The response to the abdomen as measured by force depends on how and where the force is applied and measured (Hardy et al., 2015). Specific to lap belt loading, one study found a parabolic relationship between lap belt force during submarining and abdominal injury, however this also coincided with abdominal penetration (Leung et al., 1982).

Impact energy has been correlated with the number of abdominal injuries, which increases as impact energy increases. A study by Walfisch et al. (1980) found combined force and compression limits required to produce injury (Walfisch et al., 1980). Reanalysis of these data lead to the development of the proposed injury metric Fmax*Cmax (impact energy), the product of maximum force and compression (Rouhana, 1987), which correlated well with the probability of AIS 4+ abdominal injury. An additionally study confirmed the predictive ability of Fmax*Cmax during seatbelt impacts and determined that it had a better correlation with AIS 4+ abdominal injury than the Viscous Criterion (Miller, 1989).

Abdominal injury based on pressure measurements varies widely based on where in the abdomen pressure is measured, whether it is in specific organ, vasculature, or intraperitoneal. A study of lap belt loading on swine found that AIS 3+ injuries corresponded to venous pressure and total peak force (Miller, 1989). The study produced injuries to the mesentery, small intestine, and colon. A study of pretensioned lap belt loading on the abdomens of PMHS found a delineation between injurious and non-injurious loading based on aortic pressure (Foster, et al., 2006).

Chapter 3: Methods

Rear-seat frontal sled tests were conducted using mid-sized adult male surrogates to determine occupant protection in the rear seat with respect to submarining and associated injuries. Rear seat vehicle bucks were made from modern vehicles in the US vehicle fleet. In a series of ATD tests, seven vehicles were tested under three fully frontal crash conditions, with the THOR-50M and HIII 50th-percentile male ATDs. Methods and results from the ATD test series have been published by (Bianco, Guettler, Hardy, Albert, & Kemper, 2022; Guettler, Bianco, Kemper, Albert, & Hardy, 2022). Four vehicles were selected for PMHS testing under the most severe crash condition.

Test Conditions

Vehicle Buck Selection and Fabrication

Seven vehicles were selected out of a pool of vehicles recently tested in NCAP and FMVSS 208 rigid barrier tests (MY 2017 and 2018). All vehicles were inspected for any damage to the rear structure of the vehicle that could affect this study. Seat and restraint characteristics were measured and recorded in the rear seat of each vehicle. These measurements include, but are not limited to, belt anchor locations, seat cushion stiffness, seat pan geometry, and belt routing based on an approximate 50th percentile male. These data were used to predict submarining protection and crash protection and to develop basic finite element (FE) models of some of the vehicle seats. The measurements associated with specific metrics were used to rank potential protective benefits of the restraint systems and seat designs. Submarining performance predictors included lap belt angle, seat stiffness, seat pan angle, and the presence of submarining mitigation strategies (e.g. anti-submarining bar), while the crash safety performance measurements were those associated with chest deflection, lumbar loads, and other ATD injury metrics. Basic simulations were then conducted using the vehicle-specific FE models to confirm the ranking. Seven vehicles were selected: the top, middle, and bottom performers, a vehicle in the middle of the good range, a vehicle in the middle of the bad range, and two popular vehicles with three seating rows.

Each vehicle was broken down to remove parts that were unnecessary for the bucks, including the engine compartment and its contents, windows and doors, etc. The front seats, center console, and dashboards were also removed. While the front seats provide some restraint effect for rear-seated occupants, they would introduce more variability into the test series. Therefore, front seats were removed to reduce any related test-to-test and vehicle-to-vehicle variability, and to improve line of sight for the Vicon motion capture system and high-speed cameras. In addition, with the front seats removed, the occupant compartment more closely represented novel seating arrangements that could be possible in future automated vehicles designs. Some vehicle bodies required reinforcement to prevent deformation during testing, so exoskeletons made

of steel tubing were welded to the outside of the body. Two steel tubes were welded onto the bottom of the vehicle along the longitudinal axis and had feet that were used to bolt the bucks to the sled deck. Mounting plates for the data acquisition systems were mounted into the trunk space, in the rear, of each vehicle. A mounting plate was welded to the front frame to provide a frontal onboard view of the tests. An exemplar vehicle buck is depicted in Figure 1. Two of the vehicles had three rows of seats; in those vehicles, the first and third rows were removed, and the second row of seats was used for testing.

Figure 1. Completed buck (vehicle V15) on the sled.

The seats and restraints used in this study were specific to each vehicle. New seat cushions, buckles, and belts were installed prior to each test. In some cases, if substantial damage occurred, entire seats or seat bottom frames were replaced.

Vehicles

Vehicles varied by body type, seat type, and restraint type. A summary of the study vehicles and select characteristics is provided (Table 1). The study vehicles included two mid-sized sedans, one sport utility vehicle (SUV), three crossover SUVs (CUV), and one minivan. The restraint types (rear seat/second row) fit into two categories. The first, conventional restraints, are three-point belts with continuous shoulder and lap parts, and a basic retractor (no pretensioner) at the shoulder. The second category, advanced restraints, are three-point belts with continuous shoulder and lap parts, and a pretensioner and load limiter at the retractor. As previously noted, the second seating row of each vehicle was used in this study and is referred to as the “rear seat”.

Table 1. Vehicle, seat, and restraint types selected for the study.

Buck	Model Year	Vehicle	Vehicle Type	Seat Type	Restraint Type
V1	2018	Audi Q5	CUV	Suspended	Advanced
V6	2017	Chrysler Pacifica	Minivan	Pedestal	Conventional
V10	2018	Hyundai Santa Fe	SUV	Basket	Conventional
V13	2017	Mazda CX-3	CUV	Rigid	Conventional
V14	2018	Mercedes GLC 300	CUV	Rigid	Advanced
V15	2018	Nissan Maxima	Sedan	Rigid	Conventional
V19	2018	Toyota Camry	Sedan	Rigid	Advanced

Sled Pulses

Tests were conducted using a 1.4 MN ServoSled (Seattle Safety LLC, Kent, WA). The vehicle bucks were bolted to the sled deck. The resulting sled acceleration was recorded using a single-axis accelerometer mounted to the front of the sled.

Three types of sled pulses were developed to provide three test conditions for each vehicle. First, the NCAP pulse from each vehicle's full-frontal rigid-barrier test was collected and scaled to 85% of its full magnitude. Scaling was done to remove rebound effects from the NCAP test (producing a ΔV of 56 kph) and to ensure that the ServoSled could produce the pulses. Tests using this 85% magnitude NCAP pulse are called "NCAP85" throughout the study, and each NCAP85 pulse is specific to each vehicle. The second pulse type was also specific to each vehicle; herein called the "Scaled" pulse. The Scaled pulse was created by scaling each NCAP pulse to a ΔV of 32 kph (scaling factor = 32/56). The third pulse type is a single "Generic" pulse that was used for all seven vehicles. The Generic pulse has a ΔV of 32 kph and is the point-by-point average of all seven vehicle-specific Scaled pulses.

ATD Sled Testing

Sled tests were conducted using the Hybrid III 50th-percentile male (HIII) and the THOR-50M (THOR). Sled tests were conducted with seven vehicles under three sled acceleration conditions each. For each test, the THOR was positioned in the left outboard seat (U.S. driver's side) and the HIII (U.S. passenger's side) was positioned in the right outboard seat. Both ATDs were provided by the NHTSA Vehicle Research Testing Center (VRTC), where they were calibrated and qualified.

Test Matrix

Each vehicle was tested under each of the three pulse conditions (NCAP85, Scaled, and Generic) at least once. Twenty-five tests were conducted overall (n=25), including four repeated tests. See Table 2 for the test matrix. Equipment failure during one test made that test (Test V6-3) unusable so only 24 tests are

included in this study. The three repeated tests included in this study are the Generic test for vehicle V15 and the NCAP85 tests for vehicles V14 and V19. Tests V13-2, V14-4, V15-4, and V19-4 were selected as the matched NCAP85 tests for comparison to the PMHS tests.

Table 2. ATD Series Test Matrix. The excluded test is denoted (§) and the test in which the THOR standard abdomen was used is denoted by (α).

Vehicle ID	Test Number	Pulse
V1	1	Generic
	2	Scaled
	3	NCAP85
V6	1	Generic
	2	Scaled
	3§	NCAP85
	4	NCAP85
V10	1	Generic
	2	Scaled
	3	NCAP85
V13	1	Scaled
	2	NCAP85
	3	Generic
V14	1	Generic
	2	Scaled
	3	NCAP85
	4	NCAP85
V15	1α	Generic
	2	Generic
	3	Scaled
	4	NCAP85
V19	1	Generic
	2	Scaled
	3	NCAP85
	4	NCAP85

Instrumentation

The Hybrid III had standard instrumentation and its standard abdomen, which is a soft foam covered in urethane rubber. Before testing began, the Frangible Abdomen (Rouhana, et al., 1990; Rouhana, et al., 1989), which has a more biofidelic response and can provide a quantitative measurement of lap belt penetration of the abdomen, was investigated as a possible replacement for the standard abdomen. However, use of the Frangible Abdomen required two major adaptations of the HIII: neither the standard chest potentiometer nor the lumbar load cell could be used in conjunction with the Frangible Abdomen. Alternative designs were not deemed to permit use of the lumbar load cell and the chest potentiometer. Therefore, the standard abdomen was used in this study.

The THOR-50M was fully instrumented. In one test, Test V15-1, the THOR standard abdomen, which is a pouch containing two 3D IR-TRACC assemblies to measure right and left abdominal deflection, was used. Because of the severity of some of the tests in the study and the susceptibility of the abdominal IR-TRACCs to damage, an alternative abdominal insert was desired. In Test V15-2, the standard abdomen was replaced by the Abdominal Injury and SUbmarining Prediction (ABISUP), which is a foam abdominal insert that contains right and left pressure transducers housed in deformable, fluid-filled bottles, similar to Abdominal Pressure Twin Sensors (APTS), which are used in the abdominal inserts for the Q series ATDs (Beillas et al., 2012; Hardy et al., 2015; Johannsen, et al., 2007). To determine whether or not the ABISUP would change the kinematics and kinetics of the THOR, Tests V15-1 and V15-2 were duplicate tests using the Generic pulse. The comparisons between test data were found favorable so the ABISUP prototype abdomen was deemed acceptable for use throughout the rest of the study.

Seat belt tension was also measured. Three seat belt load cells were used for each restraint. One placed on the outboard shoulder belt between the retractor and ATD shoulder, one just above the buckle on the inboard shoulder belt (effectively the inboard lap belt), and one placed between the outboard lap belt anchor and the ATD. For the Vicon system, retroreflective markers were placed on both ATDs, the vehicle buck, and the sled.

Positioning

Due to the lack of regulatory or consumer-driven frontal crash tests for rear-seated adult occupants, there are currently no positioning standards for either 50th-percentile male ATD in the rear seat. To develop a seating procedure, the Hybrid III-50M front left outboard seating procedure for FMVSS No. 208 (49 CFR § 571.208), a draft seating procedure for the THOR in either front outboard seat (provided by NHTSA), and procedures for positioning small female ATDs (Docket NHTSA-2015-0119, IIHS-2012) were consulted. Target joint angles and positioning distances for each ATD were established (Table 3).

Before the ATDs were placed in the seats, the head restraints were set to the highest position. Next, the centerline of the seat was determined using the center of the head rest and the centerline between the right and left thigh bolsters. Each ATD was centered on the seat (as defined by the centerline) with the pelvis as far rearward as possible. Pelvis angle was measured using the H-point tool for Hybrid III and internal pelvic tilt sensor in the THOR. All angles prescribed in Table 3 were used as a determination of the final angles. The palms of the hands were placed on the thighs with the thumbs on the sagittal midline of the thigh resulting in an arm angle that was approximately 40° from vertical in the sagittal plane. The seat belt was fastened and the shoulder belt was routed to cross the chest at the mid-sternum and the lap belt was set below the ASIS on the anterior pelvis. Figure 2 shows final positioning of the ATDs before one test.

Table 3. Targets for ATD positioning

	Hybrid III	THOR
Pelvis Angle	22.5 ± 2.5°	33 ± 2.5°
Head Angle	0 ± 0.5°	0 ± 0.5°
Knee Angle	100 ± 5°	100 ± 5°
Knee-to-knee Distance	269 mm	225 mm

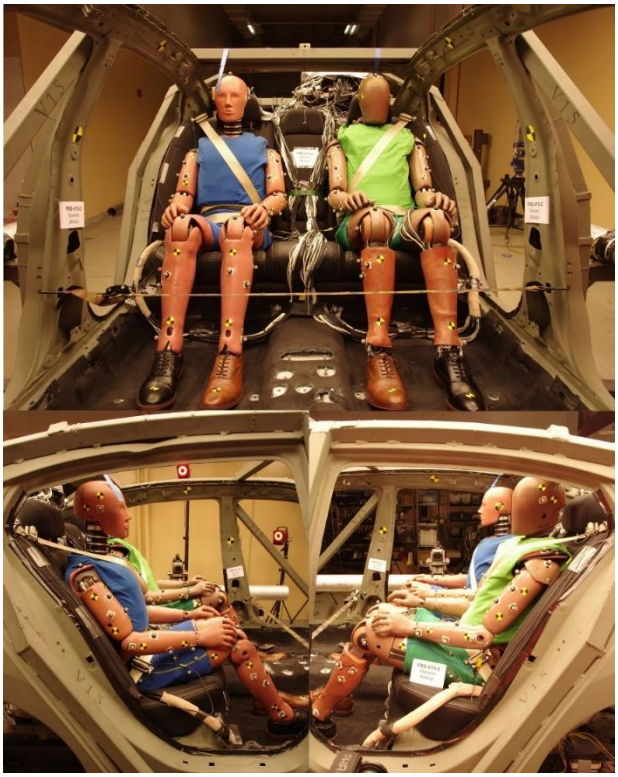

Figure 2. Pre-test positioning of HIII (blue) and THOR (green) for Test V15-2.

Without the front seats, the dummy knees can extend freely, which created the potential for hyperextension of the knee. To prevent this hyperextension of the knee and resulting damage, a strap was tied across the width of the buck on the B-pillar to arrest leg motion before the knee was fully extended. The strap was engaged by the shins late in the event, and did not alter overall ATD behavior. Figure 3 shows the location of the strap in one of the vehicles.

Figure 3. Positioning of Strap in Test V19-2.

PMHS Sled Testing

A subset of four vehicles used in the ATD study were selected for testing with post mortem human surrogates. Eight PMHS were used for a total of eight tests—each PMHS being tested once. Each vehicle was tested twice using the NCAP85 crash conditions; once using a heavier PMHS and once using a lighter PMHS, but with both falling within the range for a target mid-sized male. In all tests, the PMHS was seated in the left outboard rear seat for direct comparison to the THOR in the ATD sled tests. Figure 4 depicts the overall setup for a PMHS test in Vehicle V15.

Figure 4. Final setup for a PMHS test in Vehicle V15. The PMHS is seated in the rear left outboard seat of the vehicle buck.

Selection

The target general anthropometry for PMHS was based on recent population demographics in the National Health Statistics Report (NHSR, Dec. 2018) that are similar to the Hybrid III-50M (25th percentile male in the US). Target anthropometry values are in Table 4.

Table 4. General anthropometry values for the Hybrid III-50M and target values for PMHS.

		HIII	PMHS Target
Stature	(cm)	175.3	166.5 – 184.0
Mass	(kg)	78.2	66.4 – 89.9
BMI	(kg/m^2)	25.4	20 – 30

The PMHS were obtained from informed-consent programs. Prior to PMHS selection, anatomical donors went through serological analysis for viral risks as well as medical imaging such as plain film x-ray or computed tomography (CT) scans. Inspection of medical imaging looked for fractures, skeletal abnormalities, and osteophytes between vertebrae.

Eight PMHS were selected for use in this study. The average height was 175 cm (+/-7 cm) and the average weight was 75 kg (+/-12 kg). General information about the PMHS can be found in Table 5.

Table 5. PMHS Characteristics

PMHS	Sex	Age	Stature (cm)	Mass (kg)
SM 095	M	74	170	64
SM 129	M	79	178	63
SM 152	M	63	180	81
SM 153	M	51	168	64
SM 154	M	74	178	89
SM 155	M	65	168	85
SM 156	M	68	188	89
SM 157	M	59	173	68

Test Matrix

Four of the vehicles used for the ATD study were used in the PMHS study: vehicle V13 (CUV, conventional restraints), vehicle V14 (CUV, advanced restraints), vehicle V15 (sedan, conventional restraints), and vehicle V19 (sedan, advanced restraints). Each vehicle was tested twice in the NCAP85 crash condition. The test matrix for this series can be found in Table 6.

Table 6. PMHS Test Matrix

Buck	Test Number	PMHS
V13	4	SM129
	5	SM155
V14	5	SM156
	6	SM157
V15	5	SM152
	6	SM153
V19	5	SM154
	6	SM095

Preparation and Instrumentation

The 3D motion of the PMHS was recorded using a Vicon motion capture system and kinematics were measured at several locations on the body. Head accelerations were measured using a 9-accelerometer array (Figure 5).

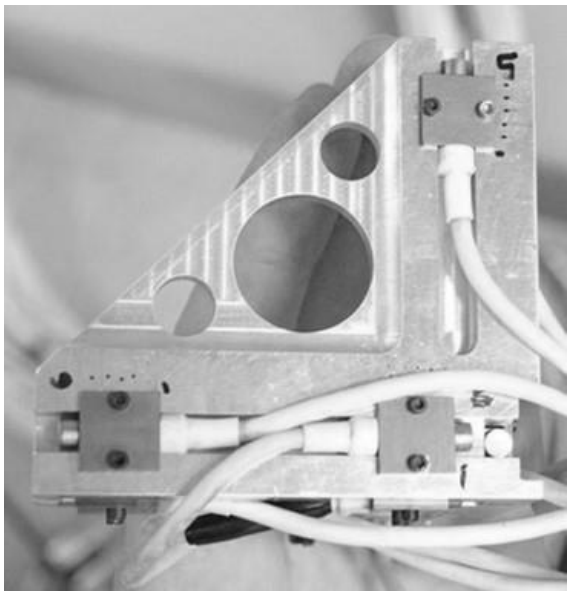

Figure 5. The 9-accelerometer array used to measure head kinematics.

Kinematics were measured at other locations using either three-degree of freedom packages (3DOF: X and Z-direction acceleration and angular speed about the Y axis) or six-degree of freedom packages (6DOF: X, Y, and Z-direction acceleration and angular speed about the X, Y, and Z axes). These measurements included packages fixed to the T1 vertebra (3DOF), T7 vertebra (6DOF), T12 vertebra (3DOF), sacrum (S1, 6DOF), pelvis (left ilium, 6DOF), and tibias (mid-diaphysis, 6DOF). The linear accelerometers used were from Endevco (7264c-2k). The angular rate sensors (ARS) used were DTS Pro (18k, 6DOF packages) or 50k (3DOF packages).

The motion blocks for the spine were fabricated using a "Pi-Omega" configuration. Two linear accelerometers and one angular rate sensor were affixed to aluminum pieces (Pi component) to create the 3DOF packages (Figure 6). These 3DOF packages were mounted to the T1 and T12 vertebrae via aluminum spine mounts (Omega component) also depicted in Figure 6. The spine mounts were also used to attach the commercially available 6DOF packages (DTS, 6DX Pro) to the T7 and S1 vertebrae. For the pelvis and tibia kinematics blocks, 3 linear accelerometers and 3 angular rate sensors were fixed to aluminum blocks to create additional 6DOF packages (Figure 7). All transducer packages were wrapped in dental dam to reduce contact with fluids.

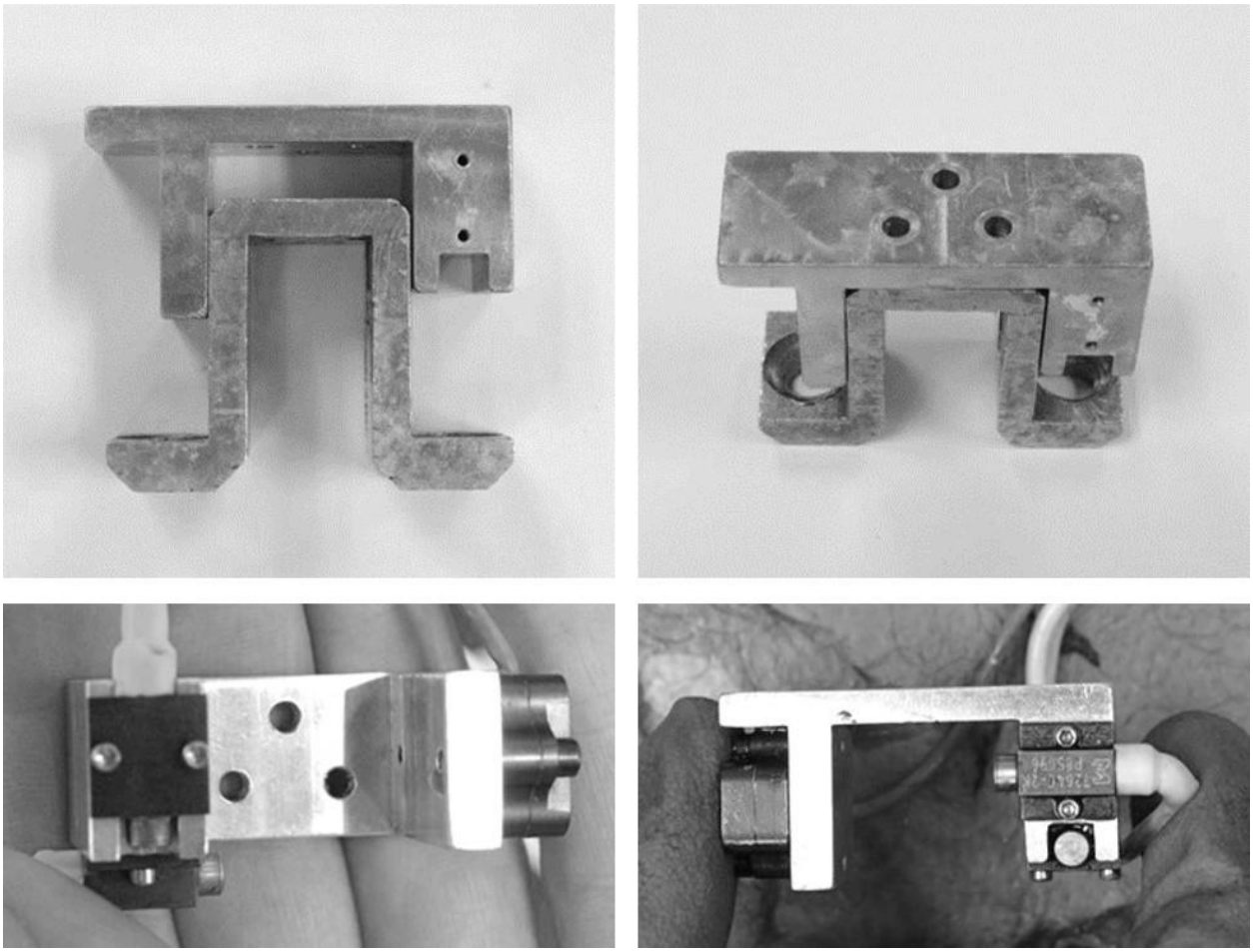

Figure 6. The aluminum mounting piece for the 3DOF packages (top) with the associated spine mounts (Pi-Omega configuration). In the bottom right and left, a loaded 3DOF Pi component with 2 linear accelerometers and 1 ARS.

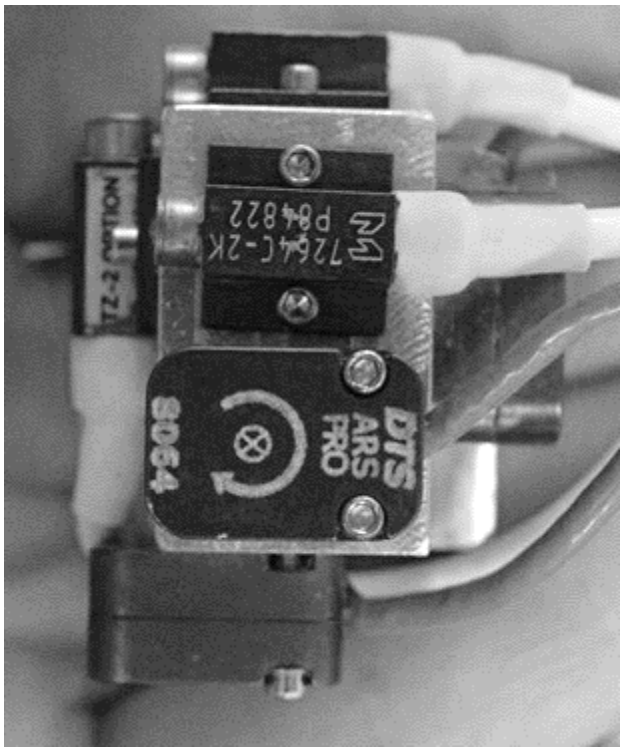

Figure 7. An exemplar 6DOF block to be used to measure the kinematics of the pelvis and both tibias.

To install the spine mounts, incisions were made at the level of each target vertebra as determined by x-ray images. Soft tissue attached to the lateral sides of the spinous processes were cut away to provide access for the spine mounts, which were fixed to the lamina using pedicle screws. Figure 8 shows an example of an installed Omega component spine mount on the T12 vertebrae with the associated Pi component 3DOF package in its appropriate orientation before being shrouded in dental dam and installation. An example of a DTS 6DOF assembly mounted to a spine assembly is provided in Figure 9. For all spine assemblies, the orientation of the instrumentation blocks was such that the wires ran superiorly out of the incision.

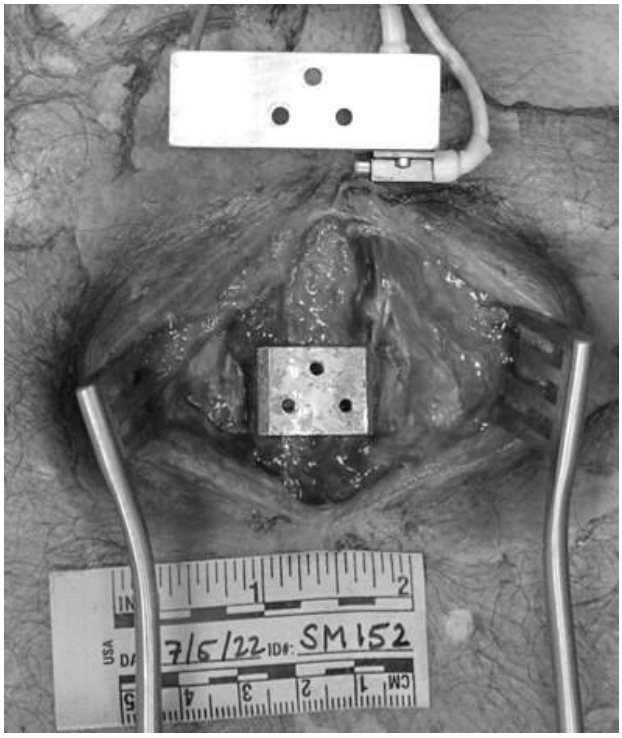

Figure 8. A spine mount installed on the T12 vertebra with the associated 3DOF package removed.

Figure 9. A DTS 6DOF assembly mounted to a spine block before being shrouded.

The pelvis 6DOF assembly was mounted to the iliac crest using a modified beam clamp and epoxy as a conformal mold. The 6DOF assemblies for the mid-shaft of the tibias were fixed to Delrin® mounts that were hose clamped to the tibias (Figure 10). The tibias were prepped by cleaning the bone and gluing sand paper to the surface to prevent the Delrin® from sliding.

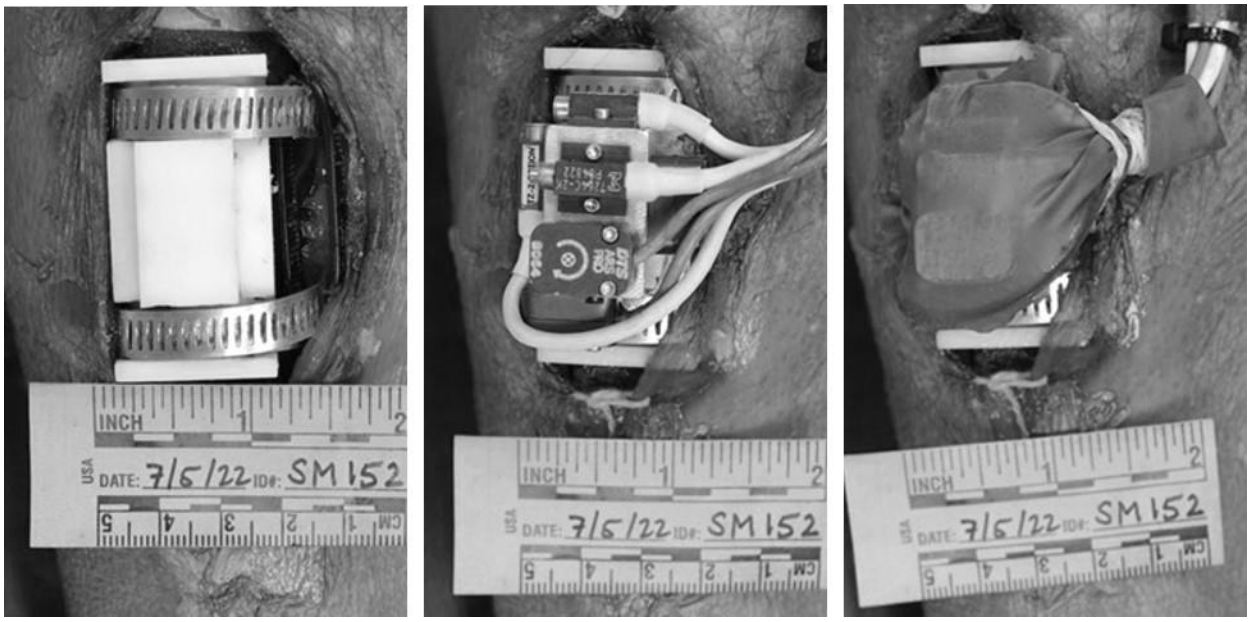

Figure 10. The Delrin block (left), mounted 6DOF assembly (middle), and wrapped assembly (right) on a tibia.

Chest deflection was measured using two 59-channel chestbands (8641, Humanetics). The chestbands were positioned at the anterior location of rib 4 and the xiphoid process (Figure 11, left). Strain gages (Micro Measurements, CEA-13-062UW-350 or CEA-13-125UN-350) were placed on the anterolateral aspects of ribs 2-9 on the right side and ribs 2-5 on the left side (Figure 11). A gage was placed on the superior aspect of the left clavicle at the midpoint and on the anterior surface of the gladiolus at the midpoint. Prior to the sled being fired, the PMHS lungs were inflated several times via compressed air applied through a tracheotomy tube.

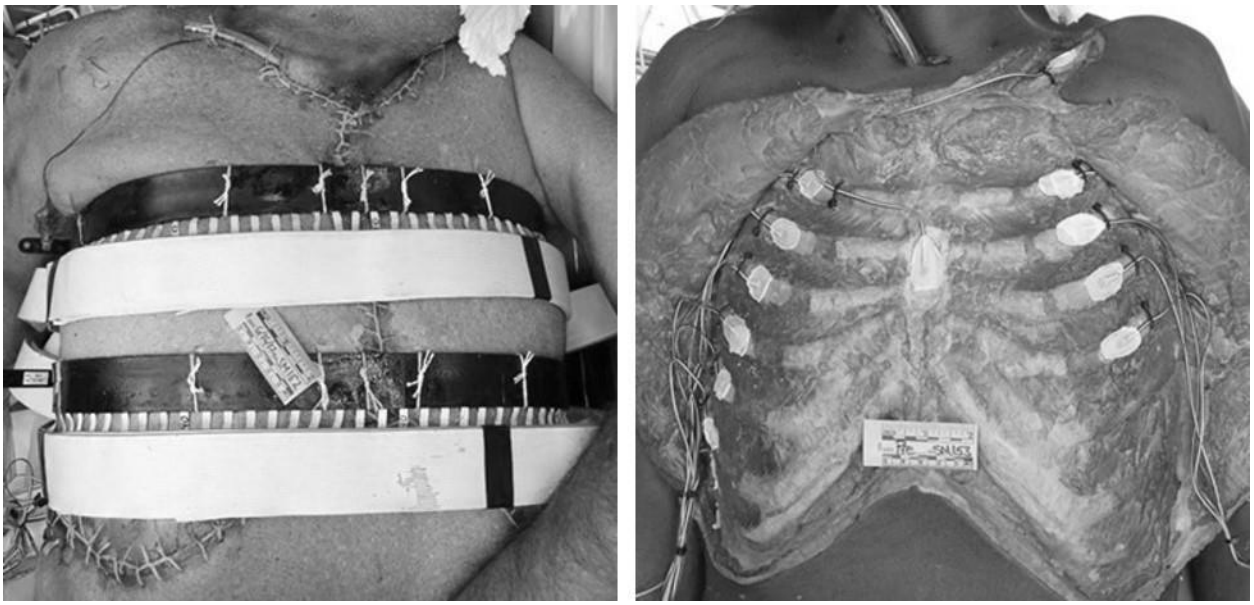

Figure 11. The chest bands positioned at the level of rib 4 and the xiphoid process (left) and the locations of the strain gages on the ribs, sternum, and left clavicle.

Abdominal pressure (Millar, SPR-350S Mikro-Tip®) was measured in the inferior vena cava (at the level of the liver) (Figure 12), the abdominal aorta (at the level of the L1-L2 vertebrae) (Figure 12), and in tissue neighboring each ASIS (slightly medial and dorsocranial) (Figure 13). The PMHS were perfused with normal saline, in most cases through the right femoral vein and the left femoral artery using Foley catheters attached to a perfusion system. T-fittings facilitated introduction of perfusion fluid and placement of the pressure transducers through the same catheters. This limited perfusion is focused on the liver and abdominal aorta/celiac trunk. Finally, three seat belt load cells were used in the same outboard shoulder (retractor), inboard shoulder (buckle), and outboard lap belt (anchor) locations as in the ATD testing phase (Figure 14).

Retroreflective markers for the Vicon motion capture system were installed on the PMHS using various methods. Markers were installed bilaterally on the femurs, arms, and above the tragion using threaded studs drilled into the bones. A plate with four markers was installed on the head. Finally, markers were stitched to the skin at the locations of the right and left acromion processes. Additional markers were fixed to Coflex® wrapped outside of the clothing on the PMHS at the knees, ankles, elbows, and wrists.

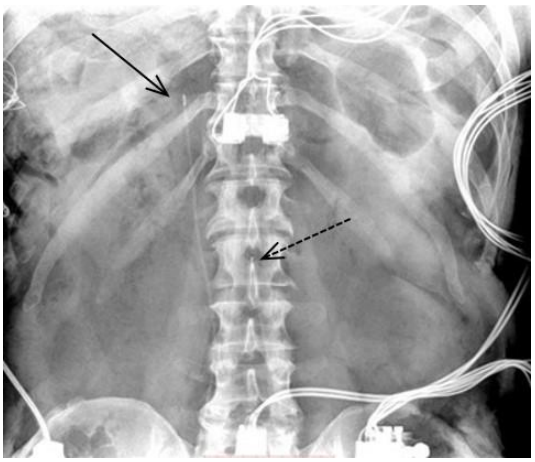

Figure 12. The locations of the pressure transducers in the inferior vena cava (solid arrow) and aorta (dashed arrow).

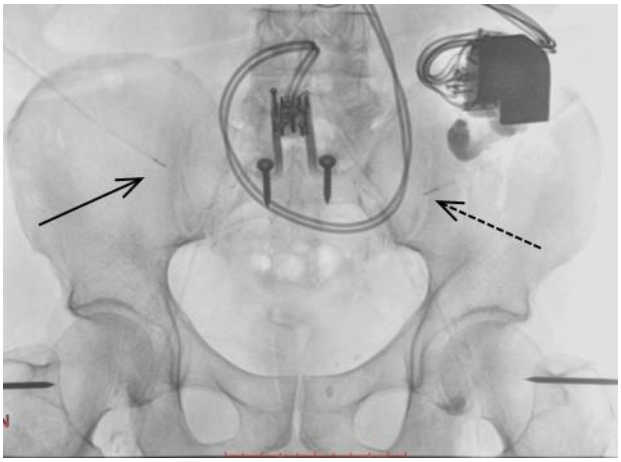

Figure 13. Right (solid arrow) and left (dashed arrow) ASIS pressure transducers.

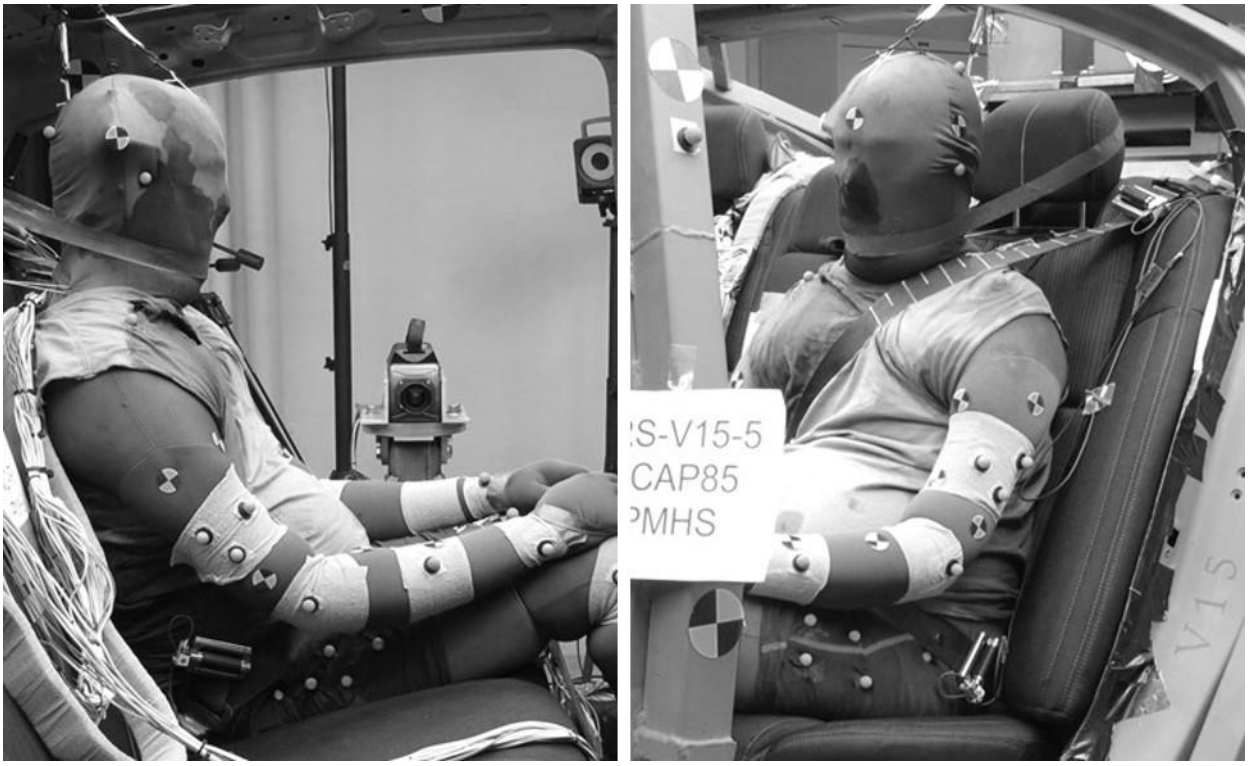

Figure 14. Locations of seat belt load cells.

Positioning

The PMHS were first dressed in a full-body spandex suit. Then, to match the ATD tests, the PMHS were fitted with 100% cotton t-shirts and shorts and the same shoes that were used for the ATD tests.

As with the ATD testing, the head restraint was set to the highest setting and the centerline of the seat was determined using the center of the head restraint and centerline between the right and left thigh bolsters. The PMHS were centered in the seat with the pelvis pushed as far rearward as possible with the torso against the seat back. First, adjustments were made to set the pelvis angle. For the PMHS, the pelvis angle was defined as the angle between the plane made by the right and left ASIS and the pubic symphysis and the horizontal (Padgaonkar, Lawson, & King, 1978). Pelvis angle was determined using a tilt sensor mounted to the right ilium at the tubercle of the iliac crest. The target pelvis angle for the PMHS was 29° to coincide with the THOR-50M pelvis geometry and angle used for the ATD testing. Next, with the torso against the seat back, the head was positioned using a marionetting technique. Positioning for the head focused on keeping the Frankfort plane horizontal and the head and neck in a "natural" position for a seated person. As was done for the THOR-50M, the feet were set so that the knee angle was 100° +/- 5° and the knees were 225 mm apart. The hands were placed on the anterior thigh so that the arms were approximately 40° from vertical. Finally, the locations of the tragion, C7, and approximate H-point were recorded relative to the

seat bight. After each positioning step the pelvis angle was checked to ensure it has not rotated. An example of the final positioning of a PMHS is provided in Figure 15.

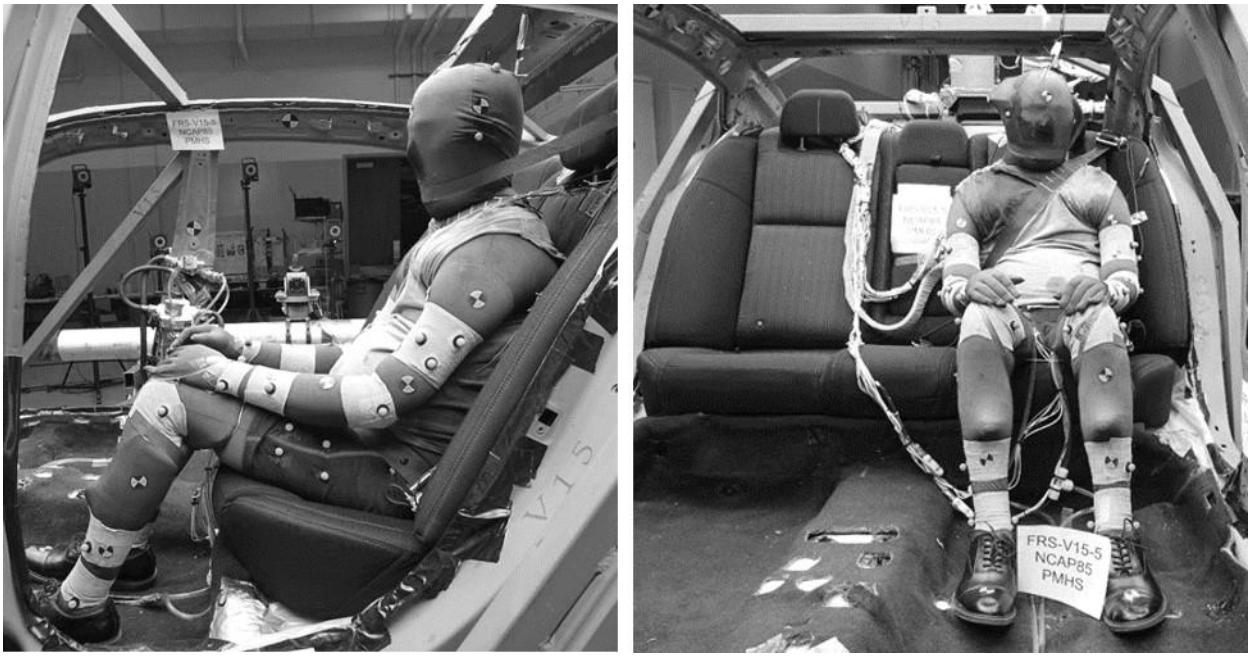

Figure 15. Final positioning of a PMHS.

Data Acquisition and Analysis

Data Acquisition and Processing

Two onboard data acquisition systems, DTS G5 and TDAS Pro (Diversified Technical Systems, Inc., Seal Beach, CA), were used for the sled tests. Data were sampled at a rate of 20,000 samples per second. Five high-speed video cameras (Phantom, V9.1, Vision Research Inc., Wayne, NJ) were also used. Three cameras were onboard during the tests, mounted to the vehicle buck (frontal view) and sled outriggers (right and left outboard views). An offboard camera was mounted above the sled for an overhead view of the tests, and another offboard camera was positioned to get a lateral view of the tests. Video was captured at 1,250 frames per second (fps). Finally, a Vicon motion capture system (Vicon Motion Systems, Oxford, UK), which includes 16 MX T-20 cameras that sample at 1,000 fps, was used to quantify the three-dimensional kinematics of the ATDs and PMHS.

Data processing followed the guidelines set by the SAE J211 standard (Society of Automotive Engineers, 2014) including filtering, data channel polarity, and coordinate system definition: X-axis is parallel to the longitudinal axis of the vehicle and is positive going from posterior to anterior, the Y-axis is positive from left to right, and the Z-axis is positive downward.

To define the body-fixed basis for the PMHS motion block data, pre-test CT scans were segmented using 3DSlicer (Open Source, (Fedorov et al., 2012)). Points were selected to obtain 3D coordinates to develop the anatomical coordinate system for each bone or body segment. The coordinate system for the pelvis is as defined by Padgaonkar (Padgaonkar et al., 1978) where the X-Y plane is defined by the left and right ASIS and the superior edge of the pubic symphysis. The origin of the coordinate system is the midpoint of the line between the right and left ASIS. The X-axis is normal to the defined plane, the Y-axis is the line connecting the left and right ASIS, and the Z-axis is normal to both the X and Y axes. Point coordinates were then taken from the segmentations to define the coordinate axes of the pelvis and sacrum motion blocks. Polarities of the pelvis body-fixed basis and the mount coordinate systems were as defined by SAE J211. Coordinate system transformations were performed to rotate the pelvis and sacrum data to the orientation of the pelvis coordinate system. The kinematics data were not, however, translated to the origin point of the pelvis.

The sled system provided a control trigger, and all data acquisition systems, cameras, and Vicon were triggered by an offboard DTS TDAS Pro, which received the trigger from the sled system. The sled launched approximately 80 ms post-trigger. During data processing, time zero for all data (transducer, video, and Vicon) was set to the beginning of the sled acceleration pulse.

Submarining Assessment

Submarining is a complex kinematic event in which the lap belt slips up and off of the anterior pelvis, ultimately loading the abdomen. This event can be difficult to identify correctly, especially with only visual analysis. For example, even with multiple camera views the lap belt can become hidden by the surrogate's clothing or out-of-plane motion, making it difficult to identify where on the surrogate the lap belt is loading. Additionally, looking at lap belt placement post-test does not indicate whether the submarining occurred during the loading phase, which is significant with respect to injury risk, or the unloading phase, which is not significant with respect to injury risk. Taking this into consideration, as many information sources as available for each surrogate must be taken into account to get an accurate assessment of submarining occurrence and severity.

ATDs

For each test, several data sources were used to identify the occurrence of submarining and to assess the severity of the submarining that occurred. Because the standard HIII abdominal insert and pelvis were used in this study, submarining assessment in the HIII was limited to post-test photographs, high-speed videos, and seat belt load cells. However, in the THOR both the standard abdomen and the ABISUP prototype abdomen measure loading of the abdomen. Additionally, the THOR pelvis has ASIS load cells that measure shear force in the X-direction and Y-axis moment, which can be used to determine loading of the pelvis

and slipping of the lap belt off of the pelvis. For submarining assessment in THOR, post-test photographs, high-speed videos, seat belt loads, ABISUP pressure, and ASIS force and moment were used to identify the occurrence of submarining and to assess its severity.

The incidences of submarining were divided into three categories. Minor submarining involved unilateral encroachment of the lap belt onto the abdomen and relatively low ABISUP pressures. In these cases, the belt slip always occurred on the buckle side, and at times was initiated by a pretensioner-initiated "belt lift" phenomenon. In pretensioner-initiated belt lift, as the pretensioner fires it lifts the shoulder belt and buckle, pulling the inboard side of the lap belt up and off of the pelvis before the ATD loads the restraints. Moderate submarining involved bilateral encroachment of the lap belt on the abdomen without substantial penetration into the abdomen. Finally, severe submarining had bilateral encroachment of the lap belt onto the abdomen, high ABISUP pressures, and departure of the ATD—specifically the pelvis—from the seat. Note that the classifications described above are based on characteristics of the data and do not include direct inferences about injury risk.

PMHS

Submarining assessment was conducted for each PMHS test using post-test photographs, high-speed video, lap belt loads, pelvis accelerations and angular rates, and abdominal pressure near each ASIS. The submarining rate of PMHS in each vehicle was compared to the submarining rate of each ATD to determine ATD better represents the submarining response of a 50th percentile male PMHS in the rear seat during frontal NCAP85 tests.

PMHS Damage Assessment

Post-test autopsies were performed on each PMHS to identify any damage related to the testing or submarining specifically. The autopsy information included and focused on herein includes damage specifically related to the pelvis, abdominal viscera, and lumbar spine. Resulting damage was compared to PMHS loading as well as ATD loading and kinematics to determine the ability of each ATD as an injury prediction tool for the abdominopelvic region.

Based on available epidemiological and experimental data, injuries related to direct lap-belt loading of the abdomen were anticipated to involve the hollow organs, mesentery, large vessels, and lumbar spine.

Kinematic Analysis of ATDs and PMHS

The Vicon motion capture data collected during the ATD tests were used to calculate pelvis angle and rotation in the THOR for the NCAP85 tests for vehicles V13, V14, V15, and V19. Pelvis rotation in the PMHS was calculated by integrating the transformed angular speed data from the pelvis or sacrum instrumentation blocks. Additionally, belt angle was determined throughout these tests by motion tracking

of the onboard high-speed video. Angle definitions used for this analysis are provided in Figure 16. The Vicon data were filtered at CFC 60Hz and the PMHS pelvis rotation and all lap belt angles were filtered at CFC 180Hz. Further comparisons of pelvis kinematics can be provided by comparisons in the pelvis acceleration data.

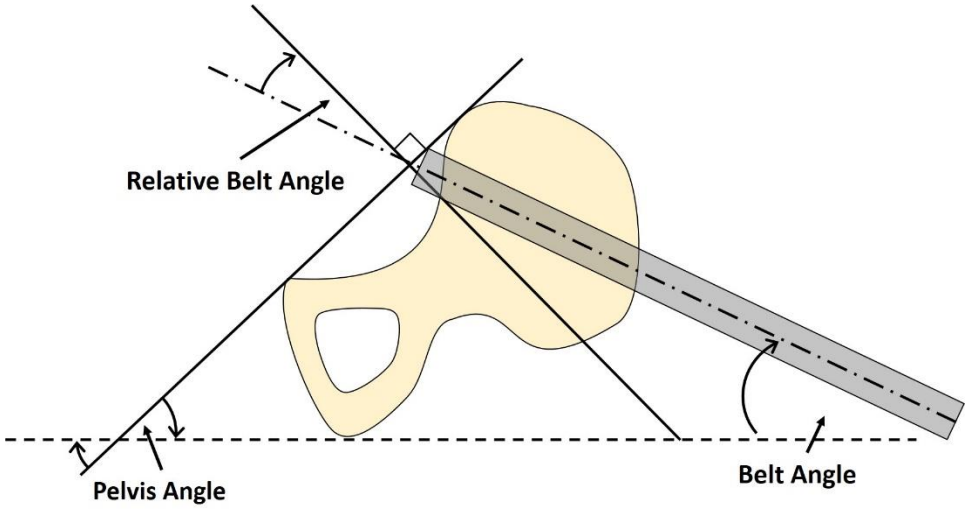

Figure 16. Definitions of the pelvis, belt, and relative belt angles

Pelvis angles are defined so that rotations follow J211. As drawn in Figure 16, rotation of the pelvis/belt angle is positive in the clockwise direction. The pelvis angle, as drawn, is negative, and would be zero when horizontal. The belt angle is positive as drawn and would also be zero when horizontal. Changes in both the pelvis and belt angle are positive for clockwise rotation. The relative belt angle is defined as the difference between the belt angle and the X-axis of the pelvis so that it is positive as the pelvis rotates rearward relative to the belt. For reference, when the belt is routed directly rearward from the pelvis, the relative belt angle is 0 degrees. As the relative angle increases, the angle between the belt and pelvis gets steeper, and is more positive. This definition of relative belt angle aligns with Nilson & Håland, 1995. Pelvis angles and relative belt angles can be used to determine thresholds for submarining for different surrogate types, these data can also be used to assess the biofidelity of the THOR's submarining response, specifically in the pelvis, and can also be used to compare the restraint conditions of the vehicles.

Rear Seat Design Characteristics and Submarining

A lot of research has been done to identify characteristics of seats, seat cushions, restraint anchoring and routing, and more that are more likely to produce submarining kinematics. However, because this study involves changing multiple factors at once between vehicles, no single design factor can be easily identified as producing submarining kinematics. Therefore, general comparisons of vehicle characteristics were made.

The selected vehicles all had varying seat pan or seat frame geometries and seat cushion characteristics such as stiffness and angle. During the vehicle selection process, basic characterizations of the seat pans were done to capture important geometries and features like anti-submarining bars and seat pan angle. Additionally, a rudimentary seat cushion stiffness was measured using varying weights and the FARO arm to approximate deflection. The basic geometries of the seat bottoms are included in Appendix A: Seat Characteristics, and a summary of key features is included in Table 7.

Table 7. Seat bottom characteristics for all seven vehicles included in the study.

Buck ID	Make and Model	Seat Pan Angle (°)	Seat Cushion Stiffness (N/mm)	Seat Cushion Angle (°)
V1	Audi Q5	29.4	11.06	12.0
V6	Chrysler Pacifica	16.5	7.49	17.0
V10	Hyundai Santa Fe	8.5	7.18	11.1
V13	Mazda CX-3	5	7.25	11.3
V14	Mercedes GLC 300	11	12.28	18.8
V15	Nissan Maxima	39.3	9.63	17.0
V19	Toyota Camry	24.6	9.78	12.6

Chapter 4: Results

A total of 32 rear-seat frontal crash sled tests were conducted with mid-sized male surrogates. In seven vehicles, the THOR and HIII were used to assess submarining risk during three crash conditions. In four vehicles, eight PMHS were tested to determine submarining risk, biofidelity of the submarining response of the ATDs, and damage to the abdominopelvic region produced during high-speed crashes. Pelvis kinematics and tissue damage of the PMHS were compared to the kinematics and loading to the THOR in the matched NCAP85 tests to determine the predictive ability of the THOR or any of its measurement capabilities.

ATD Sled Testing

Twenty-four successful sled tests were conducted to assess the response of two 50th-percentile male ATDs in the rear seat during a frontal crash. Seven vehicle bucks were tested under three frontal crash conditions including several duplicate tests. In every test the THOR was seated in the rear left outboard seat and the HIII was seated in the rear right outboard seat. In all but one test (Test V15-1) the THOR was equipped with the ABISUP prototype abdomen.

Sled Acceleration

Measured sled accelerations for all ATD tests can be found in Appendix B: Sled Accelerations. The peak acceleration (g) and the test ΔV (kph) for each test are provided in Table 8. The average ΔV's for the low energy tests are 34.5 (+/-0.3) kph and 24.1 (+/-1.8) kph for the Generic and Scaled tests, respectively. The average ΔV for the NCAP85 tests is 51.6 (+/-2.2) kph. Differences in the Generic test pulses are small, and could be due to the buck weights as well as minor variation in the sled system day-to-day.

Table 8. Peak acceleration (g) and ΔV (kph) for each test in the ATD series. The test in which the THOR standard abdomen was used is denoted (α).

Buck ID	Test Number	Pulse	Peak Acceleration (g)	ΔV (kph)
V1	1	Generic	-18.3	34.3
	2	Scaled	-21.8	34.1
	3	NCAP85	-33.7	52.3
V6	1	Generic	-17.2	34.2
	2	Scaled	-24.6	33.8
	4	NCAP85	-40.3	51.6
V10	1	Generic	-17.4	34.8
	2	Scaled	-29.2	32.0
	3	NCAP85	-41.1	46.2
V13	1	Scaled	-21.1	37.6
	2	NCAP85	-32.8	53.4
	3	Generic	-18.7	35.0
V14	1	Generic	-18.3	34.8
	2	Scaled	-18.6	33.6
	3	NCAP85	-26.0	51.0
	4	NCAP85	-26.4	53.8
V15	1^{α}	Generic	-17.6	34.2
	2	Generic	-18.3	34.4
	3	Scaled	-23.9	32.3
	4	NCAP85	-36.6	51.1
V19	1	Generic	-18.4	34.4
	2	Scaled	-23.8	35.2
	3	NCAP85	-35.5	52.2
	4	NCAP85	-35.2	52.5

THOR Abdomen Comparison

To investigate any differences in THOR kinematics or kinetics resulting from changing the abdominal insert, the Generic test condition for vehicle V15 was conducted twice. In the first test, test V15-1, the THOR standard abdomen was installed, and for the second test, the ABISUP prototype abdomen was installed.

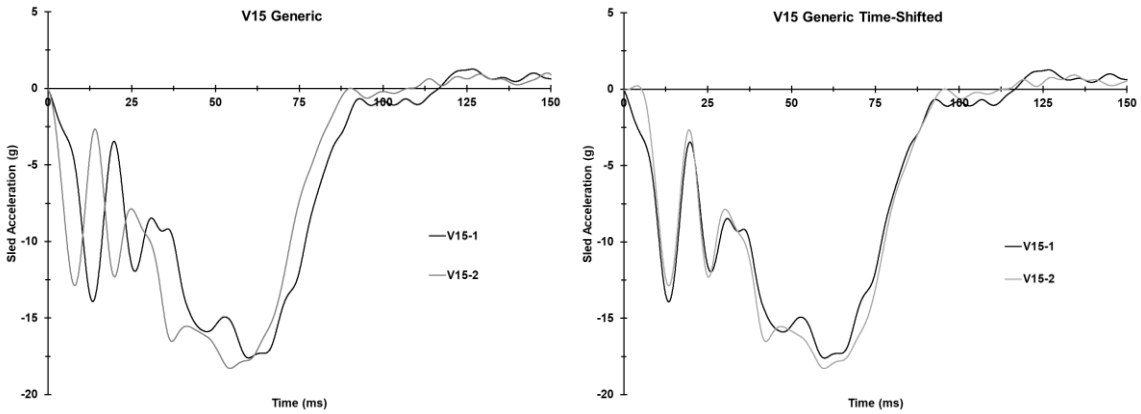

Figure 17. Sled acceleration pulses for Tests V15-1 (black) and V15-2 (gray).

As is apparent in Figure 17, the sled accelerations have a time shift between tests. For the sake of comparison, the acceleration pulses were shifted so that the first peaks were aligned. The data traces from test V15-2 have been shifted forward in time by the same amount (5.4 ms) in Figure 18-Figure 20. The un-shifted data can be found in Appendix C: THOR Abdominal Insert Comparisons. Figure 18 contains resultant head, chest, and pelvis acceleration of the THOR in tests V15-1 (black) and V15-2 (gray). Other than a slight decrease in magnitude in chest acceleration from V15-1 to V15-2, the shapes and magnitudes of the resultant accelerations match acceptably well between the two tests. In Figure 19, the Z-direction T12 loads are shown to have similar shape and magnitude. However, a difference in shear loads (X-direction) is apparent in the negative phase as the pelvis is pulled posteriorly relative to the torso. Finally, the Y-axis moments at T12 have the same loading and unloading as the torso flexes, except for near the peak, for which there is a 26% difference in magnitude. There are not enough data to identify the cause of these differences in T12 loading. Differences could be related to the abdomen characteristics, be within test-to-test variation, or even be due to specific conditions of one of the tests.

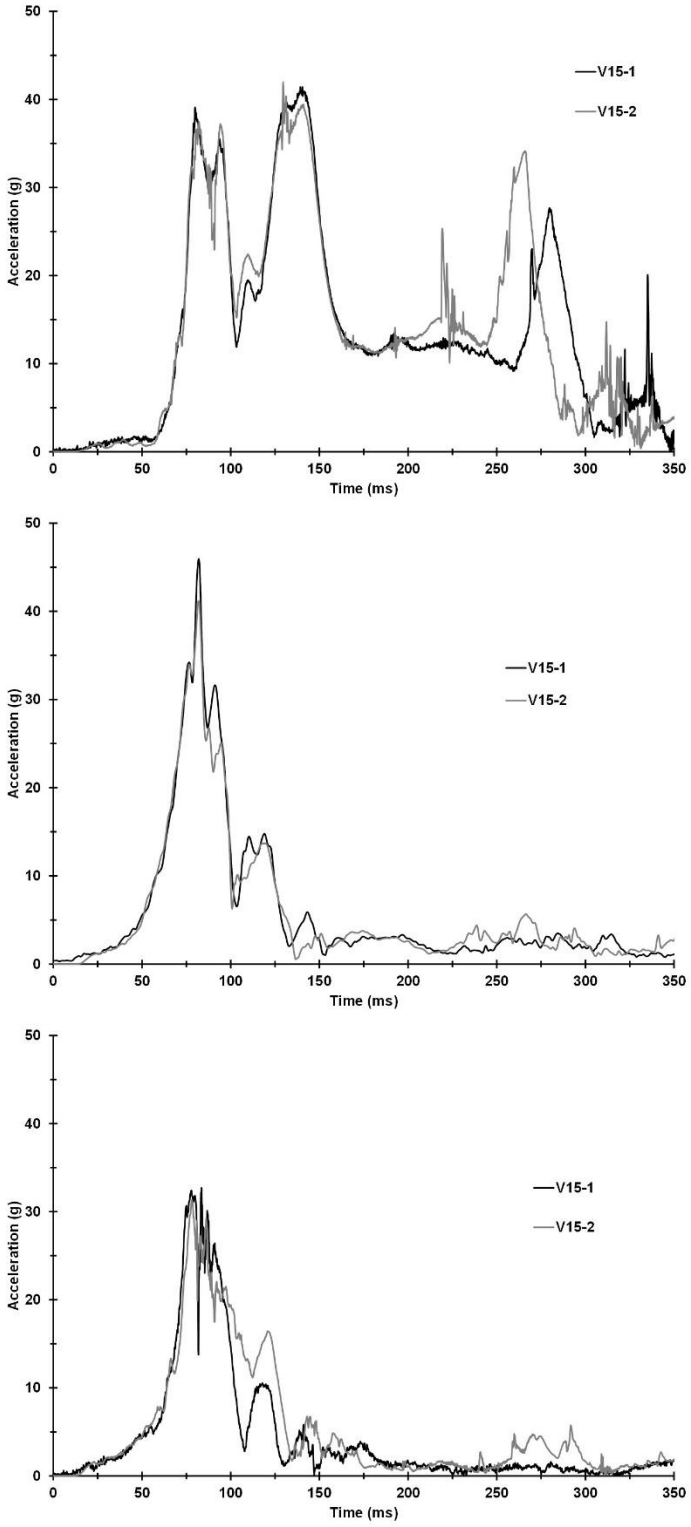

Figure 18. Resultant head (top), chest (middle), and pelvis (bottom) accelerations for tests V15-1 (black) with the standard abdomen and V15-2 (gray) with the ABISUP prototype abdomen. For the sake of comparison, the time histories from test V15-2 have been shifted forward by 5.4 ms.

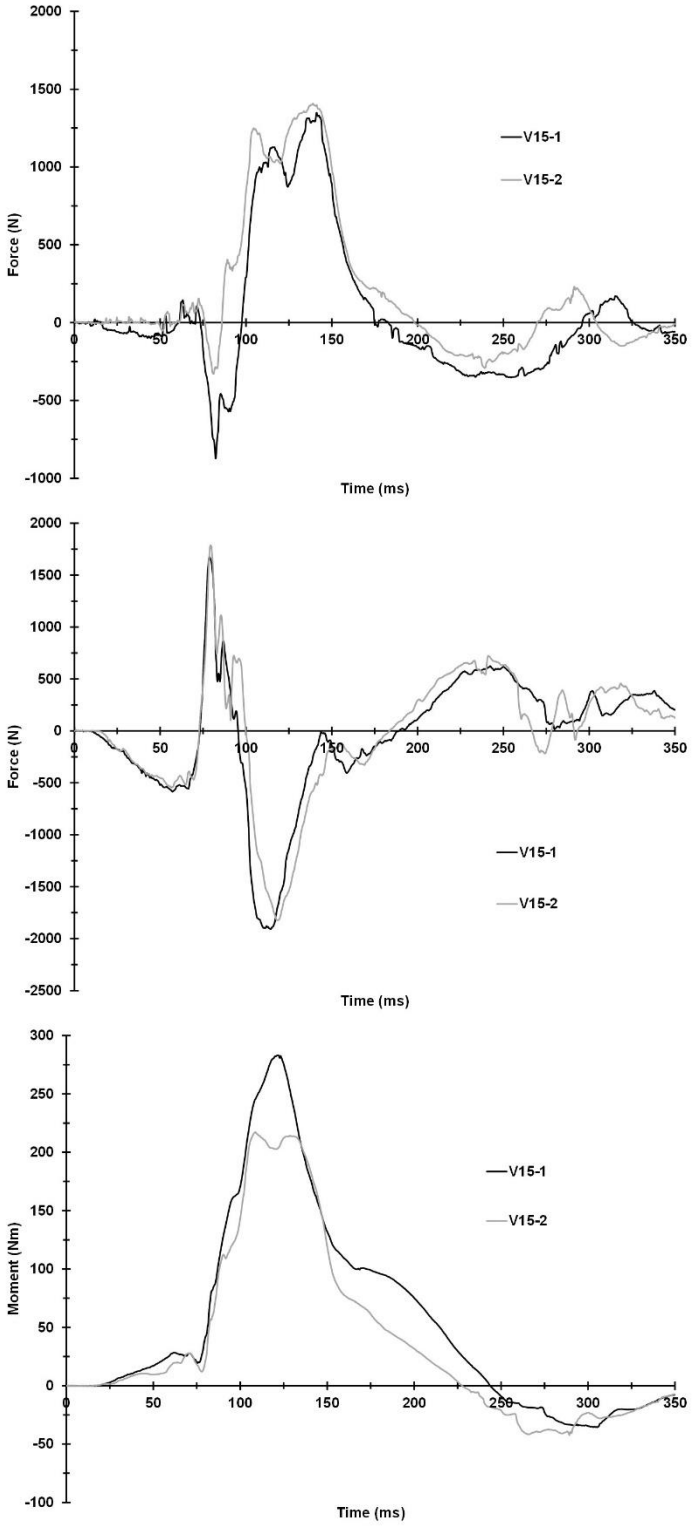

Figure 19. T12 X-direction force (top), Z-direction force (middle), and Y-axis moment (bottom) for tests V15-1 (black) with the standard abdomen and V15-2 (gray) with the ABISUP prototype abdomen. For the sake of comparison, the time histories from V15-2 have been shifted forward by 5.4 ms.

Force and moment magnitudes for the right and left ASIS are smaller for the test with the ABISUP (Figure 20). However, the right and left forces as well as the Y-axis moment on the right ASIS have similar shapes. Interestingly, an initial negative moment on the left ASIS suggests the belt first loaded the anterior pelvis inferior to the ASIS during test V15-2. The conclusion was reached that the ABISUP did not substantively alter the THOR performance, and it was decided that the ABISUP should be used in subsequent tests.

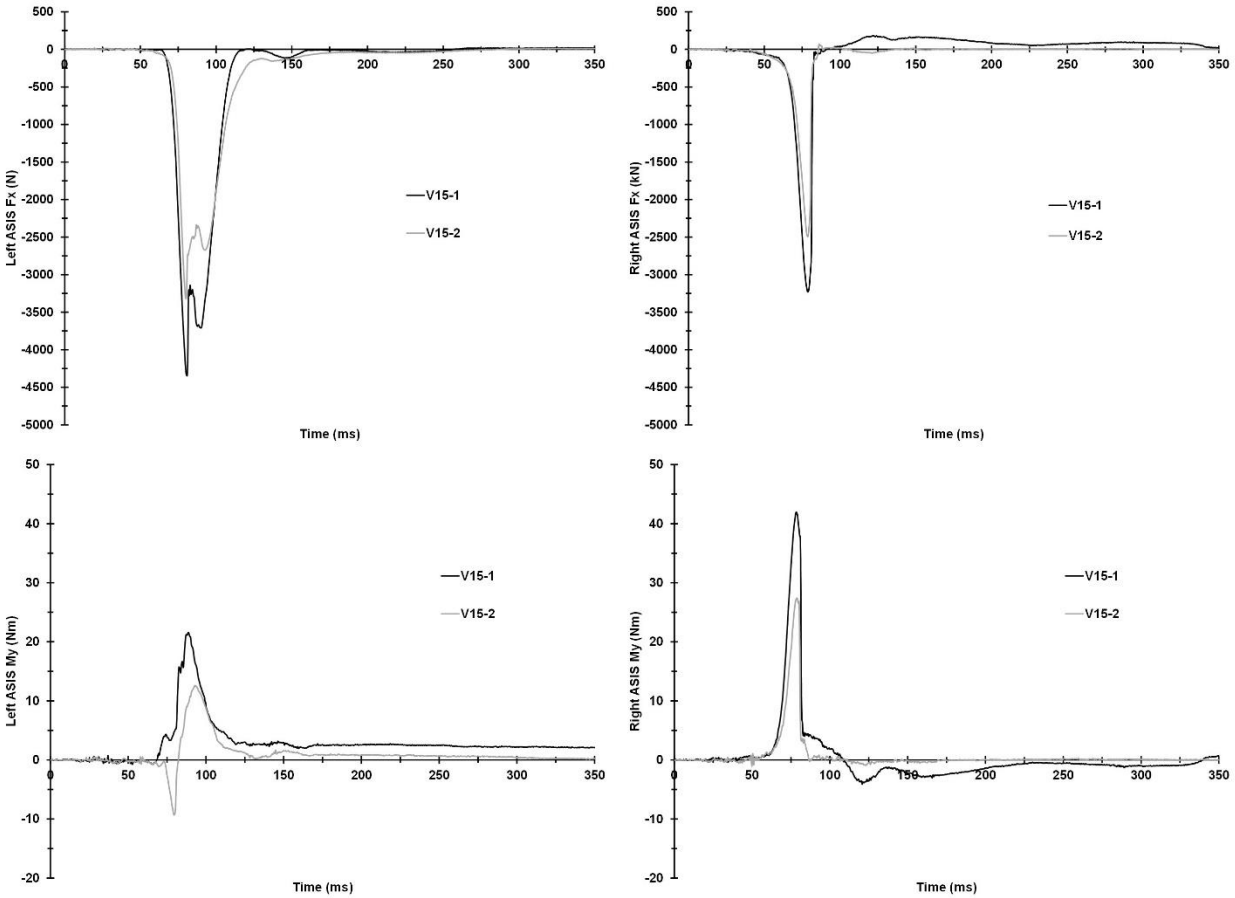

Figure 20. Left (left) and right (right) ASIS Fx (top) and My (bottom) for tests V15-1 (black) with the standard abdomen and V15-2 (gray) with the ABISUP prototype abdomen.

THOR Pelvis Loads

The THOR pelvis was instrumented with a right and left ASIS load cell that measures X-direction force (Fx) and Y-axis moment (My). These measurements are important for identifying submarining in the THOR. Plots of THOR ASIS loads are provided in Appendix D: THOR ASIS Loads. Peak forces and moments for all ATD tests are provided in Table 9.

Table 9. Peak ASIS loads and moments for the ATD tests

	Left Fx		Left My		Right Fx		Right My	
Test ID	Max	Min	Max	Min	Max	Min	Max	Min
V1-1	13.5	-2261	16.7	-1.9	300.9	-2164	12.9	-2.4
V1-2	15.3	-2477	12.4	-1.8	278.6	-2705	19.7	-3.7
V1-3	72.2	-3916	2.4	-31.0	8.4	-3301	28.1	-3.7
V6-1	7.9	-2853	14.3	-2.3	5.4	-2216	13.4	-1.5
V6-2	20.3	-2883	17.2	-1.9	15.9	-2145	8.6	-2.0
V6-4	18.4	-4792	16.3	-6.32	35.3	-3860	28.6	-2.9
V10-1	27.8	-3110	24.2	-0.9	92.6	-3127	21.7	-1.0
V10-2	58.1	-2579	22.2	-1.5	90.0	-3289	34.5	-2.2
V10-3	115.4	-2700	24.9	-1.3	150.4	-3022	29.4	-1.9
V13-1	26.2	-2807	24.6	-0.9	358.0	-3490	38.8	-0.8
V13-2	83.0	-4328	43.1	-1.3	-	-3955	46.5	-2.1
V13-3	12.5	-2439	24.4	-0.5	63.1	-1843	15.9	-2.7
V14-1	8.8	-2825	10.0	-1.8	35.6	-2581	28.8	-3.4
V14-2	17.2	-2041	10.4	-2.8	67.9	-1854	18.0	-2.7
V14-3	62.7	-3821	29.0	-3.2	27.3	-3390	18.6	-2.0
V14-4	63.2	-3893	27.9	-3.9	46.7	-4240	27.7	-1.1
V15-1	22.6	-4348	21.6	-0.8	180.7	-3230	42.0	-4.1
V15-2	18.7	-3322	12.6	-9.3	70.3	-2496	27.4	-1.1
V15-3	11.8	-2969	27.0	-0.8	43.8	-2437	25.3	-0.9
V15-4	67.1	-4517	52.7	-1.3	-	-2201	26.0	-1.7
V19-1	16.5	-3120	16.7	-1.0	-	-3323	28.6	-2.2
V19-2	12.9	-3141	21.6	-1.7	-	-3226	29.1	-1.6
V19-3	53.5	-3822	49.8	-0.7	-	-2438	20.7	-1.4
V19-4	146.6	-4587	56.5	-0.9	-	-3509	30.6	-1.6

ABISUP Pressures

For all tests except V15-1, the THOR was equipped with the ABISUP prototype abdomen. Resultant deflection from test V15-1 and the ABISUP pressures from the remaining tests are all provided in Appendix E: THOR Abdominal Loading. Peak ABISUP pressures are provided in Table 10.

Table 10. THOR peak ABISUP pressures (kPa).

Buck	Test Number	Left ABISUP	Right ABISUP
V1	1	118	191
	2	114	161
	3	127	158
V6	1	68	70
	2	76	77
	4	132	116
V10	1	224	221
	2	254	187
	3	383	375
V13	1	239	189
	2	352	294
	3	250	248
V14	1	80	93
	2	82	100
	3	118	122
	4	127	126
V15	1*	N/A	N/A
	2	90	280
	3	100	292
	4	366	326
V19	1	100	167
	2	106	220
	3	420	405
	4	428	449

Belt Loads

Belt loads were measured at the outboard and inboard shoulder belt and the outboard lap belt. Plots of belt loads for each ATD are provided in Appendix F: ATD Belt Loads. For the current study, the inboard shoulder (buckle, or inboard lap) and outboard lap belt (anchor) loads are the most relevant, but the peak loads at all locations for all ATD tests are provided in Table 11.

Table 11. Peak belt loads for the ATD tests

Test ID	HIII Outboard Shoulder	HIII Inboard Shoulder	HIII Outboard Lap	THOR Outboard Shoulder	THOR Inboard Shoulder	THOR Outboard Lap
V1-1	3796	3061	4148	3295	2906	3927
V1-2	3808	2895	4418	3446	3070	3928
V1-3	n/a	5346	5783	6897	5432	6466
V6-1	6497	5006	5839	5170	3917	5280
V6-2	6416	5098	5584	5010	3610	5371
V6-4	9477	7109	7226	8880	6129	7446
V10-1	7431	5266	6885	5956	4864	5375
V10-2	7631	5922	8047	5996	5025	5054
V10-3	10329	7746	10415	8934	6454	7770
V13-1	6613	4705	6827	5192	3959	5523
V13-2	9509	6900	9715	8908	5975	n/a
V13-3	6710	4857	6980	4987	4208	4213
V14-1	5080	3874	4632	4371	3446	5213
V14-2	5242	3840	4065	4192	3458	4277
V14-3	6318	4787	6139	n/a	4793	n/a
V14-4	5845	4986	5551	6368	4571	6767
V15-1	7524	6057	7723	5325	4253	6921
V15-2	7923	6559	7970	5423	4209	5598
V15-3	8302	6713	8496	5587	3994	5631
V15-4	11255	10068	14338	9454	6853	6559
V19-1	4072	3424	5973	3735	3388	5982
V19-2	3915	3658	6173	4068	3411	5723
V19-3	6143	5395	8880	4749	4629	6639
V19-4	7213	5328	8202	4689	4455	6505

Pelvis Kinematics

The ATDs were both instrumented with 3-axis accelerometer blocks in the pelvis. Resultant accelerations for the HIII and THOR are provided in Appendix G: Resultant Pelvis Acceleration. One NCAP85 test from each of the four vehicles selected for PMHS testing was chosen for further component-wise analysis of THOR pelvis kinematics for comparison with the PMHS: tests V13-2, V14-4, V15-4, and V19-4. X-direction and Z-direction pelvis accelerations are provided for both the HIII and THOR (Appendix H: Matched NCAP85 Pelvis X and Z-Direction Acceleration). Because only the THOR underwent submarining and no rotational pelvis instrumentation was provided for either ATD, Vicon data were used to calculate the pelvis angle of the THOR for four tests for comparison to the PMHS data. The time histories

of pelvis angle rotation from its initial position are provided in Figure 21. The lap belt angle was tracked for these four tests and are plotted with total pelvis angle in Figure 22. The relative belt angle was calculated for each test and are provided in Figure 23.

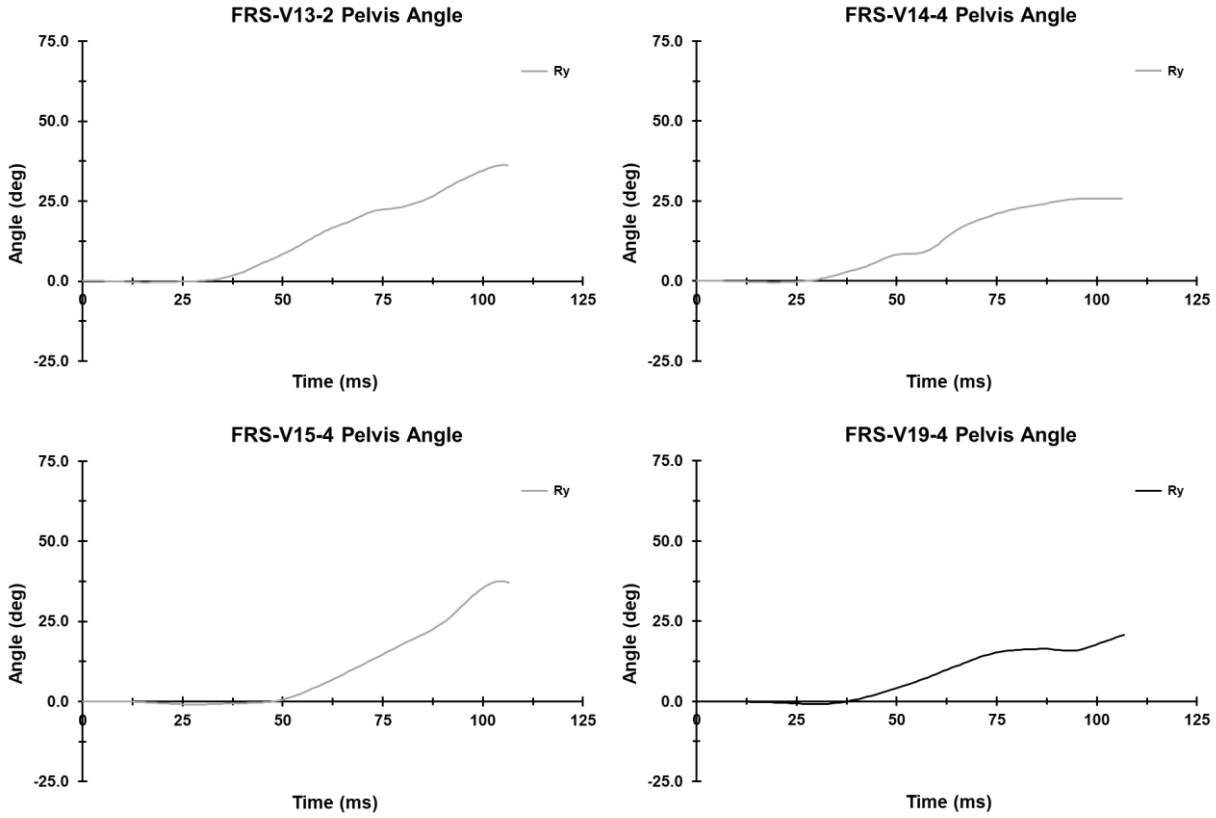

Figure 21. Pelvis rotation angle (degrees) of the THOR in four select tests.

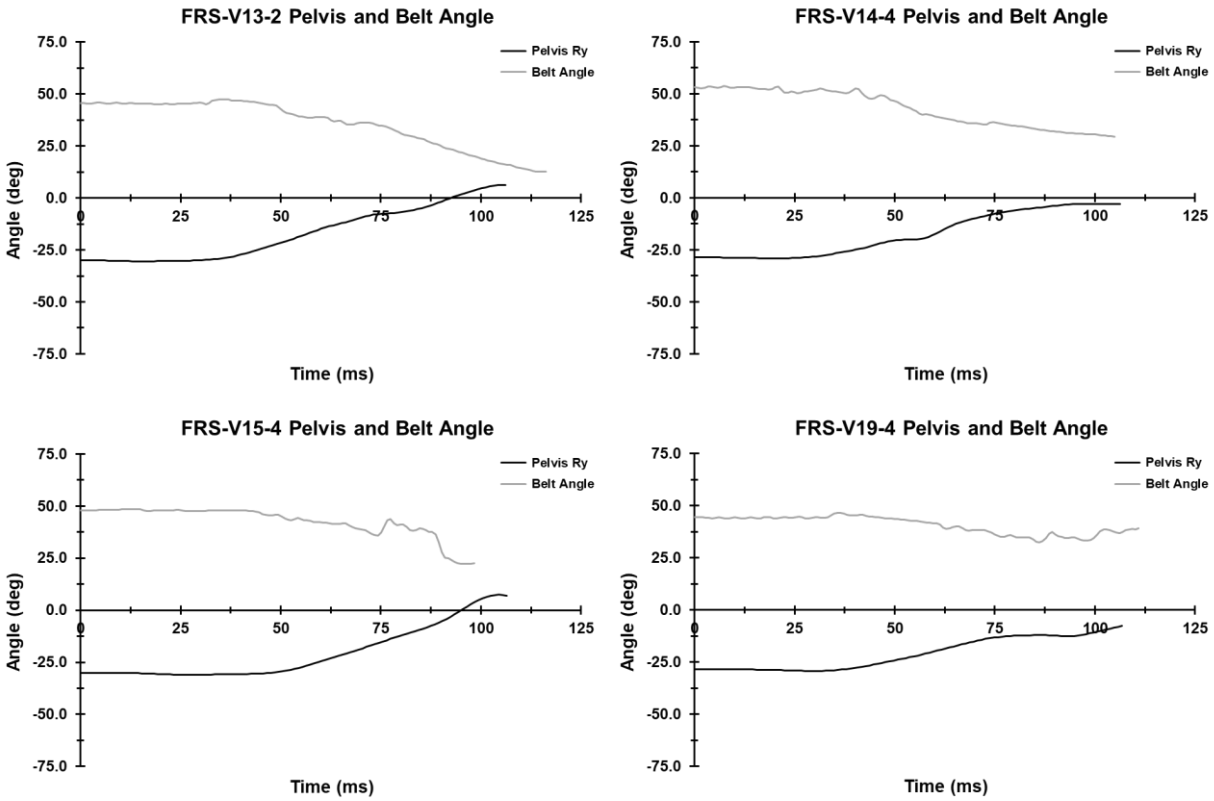

Figure 22. Pelvis and lap belt angles for THOR in four NCAP85 tests.

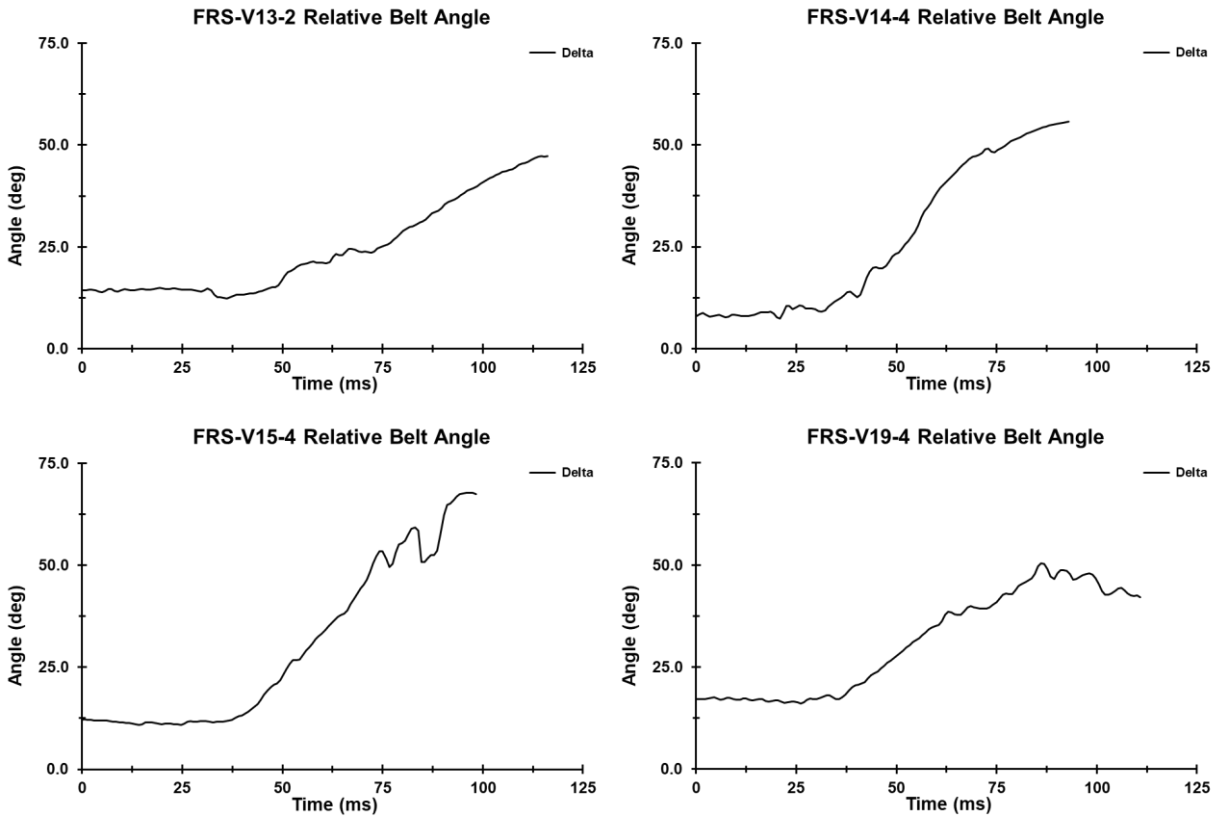

Figure 23. Relative belt angles for the THOR.

Submarining

The Hybrid III did not submarine in any test. As previously stated, this determination could only be made by post-test photographs, high-speed video, and seat belt loads; however, these data clearly show that the Hybrid III did not submarine. An exemplar set of photographs, video frames, and seat belt loading plots are provided in Figure 24.

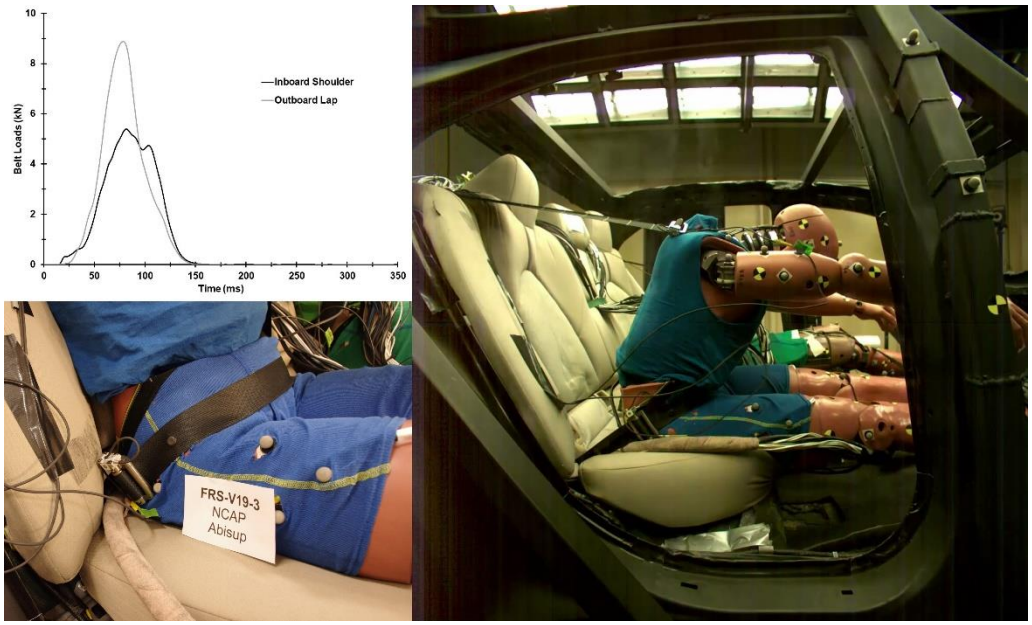

Figure 24. Hybrid III inboard shoulder (buckle) and outboard lap belt (anchor) loads (top left), post-test photograph (bottom left), and frame from high-speed video (right) for Test V19-3.

The THOR submarined in 16 of the 24 tests, including all three repeated tests. Submarining results by vehicle, restraint type, and pulse type can be found in Table 12. The THOR did not submarine during any test in two vehicles (V6 and V14), submarined in every test for four vehicles (V10, V13, V15, and V19), and submarined only in the low energy tests for vehicle V1. The THOR underwent submarining in three vehicles with conventional restraints (n=4) and two vehicles with advanced restraints (n=3). The detailed results of the assessment of the post-test photographs, high-speed videos, ABISUP abdomen pressures, ASIS loads, and seat belt loads is in Appendix I: THOR Submarining Table. Image sequences of time of submarining and maximum forward excursion are in Appendix J: Image Sequences from Matched NCAP85 Tests.

Table 12. THOR Submarining results. The test with the THOR standard abdomen is denoted (α) and the instances of pretensioner-initiated belt lift are denoted (#).

Buck	Restraint Type	Test Number	Pulse	Submarining
V1	Advanced	1	Generic	Minor[#]
		2	Scaled	Minor[#]
		3	NCAP85	None
V6	Conventional	1	Generic	None
		2	Scaled	None
		4	NCAP85	None
V10	Conventional	1	Generic	Moderate
		2	Scaled	Moderate
		3	NCAP85	Severe
V13	Conventional	1	Scaled	Moderate
		2	NCAP85	Severe
		3	Generic	Moderate
V14	Advanced	1	Generic	None
		2	Scaled	None
		3	NCAP85	None
		4	NCAP85	None
V15	Conventional	1[α]	Generic	Minor
		2	Generic	Minor
		3	Scaled	Minor
		4	NCAP85	Moderate
V19	Advanced	1	Generic	Minor[#]
		2	Scaled	Minor[#]
		3	NCAP85	Moderate
		4	NCAP85	Moderate

Post-test photographs are the least reliable for identifying submarining, as the final position of the ATD and/or the seat belt is not necessarily representative of the positions during the loading phase—when injurious submarining would occur. If submarining is not identifiable by photographs and if the submarining information from the seat belt loads is inconclusive, ASIS load and moment traces, and high-speed video can give indications of submarining. The most reliable measurement for identifying submarining was ABISUP pressure, and in most cases, ABISUP pressure traces provided clear indications of submarining. In two tests, the ABISUP pressures provided inconclusive evidence of submarining so other signals were used as a confirmation of submarining.

Some of the minor submarining cases were deemed to be initiated by pretensioner-initiated belt lift. These specific tests are identified in Table 12. These cases had the typical submarining signs in the ASIS load and moment curves (unilateral) accompanied by a slight rise in the ipsilateral ABISUP pressure. The difference primarily being the absence of the characteristic rate of pressure increase that typically occurs with instances of submarining caused by direct loading of the lap belt on the abdomen. Figure 25 contains ABISUP and ASIS loading traces from two tests in which THOR underwent minor submarining: one under typical conditions and one with pretensioner-initiated belt lift.

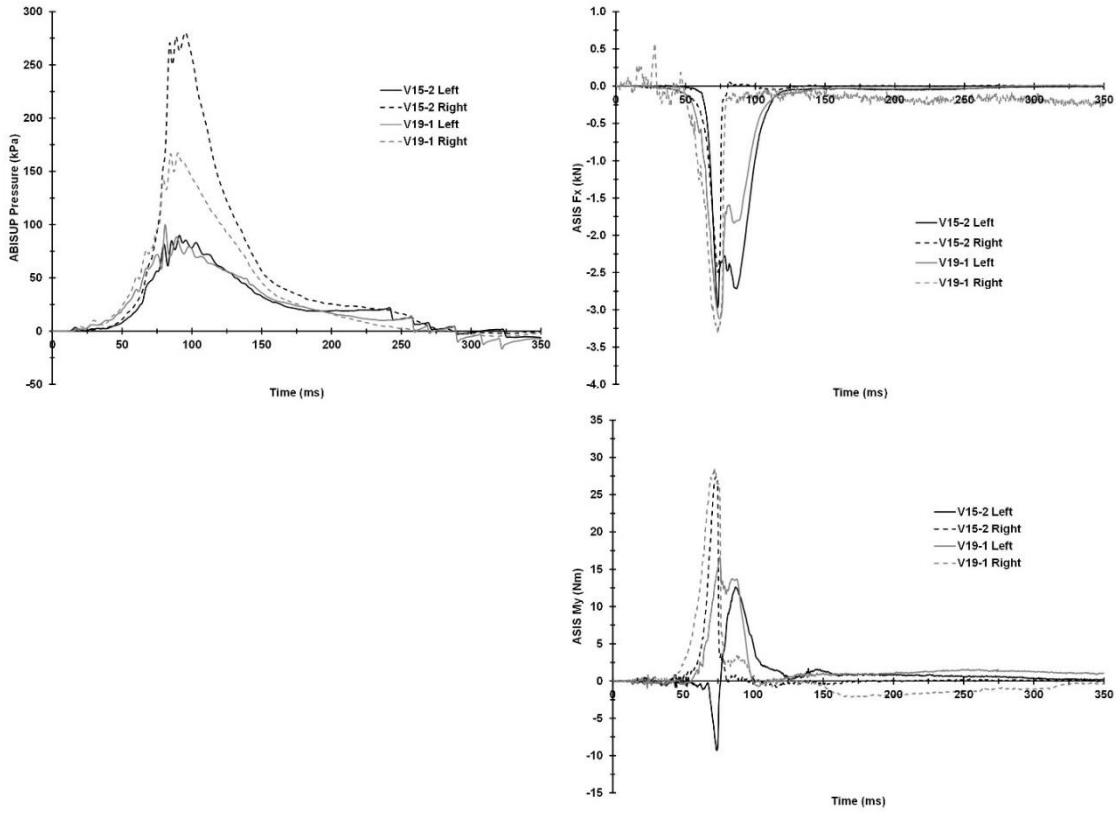

Figure 25. ABISUP (Left) and ASIS (Right) plots from Tests V15-2 and V19-1, Generic tests in which the THOR underwent minor submarining. V19-1 involved pretensioner-initiated belt lift.

For an example of a minor submarining case without pretensioner-initiated belt lift, post-test photographs and video frames from Test V15-3 are provided in Figure 26 and ASIS load and moment, ABISUP pressure, and lap belt load cell data traces are provided in Figure 27. The right ASIS X-axis force (Fx) has a similar rate of loading to the left ASIS load cell (Figure 27, top left). However, near -2.5 kN, there is a sudden drop in force indicating the belt slipped off of the pelvis. In contrast, loading of the left ASIS continues before slowly unloading around 87 ms, indicating that the belt remained in contact with the ASIS throughout the test. The Y-axis ASIS moments (My, Figure 27, bottom left) also provide indication of belt slip on the right pelvis, but not the left. In the case of ASIS My, the right side demonstrates the belt begins sliding up the

pelvis at a greater rate than the moment on the left pelvis, before it leaves the pelvis and moment drops instantaneously. The left ASIS moment suggests the belt remained in contact with the left anterior pelvis for the duration of the unloading phase. The ABISUP pressure on the right side is 300 kPa; three times that of the left side (Figure 27, top right). Finally, the lap belt loads provide inconclusive information about belt slip as the inboard side maintains its smooth bell-shaped loading curve. However, the drop in belt tension at the outboard side may indicate a brief unloading of the belt as the inboard lap belt slipped off of the ASIS.

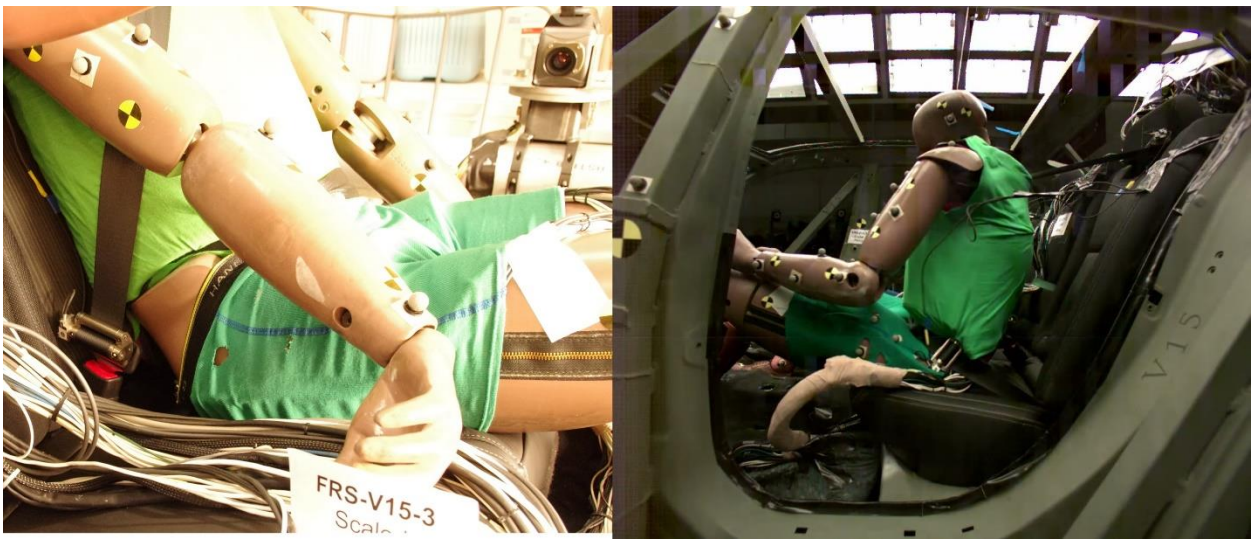

Figure 26. Post-test photograph (left) and high-speed video frame of THOR during Test V15-3.

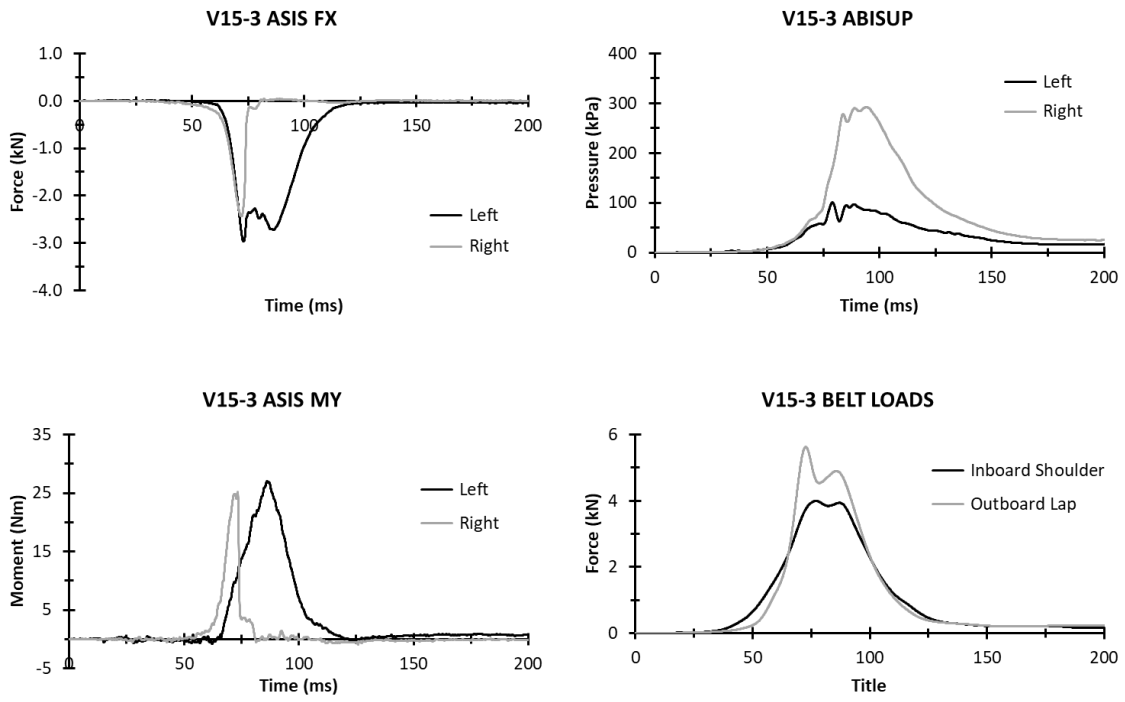

Figure 27. THOR data channels for submarining assessment in Test V15-3. In this test, minor submarining occurred on the inboard side of the pelvis.

In a severe submarining case that occurred during Test V10-3, post-test photographs and video frames (Figure 28) show obvious signs of submarining as the THOR completely departed the seat. Left and right ASIS Fx recorded nearly identical loading (Figure 29, top left), while the right ASIS experienced slightly higher loads before the sudden drop in force. The ASIS My traces (Figure 29, bottom left) are both of short duration including the characteristic drop in loading. Both right and left ABISUP pressures reached nearly 400 kPa (Figure 29, top right) and included rapid increases in pressure followed by a long duration unloading phase. Seat belt loads (Figure 29, bottom right) provide an indication of belt slip near 60 ms followed by an increased loading profile while the belt interacted with the abdomen. Signs of belt slip on both sides of the pelvis indicate bilateral encroachment of the lap belt, and high, bilateral ABISUP pressures along with the departure of the pelvis from the seat determined that this submarining case was severe.

Figure 28. Post-test photograph (left) and high-speed video frame of THOR during Test V10-3.

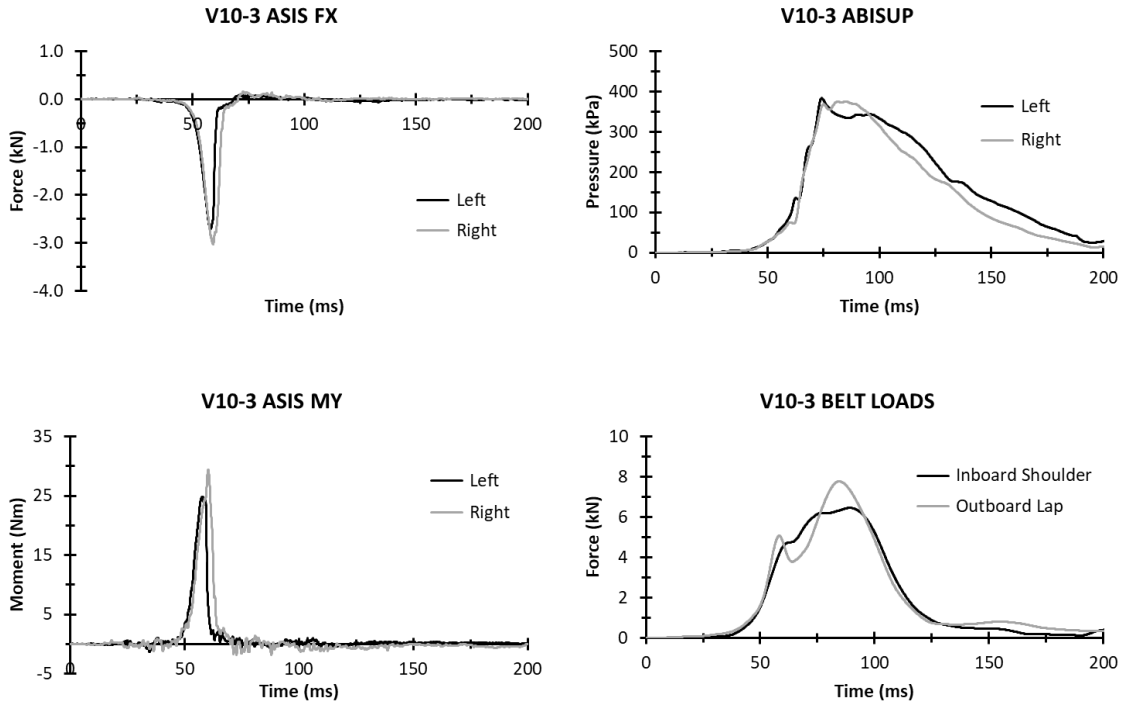

Figure 29. THOR data channels for submarining assessment for Test V10-3. In this tests, severe submarining occurred.

Test V19-4 is a test in which THOR underwent moderate submarining. The photographs and video frames in Figure 30 show the belt loading the abdomen and that the THOR (specifically the pelvis) maintained

position on the vehicle seat. The ASIS loads and moments (Figure 31, left) suggest that the submarining occurred on the right side before the left side. The left-side loading curve has an initial peak that matches that of the right followed by a slight decrease before a secondary loading before the final drop in force. The right-side moment had a similar magnitude to submarining cases in other tests, but the left moment was produced 20 ms after the right and had reached twice the magnitude before the belt finally slipped off of the left ASIS. The same delay is demonstrated in the ABISUP pressures (Figure 31, top left) although peak pressures were similar, reaching approximately 450 kPa. Finally, the outboard lap belt load has an initial peak (at nearly double the magnitude) at the same time as the inboard shoulder before it continues to load the pelvis to a peak force of 4.6 kN. After the second peak, tension drops until the outboard lap loads the abdomen. With bilateral encroachment of the lap belt on the abdomen and ABISUP pressures greater than in Test V10-3 (the severe case), there might be an indication that this was a severe submarining event. However, the THOR pelvis did not depart the seat, leading to the determination that this was a moderate submarining event per the study definitions.

Figure 30. Post-test photograph (left) and high-speed video frame of THOR during Test V19-4.

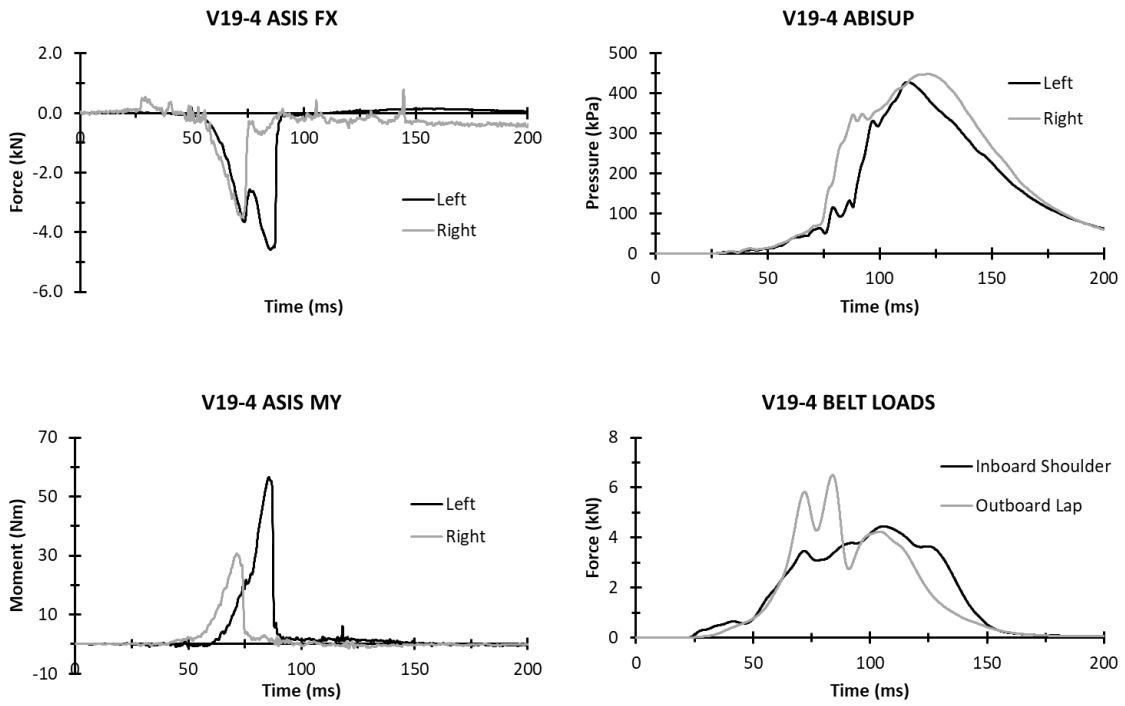

Figure 31. THOR data plots for submarining assessment for Test V19-4. In this test, moderate submarining occurred.

Submarining Timing

Submarining timing was desired for select NCAP85 tests for matched comparison to the PMHS tests. As with the pelvis kinematics, tests V13-2, V14-4, V15-4, and V19-4 are included. Belt loads, ABISUP pressure, ASIS Fx, belt angle, and high-speed video were used to estimate the time of submarining. The relative belt angle at the time of submarining for each test is provided in Table 14.

Table 13. Submarining timing derived for each data channel of the THOR for four NCAP85 tests selected for comparison to PMHS testing.

Test ID	Submarining Time	Belt Loads	Pressure	ASIS Fx	Video	Belt Angle
V13-2	62.39	60.45	63.05	60.55	66.15	61.75
V14-4	-	-	-	-	-	-
V15-4	75.35	75.35	76.95	74.75	75.45	74.25
V19-4	86.3	85.2	88.6	84.9	86.7	86.1

Table 14. THOR belt and pelvis angles at the time of submarining.

Test ID	Submarining Time (ms)	Pelvis Angle (deg)	Belt Angle (deg)	Relative Belt Angle (deg)
V13-2	62.39	-13.4	37.5	39.1
V14-4	-	-	-	-
V15-4	75.35	-14.9	37.1	37.4
V19-4	86.3	-12.0	32.3	45.6

Lower Spine Loading

Peak X-direction force (Fx), Z-direction force (Fz), and Y-axis moment (My) at the lumbar (Hybrid III) and T12 (THOR) load cells during the first 200 ms of each test are represented in Figure 32. Lumbar loading in the Hybrid III and T12 loading in the THOR both varied between vehicles and pulse types, and, in the THOR, by submarining condition. Time histories of lumbar and T12 Fx, Fz, and My are provided in Appendix K: ATD Spine Loads.

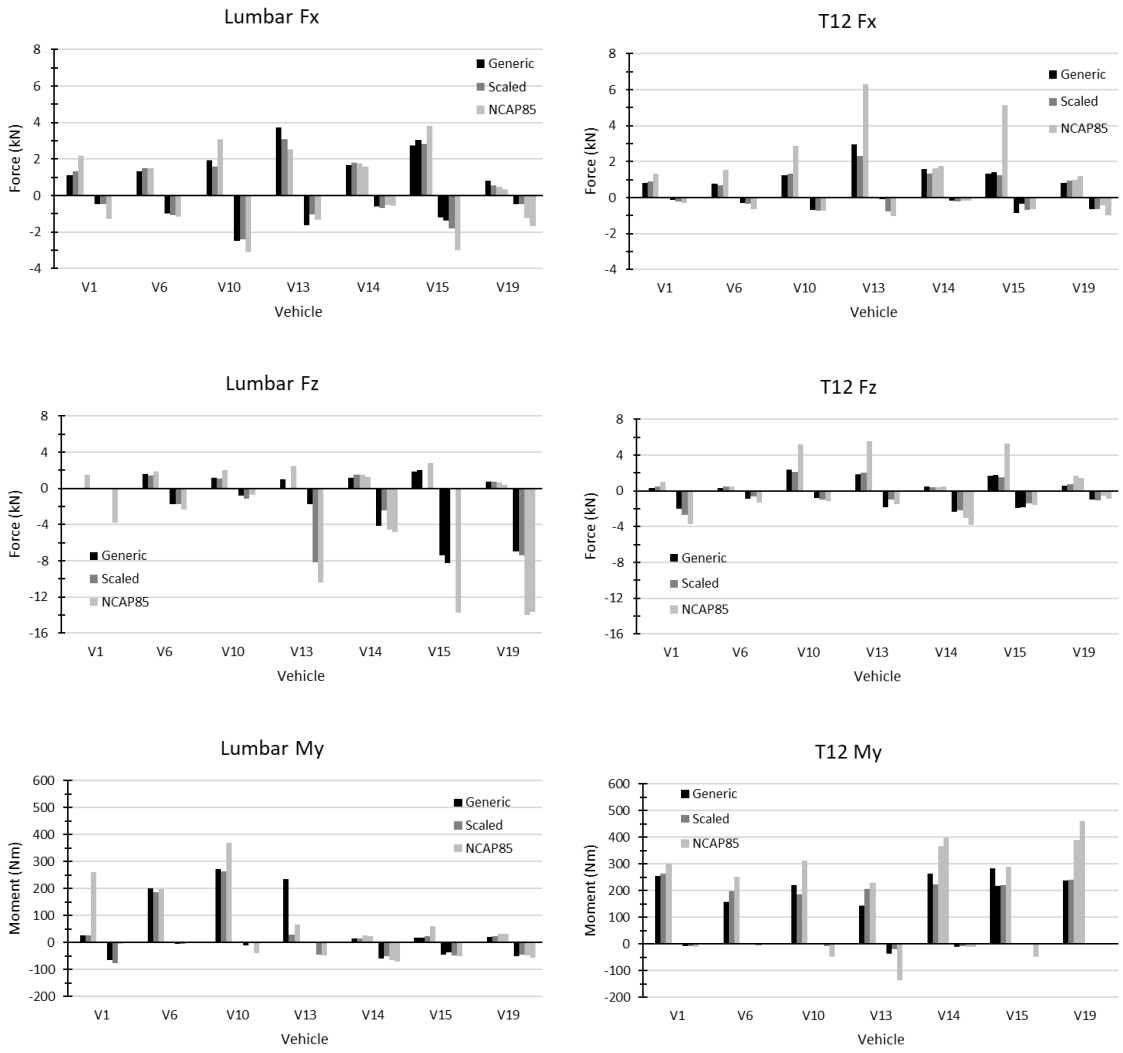

Figure 32. Peak values for lower spine loading for the Hybrid III (lumbar, left) and the THOR (T12, right).

PMHS Sled Testing

Eight sled tests were conducted in four vehicle bucks in the NCAP85 crash condition. Eight PMHS were obtained and instrumented for testing; each was tested once positioned in the rear left outboard seating position.

Sled Acceleration

Sled accelerations for all PMHS tests can be found in Appendix B: Sled Accelerations. All eight sled tests were run under the NCAP85 crash condition, in which each vehicle-specific pulse had a target ΔV of 56 kph. The average ΔV for all eight tests is 52.4 (+/-2.01) kph. The ΔV and peak acceleration for each test can be found in Table 15.

Table 15. Peak acceleration (g) and V (kph) for each test in the PMHS series.

Buck ID	Test Number	PMHS ID	Pulse	Peak Acceleration (g)	ΔV (kph)
V13	4	SM129	NCAP85	-31.0	55.6
	5	SM155	NCAP85	-31.7	55.0
V14	5	SM156	NCAP85	-27.1	49.4
	6	SM157	NCAP85	-26.9	52.1
V15	5	SM152	NCAP85	-33.3	51.9
	6	SM153	NCAP85	-32.8	50.4
V19	5	SM154	NCAP85	-33.2	52.8
	6	SM95	NCAP85	-33.3	51.8

Pelvis Kinematics

Pelvis kinematics were measured on the sacrum and the left iliac wing. Depending on the level of fusion between the sacrum and the left and right pelvic bones, there might be relative motion between the bones and therefore differences in the kinematics measured in the two locations. When there was an issue with data obtained from the pelvis mount, data from the sacrum were substituted. The data of interest for the pelvis are X and Z-direction acceleration, and resultant acceleration. Time histories for these data are presented in Figure 33-Figure 36 below. Time histories for Y-axis angular speed are presented in Figure 37-Figure 40. Angular displacement of the pelvis about the Y axis is subsequently examined within the context of lap belt angle.

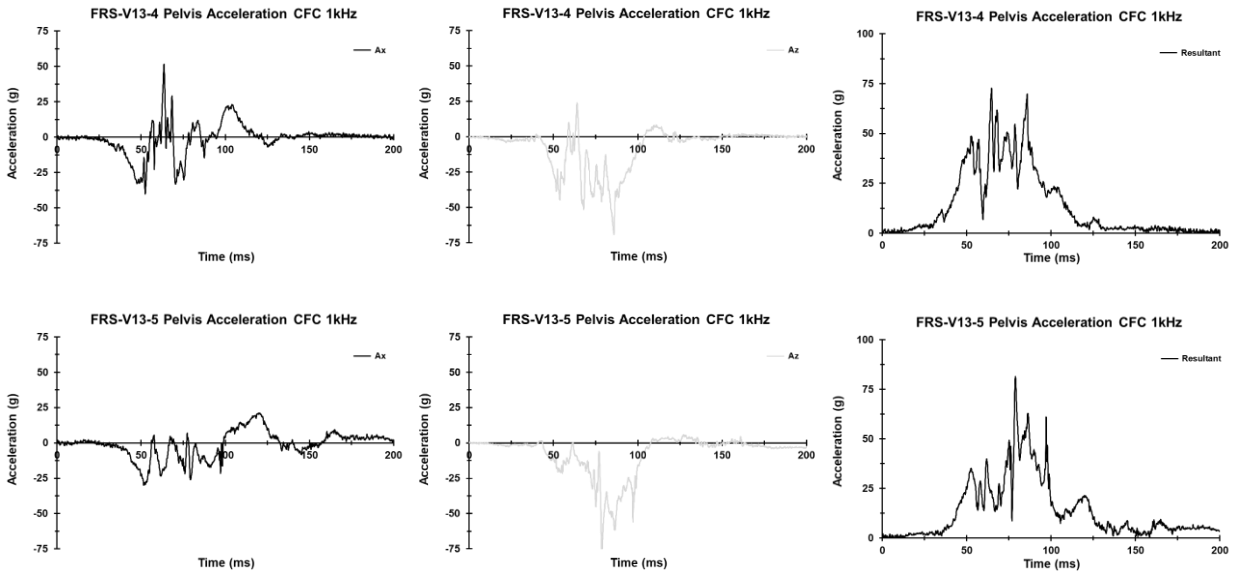

Figure 33. PMHS X and Z-direction pelvis acceleration and resultant pelvis acceleration for vehicle V13 tests

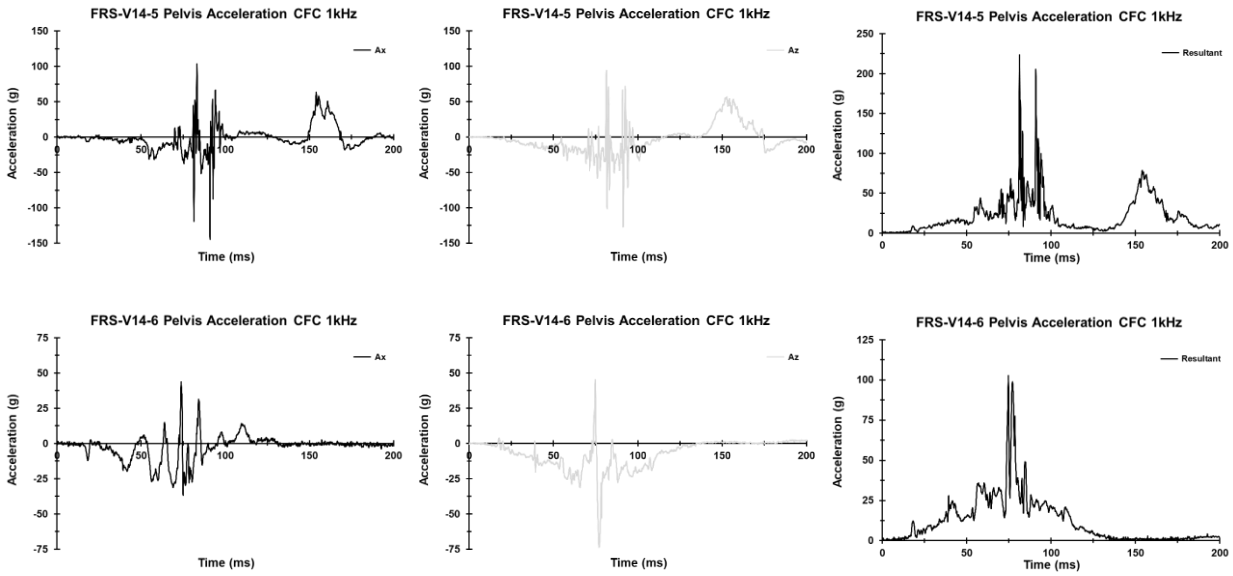

Figure 34. PMHS X and Z-direction pelvis acceleration and resultant pelvis acceleration for vehicle V14 tests

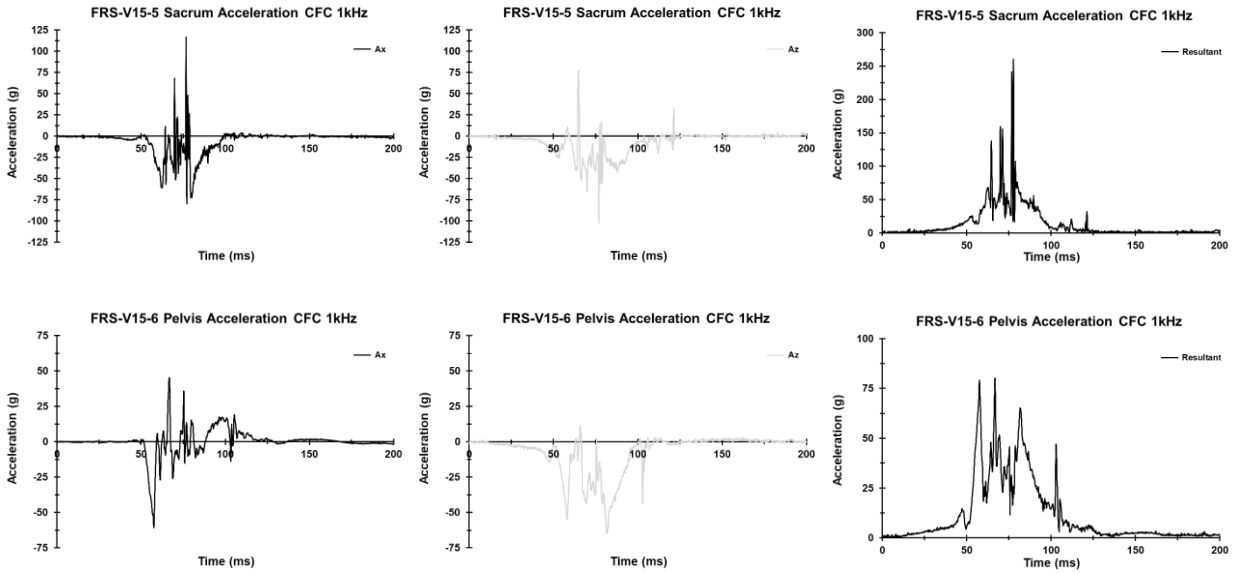

Figure 35. PMHS X and Z-direction pelvis acceleration and resultant pelvis acceleration for vehicle V15 tests

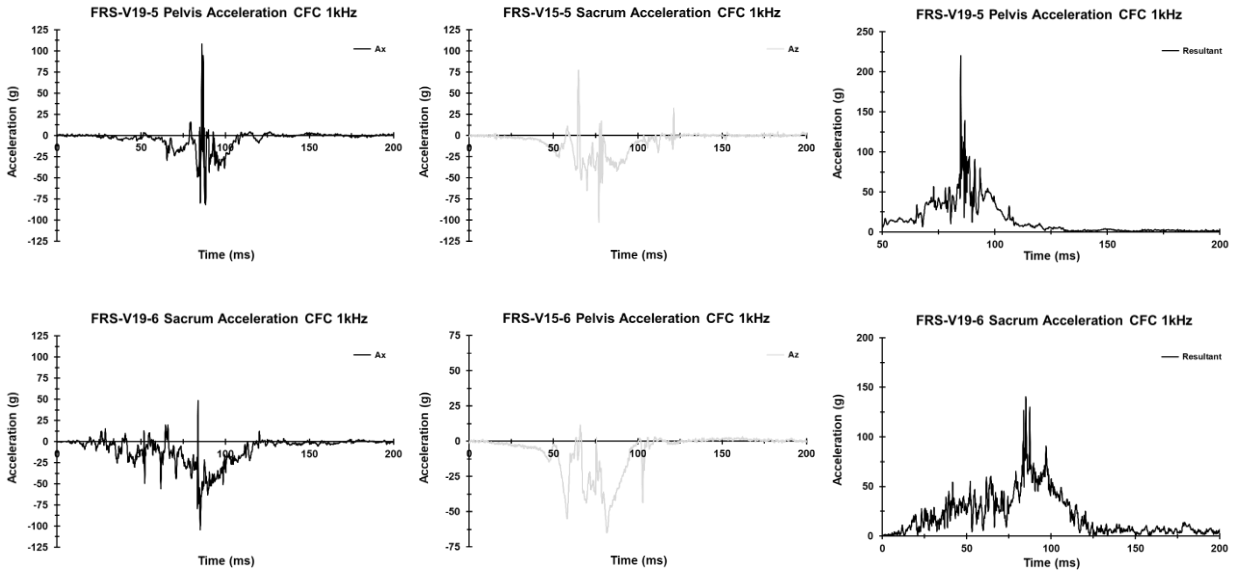

Figure 36 PMHS X and Z-direction pelvis acceleration and resultant pelvis acceleration for vehicle V19 tests

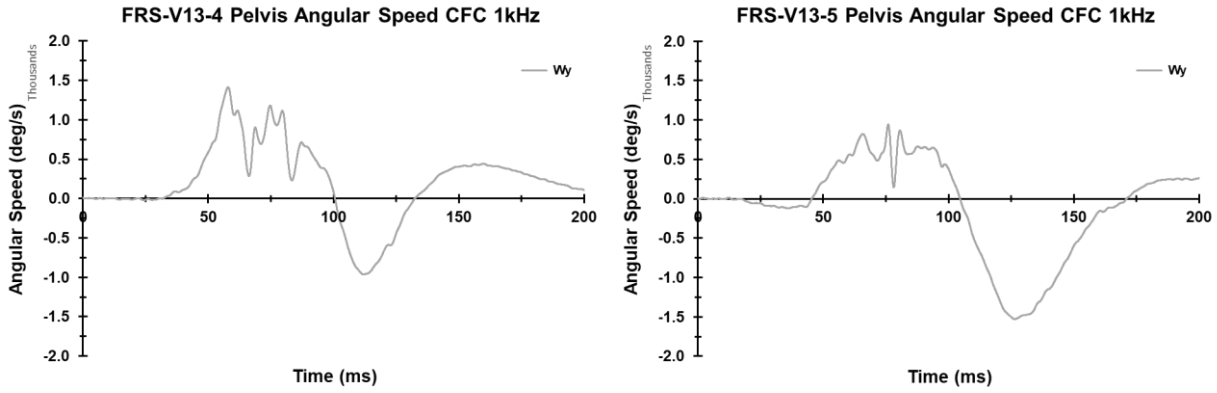

Figure 37. PMHS Y-axis angular speed for vehicle V13 tests

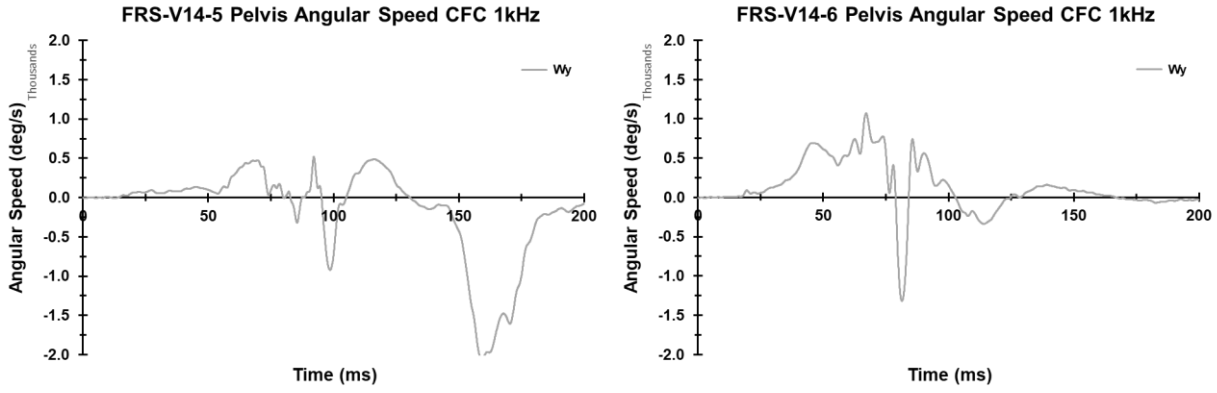

Figure 38. PMHS Y-axis angular speed for vehicle V14 tests

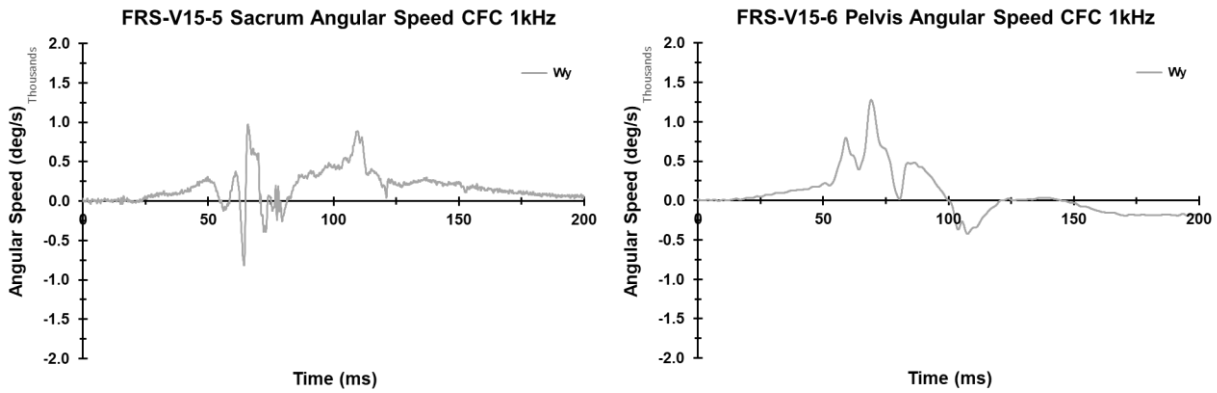

Figure 39. PMHS Y-axis angular speed for vehicle V15 tests

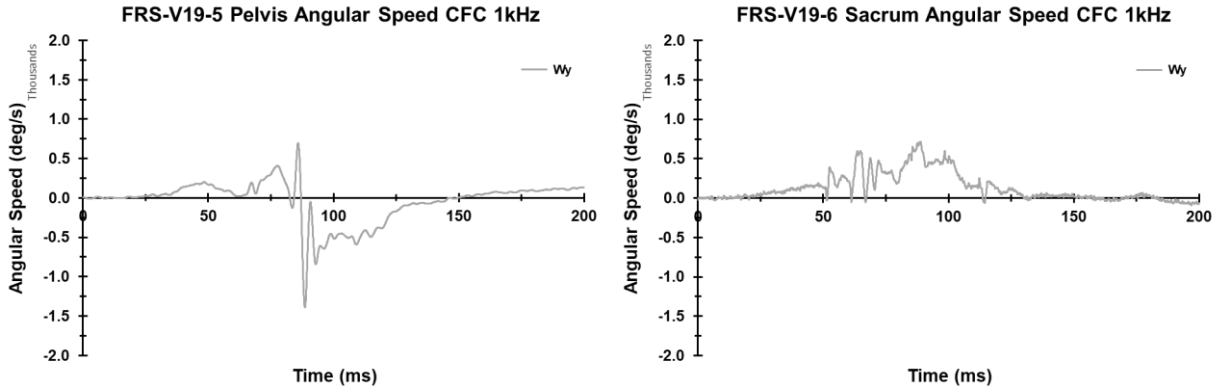

Figure 40. PMHS Y-axis angular speed for vehicle V19 tests

Plots of the pelvis rotation, pelvis angle and lap belt angle, and relative belt angle for all PMHS tests are provided in Figure 41, Figure 42, and Figure 43 (respectively).

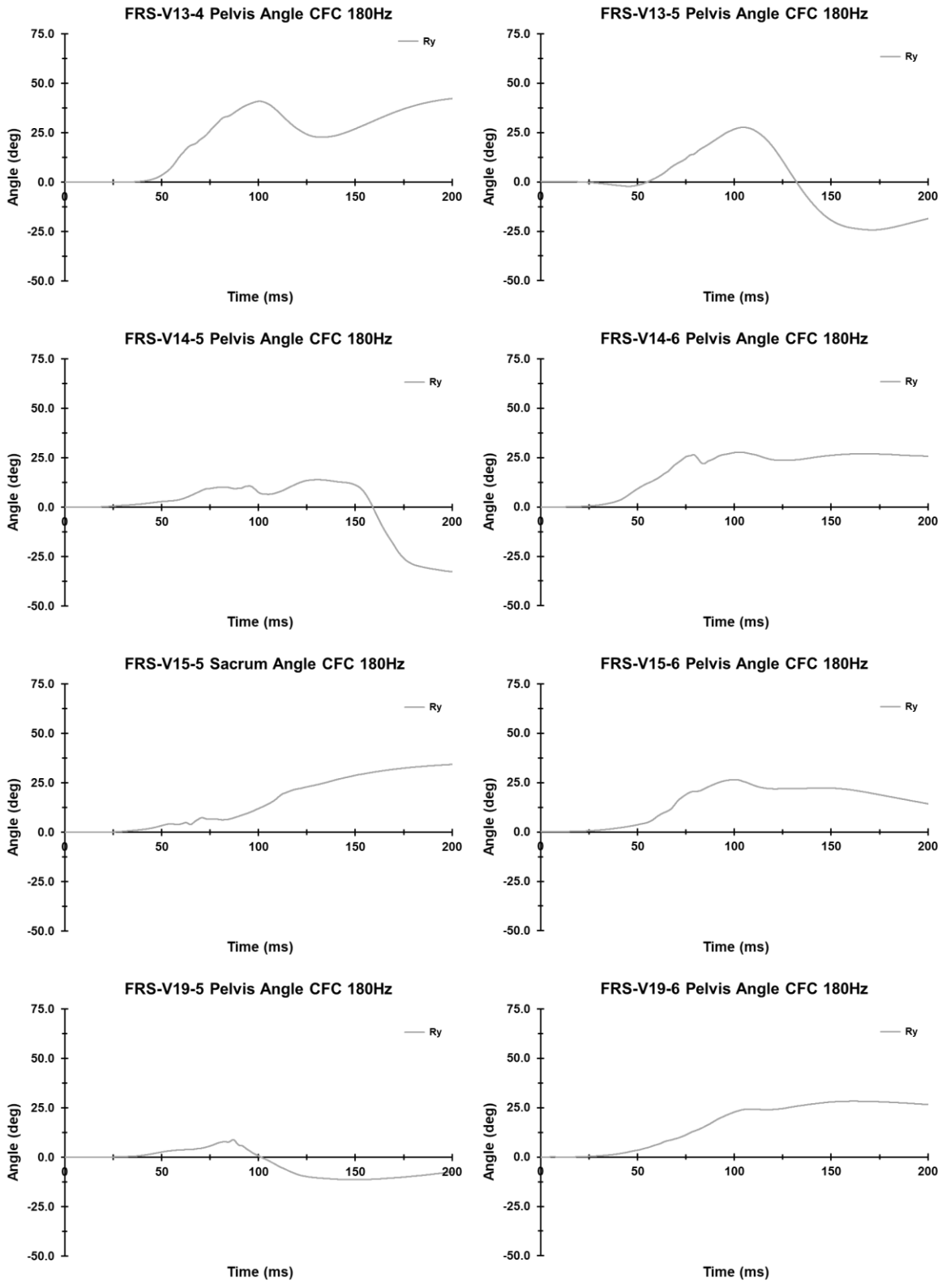

Figure 41. Pelvis rotation angle (degrees) of the PMHS

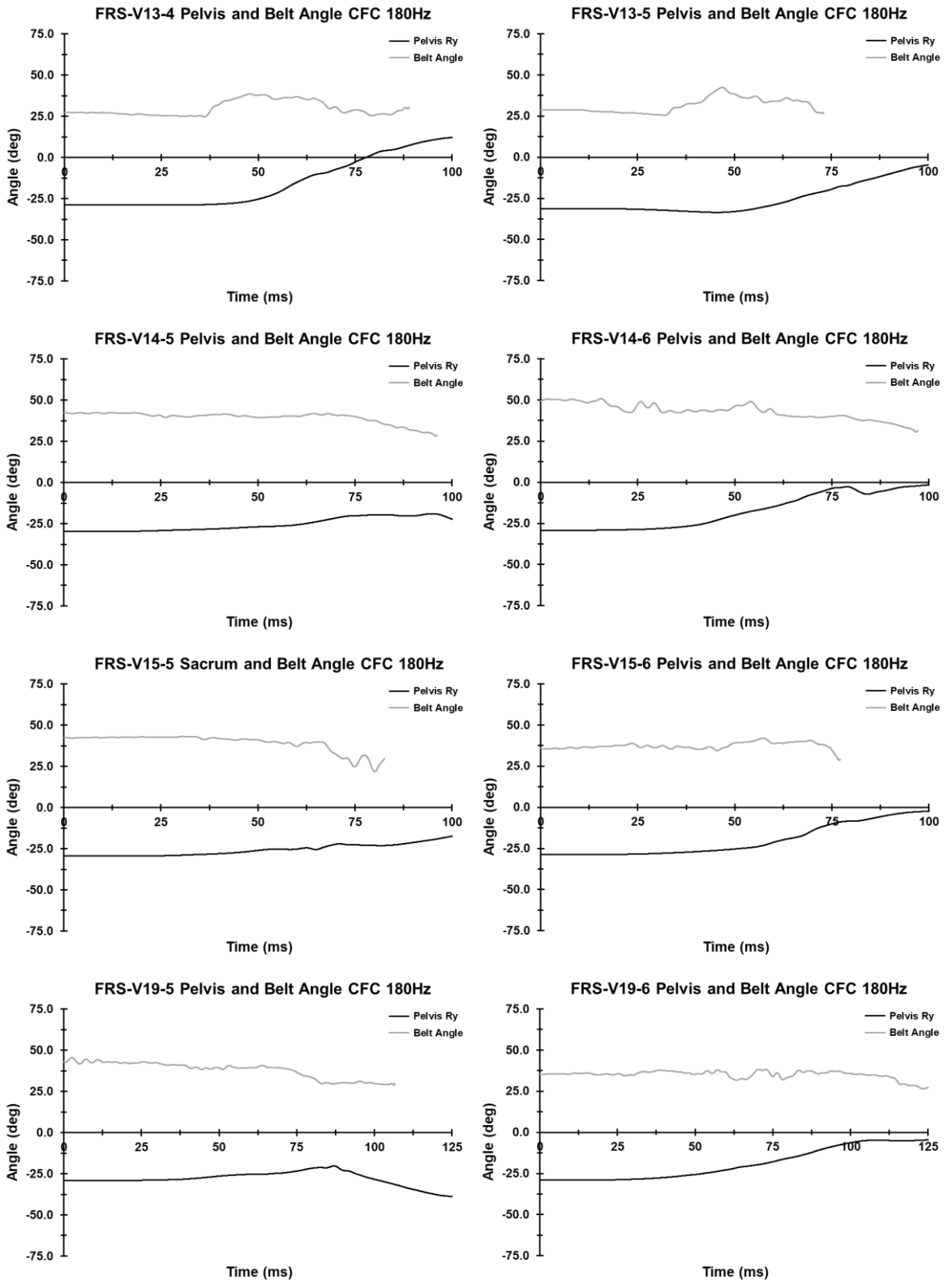

Figure 42. Pelvis and lap belt angles for the PMHS

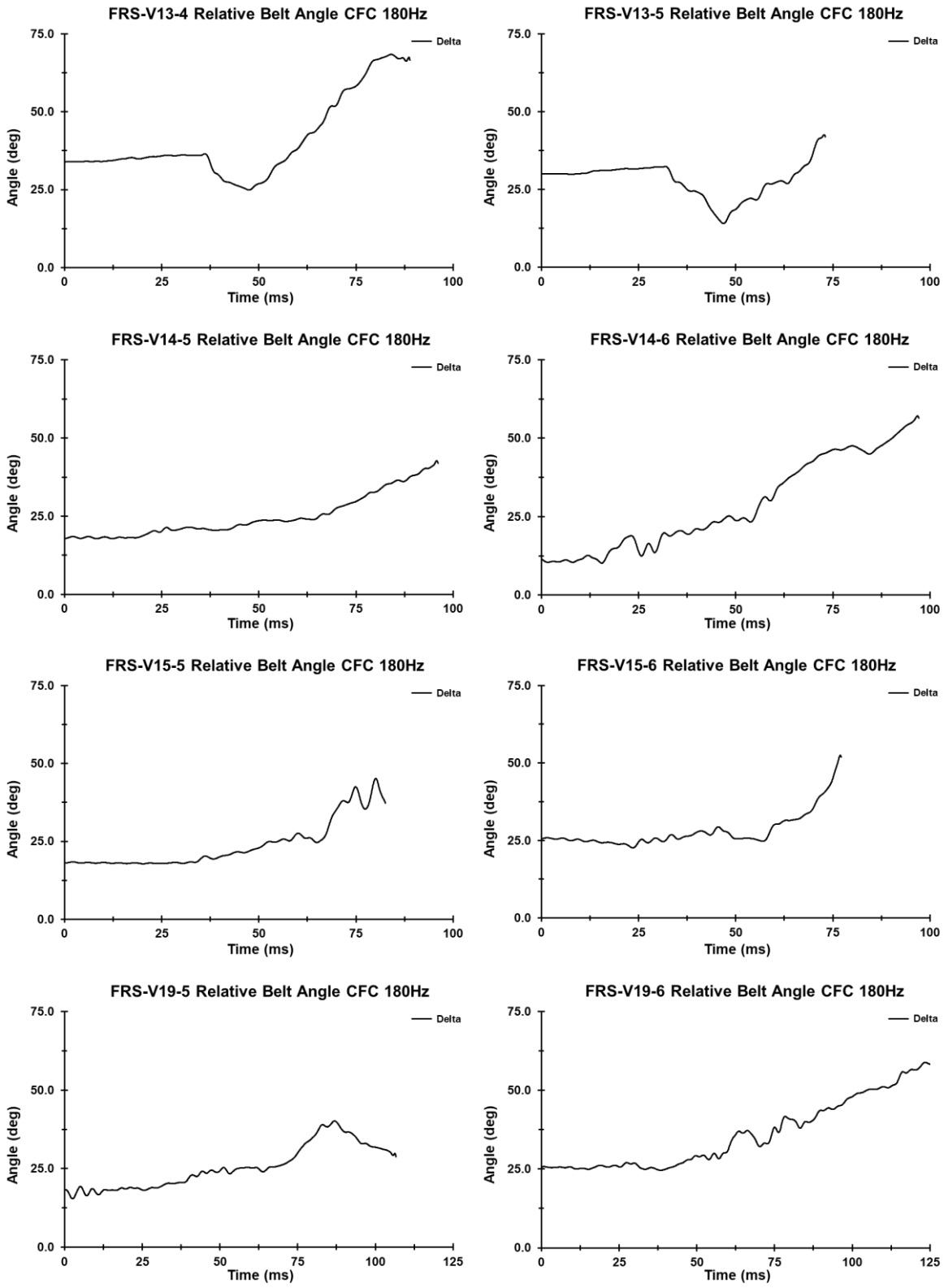

Figure 43. Relative belt angles for the PMHS

Abdominal Pressures

Abdominal pressure was measured in four locations, right and left ASIS (subcutaneous), aorta (level of L1/L2), and vena cava (near the liver). Peak abdominal pressures are provided in Table 16. Plots of abdominal pressures can be found in Appendix L: PMHS Abdominal Pressures.

Table 16. Peak abdominal pressures for PMHS tests (kPa).

Buck	Test Number	Vena Cava	Aorta	Left ASIS	Right ASIS
V13	4	100	149	127	227
	5	134	126	635	286
V14	5	119	111	74	92
	6	127	136	156	139
V15	5	120	102	220	254
	6	-	149	217	434
V19	5	107	99	106	136
	6	127	118	229	423

Belt Loads

Seat belt loads were measured at the outboard shoulder (retractor), inboard shoulder (buckle), and outboard lap (anchor) positions. All belt loads are provided in Appendix M: PMHS Belt Loads. Peak belt loads (N) are provided in Table 17.

Table 17. Peak belt loads (N) for the PMHS tests.

Buck	Test Number	PMHS ID	Outboard Shoulder (Retractor)	Inboard Shoulder (Buckle)	Outboard Lap (Anchor)
V13	4	SM129	7372	5243	5793
	5	SM155	9841	6331	8487
V14	5	SM156	6125	4846	7408
	6	SM157	6036	4652	5193
V15	5	SM152	10887	8843	8637
	6	SM153	8625	6405	7563
V19	5	SM154	5636	5247	7608
	6	SM95	4217	4880	5539

Submarining

Belt loads, abdominal pressures, high-speed videos, post-test photographs, and resultant pelvis acceleration were all used to assess submarining of the PMHS. Three PMHS submarined to some extent during these tests, in two of the four vehicle bucks. The submarining results are included in Table 18. Both PMHS

submarined in vehicle V13, and one PMHS (SM157) submarined in vehicle V14 (V14-6). The primary difference in the determination of severity in these tests is that the pelvis leaves the seat cushion in the severe submarining cases and the remains on the seat in the moderate case. Image sequences from the PMHS tests at time of submarining and maximum forward excursion are in Appendix J: Image Sequences from Matched NCAP85 Tests.

Table 18. Submarining results from the PMHS tests

Buck	Restraint Type	Test Number	PMHS Number	PMHS Submarining
V13	Conventional	4	SM129	Severe
		5	SM155	Severe
V14	Advanced	5	SM156	None
		6	SM157	Moderate
V15	Conventional	5	SM152	None
		6	SM153	None
V19	Advanced	5	SM154	None
		6	SM095	None

Abdominal pressures, belt loads (lap belt), and high-speed video were used to identify submarining. Figure 44 provides this information for test V13-4, along with a demarcation of when submarining occurred where there is a local drop in seat belt loads, increase in abdominal pressures, and a spike in the resultant acceleration at the same time. The submarining plots for tests V13-5 and V14-6 are provided in Figure 45 and Figure 46, respectively.

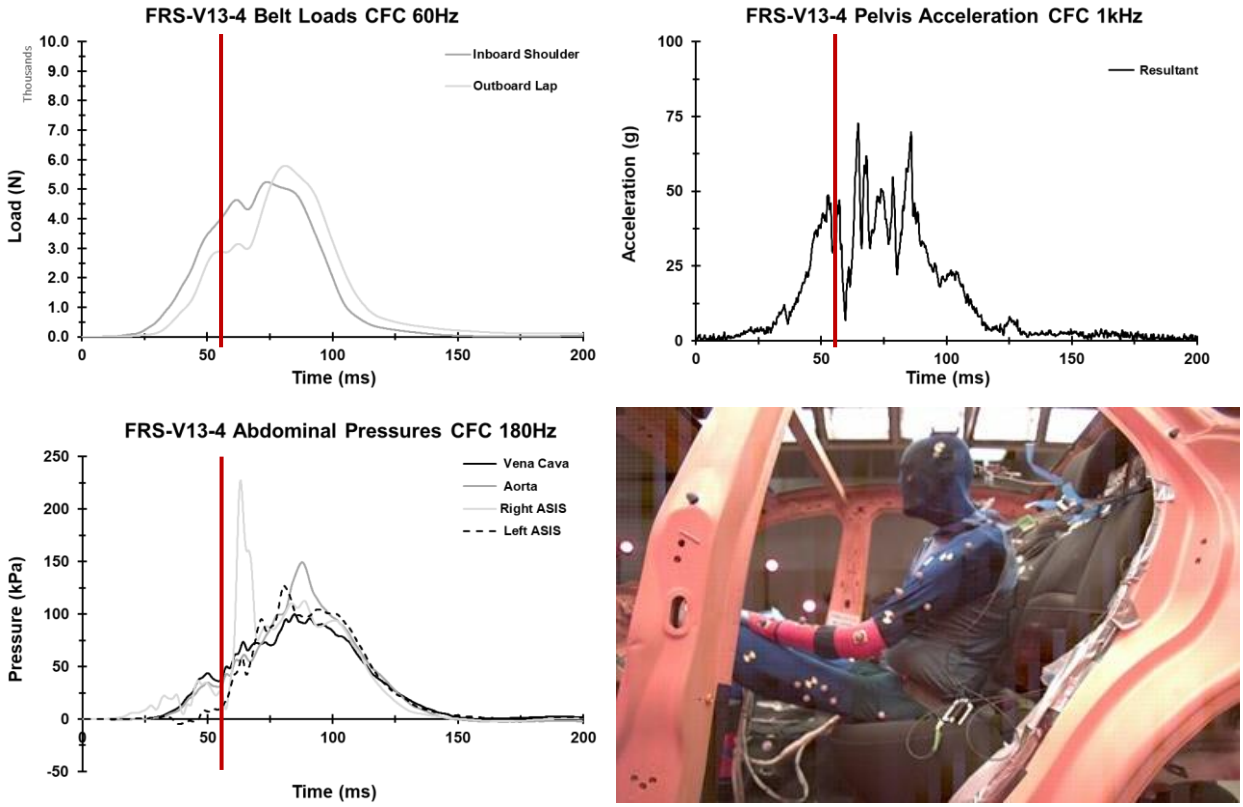

Figure 44. Submarining assessment plots for test V13-4 (SM129) and high-speed video frame at the time of submarining.

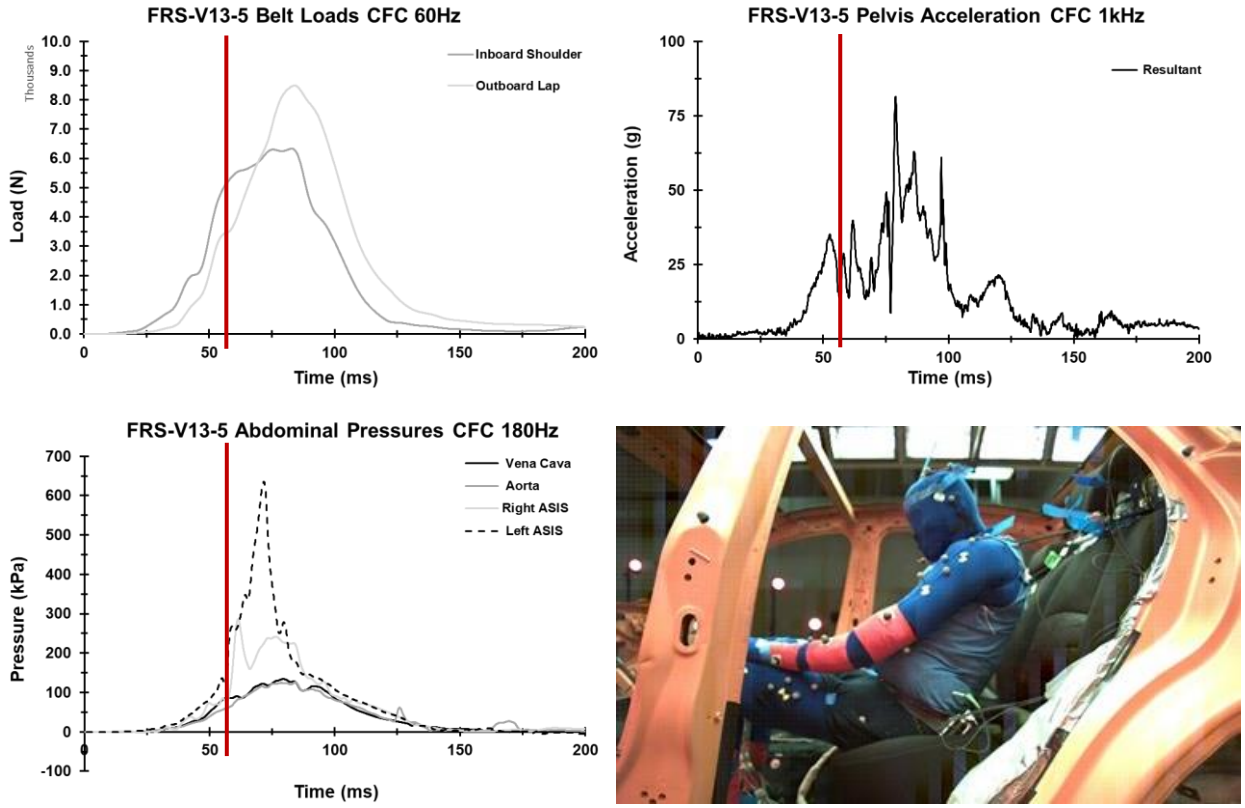

Figure 45. Submarining assessment plots for test V13-5 (SM155) with high-speed video frame at time of submarining.

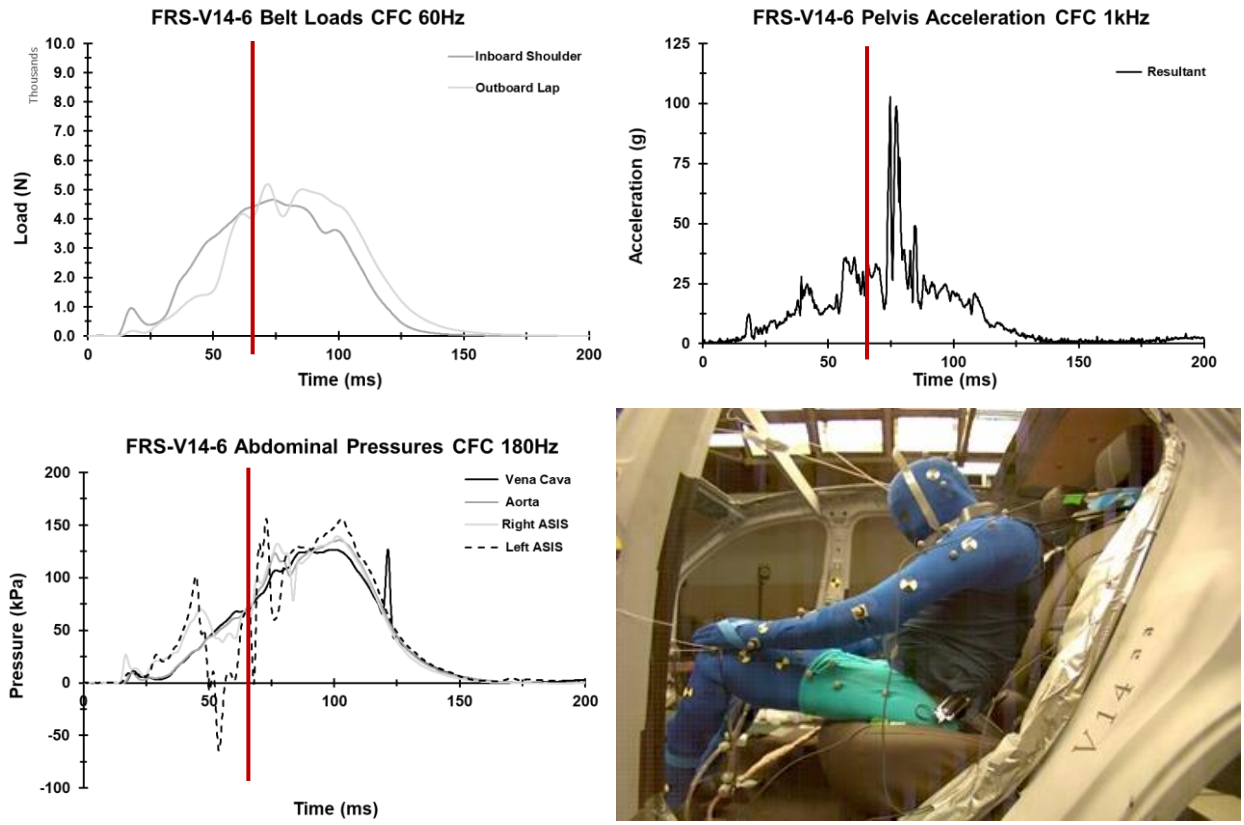

Figure 46. Submarining assessment plots for test V14-6 (SM157) with high-speed video frame at time of submarining.

Submarining Timing

The submarining timing as plotted above is provided in Table 19. Belt loads, abdominal pressures, and high-speed videos were used to estimate the time of submarining, and the average of the three was used to determine the submarining time. Resultant pelvis acceleration was used to verify the timing, looking for a rapid change in pelvis motion. The pelvis and lap belt angles at the time of submarining for the PMHS are provided in Table 20.

Table 19. Submarining timing for PMHS (ms)

Buck	Test Number	PMHS	Submarining Time	Belt Loads	Pressures	Video	Resultant Acceleration
V13	4	SM129	54.65	53.0	57.3	53.7	59.65
	5	SM155	56.15	55.75	56.45	56.25	66.75
V14	5	SM156	-	-	-	-	-
	6	SM157	64.65	63.4	66.3	64.3	64.5
V15	5	SM152	-	-	-	-	-
	6	SM153	-	-	-	-	-
V19	5	SM154	-	-	-	-	-
	6	SM095	-	-	-	-	-

Table 20. PMHS belt and pelvis angles at the time of submarining.

Test ID	PMHS	Submarining Time (ms)	Pelvis Angle (deg)	Belt Angle (deg)	Relative Belt Angle (deg)
V13-4	SM129	54.65	-21.8	35.2	33.0
V13-5	SM155	56.15	-30.9	36.4	22.7
V14-6	SM156	64.65	-11.8	40.0	38.1

Autopsy Results

Every vehicle produced damage to the abdominopelvic regions of the PMHS, to varying degrees. Damage occurred regardless of submarining occurrence.

Pelvis Fracture

Three out of the eight PMHS sustained bilateral pelvic fractures to the ala of the ilium. None of the PMHS with pelvic fractures underwent submarining. The typical fracture pattern seen indicates a medial bending of the left ilium and a lateral bending of the right ilium. It should be noted that the ilium instrumentation mount (left ala) and the tilt sensor (right ala) were both bolted to the pelvis of SM152 (test V15-5). The fractures both traveled through the mounting holes for the instrumentation; however, it appears that the fractures initiated by the same bending patterns as the other tests and were not induced by the fixation methods. Figure 47 depicts the pelvis acceleration for test V15-5, at about 70 ms, there are large magnitude spikes in acceleration, representing the time of the fracture.

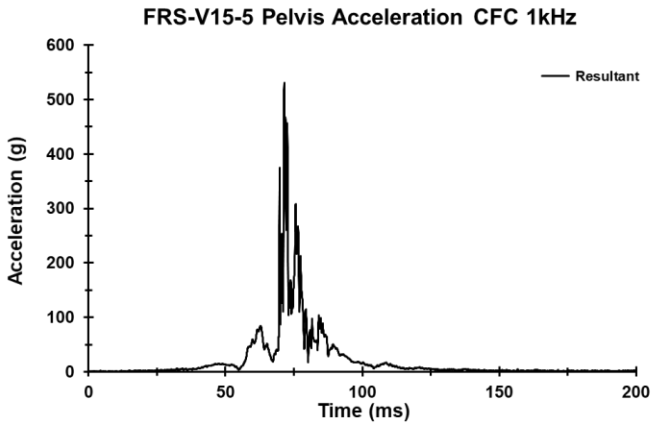

Figure 47. Pelvis acceleration from test V15-5 as measured on the left ilium of SM152.

Pelvis fracture timing was estimated with resultant pelvis acceleration and belt loads and, when possible, verified with angular speed (Y-axis) and abdominal pressures. These plots are provided for test V19-5 in Figure 48, where estimated fracture time is marked. The times estimated from the resultant acceleration and the belt loads were averaged to obtain the fracture time. These times are listed in Table 21.

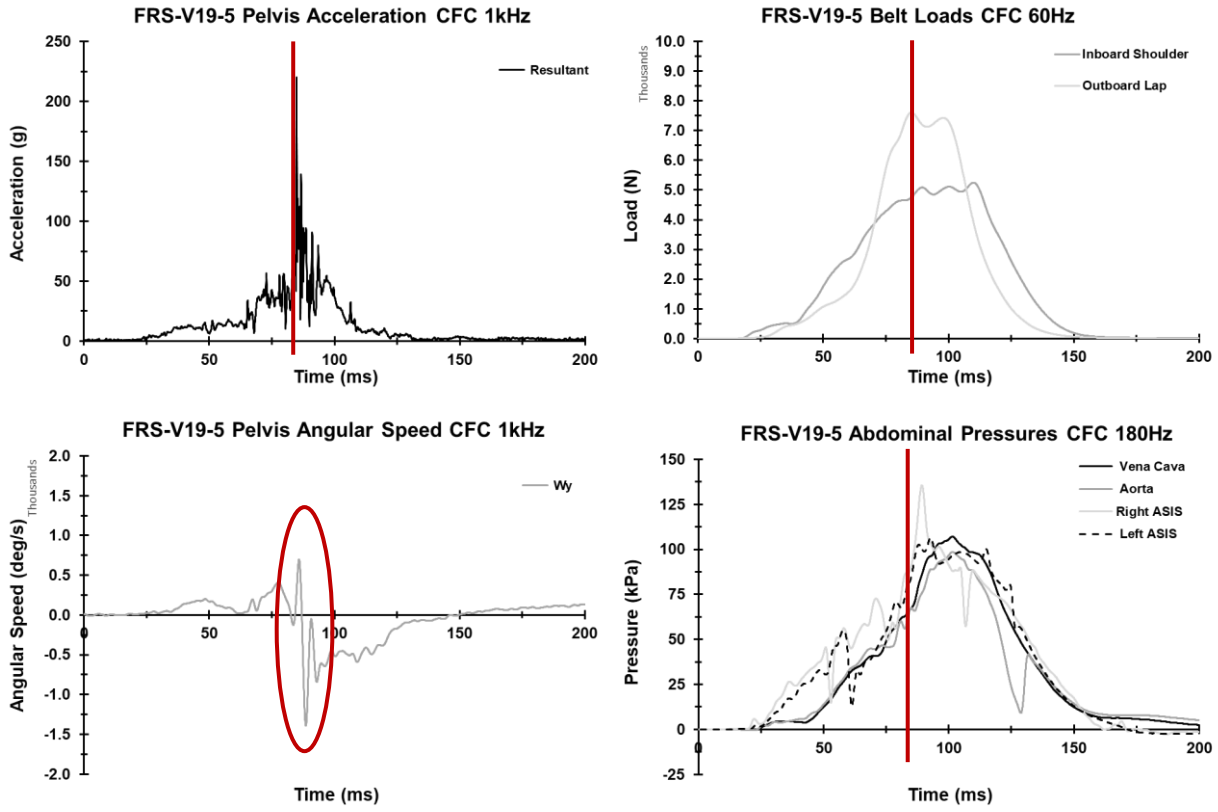

Figure 48. Fracture timing plots for test V19-5 (SM154)

Table 21. Fracture timing for PMHS (ms)

Buck	Test Number	PMHS	**Fracture Time**	Belt Loads	Resultant Acceleration	Angular Speed	Abdominal Pressures
V13	4	SM129	-	-	-	-	-
	5	SM155	-	-	-	-	-
V14	5	SM156	**80.7**	80.7	80.7	N/A	N/A
	6	SM157	-	-	-	-	-
V15	5	SM152	**69.6**	70.1	69.2	70.1	69.1
	6	SM153	-	-	-	-	-
V19	5	SM154	**85.2**	85.8	84.6	83.6	85.6
	6	SM095	-	-	-	-	-

The outboard lap belt load, belt angle, pelvis angle, and relative belt angle at the time of pelvis fracture are provided in Table 22. Image sequences from the high-speed video at the time of fracture and maximum forward excursion are in Appendix J: Image Sequences from Matched NCAP85 Tests.

Table 22. Belt loads and relative belt angle at time of pelvis fracture

Test ID	Fracture Time (ms)	Outboard Lap Belt (kN)	Pelvis Angle (deg)	Belt Angle (deg)	Relative Belt Angle (deg)
V14-5	80.7	7.4	-20	37	33
V15-5	69.6	8.6	-23	33	35
V19-5	85.2	7.6	-21	30	39

Tears in the mesentery, peritoneum, and intestines were also common regardless of the occurrence of submarining. The liver was also frequently damaged to varying degrees. Table 23 contains a brief summary of damage to the PMHS. A detailed record of the abdominopelvic damage produced in these tests is provided in Appendix N: Autopsy Results and associated images are provided in Appendix O: Autopsy Photos.

Table 23. PMHS damage summary

PMHS	Mass (kg)	FRS Test	Advanced Restraints	Submarining Degree	Pelvis Fx	Lumbar Fx	Liver	Spleen	Bowel	Mesentery	Peritoneum	Diaphragm
SM129	63	V13-4		Severe		*			Y	Y		Y
SM155	85	V13-5		Severe		L2	Y	Y	Y	Y		
SM156	89	V14-5	Y		Bilateral		Y			Y	Y	
SM157	68	V14-6	Y	Moderate			Y			Y		
SM152	81	V15-5			Bilateral		Y		Y			Y
SM153	64	V15-6					Y		Y	Y		
SM154	89	V19-5	Y		Bilateral							
SM095	64	V19-6	Y							Y		

*Multiple lateral process Fx

Chapter 5: Discussion

In one test, V14-5 (Figure 49) the sled brakes malfunctioned causing the sled to stop immediately rather than ride down. Fortunately, the sled stopped at the end of the intended sled pulse; however, the subsequent kinematic response and sustained damage of the PMHS (SM156) were altered, effectively providing a multiple-event crash scenario in which the vehicle of interest was involved in a frontal crash and was then rear-ended.

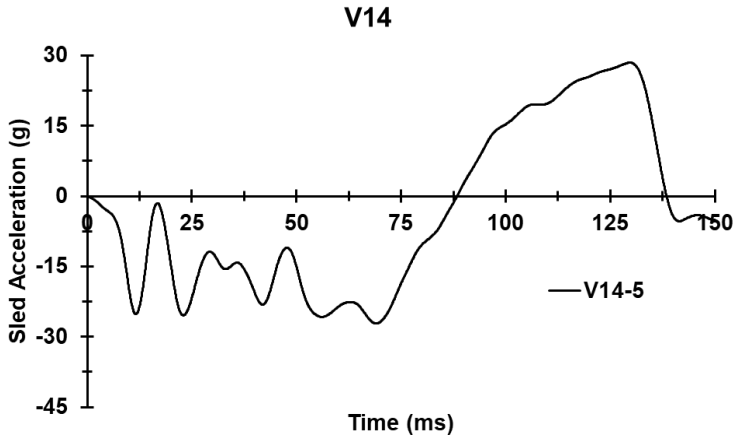

Figure 49. Sled acceleration for test V14-5, in which the brakes malfunctioned at the end of the intended pulse.

Pelvis Kinematics

When possible, X-direction and Z-direction acceleration as well as Y-axis angular speed were compared between the pelvis and sacrum instrumentation mounts. As seen in one example in Figure 50, there is reasonable agreement between the two measurement locations.

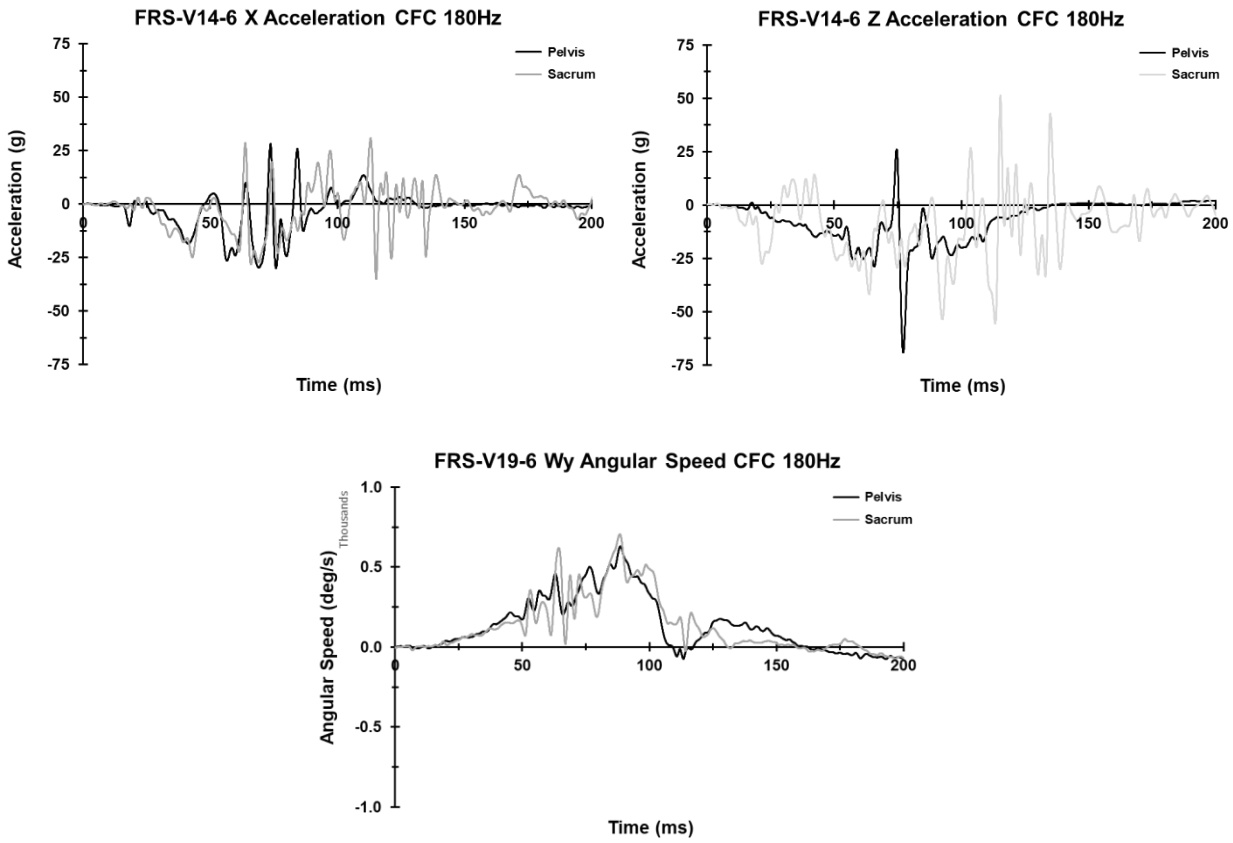

Figure 50. Test V14-6 Ax and Az (top) and Test V19-6 Wy (bottom) for the pelvis and sacrum filtered at CFC 180.

Often the sacrum kinematics are much noisier than the pelvis kinematics data due to the interaction of the sacrum motion block with the seat, especially after submarining, as displayed in the resultant acceleration for test V14-6 in Figure 51. The pelvis instrumentation is also better at identifying pelvic fracture than the sacrum instrumentation, as seen in Figure 52. The resultant acceleration recorded on the pelvis has spikes that correspond to fracture timing of the ilium. For this study, whenever possible, the kinematics as measured on the left ilium are used for pelvis kinematics, but in instances where the pelvis kinematics data are not usable (eg. lost channel or loose mount) the kinematics data from the sacrum are used.

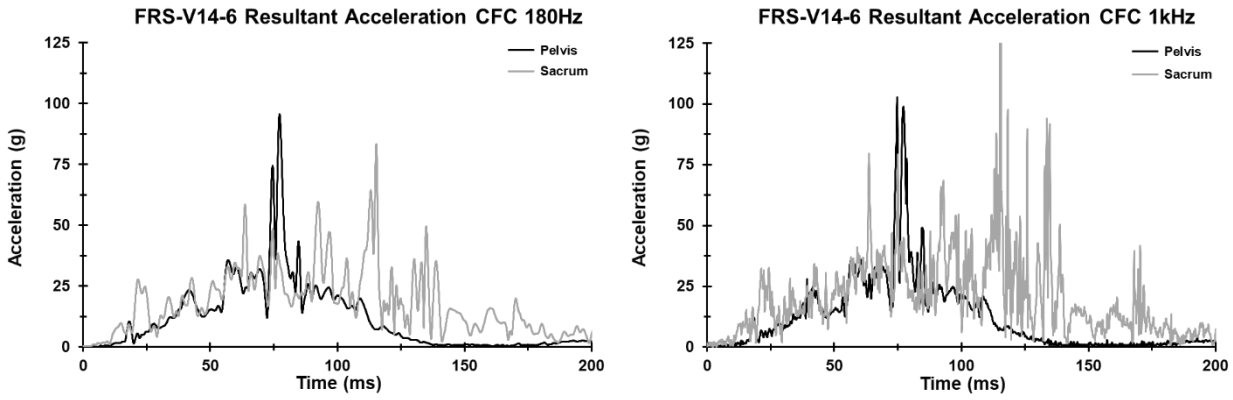

Figure 51. Test V19-6 resultant acceleration (g) of the pelvis and sacrum, filtered at CFC 180 (left) and CFC 1000 (right).

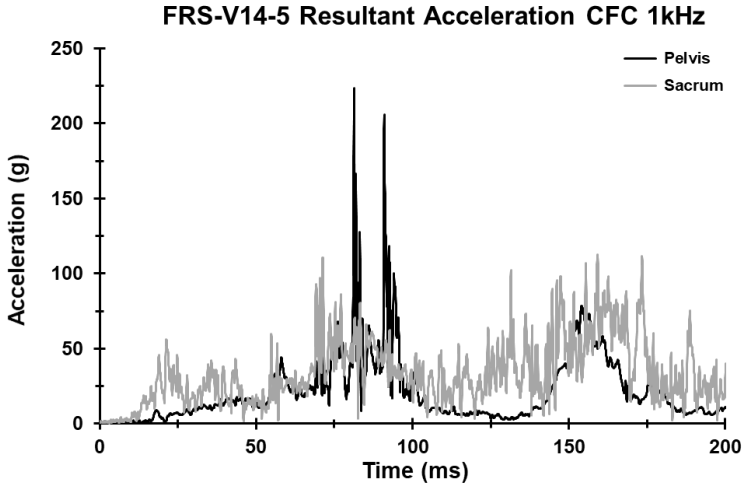

Figure 52. Resultant pelvis acceleration (g) as recorded on the left ilium (black) and sacrum (gray) during test V14-5, filtered at CFC 1000.

The pelvis and sacrum kinematics data were filtered at CFC 1000 Hfor comparison to the ATD kinematics. However, for comparison of pelvis angle to lap belt angle, kinematics data also needed to be filtered at CFC 180 Hz. The pelvis rotation angle of the PMHS in test V14-6 is plotted in Figure 53 using kinematics data

filtered at CFC 180 and 1000 Hz. As seen in the figure, there are no differences in the calculated pelvis angle between the two filtering classes.

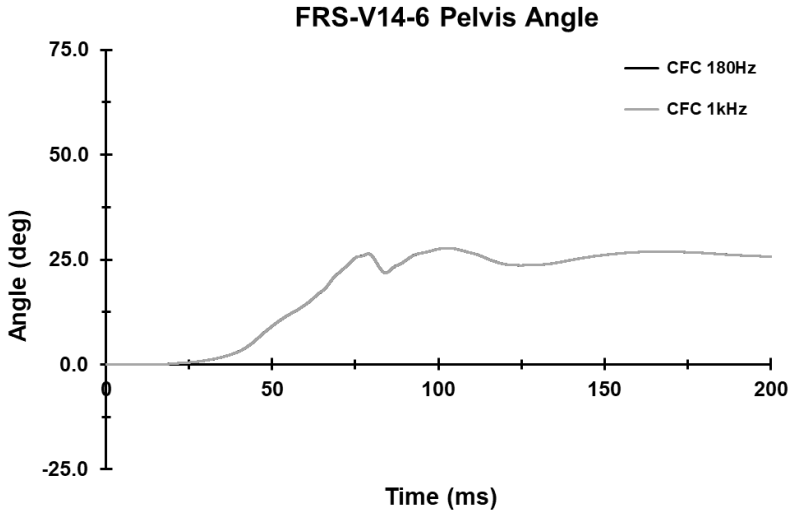

Figure 53. Pelvis rotation angle (deg) from test V14-6 filtered at CFC 180 (black) and CFC 1000 (gray).

Submarining Assessment

No single data source can accurately and consistently identify the occurrence of submarining. Therefore, all sources must be used in combination to make an informed assessment of submarining. Post-test photographs show the final position of the lap belt but cannot provide information about how the lap belt took its final position. Specifically, an investigator cannot determine if the lap belt slipped off of the pelvis during the loading phase or during the unloading phase of the event. Submarining is specific to the loading phase, during which injury occurs. High-speed videos can show the lap belt slipping off of the pelvis, but have limited fields of view which may be further reduced by movement of the surrogates. Seat belt load cells, especially those measuring load at the lap belt, disclose submarining when there is a rapid decrease in force. In cases where submarining does not occur and the lap belt remains in contact with the pelvis, the force-time histories of the lap belt load cells show a smooth curve with somewhat symmetrical loading and unloading phases. However, in the case of submarining, the force will drop off suddenly and will present as a very steep-sloped decrease in force as the belt slips off of the stiff pelvis and loads the softer abdomen. These data sources are available for both ATDs and the PMHS, although the signs of submarining are much more subtle, especially in the lap belt loads, for the PMHS. Because there are no gaps for the belt to travel between the pelvis and abdomen of the PMHS, the belt loads do not drop as distinctly as with the ATDs. Some of this effect could also be caused by the protrusion of the PMHS abdomens during this study. Even during the submarining events, the lap belt did not travel far above the pelvis, limited by the abdominal protrusion.

A benefit of the THOR is that it is equipped with additional instrumentation that provides more detailed depictions of submarining. The THOR pelvis has ASIS load cells, which measure X-direction (shear) force at the ASIS and Y-axis moment. Similar to the belt loads, both ASIS force and moment time-histories typically have smooth and symmetrical loading and unloading phases if the lap belt maintains contact and loading of the pelvis. If the lap belt slips off of the pelvis, both traces will instantaneously drop. The final data source is the ABISUP. Because it measures right and left pressure, there is no directionality of the abdominal loading. As such, without direct loading of the ABISUP by the lap belt, there will still be measured abdominal pressures from torso flexion, lateral torso flexion, compression by the shoulder belt, or indirect loading from the lap belt through the pelvic region. However, these pressures are typically low (below 180 kPa). In cases of submarining, ABISUP pressures will be much higher and will have steeper loading curves after the belt slips off of the pelvis. Additionally, ABISUP loading was sustained over a longer duration in submarining events compared to when no submarining occurred.

Belt Loads

Based on a study that assessed submarining of the HIII-5F in the front and rear seats, the ratio of lap belt load to shoulder belt load was calculated (Tylko & Dalmotas, 2005). For this study ratios are calculated with the outboard lap belt (anchor) and the outboard shoulder belt (retractor) loads, and are provided in Table 24. In the 2005 study, a belt force ratio of less than 0.5 indicated submarining, while a ratio of about 1.0 indicated no submarining. As seen in Table 24, none of the matched NCAP85 tests produced ratios of 0.5 or less. However, there is a delineation of ratios below and above 1.0. Vehicles with conventional restraints (V13 and V15) had ratios that ranged from 0.69-0.88. These tests include a mix of submarining and surrogate type. Vehicles V14 and V19, with the exception of test V14-6 (0.86), had ratios ranging from 1.06-1.35. While there is not enough information to identify the exact cause of the outlier, or why this trend might be occurring, in this study this ratio seems to be related to vehicle design rather than an indication of submarining. In general, differences between the magnitudes of this ratio between these two studies is likely related to differences between the stature and mass of the ATDs used for each.

Table 24. Ratio of lap belt load to shoulder belt load for the matched NCAP85 tests

Buck	Test Number	Surrogate	Submarining?	Outboard Lap (Anchor)	Outboard Shoulder (Retractor)	Anchor / Retractor
V13	2	THOR	Yes	N/A	9509	N/A
	4	SM129	Yes	5793	7372	0.79
	5	SM155	Yes	8487	9841	0.86
V14	4	THOR	No	6767	6368	1.06
	5	SM156	No	7408	6125	1.21
	6	SM157	Yes	5193	6036	0.86
V15	4	THOR	Yes	6559	9454	0.69
	5	SM152	No	8637	10887	0.79
	6	SM153	No	7563	8625	0.88
V19	4	THOR	Yes	6505	4689	1.39
	5	SM154	No	7608	5636	1.35
	6	SM095	No	5539	4217	1.31

Differences in Surrogate Submarining Response

HIII and THOR

The submarining responses of the two ATDs were quite different. While the Hybrid III did not submarine in any test, the THOR submarined in 16 out of 24 tests in 5 out of 7 vehicles. This is not the first study to identify a difference in the frequency of submarining between the HIII and the THOR. A study in 2015 compared the submarining responses of the Hybrid II, HIII, and THOR ATDs in multiple seating configurations during 50 kph sled tests (Uriot, Potier, Baudrit, Trosseille, Richard, et al., 2015). In those tests, the HIII never submarined while the THOR submarined in some of the seating conditions.

There are significant differences in the design and geometry of the ATDs, which could cause the substantial differences in submarining response between them. There are several characteristics of the pelvis that can affect how the lap belt interacts with it. Pelvis angle and the geometry of the anterior pelvis have both been found to be key factors as to whether or not the lap belt will slip off of the pelvis. The HIII has a taller pelvis (from superior-most point of the ilium to the inferior-most point of the ischium) with a flat anterior surface providing a larger surface area for lap belt loading. The high pelvis flesh also provides a greater distance for the belt to travel before sliding off of the pelvis. In contrast, the THOR has a shorter pelvis than the HIII overall, with a shorter distance between the anterior thigh and ASIS while seated. Therefore, the THOR has a smaller surface area for lap belt loading and a shorter distance for the lap belt to travel before sliding off of the anterior pelvis. Additionally, the THOR pelvis has ASIS load cells intended to mimic the

geometry of the human pelvis, which is vastly different from the flat surface of the anterior pelvis of the HIII. These design differences, among others, change loading pathways and load distribution between the two pelvises, and could change lap belt kinematics during a crash.

In addition to pelvis geometry, the angle of the pelvis before a crash event and throughout the event are key factors in whether or not submarining will occur. While initial pelvis angle can be set during test setup, rotation of the pelvis during a crash event is inherent to each ATD's design. The spine of the HIII is very stiff compared to the THOR, limiting torso flexion, which might make pelvis rotation less likely, especially independent from the ATD torso. In fact, in this study the HIII lumbar spine only went into flexion when the entire seat bottom deformed toward the vehicle floor in vehicles V6 and V10. In contrast, the THOR T12 load cell always measured flexion moments except for the test in which the THOR pelvis left the seat (test V13-2). Previous studies have found that the flexibility of the lumbar spine directly relates to pelvis rotation and likelihood of submarining (Leung et al., 1982), and that the HIII requires reward rotation of the entire torso rather than the pelvis in order to undergo submarining (Luet et al., 2012). So, lumbar spine stiffness must be considered in addition to pelvis geometry when assessing submarining kinematics of the ATDs.

The ATD abdominal inserts could also affect the interaction of the lap belt and the ATD. In the HIII, the abdominal insert is positioned behind the anterior pelvis flesh and does not fill the entirety of the abdominal cavity. These factors in conjunction with the rounded shape and flimsiness of the insert itself lead to the lap belt sliding up and over the insert directly loading the lumbar spine if submarining occurs. The ABISUP fills more of the abdominal cavity of the THOR, has a flatter anterior surface, and is more compliant and biofidelic, which allows the lap belt to directly load the abdomen. These factors ultimately lead to different lap belt trajectories and can change the ATD kinematics.

ATDs and PMHS

With such different submarining responses between the two ATDs, it is important to determine which ATD better predicts submarining risk for a PMHS. In this study, the HIII did not submarine in any vehicle or test condition; and, out of the matched NCAP85 tests, the THOR submarined in three out of four vehicles. Three out of eight PMHS submarined in matched NCAP85 tests (Table 25). The PMHS submarined in two vehicles. On this determination alone, the HIII was not sensitive enough to predict submarining in rear-seated PMHS during frontal crashes, as seen in previous studies (Uriot, Potier, Baudrit, Trosseille, Richard, et al., 2015).

Table 25. Submarining results for the PMHS and THOR

Buck	Restraint Type	Test Number	PMHS Number	PMHS Submarining	THOR Submarining
V13	Conventional	4	SM129	Severe	Severe
		5	SM155	Severe	
V14	Advanced	5	SM156	None	None
		6	SM157	Moderate	
V15	Conventional	5	SM152	None	Moderate
		6	SM153	None	
V19	Advanced	5	SM154	None	Moderate
		6	SM095	None	

The results get much more complicated when considering the THOR. In vehicle V13, the THOR underwent severe submarining (test V13-2), and both PMHS (SM129 and SM155) underwent severe submarining (tests V13-4 and V13-5). However, in vehicles V15 and V19, in which the THOR underwent moderate submarining during the NCAP85 tests, neither PMHS submarined. Finally, in vehicle V14, the best performing vehicle in terms of submarining protection for the ATDs, one PMHS did not submarine (SM156, test V14-5) and one submarined in moderate severity (SM157, test V14-6). SM157 had a very short distance between the ASIS and the top of the thigh, limiting the area available for the lap belt to engage the pelvis. Vehicle V14 also has advanced restraints that could have caused pretensioner-initiated belt lift. In these tests, the THOR accurately predicted submarining in one vehicle (V13), which generated the most severe submarining for the THOR and PMHS, but provided mixed results in the other three vehicles included in the matched ATD and PMHS tests.

The THOR was able to accurately predict severe submarining in vehicle V13, during which the two PMHS sustained substantial damage to the abdominal viscera, and in one case, the lumbar spine. In contrast the THOR was not sensitive enough to predict a submarining case in which the PMHS sustained major damage to the small intestine, mesentery, and peritoneum. This result is somewhat contrary to previous studies in which the THOR accurately predicted positive and negative submarining results in the PMHS (Uriot, Potier, Baudrit, Trosseille, Richard, et al., 2015).

There could be several factors that caused this mismatch in submarining occurrence between ATDs and PMHS. Some are specifically related to surrogate type, including pelvis geometry, flesh stiffness, spine design and stiffness, and more. Others could be related to specific test conditions related to the surrogate types. One in particular is friction. The ATDs and PMHS were all dressed in the standard-required all-cotton shirts and shorts. However, the ATDs were tested in dry clothing on a dry seat with a dry lap belt.

This condition is the standard for consideration of reproducibility of friction conditions during regulatory tests. In contrast, the PMHS had damp shorts and potentially damp seats and restraints, increasing friction between the PMHS pelvis and the seat bottom as well as between the anterior pelvis and the lap belt in comparison to the ATDs. Several steps were taken to mitigate the leaking of fluids from the PMHS. First, the PMHS were not dressed in the shorts or shirts until the day of the test. Second, the seats were covered in plastic with the PMHS seated in the right outboard rear seat just before PMHS positioning, at which point the PMHS was moved into the testing position (rear left outboard) and the plastic was removed. Regardless of these strategies, the friction coefficients between the PMHS pelvises, restraints, and the seat bottoms were likely different in the PMHS tests compared to the ATD tests.

Increasing the coefficient of friction between the lap belt and surrogate pelvis has been shown to increase the required relative belt angle to induce belt slipping (Horsch & Hering, 1989; Leung et al., 1982). A potential increase in friction between the lap belt and the PMHS in vehicles V15 and V19 could have increase the critical angle for belt slip enough to prevent the PMHS from submarining, causing a discrepancy in submarining results between the PMHS and THOR.

The PMHS in test V14-6 (SM157) had a short distance between the top of the thigh flesh and the ASIS. In a study that used CT scans to identify key pelvis geometry and lap belt interaction parameters in male and female volunteers, ASIS to thigh flesh height was a key factor in how well the lap belt interacted with the pelvis (Tanaka et al., 2022). The study compared the results to the Hybrid III AM50, Hybrid III AF05, and THOR models. The THOR had a smaller difference between the ASIS and thigh flesh heights than the other ATDs, but larger than volunteers. However, the ischium flesh was over 20 mm thicker than all other surrogates and all volunteers, allowing for more compression before loading the rigid pelvis. Two major results from the CT study can inform the results of the current study. First, that the THOR pelvis has a much larger distance of downward vertical excursion before it loads its pelvis than other surrogates, increasing its chance for submarining over the HIII and PMHS. Second, that the distance between the ASIS and thigh flesh affects the ability of the lap belt to load the pelvis, so a PMHS with a distance similar to or shorter than the THOR would have a higher probability of submarining. A potential compounding factor is the pretensioners in vehicle V14. Lift of the buckle by the shoulder belt via the pretensioner can increase the probability of submarining.

Submarining Trends by Vehicle

The vehicle bucks used in this study have a number of differences that, isolated or combined, could lead to differences in submarining prevention for rear-seated occupants. The study fleet had different types of vehicles, seat types, restraints, and different crash pulses.

THOR

Vehicles V1, V6, and V14 produced no substantive submarining. Vehicles V6 and V14 produced no submarining in any test although one has advanced restraints (V14) and one has conventional restraints (V6). Vehicle V1 has advanced restraints and the THOR did not undergo submarining in the NCAP85 test (Test V1-3), but the THOR did undergo minor submarining in the two low energy tests. In these cases, the submarining was a lifting of the buckle (and inboard lap belt) initiated by the pretensioner. In both tests, evidence of lap belt encroachment was found in the right ASIS loads and moments, but resulted in no substantial abdominal loading or kinematic changes. All three vehicles also had different seat types: rigid/bench (V14), suspended frame (V1), and pedestal style (V6). As depicted in Figure 64, vehicles V1 and V14 both had seat bottoms/pans that were not flat but more ramped, as well as the stiffest seat cushions of the study. In contrast, vehicle V6 (Figure 67) had a relatively flat seat frame and a softer cushion, similar to that in the vehicles with poor submarining protection for the THOR. Vehicle V6 was a second-row pedestal-style seat with the buckle mounted to the seat itself. In each test, the pedestal of the seat deformed causing the seat and ATDs to drop; however, because the buckle traveled with the seat, the lap belt was able to maintain contact with the pelvis and prevent submarining.

Severe submarining of the THOR occurred in vehicles V10 and V13 during the NCAP85 tests (V10-3 and V13-2). Moderate submarining was produced in both of these vehicles during the low energy tests. These vehicles had conventional restraints, soft seat cushions and flat seat bottoms/pans (Figure 66). During each test, the basket-style seats in vehicle V10 were bent downward by both ATDs. Despite this drastic downward motion of both the seat bottom and ATD, the lap belt still maintained contact with the HIII anterior pelvis. In contrast, the THOR pelvis slid under the lap belt in all vehicle V10 tests, contributing to the severity of the submarining. The most pronounced submarining occurred in vehicle V13, which had a relatively flat seat pan. While there was no deformation of the seat bottom in this case, the THOR still underwent submarining and during the NCAP85 test (V13-2) departed from the seat cushion, its pelvis nearly making contact with the floor of the occupant compartment.

The two sedans in the study, vehicles V15 and V19, both produced submarining of the THOR. One of these vehicles had conventional restraints (V15) and the other had advanced restraints (V19). These vehicles each had medium stiffness seat cushions and reasonable anti-submarining angles in the seat pans (Figure 65). Because the extent of the submarining was much less severe in these vehicles, they were determined to provide moderate submarining protection for the THOR. Similar to vehicle V1, during the low energy tests in vehicle V19, the minor submarining was initiated by pretensioner belt lift, producing little increase in ABISUP loading.

The seats of vehicles V6 and V10 were both second row seats with soft seat cushions and little-to-no anti-submarining geometry in the seat frames. However, vehicle V6 provided excellent submarining protection while vehicle V10 provided no submarining protection for the THOR. In both vehicles, the seat bottoms were suspended on frames rather than a seat pan, and both deformed during the tests. The seat in vehicle V6 was supported on all corners by the seat frame, which was collapsible for stowing capabilities. The whole seat deformed downward through the pedestal. In contrast, the seat bottom in vehicle V10 was fixed by a hinge at the bottom of the seat back. In these tests, the seat bottom cantilevered, so that the front of the seat cushion deformed toward the floor. In the case of the THOR, this allowed the pelvis to slip under the lap belt because the lap belt anchor and buckle maintained their initial positions.

While the pretensioners in two of the vehicles initiated belt lift that resulted in minor submarining, this does not detract from their potential benefit to occupant safety in the rear seat. The submarining produced by pretensioner belt lift produced different abdominal loading than standard minor submarining in this study. For example, the peak ABISUP pressure on the right side of the abdomen during the pretensioner-initiated belt lift in vehicle V1 was nearly the same as the peak pressure in the non-submarining test (Test V1-3, NCAP85). In comparing vehicles V15 and V19, peak pressure for the right side was higher for vehicle V15, which does not have pretensioners. Based on this, belt-lift induced submarining is not expected to have relevance toward injury risk.

Overall, given the different vehicle designs used in this study, advanced restraints did not universally mitigated submarining in the THOR. In general, a stiffer seat cushion appeared to contribute to better submarining protection and steeper angles in the seat pan or seat frame appears to have reduced submarining severity. In one case, seat bottom characteristics directly induced submarining (i.e. the seat bottom deflection in vehicle V10). In general, many features appeared to either improve upon submarining protection or exaggerate submarining kinematics, but often no single factor could be determined for the cause of submarining or the success in submarining mitigation.

PMHS

Neither PMHS in vehicles V15 nor V19 underwent submarining. The submarining of the THOR in the NCAP85 tests of both vehicles was moderate. Differences in pelvis geometry and spine stiffness could cause the discrepancy in submarining response between the THOR and the PMHS in both vehicles.

Both PMHS submarined in vehicle V13, the vehicle in which the THOR underwent the most severe submarining. Vehicle V13 had a relatively flat seat pan with a minor anti-submarining feature at the front. It also had a soft seat cushion and conventional restraints, all which could have contributed to submarining kinematics in all three surrogates.

Finally, one PMHS underwent submarining (SM157) and one did not (SM156) in vehicle V14. This result differed from the THOR, which did not undergo any submarining to any extent during all three crash conditions. Vehicle V14 had a moderately sloped seat pan, a stiff seat cushion, and advanced restraints, indicating an expected good level of submarining protection. However, in the PMHS tests, the PMHS that underwent submarining was the smaller of the two PMHS and had a shorter ASIS relative to the top of the thigh—similar to the geometry of the THOR pelvis—which increases the likelihood of submarining. In contrast, the non-submarining PMHS was larger, had a larger distance between the ASIS and the top of the thigh (similar to HIII), and sustained bilateral iliac wing fractures.

Relative Belt Angles

Trends by Vehicle

Submarining event timing and the pelvis and belt angles at that time are important information for understanding the differences in submarining between vehicles and surrogates. The time of submarining with the associated pelvis, belt, and relative belt angles are provided in Table 26. Time of pelvis fracture and the associated angles are also included.

Table 26. Submarining and pelvis fracture timing for matched NCAP85 tests with pelvis and belt angles at that time.

Buck	Test Number	Surrogate	Submarining/ Fracture	Sub/Fx Time (ms)	Pelvis Angle (deg)	Belt Angle (deg)	Relative Belt Angle (deg)
V13	2	THOR	Submarining	62.39	-13.6	37.5	22.4
	4	SM129	Submarining	54.65	-21.8	35.2	33.0
	5	SM155	Submarining	56.15	-30.9	36.4	22.7
V14	4	THOR	-	-	-	-	-
	5	SM156	Fracture	80.7	-20	37	33
	6	SM157	Submarining	64.65	-11.8	40.0	38.1
V15	4	THOR	Submarining	75.35	-15.1	37.1	53.4
	5	SM152	Fracture	69.6	-23	33	35
	6	SM153	-	-	-	-	-
V19	4	THOR	Submarining	86.3	-12.0	32.3	50.5
	5	SM154	Fracture	85.2	-21	30	39
	6	SM095	-	-	-	-	-

Of all the matched NCAP85 tests, submarining occurred the earliest in the vehicle V13 tests, and both PMHS in V13 submarined before the THOR. The relative belt angle at the time of submarining was also the smallest in this vehicle. Studies that have used critical angle to estimate submarining risk state that the tangent of the relative belt angle needs to exceed the friction coefficient between the belt and pelvis to cause

submarining (Horsch & Hering, 1989). No specific value was given, but this would indicate that a larger relative belt angle would make it more likely for the surrogate to submarine. Relatively small relative belt angles in the V13 tests then indicates that submarining is occurring readily, and under much lower loading than expected.

The initial relative belt angles of the surrogates in the V13 tests (Figure 54) had the largest difference between THOR and the PMHS of any other vehicle, with the minimum difference between the THOR and one of the PMHS (SM155) being 16 degrees. This difference was caused by the large difference in initial lap belt angle between the THOR and the PMHS. While the initial lap belt angle for the THOR was approximately 46 degrees, the initial lap belt angles (from horizontal) for PMHS were about 28 degrees. The small initial belt angle in the PMHS tests was caused by a wrapping of the belt over the top of the seat cushion. As the PMHS began to the load the restraints, the pelvis angle increased as the belt compressed the seat cushion and straightened, causing the decrease in relative belt angle from 32-48 ms. While the belt was straightening, the pelvis was allowed to translate forward without a rotational force. After the belt straightened out completely, the load applied to the restraint caused rearward rotation of the pelvis, producing the increase in relative belt angle. In both cases, submarining occurred during the pelvis rotation phase. Because the pelvis angle was greater for the THOR, the belt was relatively straight to start. The belt therefore produced rearward rotation of the pelvis and decreased in angle starting at the time of restraint loading. During this rotation/loading phase, the slopes of the relative belt angle curves are similar for all three surrogates. Each surrogate in vehicle V13 submarined when the lap belt angle was between 35 and 37 degrees during a phase of decreasing belt angle. The other rotation parameters at the time of submarining were not consistent between tests.

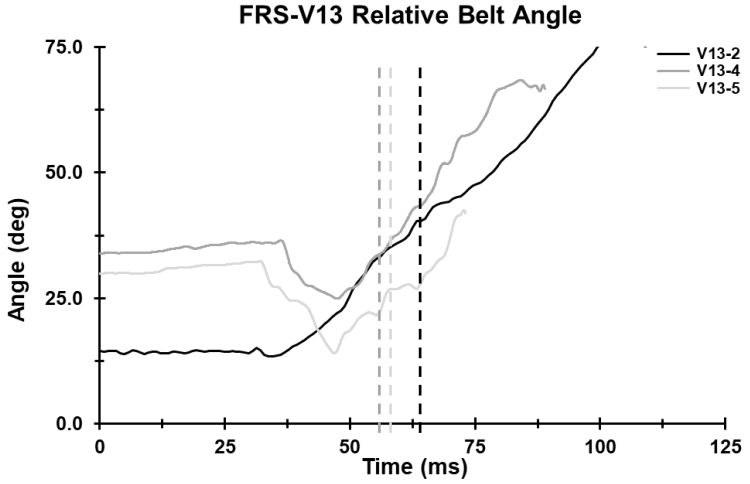

Figure 54. Relative belt angle for THOR (V13-2), SM129 (V13-4), and SM155 (V13-5). Submarining occurrence is indicated by vertical lines.

In vehicle V14 the THOR did not submarine, one PMHS (SM157) submarined, and one PMHS (SM156) sustained bilateral pelvis fractures. The relative belt angles for these tests are shown in Figure 55. As with the other pelvis fracture cases, SM156 was a larger PMHS. The time history of the relative belt angle for the pelvis fracture test (V14-5) involved little relative rotation until late in the event, with only slight rearward rotation of the pelvis.

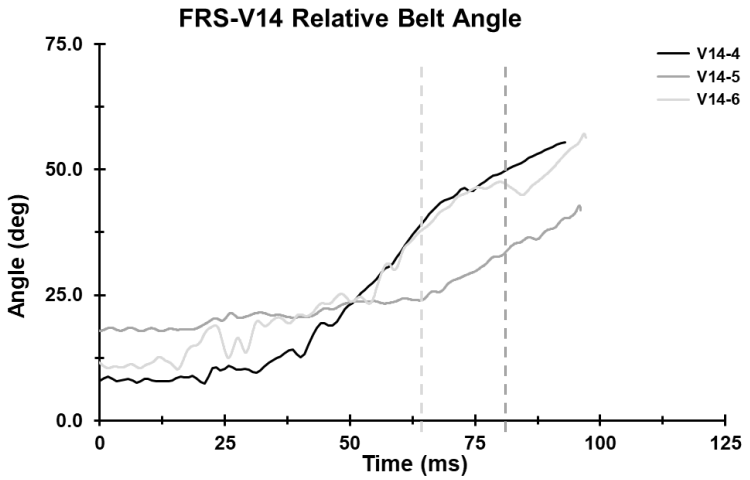

Figure 55. Relative belt angle for THOR (V14-4), SM156 (V14-5), and SM157 (V14-6). Submarining or fracture occurrence is indicated by vertical lines.

The PMHS (SM157) that submarined was smaller and had a very similar initial belt angle and time history of relative belt angle to those of the THOR. This gives further evidence that SM157 had similar relative geometry to the THOR, perhaps with taller thighs than the larger PMHS, causing a steeper belt angle. Submarining occurred at a very small pelvis angle, and relatively steep belt angle. The pelvis geometry volunteer study found that the THOR thigh flesh was taller than the HIII and most of the volunteers in the study (Tanaka et al., 2022), which might explain why the initial belt angles were typically larger for the THOR than the PMHS. The anthropometry of SM157 and its relative belt angle trajectory could explain why it might have submarined in a vehicle that was considered to have excellent submarining protection during the ATD tests. This does not explain why the THOR did not then submarine in vehicle V14 in either of the two NCAP85 tests. One possibility could be that the lap belt and pelvis rotated differently for the THOR and SM157 but created the same relative belt angles. As displayed in Figure 56, the pelvis angles and belt angles of the THOR and SM157 were nearly the same.

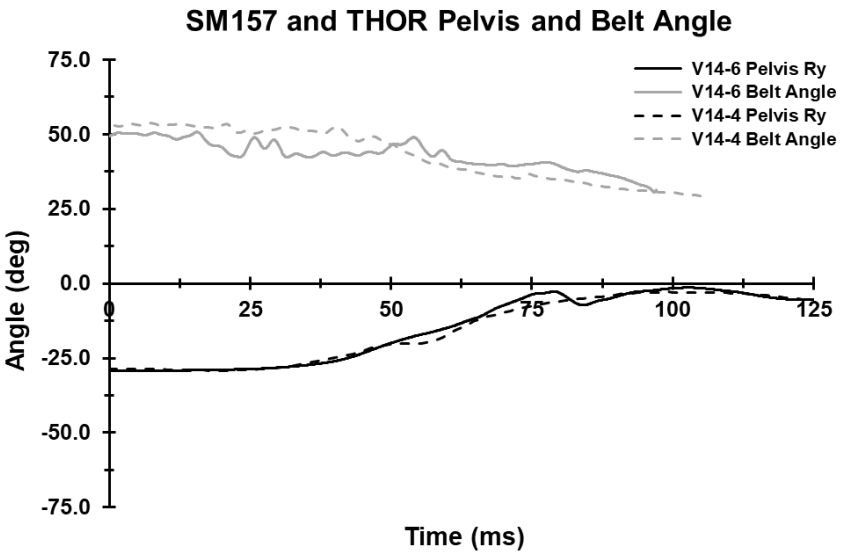

Figure 56. Pelvis and belt angles of SM157 (V14-6) and the THOR (V14-4).

This case is a exemplifies the complexity of the problem of submarining prediction and protection. There are many factors in a real-world environment that can affect the kinematics of any given occupant, and it is not likely to be able to reduce the analysis of such into one kinematic analysis or variable.

Vehicle V15 produced moderate submarining of the THOR, but neither PMHS submarined. Again, the larger PMHS (SM153) sustained bilateral pelvis fractures. There was a wide array of initial relative belt angles in this vehicle (Figure 57), with the smaller PMHS having the largest relative belt angle (smallest initial belt angle), and the THOR having the smallest relative belt angle initially. It is possible that the pelvis geometry of the smaller PMHS in this test (SM152) allowed for better engagement of the anterior pelvis by the belt, preventing submarining. It could also mean that the THOR submarines too readily in this specific buck environment. Regardless, further analysis would be required to obtain these answers.

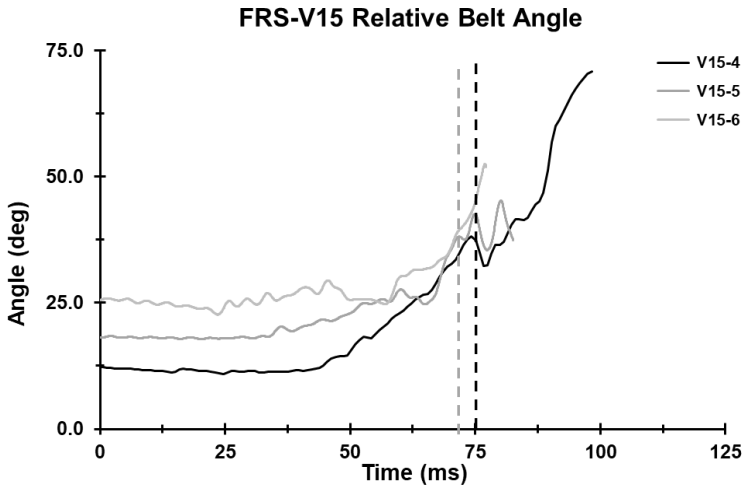

Figure 57. Relative belt angle for THOR (V15-4), SM152 (V15-5), and SM153 (V15-6). Submarining or fracture occurrence is indicated by vertical lines.

Vehicle V19 was similar to V15 in that the THOR submarined, but neither PMHS did. In the first PMHS test, SM154 (the larger PMHS) sustained pelvis fractures. The THOR and SM154 had similar initial relative belt angles (Figure 58) while the initial relative belt angle of SM95 was approximately 10 degrees greater. All three curves are similar, but none reflect similar kinematics between surrogates.

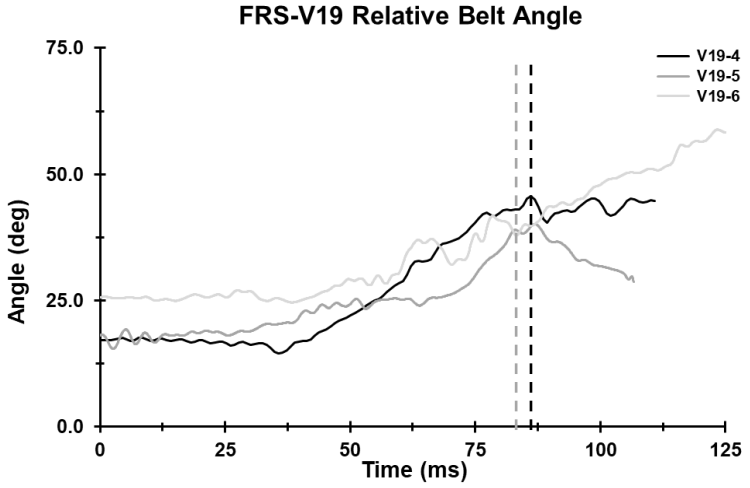

Figure 58. Relative belt angle for THOR (V19-4), SM154 (V19-5), and SM95 (V19-6). Submarining or fracture occurrence is indicated by vertical lines.

Trends by Restraint Type

The relative belt angles for THOR and the PMHS are plotted by restraint type in Figure 59 and Figure 60, respectively. As with the submarining trends themselves, there are no apparent trends in relative belt angle between vehicles with advanced and conventional restraints, regardless of surrogate type. However, it is interesting to note the similarities between the relative belt angle responses for each type of restraint for

both the ATD and PMHS tests. As with submarining, pelvis fractures also occurred in vehicles with both types of restraints, which as indicated in Figure 60, occurred later in the tests than submarining for that restraint type.

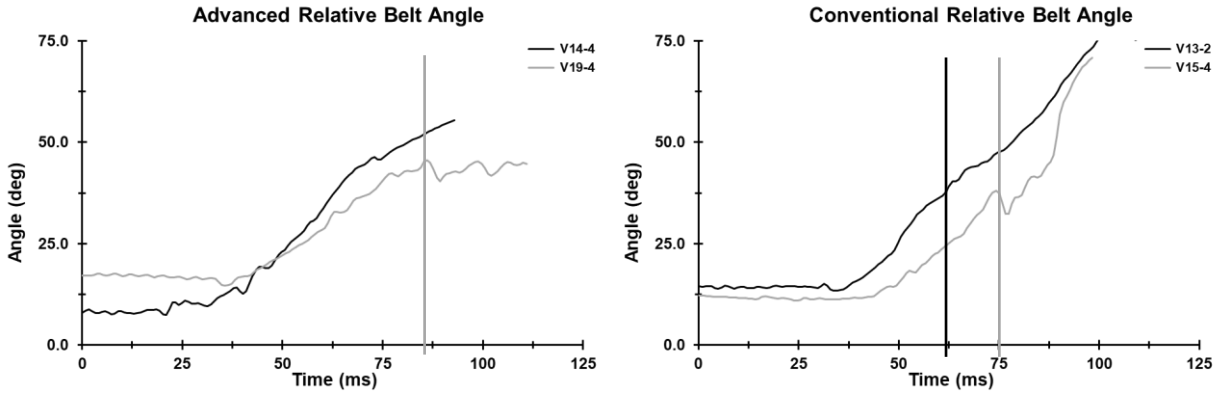

Figure 59. Relative belt angle for advanced restraints (left) and conventional restraints (right). Submarining or fracture occurrence is indicated by vertical lines.

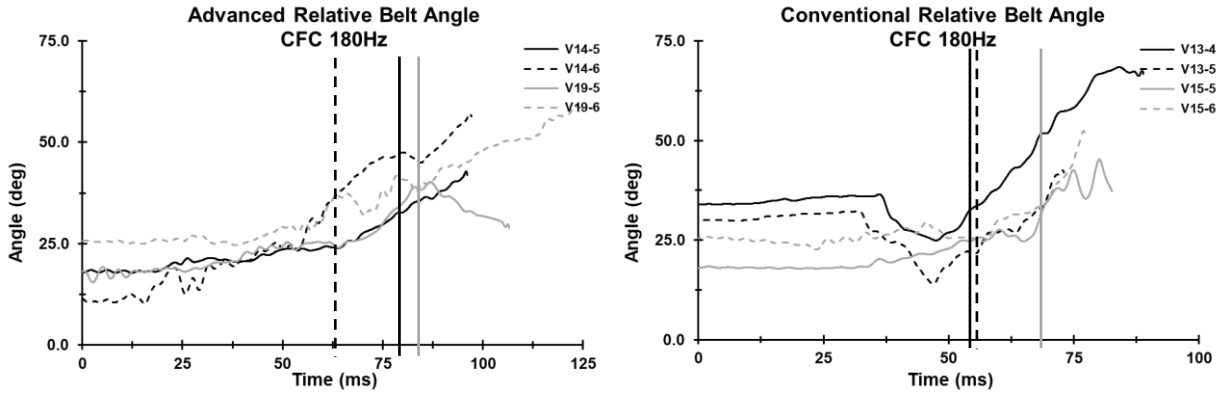

Figure 60. Relative belt angle (PMHS) for advanced restraints (left) and conventional restraints (right). Submarining or fracture occurrence is indicated by vertical lines.

Trends in THOR

Despite the different submarining results and different environments of each vehicle buck, there are no significant differences between the relative belt angles (Figure 61) in the submarining group compared to the non-submarining test, V14-4. The initial relative belt angle ranged from 8 to 17 degrees depending on the vehicle. V14 had the smallest initial relative belt angle (largest initial belt angle) and V19 had the largest initial relative belt angle. In vehicle V13, the THOR had similar pelvis, belt, and relative belt angles at the time of submarining as the PMHS. However, in vehicles V15 and V19, the relative belt angle at the time of submarining was much larger, approximately 50 degrees rather than 20. The pelvis and belt angles at the

time of submarining were also very similar between V15 and V19. This may be an indication that the relative belt kinematics alone are not sufficient indicators of submarining likelihood in the THOR, but that other vehicle-specific factors must be taken into account also. Some studies have included comparisons of lap belt loads as part of this analysis, but no trends were found in the current study (Nilson & Håland, 1995).

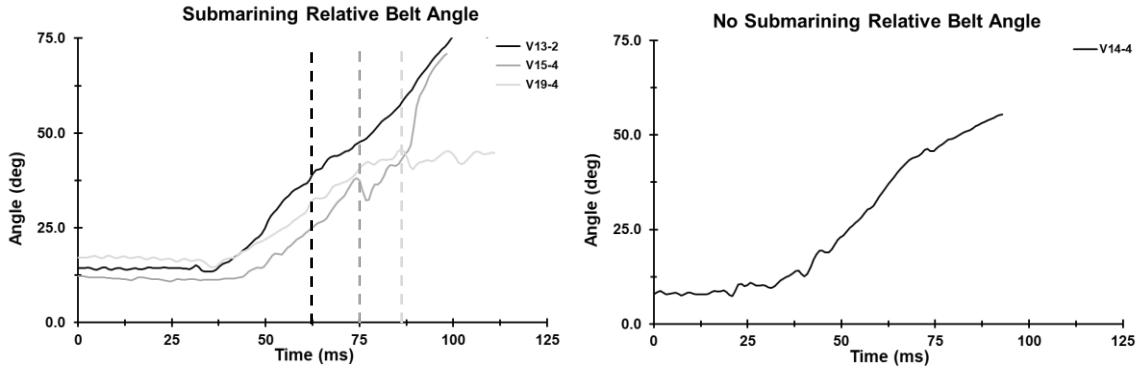

Figure 61. Relative belt angle for the THOR in submarining tests (left) and a no submarining test (right). Submarining occurrence is indicated by vertical lines.

Trends in PMHS

When comparing only the PMHS belt/pelvis data, analyses of relative belt angles can be collected by event type—i.e. submarining, pelvis fracture, and no submarining/no fracture. Relative belt angles are plotted by event type: submarining, no submarining or pelvis fracture, and pelvis fracture in Figure 62. Because the curves for the vehicle V13 tests have such a unique shape because of the seat compression by the belt, there isn't a clear trend between those tests and test V14-6. However, near the time the belts begin to produce pelvis rotation in the V13 tests, the relative belt angle for V14-6 increases and has the same slope as the two other tests. The relative belt angle from the tests with pelvis fractures (V14-5, V15-5, and V19-5) are nearly identical through the time of the earliest pelvis fracture. The initial relative belt angle for all three tests was 18 degrees (initial belt angles were 42-43 degrees), and the relative belt angle remained relatively constant through the first 60 ms of each test, only increasing by 8 degrees. Finally, the two tests that produced no submarining and no pelvis fractures are also very similar through the first 60 ms of the tests. Both tests had an initial relative belt angle of 26 degrees (initial belt angles were 37 and 35 degrees). The overall increase in relative belt angle was only 5 degrees in the first 60 ms of each test.

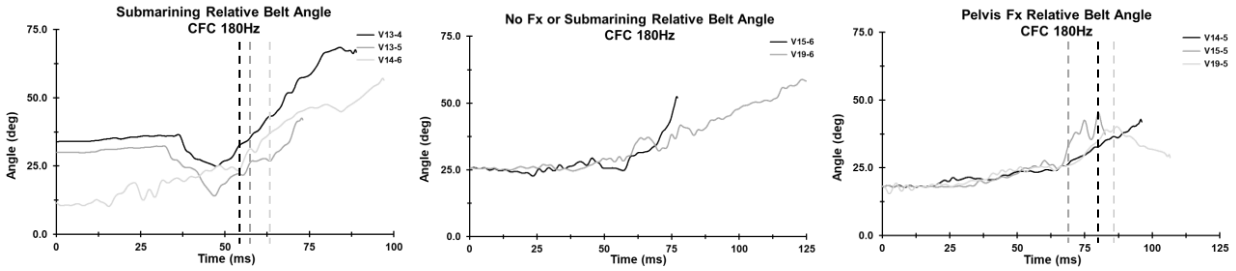

Figure 62. Relative belt angles of PMHS by submarining (left), no submarining or fracture (middle), and pelvis fracture (right). Submarining or fracture occurrence is indicated by vertical lines.

PMHS Submarining and Damage Trends

Summary of Damage and Submarining

V13-4

Test V13-4 produced severe submarining in SM129, during which the pelvis came partially off of the seat. The PMHS sustained a multitude of rib fractures (47), a fracture to the gladiolus, and a fracture to the left clavicle. However, there was no damage to the liver or spleen, organs that are frequently damaged by fractured ribs. The PMHS sustained a large tear to the peritoneum near the bifurcation of the abdominal aorta, several mesenteric tears, a transection of the small intestine, and tears in the ileocecal junction and in the sigmoid colon. Many of these tears were positioned between the ala of the pelvis *in situ*. During submarining, the lap belt loaded the abdomen just above the iliac crests, but below the bulk of the abdominal protrusion, likely compressing the abdominal viscera against the lumbar spine while providing tension between viscera positioned inferior to the lap belt and the viscera trapped in the abdominal distension. This division caused by the lap belt can be clearly seen in the high-speed video frame at peak forward excursion Figure 113, Appendix J: Image Sequences from Matched NCAP85 Tests. SM129 also sustained fractures to the transverse processes of the L2 and L4 vertebrae, possibly caused by this compression or the loading of the lumbar spine on the seat bottom.

V13-5

During test V13-5, SM155, the larger of the two PMHS in vehicle V13, also underwent severe submarining. This PMHS came completely off of the seat bottom before the lumbar spine slammed against the anterior edge of the seat. Again, the lap belt remained below the abdominal distension, which was much larger in this PMHS, and with the larger excursion of the pelvis off of the seat, the lap belt pulled the abdominal contents anteriorly away from the pelvis. SM155 sustained many rib fractures (46) and a fracture of the sternum. In contrast to SM129, SM155 sustained multiple surface disruptions, abrasions, and fractures to the diaphragmatic and visceral surfaces of the liver, as well as two capsular tears of the spleen. There were two complete transections of the small intestine that created a 124 cm long segment and a mesenteric tear

with a 6 cm long “sleeve” in the large intestine. Finally, there was a cranial and caudal ventral avulsion of the L2 vertebra along with fractures to most of the transverse processes of the lumbar vertebrae.

Based on location and characteristics of damage to the liver and spleen, the damage was likely due to a combination of interactions with rib fractures and pressure. The transections of the small intestine were likely due to the compression of the lap belt against the lumbar spine during forward excursion and follow expected trends of lap belt related injuries specifically from submarining. The stretching damage to the large intestine could have been produced by the tension caused by the lap belt restraining the distended portion of the abdomen while the pelvis continued its forward and downward excursion from the seat cushion. Finally, the avulsion of L2 could have been caused by the extreme extension, tension, and shear loading on the lumbar spine during submarining. In test V13-2, the THOR underwent severe submarining with its pelvis leaving the seat cushion. The THOR experienced a peak tensile force of 5.4 kN, positive shear force of 6.1 kN, and peak extension of 134 Nm at T12—all after submarining. This loading was likely caused by the wrapping of the pelvis and lumbar spine around the anterior of the seat cushion. This was the only test in which the THOR T12 load cell measured extension during the loading phase.

V14-5

Test V14-5 involved the larger PMHS for vehicle V14, SM156. SM156 did not undergo submarining, but sustained fractures to the ala of the right and left ilium. Sustaining several rib fractures (22) and a fracture of the manubrium, SM156 had a 4.3 cm long fracture on the diaphragmatic surface of the liver, possibly related to rib fractures. This PMHS also sustained a small tear in the mesentery and a 6 cm long tear of the peritoneum at the level of the L5 vertebra. In the absence of submarining and direct loading of the lap belt on the abdomen, it is suspected that this damage was caused by tension during inertial loading from the abdominal viscera.

V14-6

Contrary to the results from the ATD tests, SM157 underwent submarining (moderate) in vehicle V14. The liver of SM157 had a long superficial disruption on the diaphragmatic surface, possibly related to the many rib fractures on the right side of the thoracic cage. There was a transverse tear in the mesentery that was 17 cm in length, as well as a contused ileum with a mesenteric tear with a radial length of 8.5 cm. Again, the lap belt did not travel superiorly on the abdomen and loaded the abdomen below the large distension. While the pelvis did not depart the anterior border of the seat cushion in this test, there was still possible tensile loading of the abdominal viscera.

V15-5

The first test run in the PMHS series, the pelvis instrumentation in test V15-5 was bolted to the left iliac wing and the tilt sensor was bolted to the right iliac wing. SM152 sustained fractures to the ala of the right and left ilium and sustained a separation of the sacroiliac joint on the left side. Although the instrumentation fixation was deemed to not be involved in fracture initiation, the instrumentation was mounted to the pelvis in manner that did not compromise the bone after this test. The pelvis fracture patterns seen in test V15-5 were repeated in other tests, reinforcing confidence in this assessment. SM152 was the larger PMHS of the two tested in this vehicle, as with SM156 in test V14-5. In this test, SM152 sustained many rib fractures (40) and a fracture of the manubrium and left clavicle, indicating substantial loading by the shoulder belt. There were lacerations to the pleural surface of the diaphragm bilaterally and a very large fracture or puncture on the diaphragmatic surface of the liver with a second, smaller fracture. Again, these could be related to the plethora of rib fractures or due to intra-abdominal pressure. There was also a 10 cm long contusion to the ileum. Despite the lack of submarining, the shoulder belt loading could have produced increased pressure in the abdomen, or damage could be related to inertial loading from the abdomen itself.

V15-6

Test V15-6 did not involve submarining or pelvis fracture of SM153. The liver sustained significant damage with multiple deep fractures, some of which pass through from the diaphragmatic to visceral surfaces. There were also multiple superficial disruptions of the diaphragmatic surface. There were two tears in the mesentery anchoring the small intestine and a long tear in the mesentery along the sigmoid colon, with a complete transection in the descending colon proximal to the mesenteric tear. Again, the inertial loading of the abdomen seems to be producing the damage to the bowels and mesentery.

V19-5

During test V19-5, SM154 sustained pelvis fractures to the alas of the right and left ilium, but no damage to the abdominal viscera was found. This was a larger PMHS that did not undergo submarining.

V19-6

As for the smaller PMHS tested in vehicle V19, SM95 did not sustain a pelvis fracture. SM95 also did not undergo submarining. Similar to other tests, SM95 had a 53-cm long longitudinal tear in the mesentery with possible stretching of the small intestine on either end. With no other damage found to the abdominal viscera, it is suspected that this damage was caused by tension due to the inertial loading from the abdomen.

Pelvis Fractures

There were no instances in which a PMHS underwent submarining and sustained pelvis fractures. Pelvis fractures all occurred at or above 7.4 kN belt load (outboard lap or anchor load cell location), which is well

above the typical belt load at the time of submarining. There was only one test (V15-6) during which the outboard lap load exceeded 7.6 kN that did not result in pelvis fracture. All pelvis fracture cases occurred in the heavier PMHS tested in each vehicle, which were also heavier than the ATDs, all weighing more than 80 kg. According to the belt and pelvis angles at the time of fracture listed in Table 26, the pelvis fractures occurred at pelvis angles between -20 and -23 degrees, belt angles 30-37 degrees from horizontal, and relative belt angles between 33 and 39 degrees.

These bilateral pelvis fractures without submarining are not common in the literature. In a study by Luet et al. (2012), five PMHS sustained pelvis fractures; all of which also submarined. In that study, only two PMHS submarined without pelvis fractures. Additionally, the majority of the fractures in the study were unilateral, occurring either to the right or left sides of the pelvis (Luet et al., 2012). Lap belt loads were also lower, ranging from 4-6 kN at the time of fracture. These tests were conducted on a rigid seat pan of which the angle ranged from 0-5° depending on the test configuration. Additionally, to reduce variability in lap belt loading caused by shoulder belt lift, the shoulder and lap belts were separated, each anchored independently at two points: the lap belt with retractors at either end and the shoulder belt with a retractor at the upper shoulder only.

In a later study, a similar setup was used to compare submarining kinematics of mid-sized male PMHS in front and rear seat conditions (Uriot, Potier, Baudrit, Trosseille, Petit, et al., 2015). For this study, the rigid seat pan was replaced with a semi-rigid seat pan which allowed for control of the seat angle, included an anti-submarining ramp, and allowed for deformation of the seat bottom during the test. Seat pan angle and angular stiffness, as well as anchor locations, were changed to represent the front and rear seat conditions. No PMHS sustained pelvis fractures in the front seat configuration, but every PMHS in the rear seat configuration sustained pelvis fractures. This study limited the outboard lap belt forces to 5 kN, which was exceeded in every test. This study could not identify any submarining, but noted that with this test setup it was not possible to separate iliac wing fractures from submarining.

Abdominal Pressure and Submarining

ABISUP Pressures

In addition to the pressure time-histories being a reliable source for submarining assessment, peak ABISUP pressures gave a good indication of submarining severity. When the lap belt does not encroach on the abdomen, ABISUP pressures range from 68 to 114 kPa during low energy tests. This includes the non-slipping side in minor submarining cases. For these conditions during NCAP85 tests, pressures range from 116 to 158 kPa. Abdominal pressures on the sides on which the belt encroaches the abdomen reach from 161 to 292 kPa during low energy tests and 204 to 499 kPa in NCAP85 tests. Note that submarining

occurring during low energy tests was rated minor or moderate while submarining during NCAP85 tests was moderate-to-severe.

ABISUP pressures can be difficult to interpret because they do not relate only to lap belt loading. Both increased pressure from torso flexion and loading from the shoulder belt confound potential injury risk assessment. Additionally, because of these factors, if it not possible to directly relate ABISUP pressures to deflection or specifically the IR-TRACC deflection measurements in the standard THOR abdomen.

PMHS Abdominal Pressures

The aorta and vena cava pressures display different potential trends with respect to damage to the abdominal viscera. Table 27 compares peak vascular abdominal pressures to submarining, pelvis fracture, and abdominal viscera damage. While there was only one tests in which no damage to the abdominal viscera was found (V19-5), there could still be a delineation between pressure and damage. The minimum peak aorta pressure related to any abdominal damage is 102 kPa, with the peak in the test with no abdominal injury being 99 kPa. For the vena cava, the lowest pressure sustained with abdominal damage was 100 kPa, and the pressure in the test with no abdominal damage was 107 kPa. Note that while V19-5 did not include damage to the abdominal viscera, there was a bilateral pelvis fracture during this test. These pressures are within the range of a previous study in which the lowest abdominal aorta pressure related to abdominal injury was 89 kPa, and the highest aorta pressure related to a non-injurious event was 103 kPa (Foster et al., 2006). Foster et al. also stated that pressure in the abdominal aorta could potentially be used as an indicator for liver injury. A later study found the threshold for abdominal damage to be 57 kPa, and for which AIS 2 and 3 abdominal damage was associated with peak aorta pressures between 74 and 97 kPa (Ramachandra et al., 2016). In the current study, the vena cava pressure (measured near/at the liver) reflects a stronger indication of a trend, with the delineation between injury and non-injury being approximately 125 kPa. Peak aorta pressure may also indicate the risk of damage to the mesentery, the non-injurious to injurious range being from 107-111 kPa in these data. It is important to remember that strict interpretation of abdominal pressure is difficult for these tests given the complex response of the abdomen related to interaction with restraints combined with inertia. Boundary and loading conditions will affect the pressure responses for different modes of testing.

Table 27. Summary of damage to the abdominal viscera and peak abdominal pressures measured in the abdominal aorta and the inferior vena cava

PMHS	Mass (kg)	FRS Test	Submarining Degree	Peak Aorta Pressure (kPa)	Peak Vena Cava Pressure (kPa)	Pelvis Fx	Liver	Spleen	Bowel	Mesentery	Peritoneum	Diaphragm
SM129	63	V13-4	Severe	149	100				Y	Y		Y
SM155	85	V13-5	Severe	126	134		Y	Y	Y	Y		
SM156	89	V14-5		111	119	Bilateral	Y			Y	Y	
SM157	68	V14-6	Moderate	136	127		Y			Y		
SM152	81	V15-5		102	120	Bilateral	Y		Y			Y
SM153	64	V15-6		149	-		Y		Y	Y		
SM154	89	V19-5		99	107	Bilateral						
SM095	64	V19-6		118	127					Y		

In all but one case (test V15-6), the peak aorta pressures were 118 kPa or lower during tests with no submarining. Peak aorta pressure during submarining events was at least 126 kPa. However, in test V15-6, in which SM153 did not submarine, the peak abdominal pressure aorta was 149 kPa, the same as during a severe submarining event in test V13-4. Extensive damage to the liver was produced in test V15-6 (Figure 63) that could be related to the high abdominal pressure produced even in the absence of submarining. This is likely related to strong engagement with the shoulder belt.

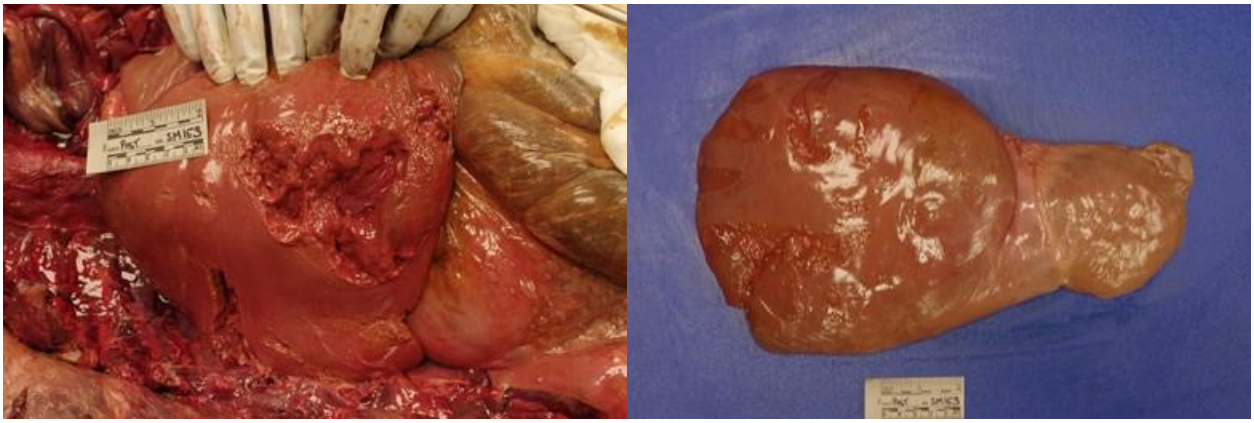

Figure 63. Photos of liver damage to SM153 in test V15-6

Peak ASIS pressures ranged from 74 to 635 kPa with the highest pressure coming from a submarining test (V13-5) and the next highest peak pressure (434 kPa) occurring during a non-submarining, no pelvis-fracture test. ASIS pressures varied the most of all of the pressure measurements, but are difficult to

interpret, as indicated previously. Part of the variability in ASIS pressures could be caused by the final testing position of the transducers. The placement relative to other structures achieved during preparation might not be maintained once the specimen is positioned in a seat. It was also not guaranteed that the transducers would be in the line of lap belt loading.

As with the ABISUP pressures, the abdominal pressures measured in the vasculature were likely confounded by loading from the shoulder belt and torso flexion during testing. Additionally, the placement and fixation of the chest bands caused the abdomen of each PMHS to distend more than typical for a PMHS that was quite turgid. This distension of the abdomen: prevented the lap belt from sliding very far up the abdomen, changed the inertia of the abdominal contents, and very likely changed the pressures within the abdominal viscera. The forward excursion of the abdomen due to inertial loading also confounded the interpretation of the pressure values. While some trends were described here, there is not enough clear delineation to make any conclusive statements. The damage to the abdominal viscera described in this study was not coded for severity, which could clarify or strengthen some of the observed trends.

Buck Environments

Using seven different rear-seat bucks made from modern vehicles provides major advantages for this study. First, vehicle statistics from the current US vehicle fleet can be compared to the submarining and abdominal injury data obtained in these sled tests to get an indication of the expansiveness of current technologies and possible gaps in occupant protection. Two ATDs were used to determine occupant submarining risk in the seven vehicles at different crash severities. This information related to a variety of seat type, restraint types, and vehicle geometry can give indications of ways to improve occupant protection with respect to submarining. Using PMHS in these same vehicles allows for interpretation of the differences in ATD responses by providing a benchmark for the biofidelity of the submarining response of each ATD in addition to providing potential injury information.

The complex environments of each buck and the complex combinations of vehicle, seat, and restraint variables necessitates comprehensive analysis of these features to make effective decisions for the improvement of rear seat occupant safety. Most other studies discussed herein used simplified lab seats or older model modified vehicle seats in which specific variables can be controlled or changed. However, while only using one seat with no cushion might allow for the determination of how different anchor positions might affect submarining response, there is no information or opportunity for inference about how those anchor positions would make the lap belt interact with the seat cushion, as it did in the vehicle V13 PMHS tests. Similarly, only using one surrogate or surrogates that are all the same size might not

demonstrate how different pelvis and lower extremity geometries might affect the initial lap belt angle or degree of interaction of the lap belt with the pelvis.

In an effort to reduce variability between tests caused by shoulder belt lift of the buckle, studies have separated the lap and shoulder belt parts (Horsch & Hering, 1989; Luet et al., 2012; Trosseille et al., 2018; Uriot, Potier, Baudrit, Trosseille, Petit, et al., 2015). In the current study several instances of submarining were initiated by this kind of mechanism, which reflects a more realistic environment. The continuity between the shoulder and lap belts is a major factor in control of torso kinematics as well as restraint of the pelvis. Separating the belt into these two parts limits the comparability of research data to real world occupant protection. While these studies can identify specific factors that can affect submarining or general occupant response, they can be difficult to translate into the complex environments of actual vehicles.

Front Seats

The front seats were removed from the vehicle bucks to reduce variability between vehicles and to improve sight lines for high-speed video the Vicon motion capture system, which were critical for assessing occupant kinematics and submarining.

The front seat is often considered part of the restraint system for the rear-seated passengers. However, the restraint effect of the front seat is dependent on seat-track position, seat back angle, and occupant presence or mass. These conditions would be difficult to match or account for in these tests. The restraint of rear-seated occupants by the front seat may not reduce the risk of submarining at all. During their assessment of rear-seat occupant protection, Hu et al. investigated changes in protection for different occupant sizes and front seat locations (Hu et al., 2015). Regardless of knee-to-seat back distance, the THOR underwent bilateral submarining in severe tests, while a smaller knee-to-seat back distance limited submarining to one side during the less severe tests. Overall, even with 70 mm between the knees and the front seat, the THOR submarined in high-speed (ΔV=63 kph) tests. In fact, an early study of submarining kinematics suggested that the constraint of a rear-seated occupant's feet could increase submarining risk (Håland & Nilson, 1993).

Finally, part of the purpose of focusing on rear-seat occupant protection in this study is to determine potential risks associated with alternative seating arrangements — including no front seating row or no front-seated occupants in fully autonomous vehicles. In these scenarios, a rear-seated occupant would have additional protection from the presence of a seat in front of them.

Limitations

A major limitation of the use of surrogates, whether they are ATDs or PMHS, is that there is no way to represent a living human occupant. While the biofidelity of ATDs is assessed against the response of

PMHS, PMHS do not necessarily have the same kinematic or injury response as a human. Two key factors are the lack of blood pressure and muscle tension. Both likely affect loading mechanisms, especially to the viscera, but muscle tension could affect overall kinematics, even at these high loading rates. With specific considerations for abdominal injury, the lack of blood pressure has a large effect. The positions of the thoracoabdominal contents are shifted inferiorly in PMHS relative to humans; in several studies, inversion of the PMHS allowed for loading of the thorax and abdomen with the viscera in more accurate position (Hardy et al., 2006; Howes, Gregory, Hardy, & Beillas, 2012; Howes, Hardy, & Beillas, 2013). The benefits of inverting PMHS are improved interaction of the belt with the abdominal viscera and therefore more accurate description of potential injuries. However, in full-body sled tests inversion is not possible. Additionally, valuable information about submarining tendency and potential damage mechanisms can still be observed.

Another limitation for biofidelity of PMHS in this study is related to the effects of the chest band implementation on abdomen characteristics. Two chest bands were applied to each PMHS, compressing the thorax, and restricting thorax expansion. This moved the thoracoabdominal viscera inferiorly, which caused a distension of the abdomen, which varied in size. These distensions were firm and restricted motion of the lap belt and potentially restricted motion of the abdominal viscera during loading. By visual inspection of the high-speed videos and the post-test autopsy damage, it appears that there was inertial loading caused by the restricted abdominal contents, potentially confounding the damage sustained by the PMHS regardless of submarining in this study.

One of the strengths of this study is that the bucks are made from rear-world vehicle seats and have modern rear-seat environments. While this provides invaluable information about the state of rear-occupant safety in modern vehicles, it also makes the analysis and identification of variables affecting submarining and injury protection more difficult. For example, many studies will change one factor at a time, like anchor position or seat cushion stiffness, to determine which conditions will improve submarining protection. In this study, each vehicle has different seat frame and seat pan designs, seat cushion stiffness, restraint anchoring locations, restraint types, and crash pulses.

This study only focuses on a mid-sized adult male occupant. However, even with this small target demographic, the results of this study highlight the importance of overall occupant size and anthropometry on injury and submarining risk. Even within the range considered a mid-sized male, differences in mass and pelvis geometry produced different outcomes, emphasizing importance of studying a wide array of occupants to better represent the protective abilities of the rear-seat environment for the entire population.

Finally, this dissertation only addresses the risk of submarining and abdominal injury in a rear-seated occupant; but this does not take into account the entire occupant protection picture. Thoracic loading and injury are massively important in determining the overall effectiveness of occupant protection in these vehicles. There are often tradeoffs in design parameters for given injury risks to different body regions, so the whole-body response must be considered when making those types of conclusions.

Future Work

Thus far, eight PMHS have been tested, two per vehicle. Four more PMHS will be tested in this study, one per vehicle. The work conducted so far included PMHS and at the outer bounds of the target heights and weights, so emphasis is being placed on obtaining PMHS in the middle of the height and weight ranges so that a complete picture of the response of the mid-sized male occupant can be obtained for each vehicle.

The results of this study will be used to get a real-world risk assessment for rear-seat occupants. A survey of the current US fleet will be conducted to determine the numbers of vehicles that match or are similar to the vehicles in this study. Results of kinematics and injury risk can then be compared to exposure data of the US fleet to get an overall assessment of risk.

This dissertation does not cover the full breadth of potential analyses that could pertain to submarining and abdominal injury. More can be done to attempt to identify specific trends, especially with data from the third PMHS test for each vehicle.

Chapter 6: Summary

Thirty-two frontal crash sled tests were conducted using mid-sized male surrogates. Seven rear-seat vehicle bucks were created from modern vehicles (MY 2017 and 2018). Each of the seven vehicles was tested under three crash conditions with the Hybrid III 50th-percentile male and THOR-50M ATDs. Twenty-four tests were included in the ATD study, including at least one test per buck per crash condition and 3 repeat tests. Four vehicle bucks were chosen for use in matched NCAP85 PMHS tests. Two NCAP85 tests were conducted on each vehicle, each PMHS being tested only once (8 PMHS for 8 tests). A summary of key takeaways is included below.

- The HIII did not submarined in any test, but the THOR submarined in 16 out of 24 tests.
- While multiple information sources were used to identify and categorize submarining in the THOR, abdominal pressure, as measured by the ABISUP prototype abdomen, was the most reliable parameter for correctly identifying submarining occurrence.
- Restraint type was not indicative of whether or not the THOR would submarine; due to the complex differences between rear seat environments in this study, individual characteristics that increase submarining risk of the THOR are difficult to isolate. This was also true for PMHS testing.
- Three out of eight PMHS underwent submarining, in only two out of the four vehicles. While the worst-performing vehicle produced submarining in the THOR and both PMHS, the third PMHS submarined in the best-performing vehicle from the ATD tests. While the Hybrid III is insensitive to PMHS submarining risk in the conditions of the matched NCAP85 tests, the THOR is not a perfect predictor of PMHS submarining either.
- The most severe submarining for both the THOR and PMHS was associated with a vehicle having conventional restraints (V13). However, this vehicle also had a relatively flat seat pan. Interpretation of relative belt angles revealed the complex nature of restraint and occupant interaction with respect to submarining or injury outcomes.
- PMHS heavier than the target mid-sized male that did not undergo submarining sustained bilateral pelvis fractures.
- Substantial damage to the abdominal viscera was produced regardless of submarining, and specific injury mechanisms are difficult to identify due to many confounding factors related to study design. However, substantial engagement with the shoulder belt in the absence of submarining is likely an important factor.
- Considering only the abdomen and pelvis, the PMHS kinematics and damage results suggest that V13 (severe submarining and abdominal viscera damage) is associated with the greatest potential

for injury, while V19 is associated with the least potential for injury, with V14 and V15 falling between.

- Considering only the abdomen and pelvis, comparison between the PMHS and ATD responses suggests the THOR might be more appropriate for use in rear seat occupant protection than the Hybrid III.

This study provides a massive database of information regarding submarining and abdominal injury for three surrogate types, two crash severities, and seven modern, real-world vehicle environments. The occupant responses identified by this study inform of major gaps in occupant protection in the rear seats of modern vehicles.

References

Adomeit, D. (1977). Evaluation Methods for the Biomechanical Quality of Restraint Systems During Frontal Impact. *SAE Technical Paper Series*, 3244–3251. https://doi.org/10.4271/770936

Adomeit, D., & Heger, A. (1975). Motion Sequence Criteria and Design Proposals for Restraint Devices in Order to Avoid Unfavorable Biomechanic Conditions and Submarining. *SAE Technical Paper*, 3150–3159.

Anderson, P. A., Rivara, F. P., Maier, R. V, & Drake, C. (1991). The epidemiology of seatbelt-associated injuries. *The Journal of Trauma*, *31*(1), 60–67.

Beillas, P., Alonzo, F., Chevalier, M.-C., Lesire, P., Leopold, F., Trosseille, X., & Johannsen, H. (2012). *Abdominal twin pressure sensors for the assessment of abdominal injuries in q dummies: in-dummy evaluation and performance in accident reconstructions*. SAE Technical Paper.

Bhat, G., Beck, L., Bergen, G., & Kresnow, M. (2015). Predictors of rear seat belt use among US adults, 2012. *Journal of Safety Research*, *53*, 103–106.

Bianco, S., Guettler, A. J., Hardy, W. N., Albert, D. L., & Kemper, A. R. (2022). Evaluation and comparison of thoracic injury risk for the Hybrid III and THOR 50th-percentile male anthropomorphic test devices in the rear seat during frontal impacts. *SAE International Journal of Transportation Safety*, *10*(09-10-02–0015).

Bilston, L. E., Du, W., & Brown, J. (2010). A matched-cohort analysis of belted front and rear seat occupants in newer and older model vehicles shows that gains in front occupant safety have outpaced gains for rear seat occupants. *Accident Analysis & Prevention*, *42*(6), 1974–1977.

Bondy, N. (1980). Abdominal injuries in the national crash severity study. *National Center for Statistics and Analysis Collected Technical Studies*, *2*, 59–80.

Daniel, R. (1974, October 15). Test dummy submarining indicator system. Google Patents.

Doersch, K. B., & Dozier, W. E. (1968). The seat belt syndrome: the seat belt sign, intestinal and mesenteric injuries. *The American Journal of Surgery*, *116*(6), 831–833.

Elhagediab, A. M., & Rouhana, S. W. (1998). Patterns of abdominal injury in frontal automotive crashes. In *The 16th International Technical Conference on the Enhanced Safety of Vehicles*.

Fedorov, A., Beichel, R., Kalpathy-Cramer, J., Finet, J., Fillion-Robin, J.-C., Pujol, S., … Sonka, M. (2012). 3D Slicer as an image computing platform for the Quantitative Imaging Network. *Magnetic Resonance Imaging*, *30*(9), 1323–1341.

Forman, J., Lopez-Valdes, F. J., Lessley, D., Kindig, M., Kent, R., & Bostrom, O. (2009). The effect of obesity on the restraint of automobile occupants. In *Annals of Advances in Automotive Medicine/Annual Scientific Conference* (Vol. 53, p. 25). Association for the Advancement of Automotive Medicine.

Forman, J., Lopez-Valdes, F., Lessley, D., Kindig, M., Kent, R., Ridella, S., & Bostrom, O. (2009). *Rear seat occupant safety: an investigation of a progressive force-limiting, pretensioning 3-point belt system using adult PMHS in frontal sled tests*. SAE Technical Paper.

Forman, J., Michaelson, J., Kent, R., Kuppa, S., & Bostrom, O. (2008). Occupant restraint in the rear seat: ATD responses to standard and pre-tensioning, force-limiting belt restraints. In *Annals of Advances in Automotive Medicine/Annual Scientific Conference* (Vol. 52, p. 141). Association for the

Advancement of Automotive Medicine.

Foster, C. D., Hardy, W. N., Yang, K. H., King, A. I., & Hashimoto, S. (2006). High-speed seatbelt pretensioner loading of the abdomen. *Stapp Car Crash Journal*, *50*, 27.

Frampton, R., Lenard, J., & Compigne, S. (2012). An in-depth study of abdominal injuries sustained by car occupants in frontal crashes. In *Annals of Advances in Automotive Medicine/Annual Scientific Conference* (Vol. 56, p. 137). Association for the Advancement of Automotive Medicine.

Garrett, J. W., & Braunstein, P. W. (1962). The seat belt syndrome. *Journal of Trauma and Acute Care Surgery*, *2*(3), 220–238.

Guettler, A. J., Bianco, S. T., Kemper, A. R., Albert, D. L., & Hardy, W. N. (2022). Submarining protection for 50th-percentile male anthropomorphic test devices in the rear seat during frontal crash sled tests. *SAE International Journal of Transportation Safety*, *10*(09-10-02–0016).

Håland, Y., & Nilson, G. (1993). Seat belt pretensioners to avoid the risk of submarining-a study of lap-belt slippage factors. In *Proceedings: International Technical Conference on the Enhanced Safety of Vehicles* (Vol. 1993, pp. 1060–1068). National Highway Traffic Safety Administration.

Hardy, W. N., Howes, M. K., Kemper, A. R., & Rouhana, S. W. (2015). Impact and injury response of the abdomen. In *Accidental Injury* (pp. 373–434). Springer.

Hardy, W. N., Shah, C. S., Kopacz, J. M., Yang, K. H., Van Ee, C. A., Morgan, R., & Digges, K. (2006). *Study of potential mechanisms of traumatic rupture of the aorta using insitu experiments*. SAE Technical Paper.

Horsch, J. D., & Hering, W. E. (1989). A kinematic analysis of lap-belt submarining for test dummies. *SAE Transactions*, 1847–1854.

Howes, M. K., Gregory, T. S., Hardy, W. N., & Beillas, P. D. (2012). *Kinematics of the thoracoabdominal contents under various loading scenarios*. SAE Technical Paper.

Howes, M. K., Hardy, W. N., & Beillas, P. (2013). The effects of cadaver orientation on the relative position of the abdominal organs. *Annals of Advances in Automotive Medicine*, *57*, 209.

Hu, J., Fischer, K., Lange, P., & Adler, A. (2015). *Effects of crash pulse, impact angle, occupant size, front seat location, and restraint system on rear seat occupant protection*. SAE Technical Paper.

Hu, J., Reed, M. P., Rupp, J. D., Fischer, K., Lange, P., & Adler, A. (2017). *Optimizing seat belt and airbag designs for rear seat occupant protection in frontal crashes*. SAE Technical Paper.

Huelke, D. F., & Compton, C. P. (1995). The effects of seat belts on injury severity of front and rear seat occupants in the same frontal crash. *Accident Analysis & Prevention*, *27*(6), 835–838.

Johannsen, H., Alonzo, F., & Schindler, V. (2007). Abdominal sensors for child dummies of the Q family, injury criteria and injury risk curves. In *International Research Council on Biomechanics of Injury (IRCOBI) Conference Proceedings*.

Kearney, P. A. (1989). Blunt trauma to the abdomen. *Annals of Emergency Medicine*, *18*(12), 1322–1325.

Kent, R., Forman, J., Parent, D., & Kuppa, S. (2007). Rear seat occupant protection in frontal crashes and its feasibility. In *20th International Conference on the Enhanced Safety of Vehicles* (pp. 18–21).

Klinich, K. D., Flannagan, C. A. C., Nicholson, K., Schneider, L. W., & Rupp, J. D. (2010). *Factors associated with abdominal injury in frontal, farside, and nearside crashes*. SAE Technical Paper.

Kuppa, S., Saunders, J., & Fessahaie, O. (2005). Rear seat occupant protection in frontal crashes. In *19th International Conference on the Enhanced Safety of Vehicles*. Citeseer.

Lamielle, S., Cuny, S., Foret-Bruno, J.-Y., Petit, P., Vezin, P., Verriest, J.-P., & Guillemot, H. (2006). Abdominal injury patterns in real frontal crashes: influence of crash conditions, occupant seat and restraint systems. In *Annual Proceedings/Association for the Advancement of Automotive Medicine* (Vol. 50, p. 109). Association for the Advancement of Automotive Medicine.

Lau, I. V, & Viano, D. C. (1986). The viscous criterion—bases and applications of an injury severity index for soft tissues. *SAE Transactions*, 672–691.

Lee, J. B., & Yang, K. H. (2002). Abdominal injury patterns in motor vehicle accidents: a survey of the NASS database from 1993 to 1997. *Traffic Injury Prevention*, *3*(3), 241–246.

Leung, Y. C., Tarriere, C., Fayon, A., Mairesse, P., & Banzet, P. (1981). An anti-submarining scale determined from theoretical and experimental studies using three-dimensional geometrical definition of the lap-belt. *SAE Transactions*, *90*, 3232–3253.

Leung, Y. C., Tarriere, C., Fayon, A., Mairesse, P., Delmas, A., & Banzet, P. (1979). A comparison between part 572 dummy and human subject in the problem of submarining. *SAE Transactions*, 3537–3556.

Leung, Y. C., Tarriere, C., Lestrelin, D., Got, C., Guillon, F., Patel, M. M., & Hureau, J. (1982). Submarining injuries of 3-point belted occupants in frontal collisions-description, mechanisms and protection. In *Proceedings: Stapp Car Crash Conference* (Vol. 26, pp. 173–205). Society of Automotive Engineers SAE.

Luet, C., Trosseille, X., Drazétic, P., Potier, P., & Vallancien, G. (2012). Kinematics and Dynamics of the Pelvis in the Process of Submarining using PMHS Sled Tests. *Stapp Car Crash Journal*, *56*, 411.

Mayrose, J., & Priya, A. (2008). The safest seat: effect of seating position on occupant mortality. *Journal of Safety Research*, *39*(4), 433–436.

Michaelson, J., Forman, J., Kent, R., & Kuppa, S. (2008). *Rear seat occupant safety: kinematics and injury of PMHS restrained by a standard 3-point belt in frontal crashes*. SAE Technical Paper.

Miller, M. A. (1989). The biomechanical response of the lower abdomen to belt restraint loading. *The Journal of Trauma*, *29*(11), 1571–1584.

Mitchell, R. J., Bambach, M. R., & Toson, B. (2015). Injury risk for matched front and rear seat car passengers by injury severity and crash type: An exploratory study. *Accident Analysis & Prevention*, *82*, 171–179.

Moore, K. L., Dalley, A. F., & Agur, A. M. R. (2013). *Clinically oriented anatomy*. Lippincott Williams & Wilkins.

Nie, B., Gan, S., Chen, W., & Zhou, Q. (2020). Seating preferences in highly automated vehicles and occupant safety awareness: A national survey of Chinese perceptions. *Traffic Injury Prevention*, *21*(4), 247–253.

Nilson, G., & Håland, Y. (1995). An analytical method to assess the risk of the lap-belt slipping off the pelvis in frontal impacts. *SAE Transactions*, 2928–2939.

Padgaonkar, A. J., Lawson, S. M., & King, A. I. (1978). Anatomical coordinate systems for human body segments. In *Proceedings of the Human Factors and Ergonomic Society annual meeting* (Vol. 22, pp. 676–679). SAGE Publishing.

Padmanaban, J., & Ray, R. M. (1992). *Safety performance of rear seat occupant restraint systems*. SAE

Technical Paper.

Parenteau, C., & Viano, D. C. (2003). *Field data analysis of rear occupant injuries part I: adults and teenagers*. SAE Technical Paper.

Ramachandra, R., Kang, Y.-S., Bolte, J. H., Hagedorn, A., Herriott, R., Stammen, J. A., & Moorhouse, K. (2016). *Biomechanical responses of PMHS subjected to abdominal seatbelt loading*. SAE Technical Paper.

Rouhana, S. W. (1987). *Abdominal injury prediction in lateral impact-an analysis of the biofidelity of the Euro-SID abdomen*. SAE Technical Paper.

Rouhana, S. W., Horsch, J. D., & Kroell, C. K. (1989). *Assessment of Lap-ShouIder Belt Restraint Performance in Laboratory Testing*. SAE Technical Paper.

Rouhana, S. W., Jedrzejczak, E. A., & McCleary, J. D. (1990). Assessing submarining and abdominal injury risk in the Hybrid III family of dummies: part II—development of the small female frangible abdomen. *SAE Technical Paper*, 1760–1788.

Rouhana, S. W., Lau, I. V, & Ridella, S. A. (1985). Influence of velocity and forced compression on the severity of abdominal injury in blunt, nonpenetrating lateral impact. *The Journal of Trauma*, *25*(6), 490–500.

Rouhana, S. W., Viano, D. C., Jedrzejczak, E. A., & Mccleary, J. D. (1989). Assessing Submarining and Abdominal Injury Risk in the Hybrid III Family of Dummies, *98*(1989), 1824–1846.

Rutledge, R., Thomason, M., Oller, D., Meredith, W., Moylan, J., Clancy, T., … Baker, C. (1991). The spectrum of abdominal injuries associated with the use of seat belts. *The Journal of Trauma*, *31*(6), 820–825.

Smith, K.M., & Cummings, P. (2006). Passenger seating position and the risk of passenger death in traffic crashes: a matched cohort study. *Injury Prevention*, *12*(2), 83–86.

Smith, Kathleen M, & Cummings, P. (2004). Passenger seating position and the risk of passenger death or injury in traffic crashes. *Accident Analysis & Prevention*, *36*(2), 257–260.

Society of Automotive Engineers. (2014). SAE J 211-1: Instrumentation for Impact Test - Part 1 - Electronic Instrumentation. SAE International. https://doi.org/https://doi.org/10.4271/J211/1_201403 UI - J211/1_201403

Tanaka, Y., Nakashima, A., Feng, H., Mizuno, K., Yamada, M., Yamada, Y., … Jinzaki, M. (2022). *Analysis of lap belt fit to human subjects using CT images*. SAE Technical Paper.

Tatem, W. M., & Gabler, H. C. (2019). Differential fatality risk between rear and front seat passenger vehicle occupants in frontal crashes. In *Proceedings of the 2019 International IRCOBI Conference on the Biomechanics of Injury* (pp. 554–560).

Trosseille, X., Petit, P., Uriot, J., Potier, P., Baudrit, P., Richard, O., … Douard, R. (2018). Reference PMHS sled tests to assess submarining of the small female. *Stapp Car Crash Journal*, *62*, 93–118.

Tylko, S., & Dalmotas, D. J. (2005). Protection of rear seat occupants in frontal crashes. In *Proceedings: International Technical Conference on the Enhanced Safety of Vehicles* (Vol. 2005, pp. 8p-8p). National Highway Traffic Safety Administration.

Uriot, J., Potier, P., Baudrit, P., Trosseille, X., Petit, P., Richard, O., … Douard, R. (2015). Reference PMHS sled tests to assess submarining. *Stapp Car Crash Journal*, *59*, 203.

Uriot, J., Potier, P., Baudrit, P., Trosseille, X., Richard, O., & Douard, R. (2015). Comparison of HII, HIII and THOR dummy responses with respect to PMHS sled tests. In *Proceedings of the International Research Conference on the Biomechanics of Impact, IRCOBI, Lyon, France, 9th September-11th September*. *IRC-15-55*.

Viano, D. C., & Lau, I. V. (1985). *Thoracic impact: a viscous tolerance criterion* (No. 856025). *SAE Technical Paper*.

Viano, D. C., & Lau, I. V. (1988). A viscous tolerance criterion for soft tissue injury assessment. *Journal of Biomechanics, 21*(5), 387–399.

Walfisch, G., Fayon, A., Tarriere, C., Rosey, J. P., Guillon, F., Got, C., … Stalnaker, R. L. (1980). *Designing of a dummy's abdomen for detecting injuries in side impact collisions*.

Zellmer, H., Lührs, S., & Brüggemann, K. (1998). Optimized restraint systems for rear seat passengers. *Thorax, 7*, 1.

Zhu, M., Cummings, P., Chu, H., & Cook, L. J. (2007). Association of rear seat safety belt use with death in a traffic crash: a matched cohort study. *Injury Prevention*, *13*(3), 183–185.

Appendix A: Seat Characteristics

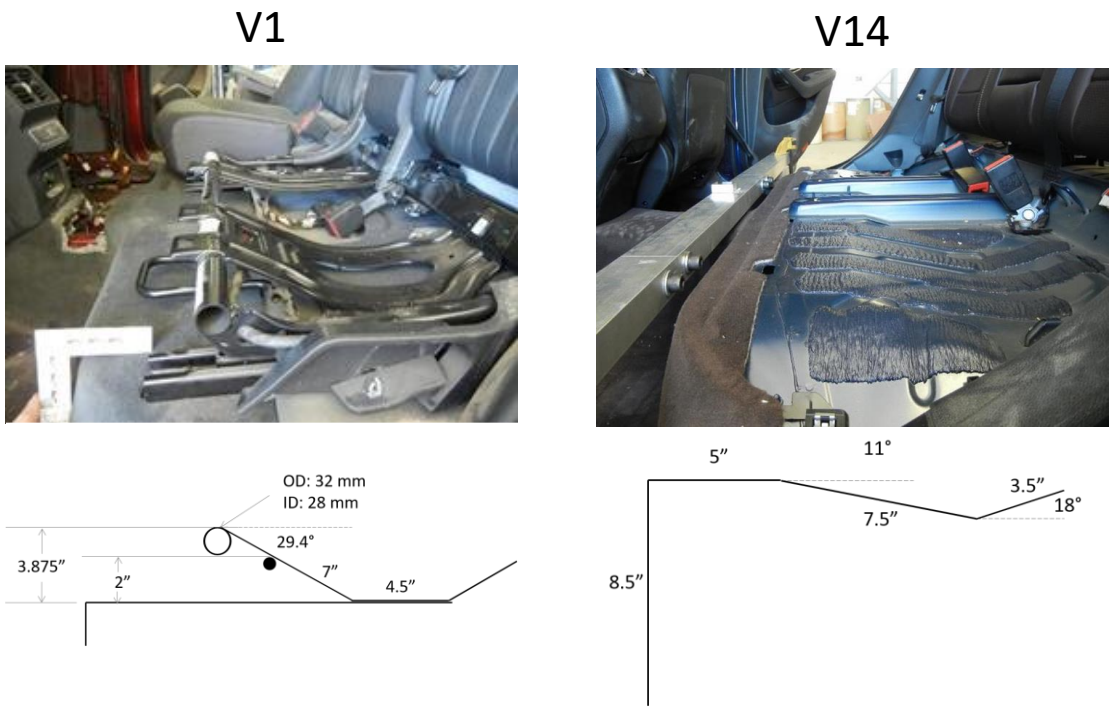

Figure 64. Seat characteristics for vehicles V1 and V14, which provided excellent submarining protection for the THOR.

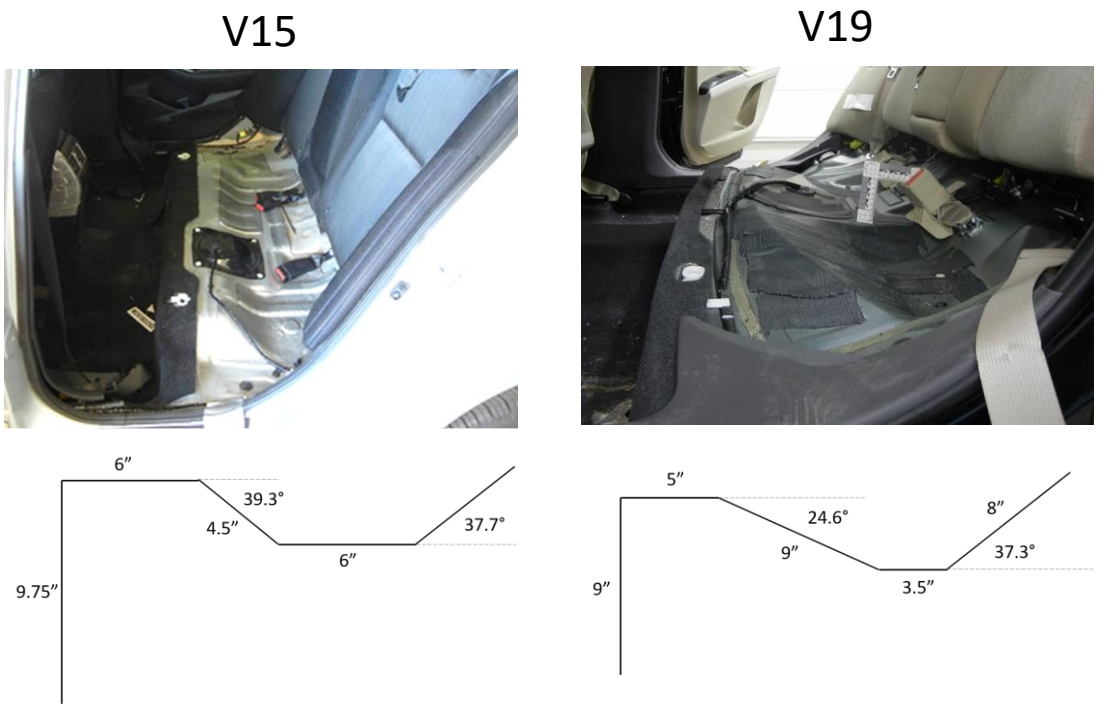

Figure 65. Seat characteristics for vehicles V15 and V19, which provided some submarining protection for the THOR.

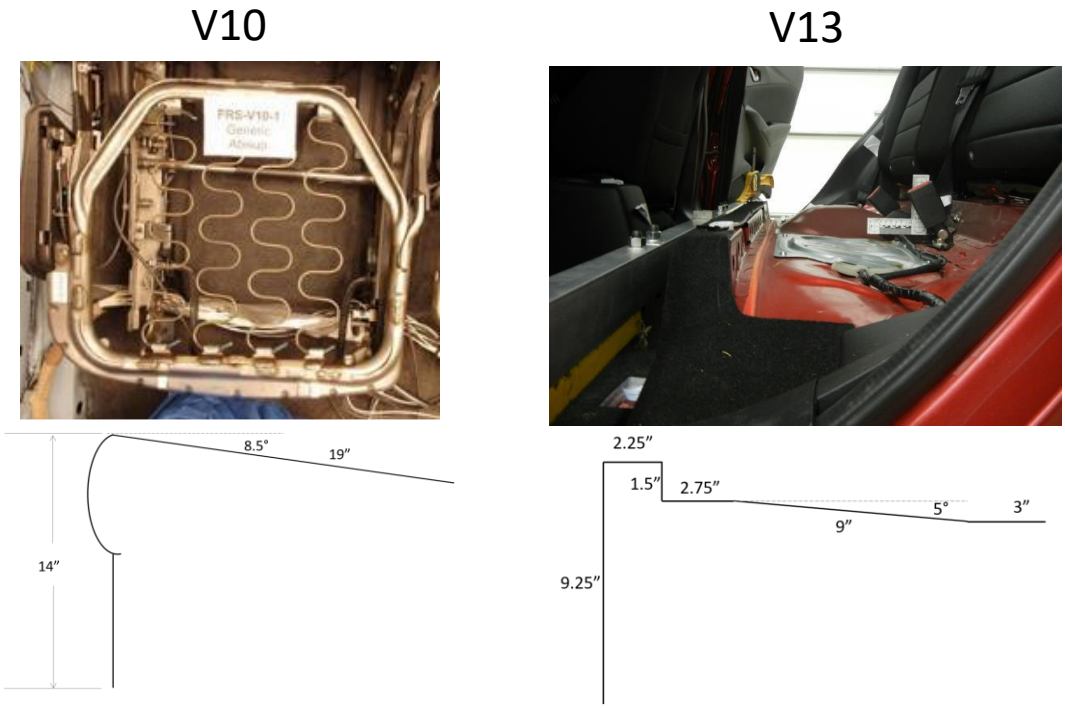

Figure 66. Seat characteristics for vehicles V10 and V13, which provided no submarining protection for the THOR.

V6

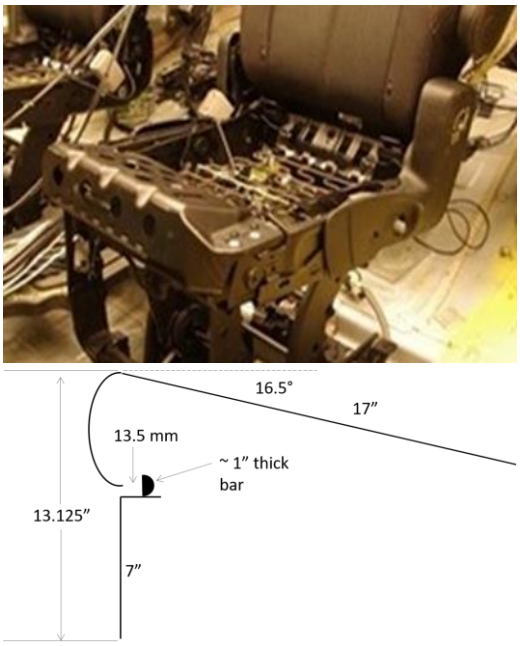

Figure 67. Seat characteristics for vehicle V6, which provided good submarining protection for the THOR, but had characteristics similar to those in the poor group.

Appendix B: Sled Accelerations

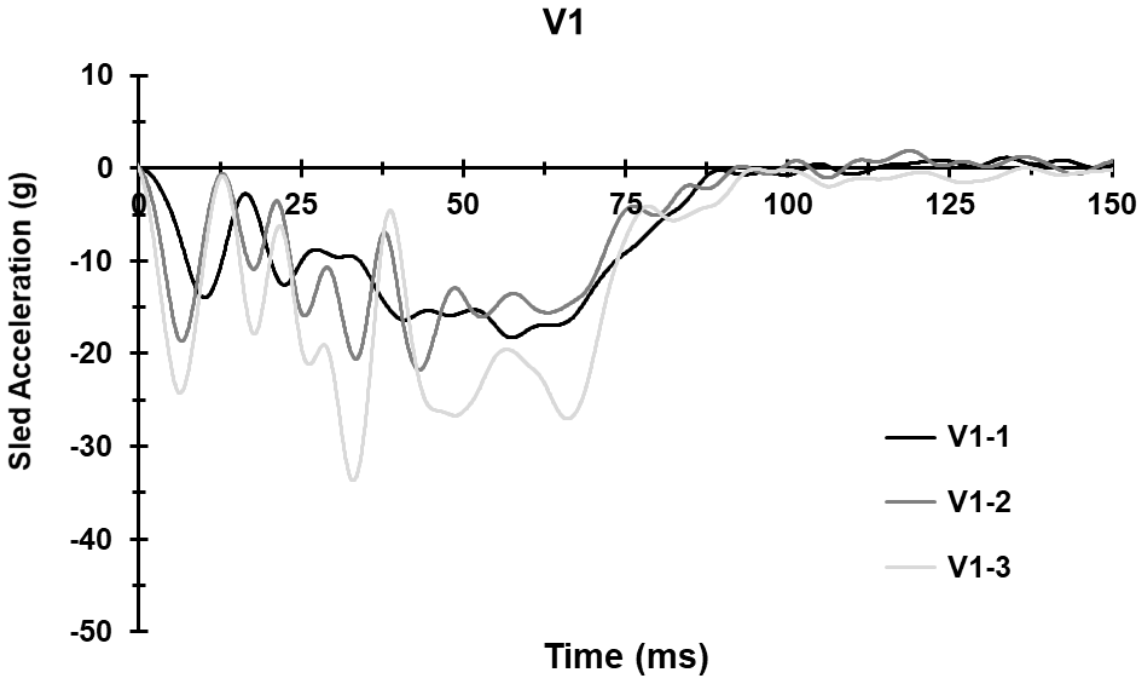

Figure 68. Vehicle V1 sled accelerations (g)

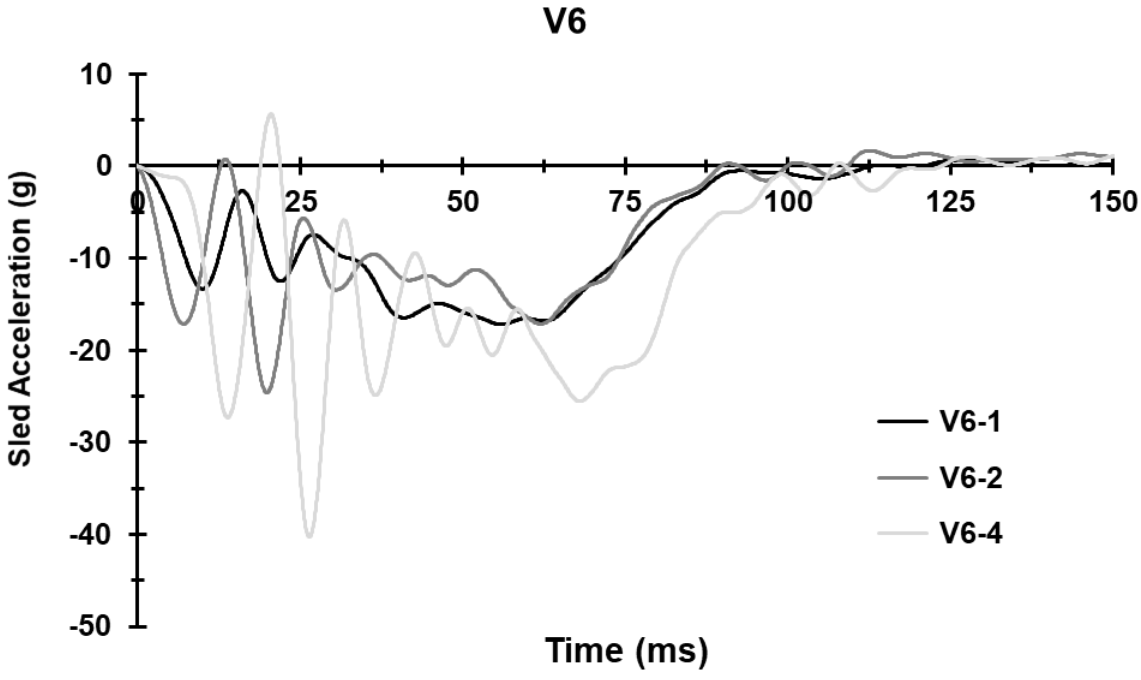

Figure 69. Vehicle V6 sled accelerations (g)

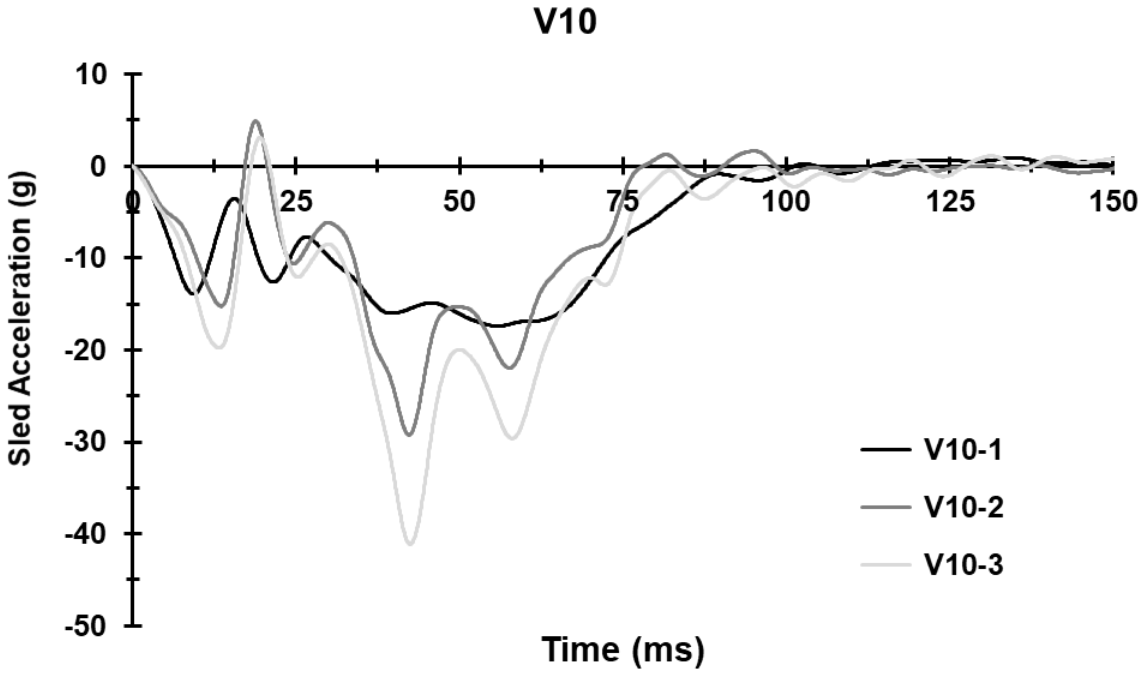

Figure 70. Vehicle V10 sled accelerations (g)

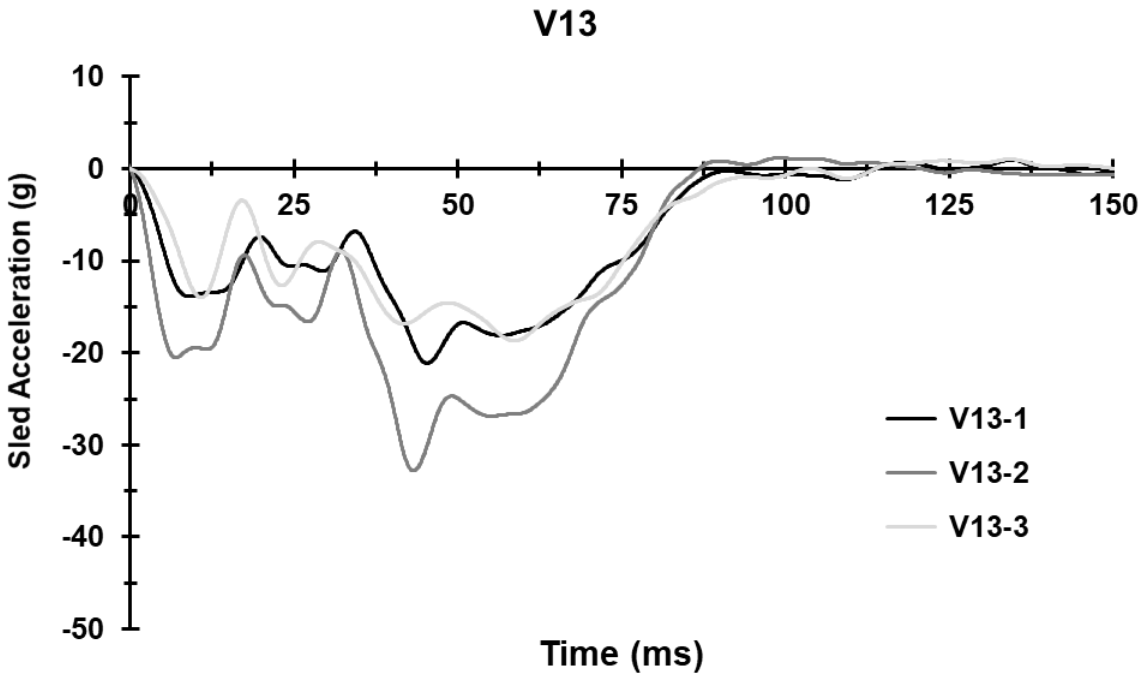

Figure 71. Vehicle V13 sled accelerations (g) for ATD tests

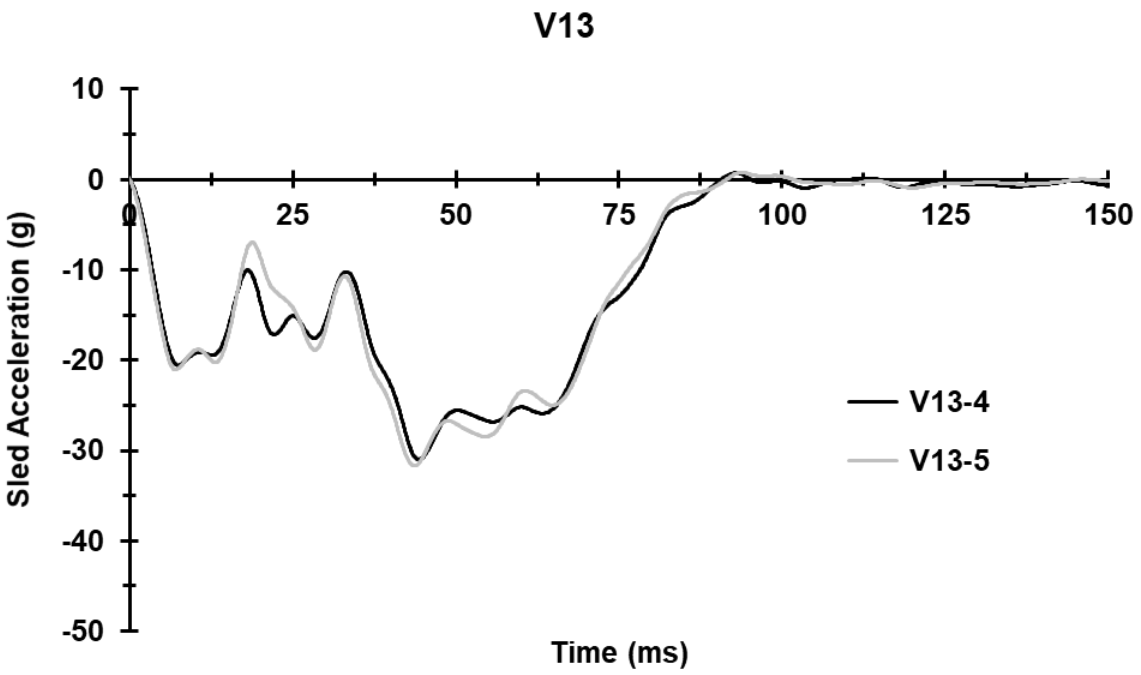

Figure 72. Vehicle V13 sled accelerations (g) for PMHS tests

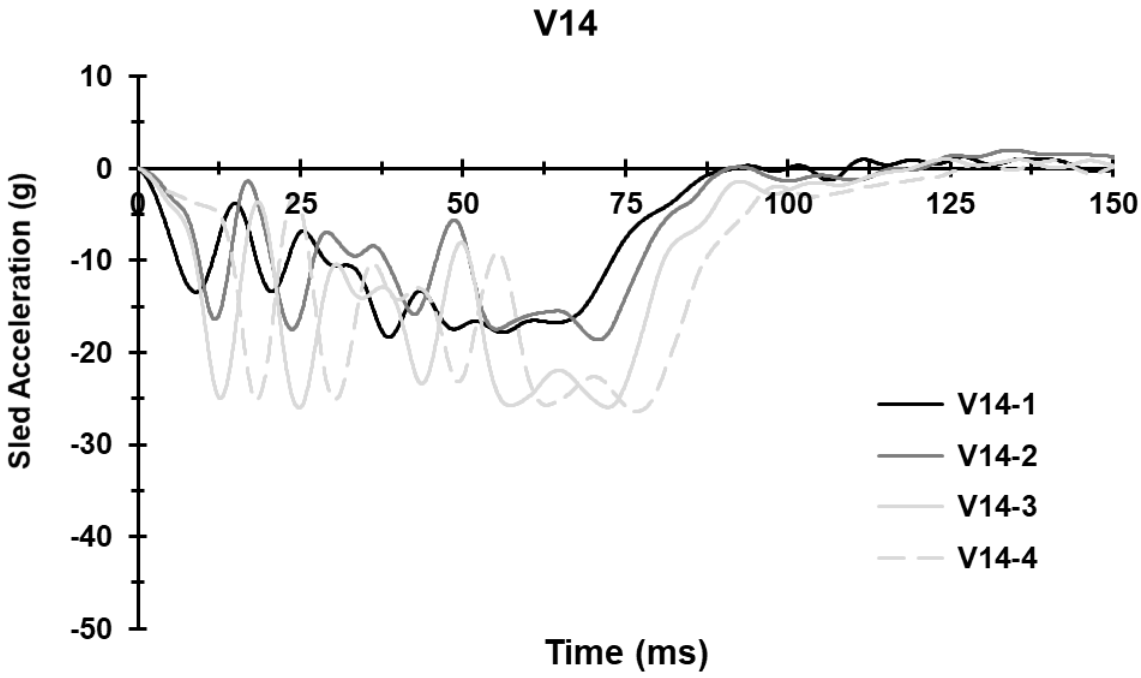

Figure 73. Vehicle V14 sled accelerations (g) for ATD tests

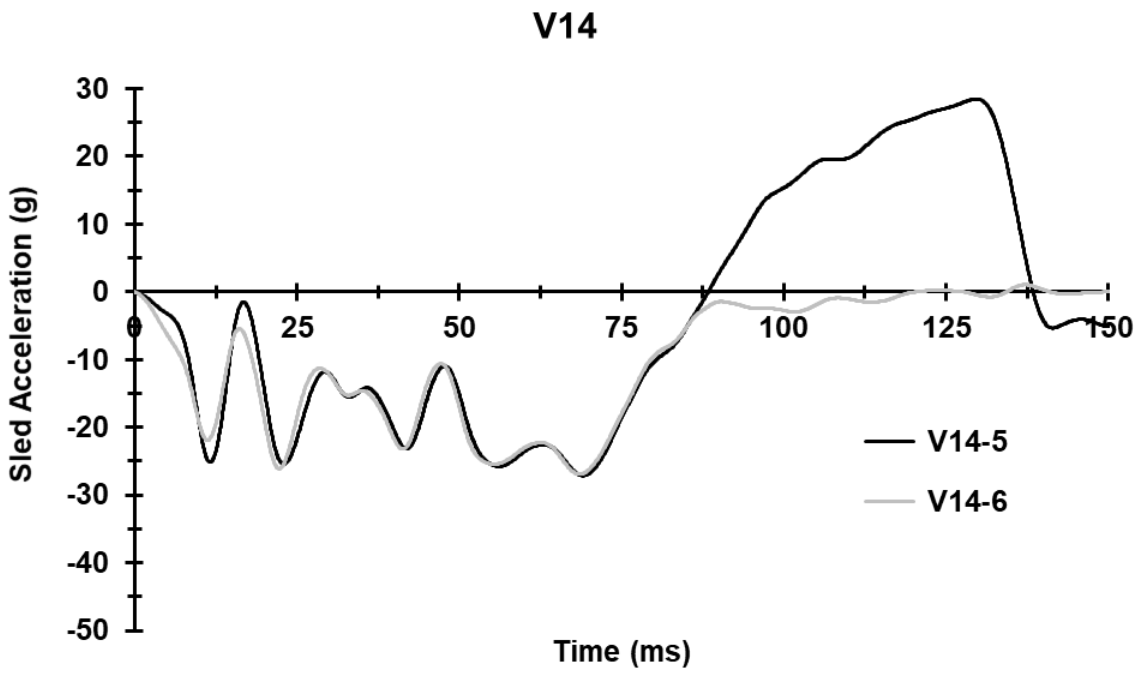

Figure 74. Vehicle V14 sled accelerations (g) for PMHS tests

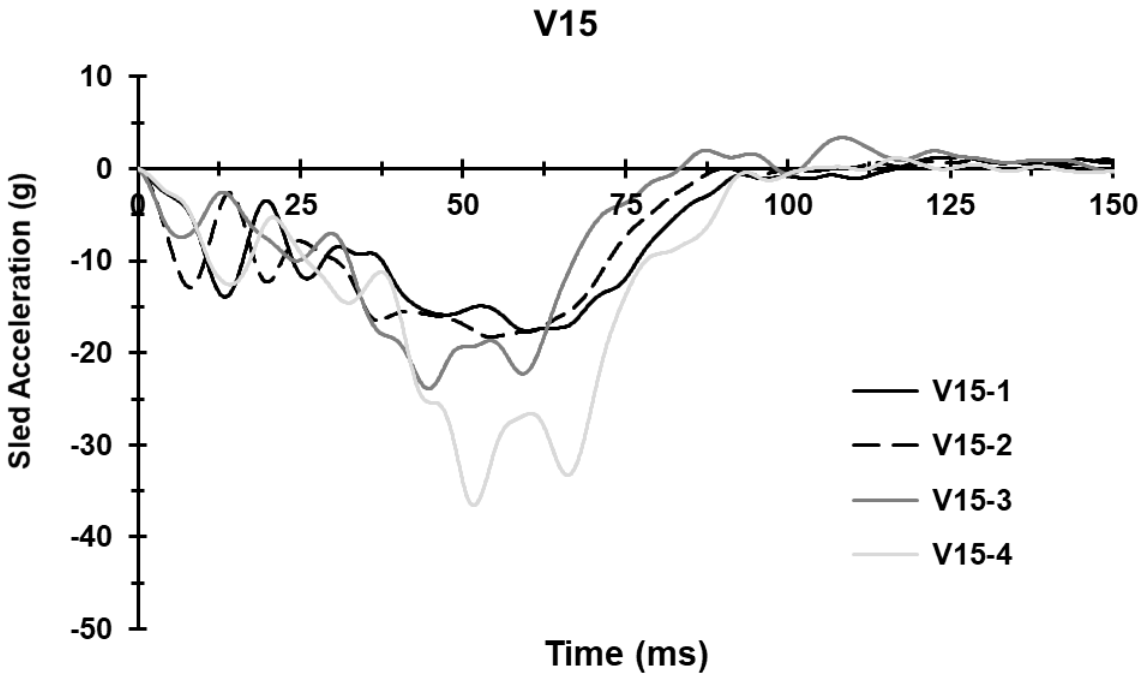

Figure 75. Vehicle V15 sled accelerations (g) for ATD tests

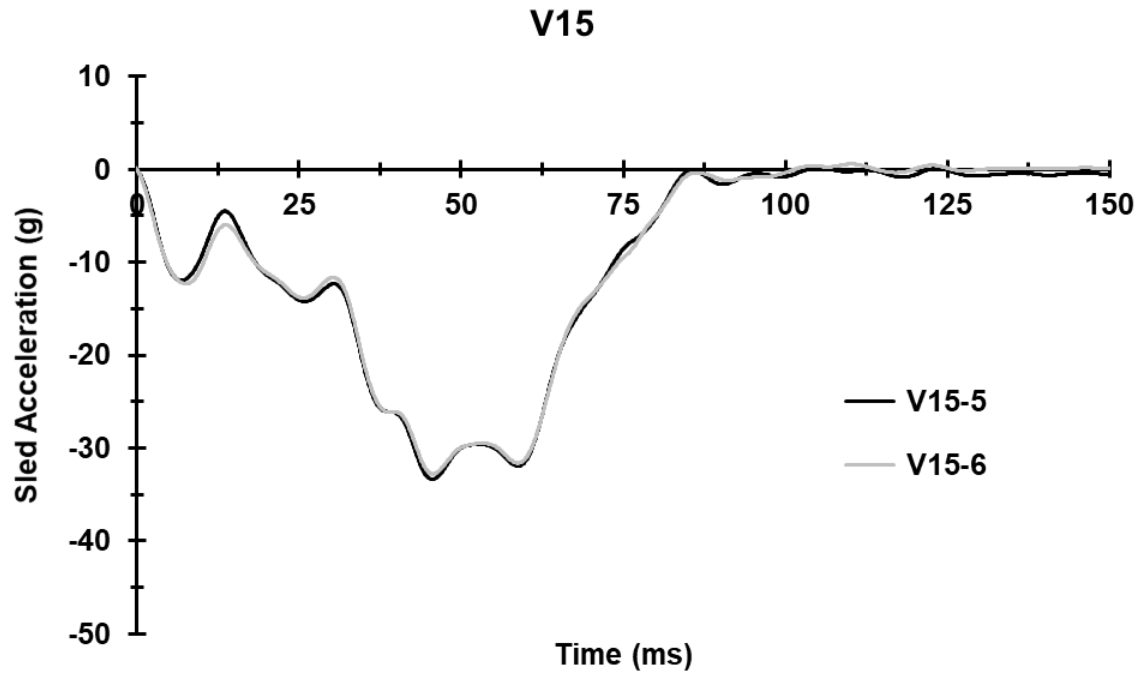

Figure 76. Vehicle V15 sled accelerations (g) for PMHS tests.

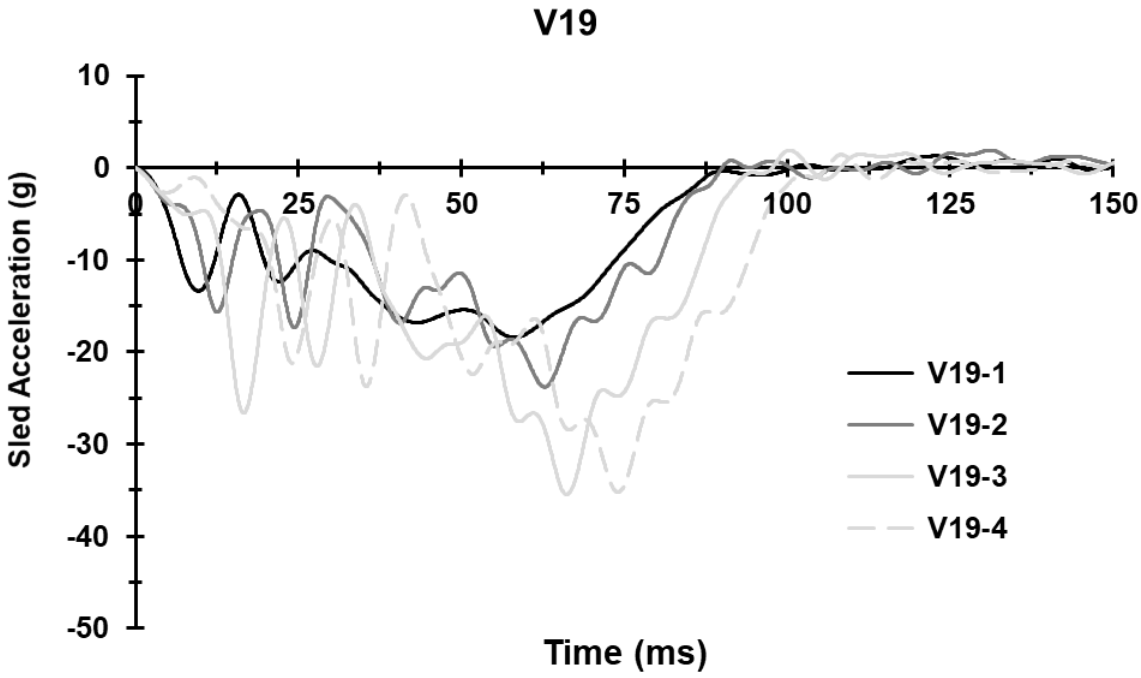

Figure 77. Vehicle V19 sled accelerations (g) for ATD tests

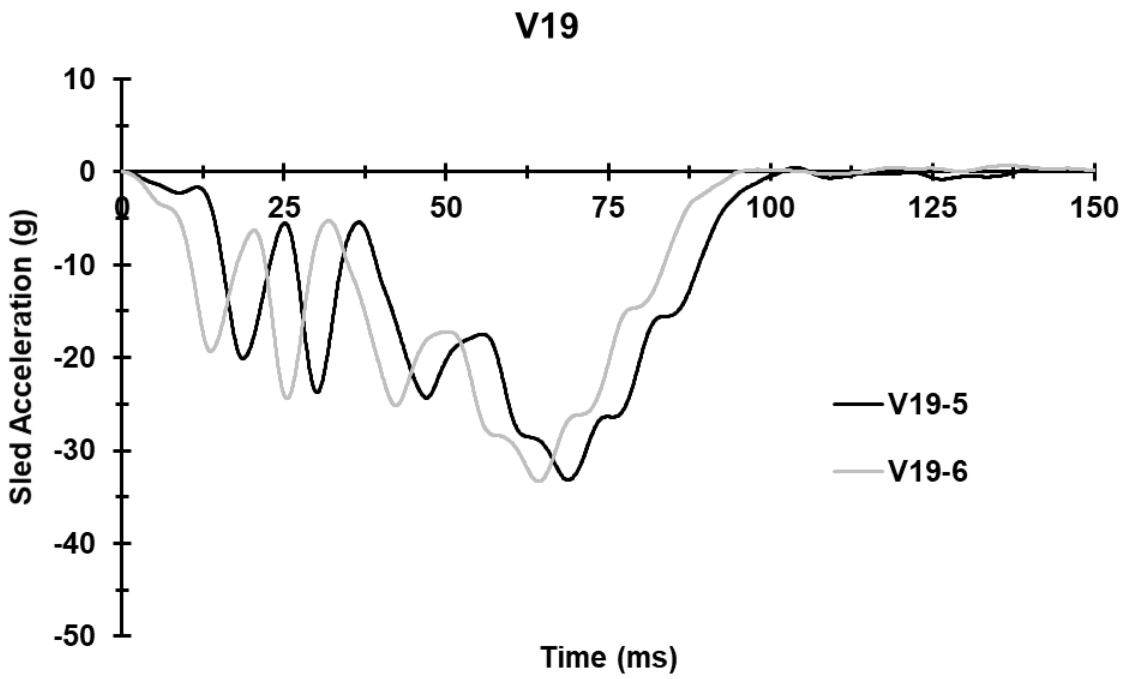

Figure 78. Vehicle V19 sled accelerations (g) for PMHS tests

Appendix C: THOR Abdominal Insert Comparisons

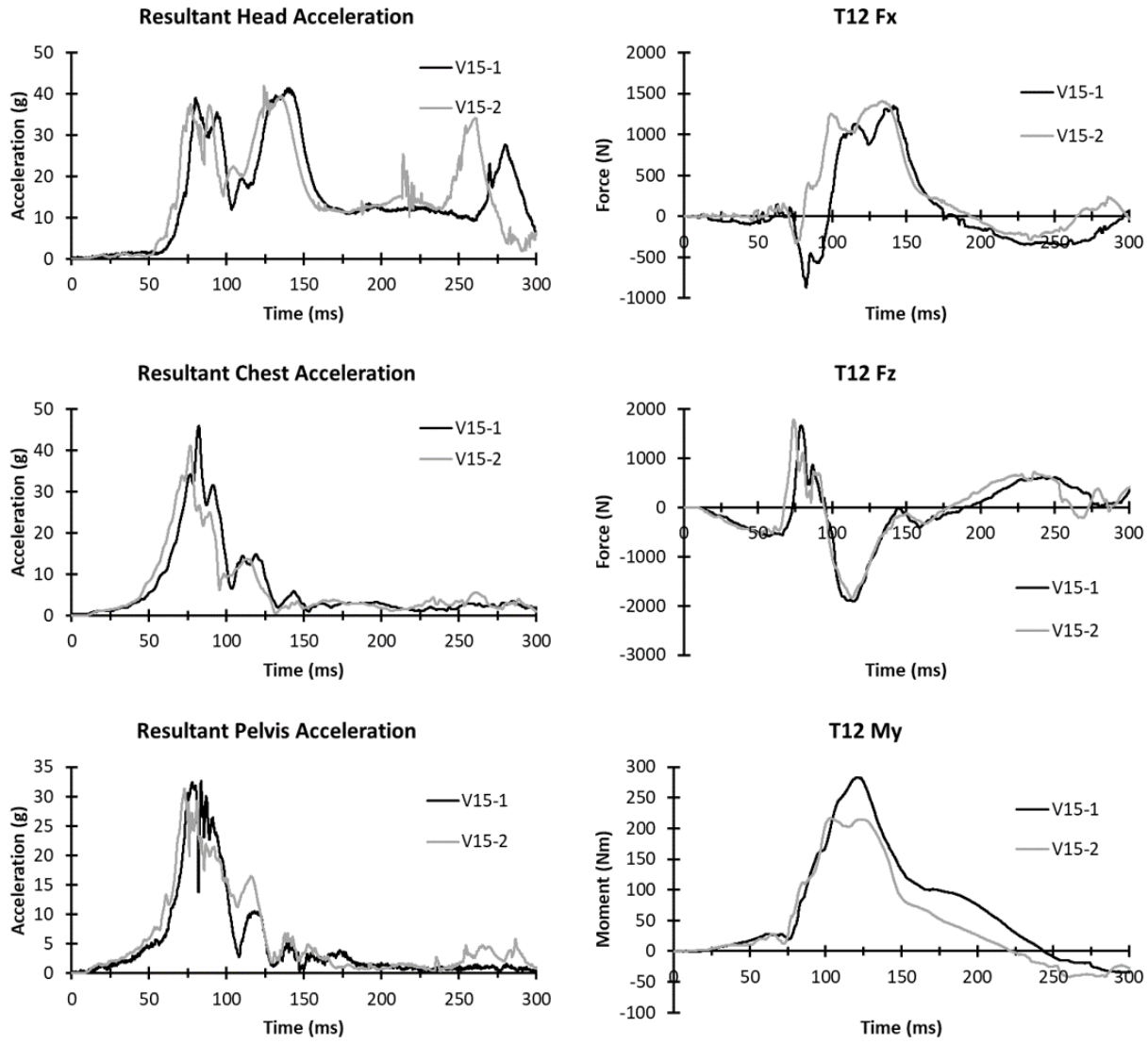

Figure 79. Un-shifted resultant head, chest, and pelvis acceleration for the THOR-50M (left) and the T12 Fx, Fz, and My (right). THOR had standard abdomen (black, V15-1) and ABISUP abdomen (gray, V15-2).

Appendix D: THOR ASIS Loads

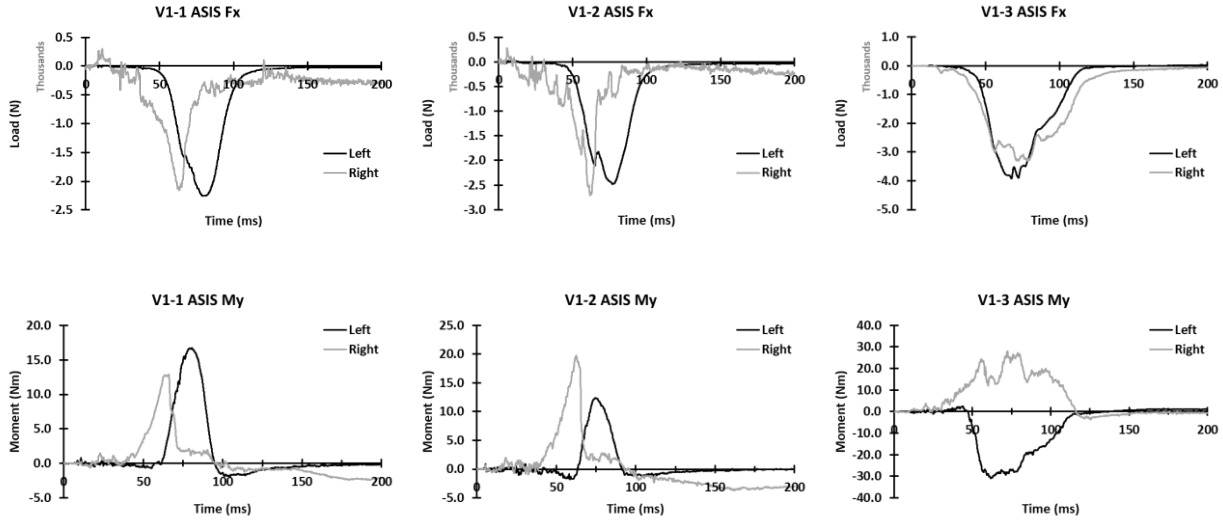

Figure 80. THOR ASIS Fx (top row) and My (bottom row) in vehicle V1

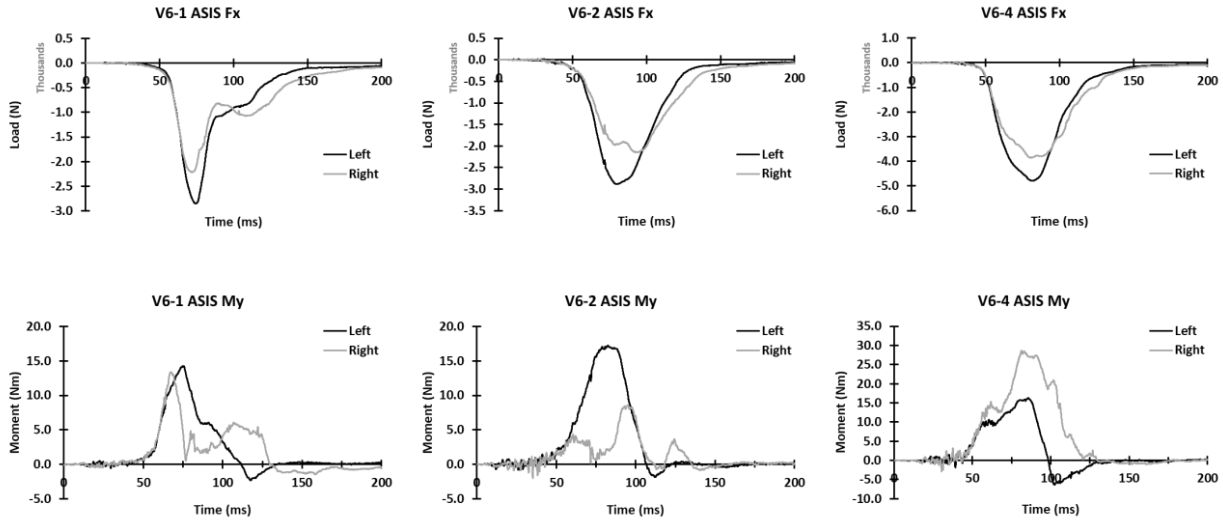

Figure 81. THOR ASIS Fx (top row) and My (bottom row) in vehicle V6

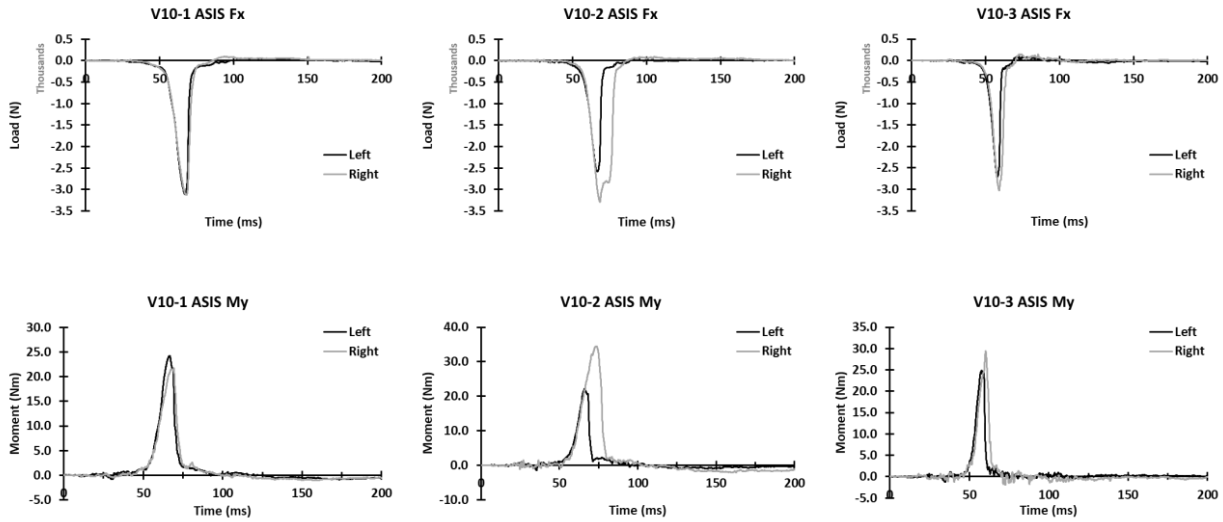

Figure 82. THOR ASIS Fx (top row) and My (bottom row) in vehicle V10

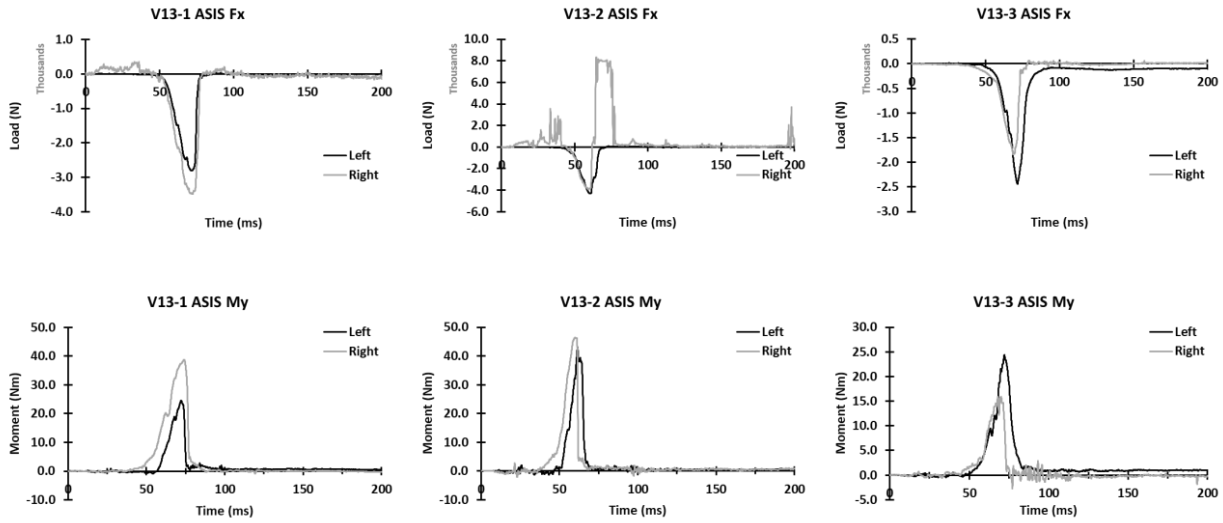

Figure 83. THOR ASIS Fx (top row) and My (bottom row) in vehicle V13

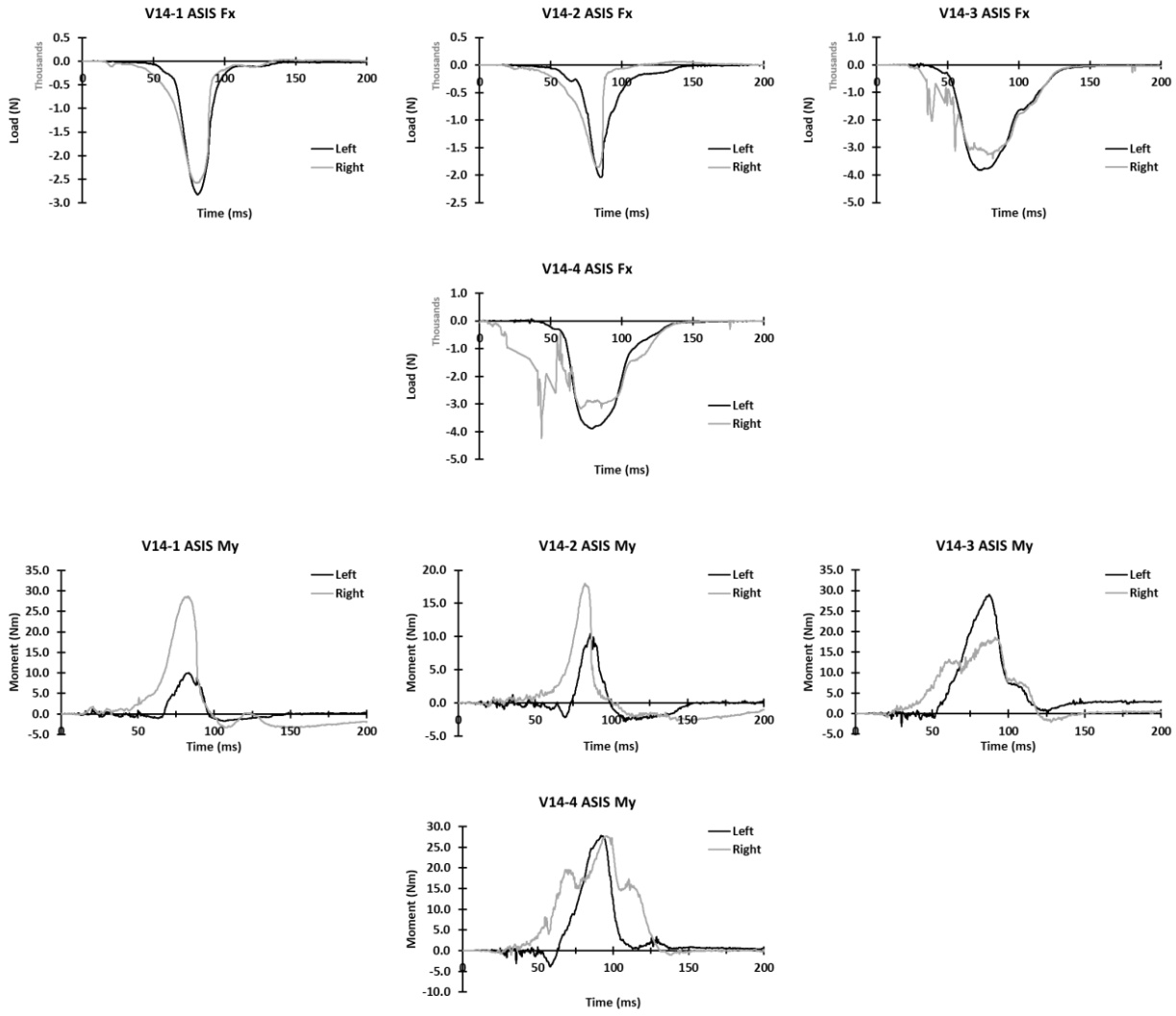

Figure 84. THOR ASIS Fx (top rows) and My (bottom rows) in vehicle V14

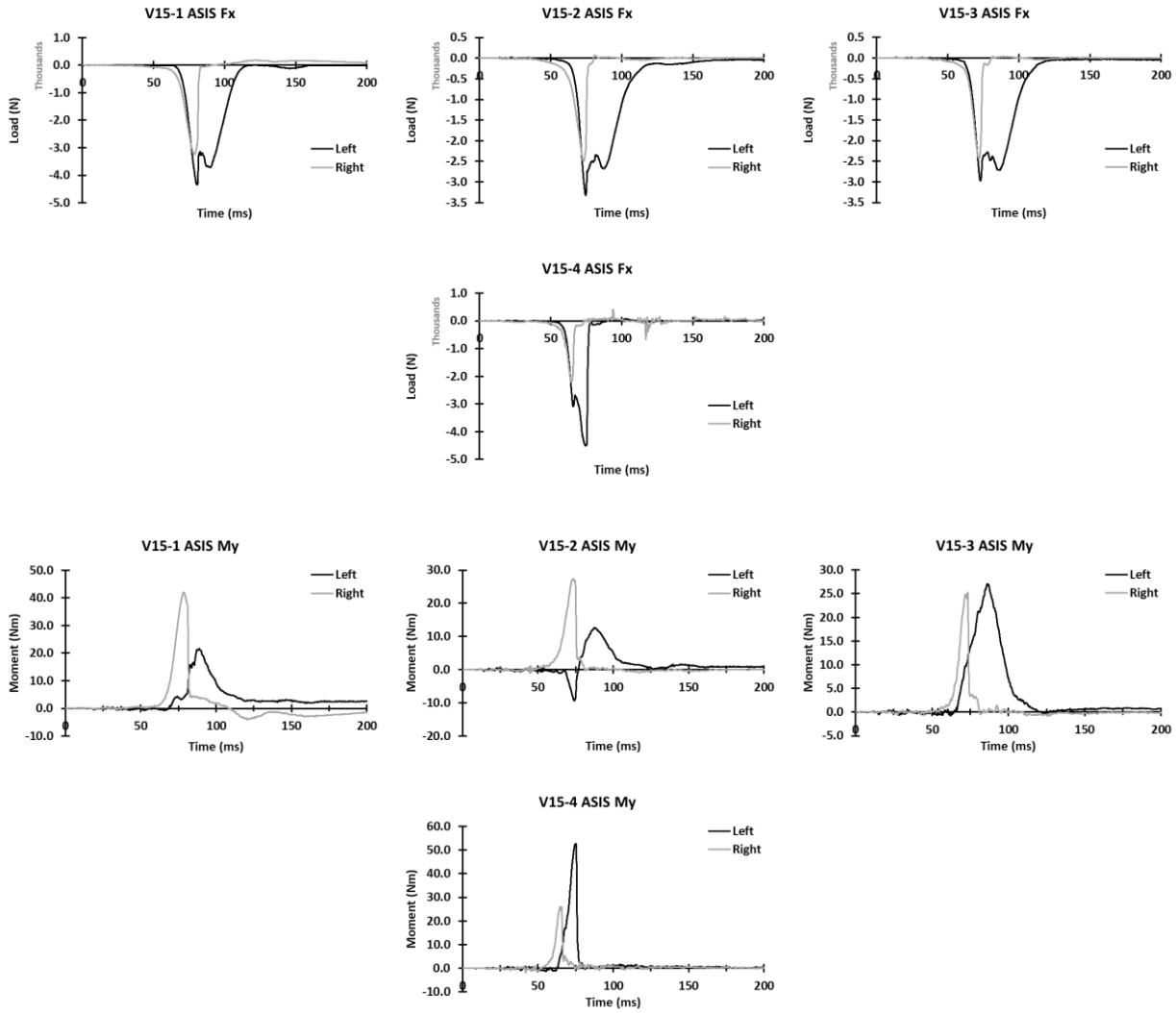

Figure 85. THOR ASIS Fx (top rows) and My (bottom rows) in vehicle V15

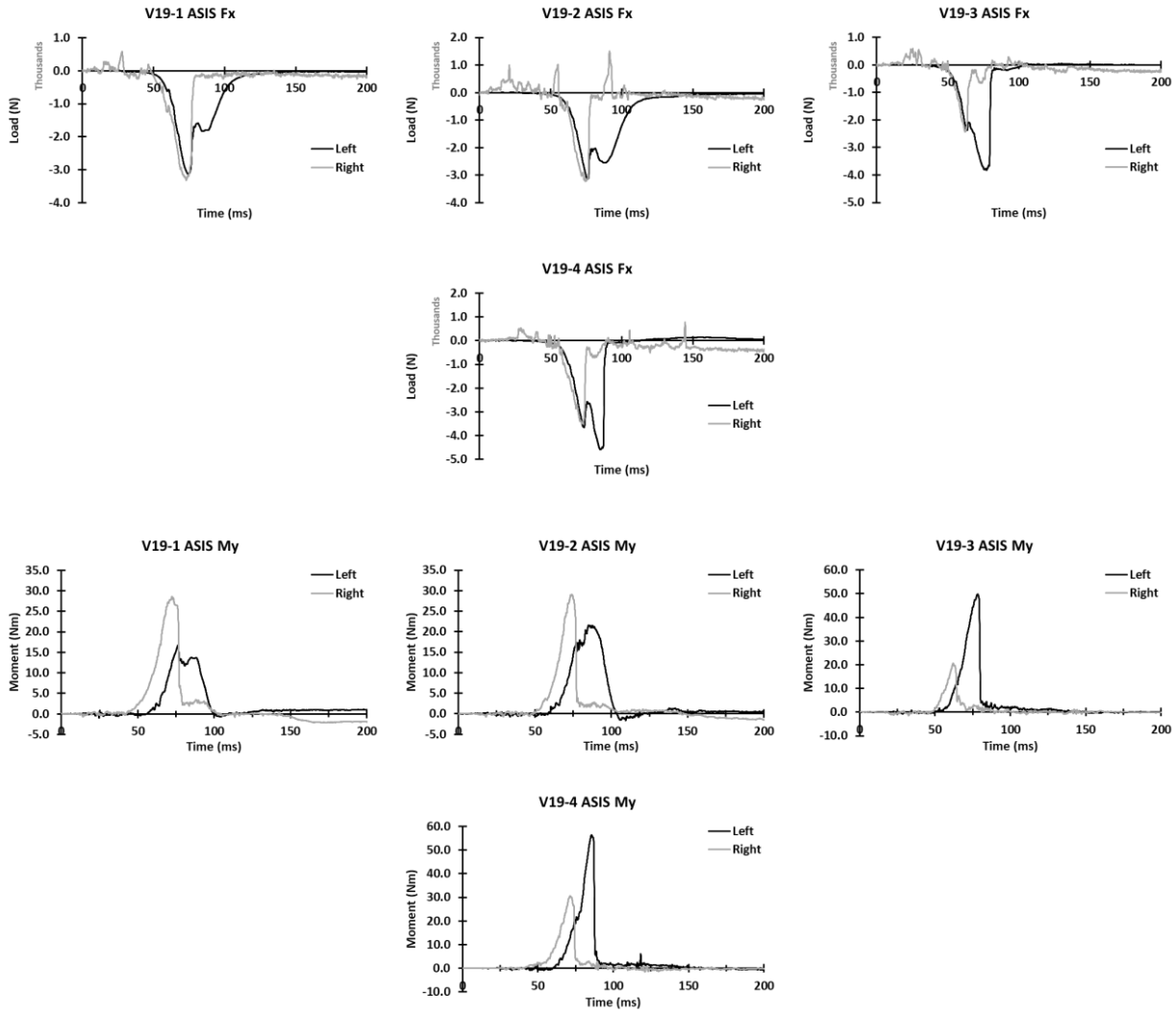

Figure 86. THOR ASIS Fx (top rows) and My (bottom rows) in vehicle V19

Appendix E: THOR Abdominal Loading

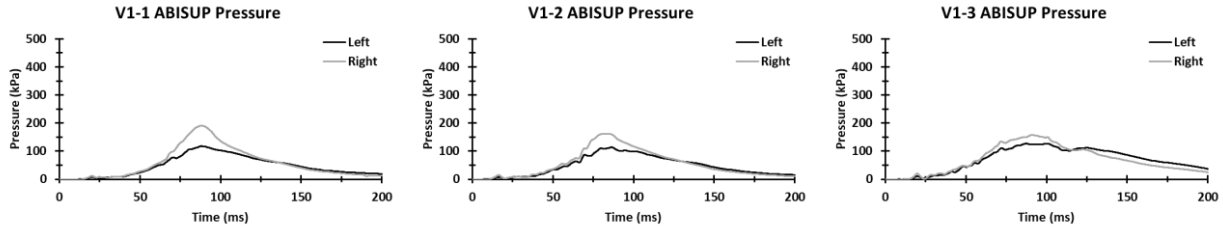

Figure 87. THOR ABISUP pressure (kPa) for vehicle V1

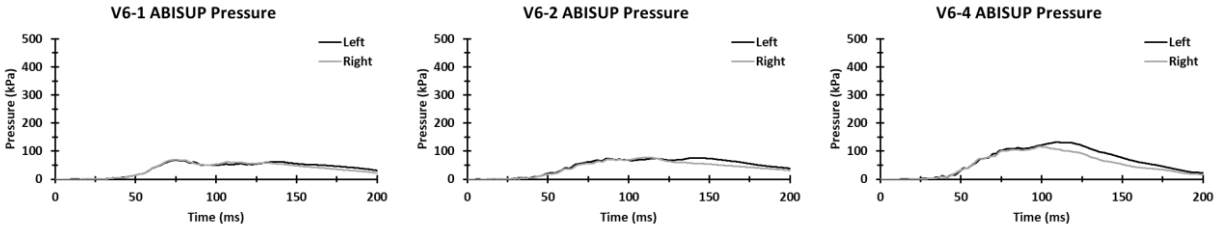

Figure 88. THOR ABISUP pressure (kPa) for vehicle V6

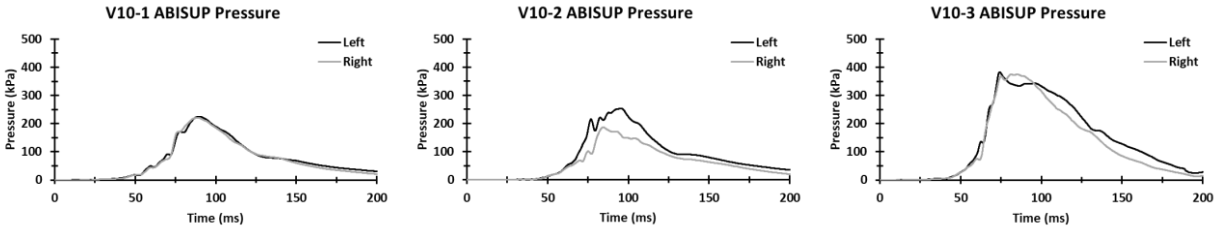

Figure 89. THOR ABISUP pressure (kPa) for vehicle V10

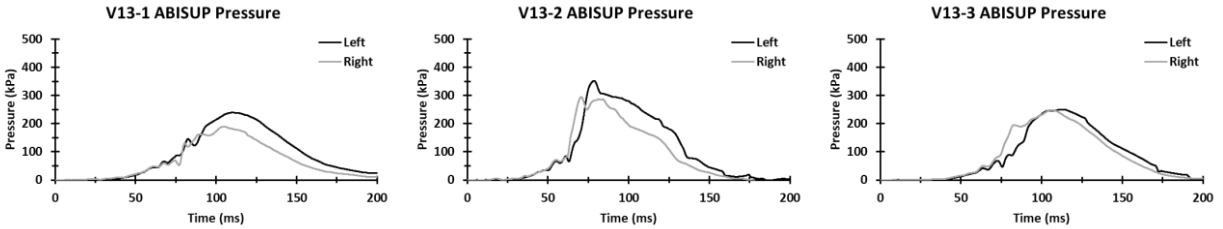

Figure 90. THOR ABISUP pressure (kPa) for vehicle V13

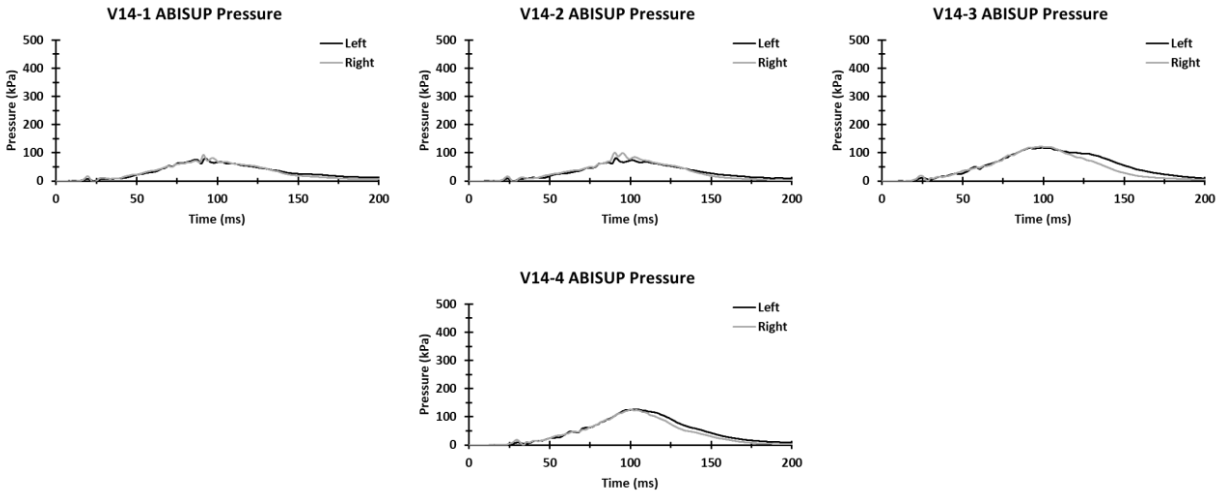

Figure 91. THOR ABISUP pressure (kPa) for vehicle V14

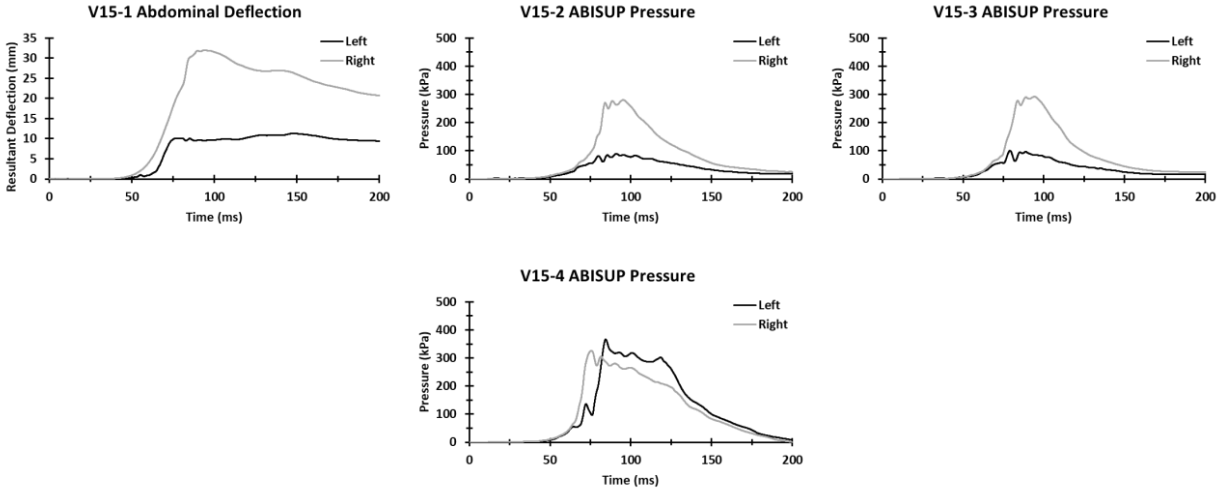

Figure 92. THOR abdominal deflection (mm) and ABISUP pressure (kPa) for vehicle V15

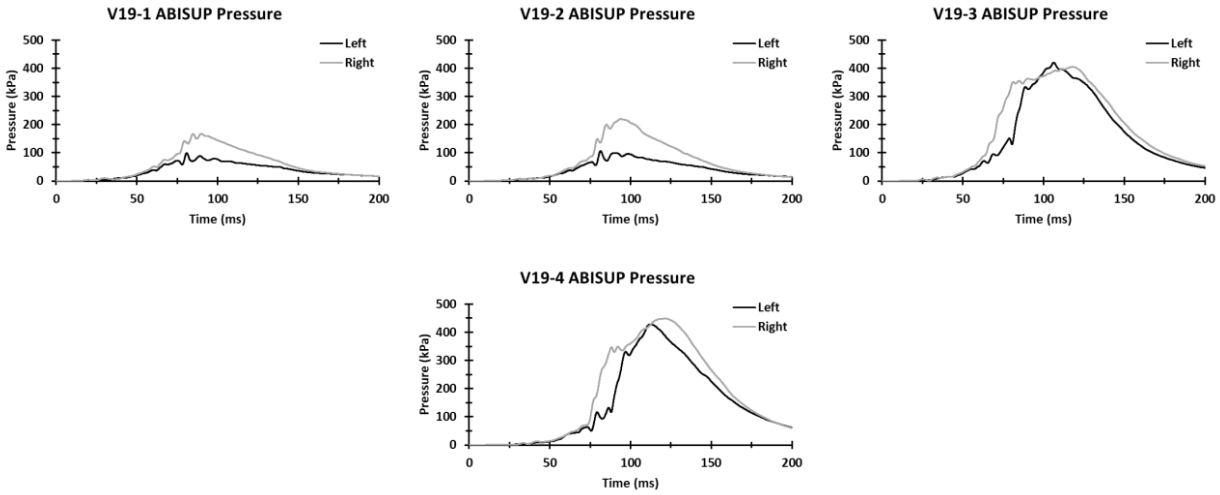

Figure 93. THOR ABISUP pressure (kPa) for vehicle V19

Appendix F: ATD Belt Loads

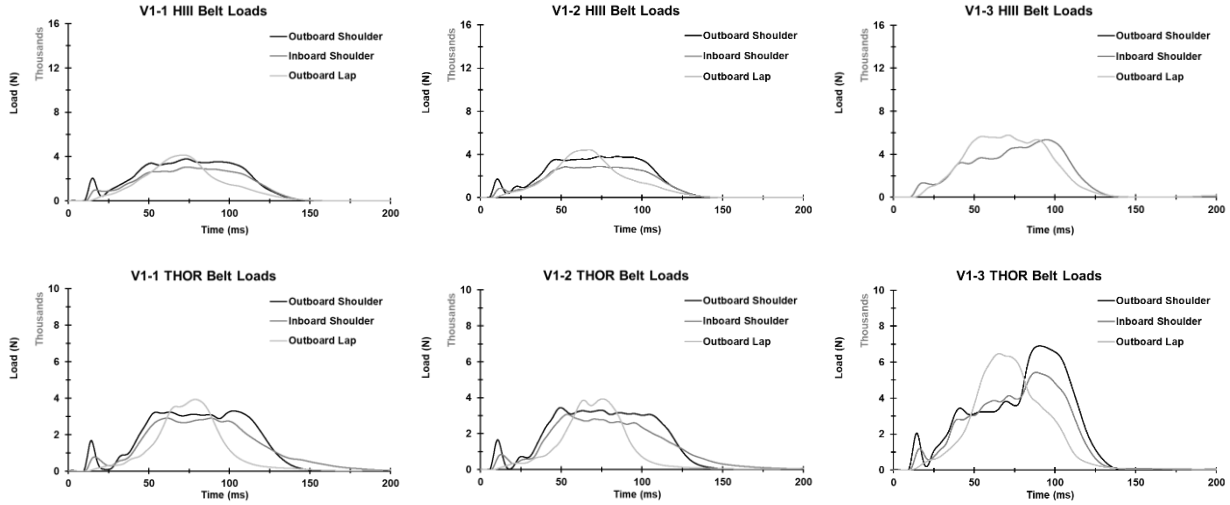

Figure 94. Belt loads for the HIII (top row) and THOR (bottom row) in vehicle V1

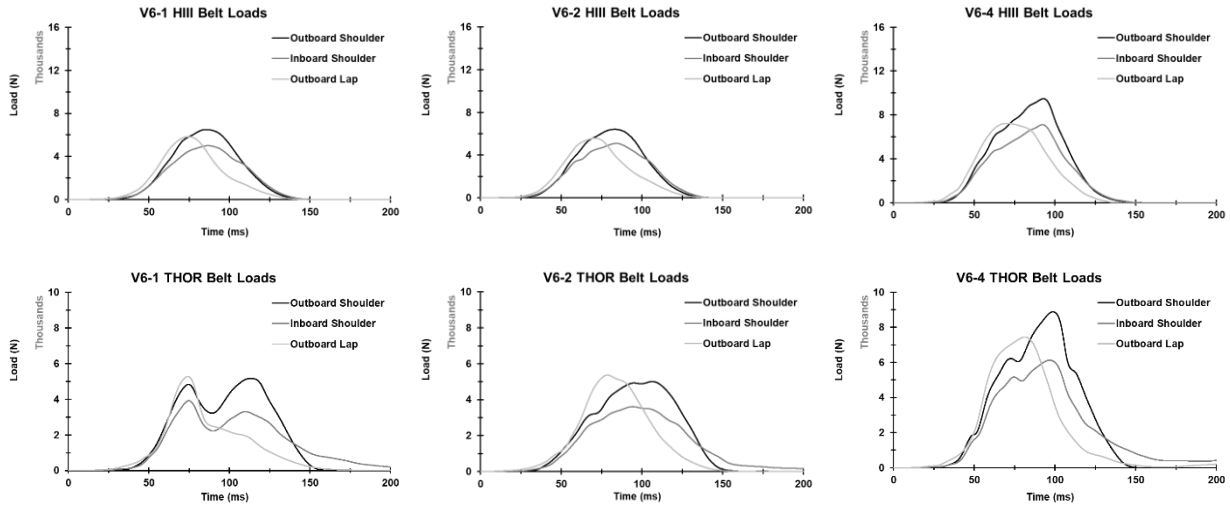

Figure 95. Belt loads for the HIII (top row) and THOR (bottom row) in vehicle V6

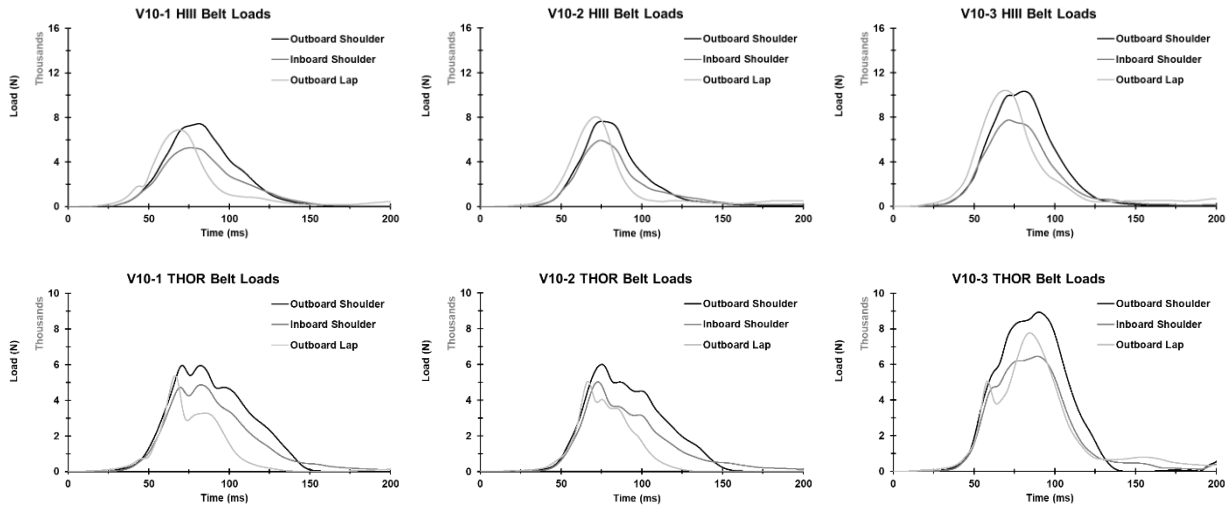

Figure 96. Belt loads for the HIII (top row) and THOR (bottom row) for vehicle V10

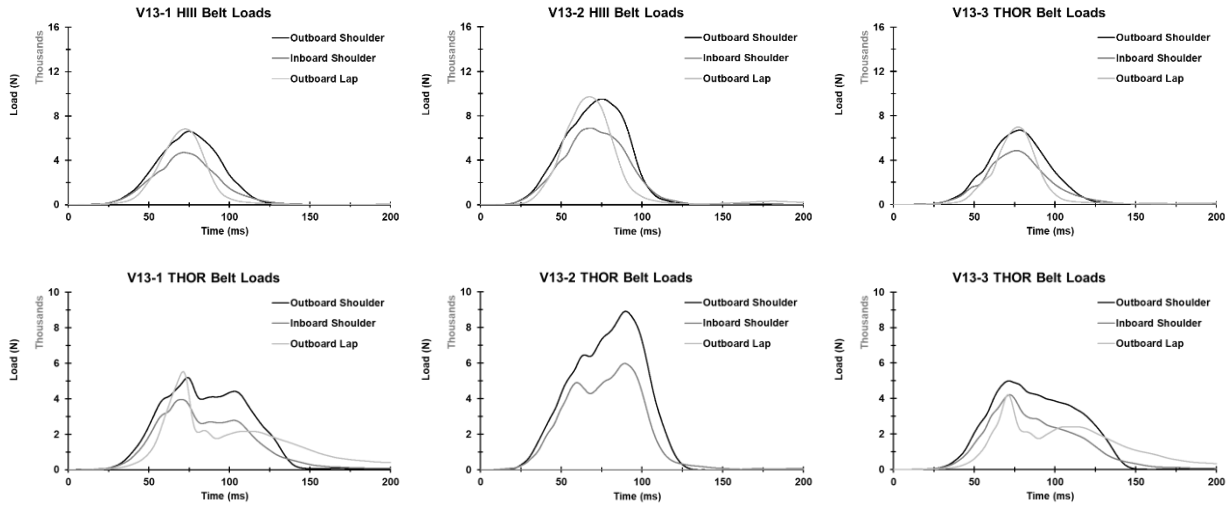

Figure 97. Belt loads for the HIII (top row) and THOR (bottom row) for vehicle V13

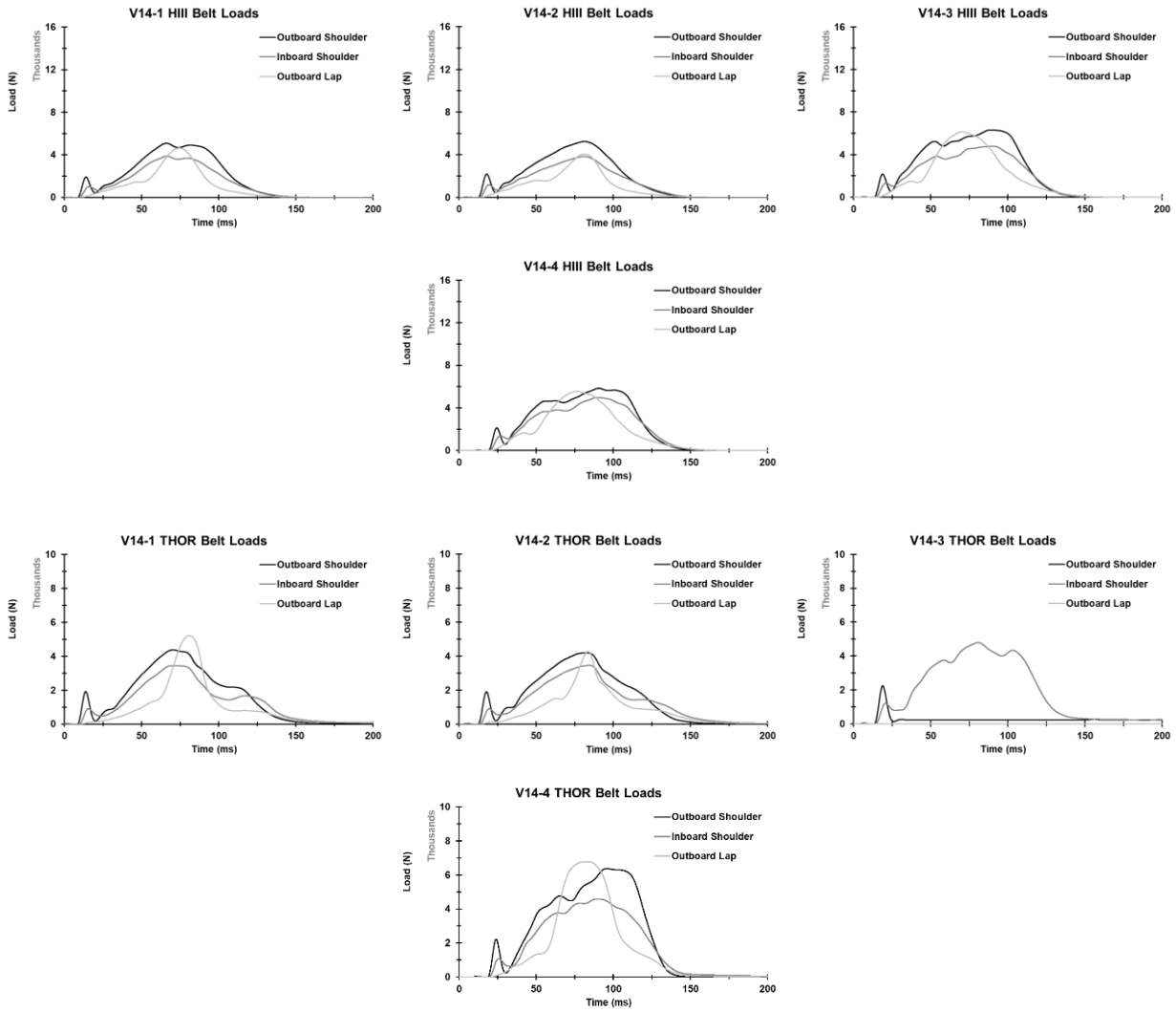

Figure 98. Belt loads for the HIII (top rows) and THOR (bottom rows) for vehicle V14

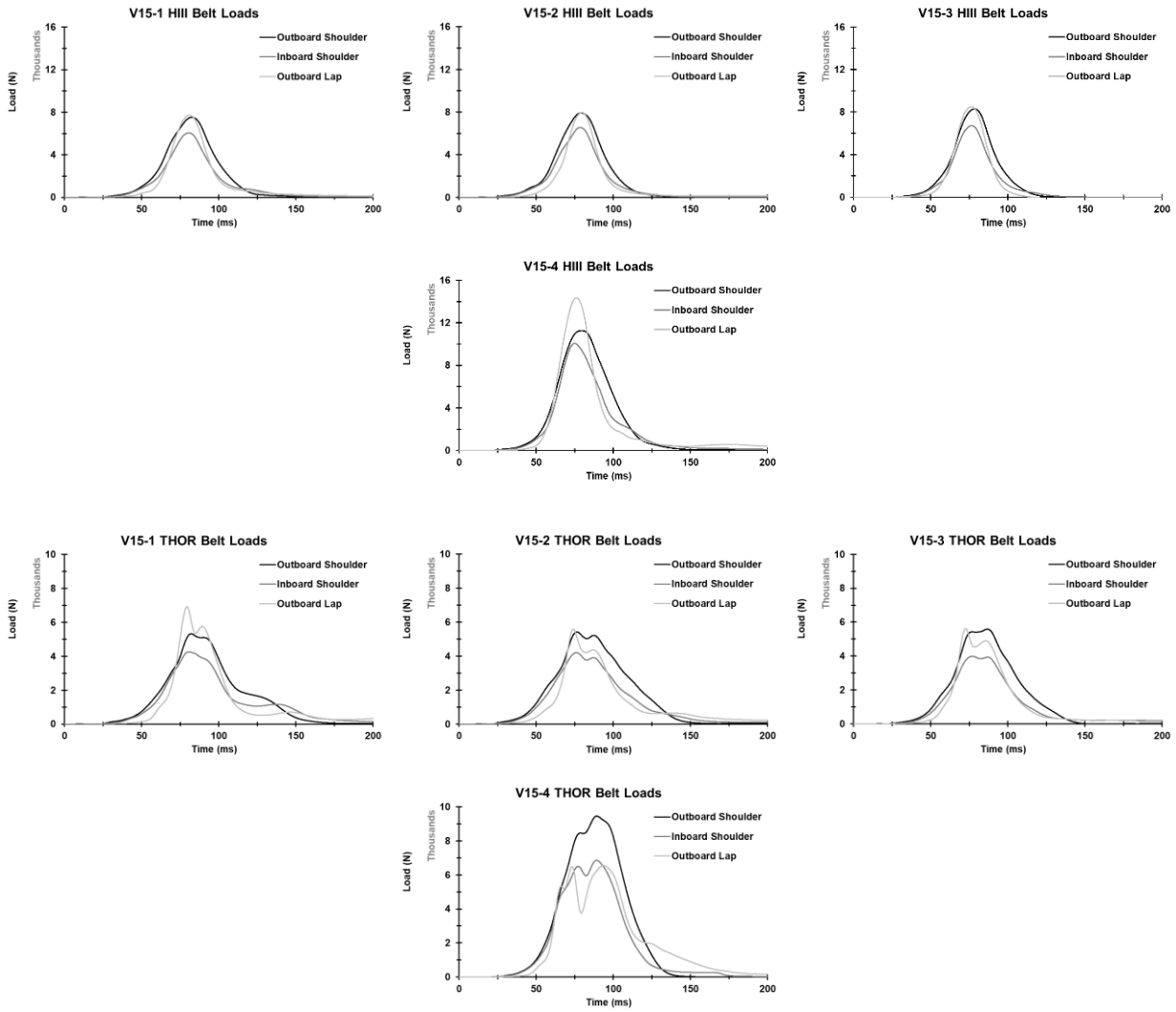

Figure 99. Belt loads for HIII (top rows) and THOR (bottom rows) for vehicle V15

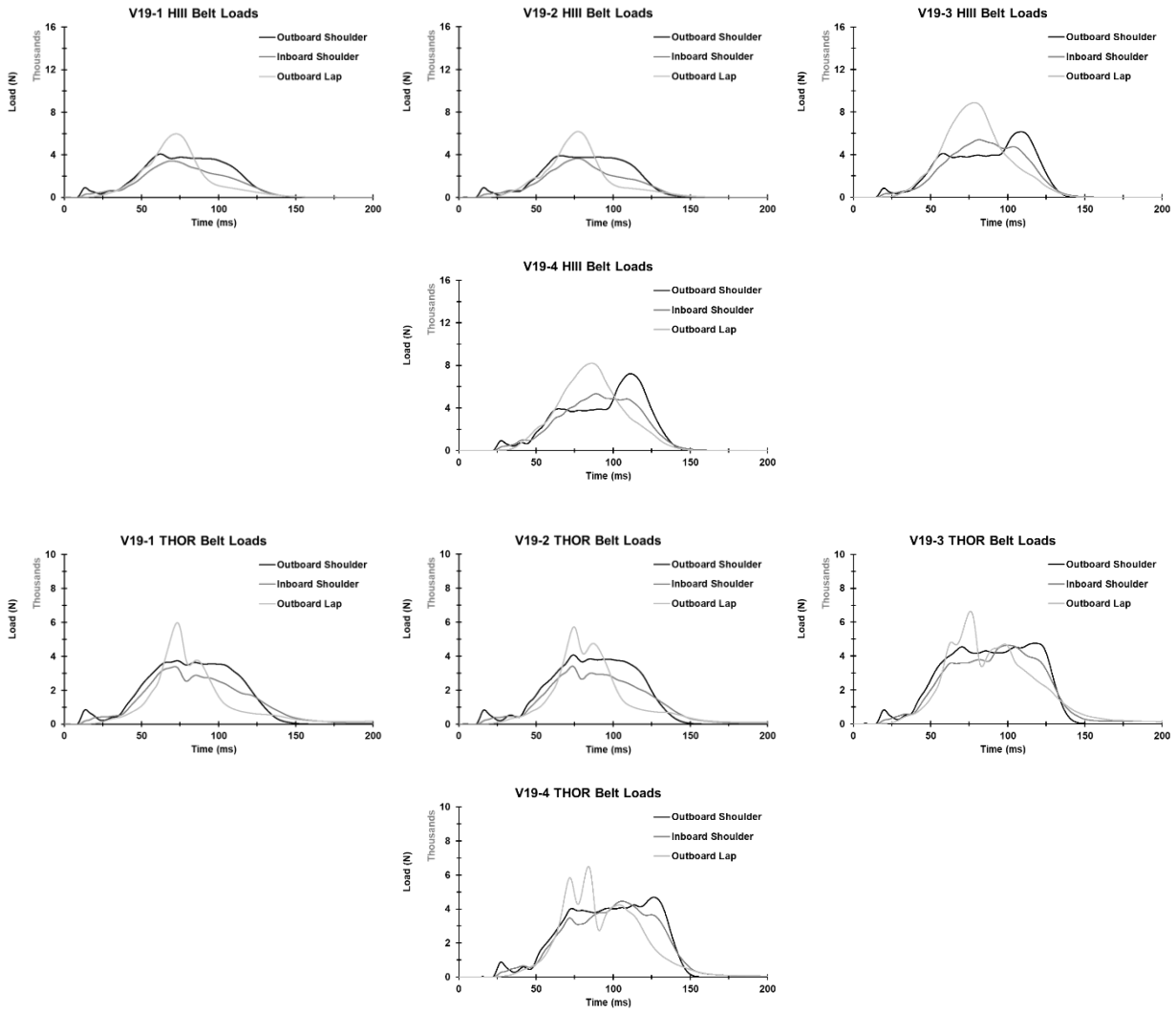

Figure 100. Belt loads for HIII (top rows) and THOR (bottom rows) for vehicle V19.

Appendix G: Resultant Pelvis Acceleration

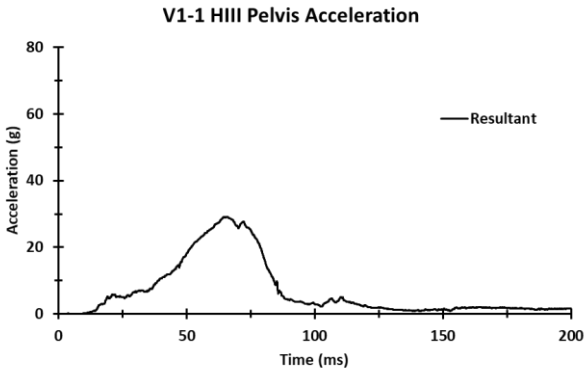

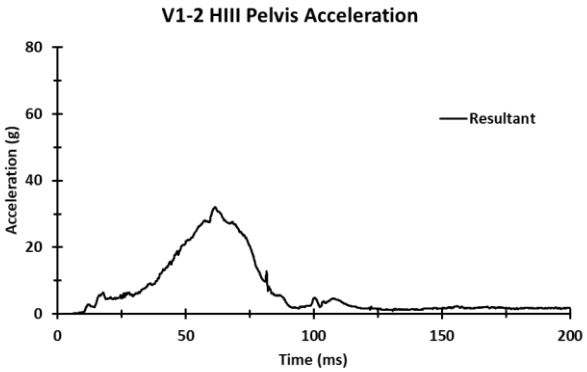

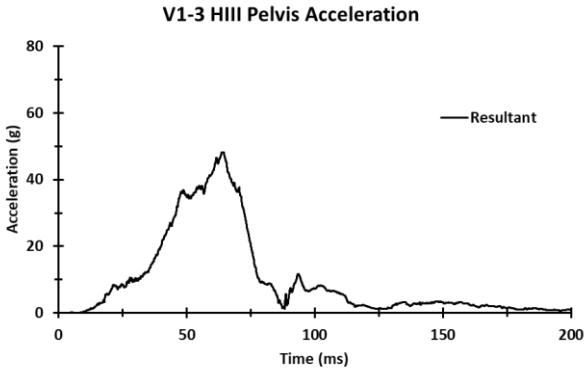

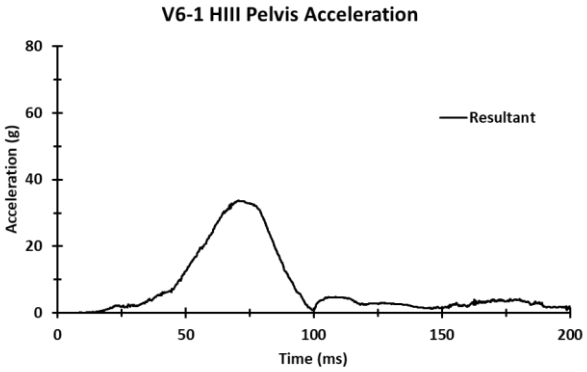

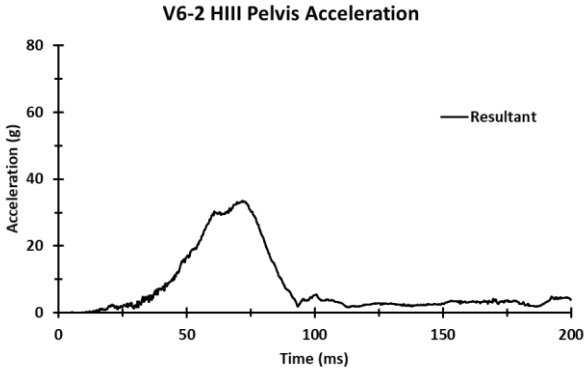

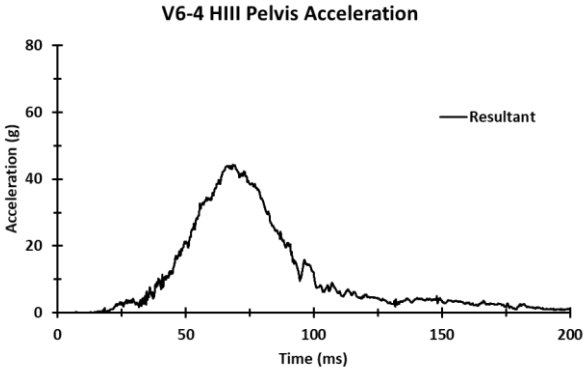

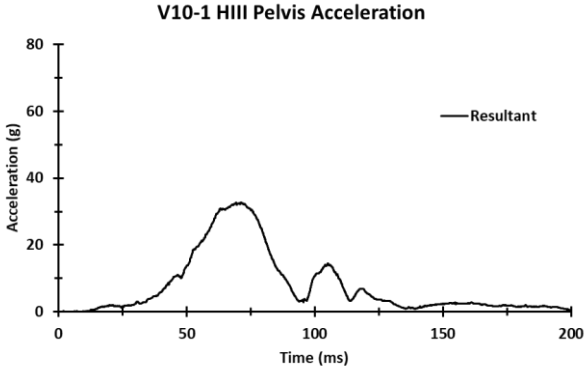

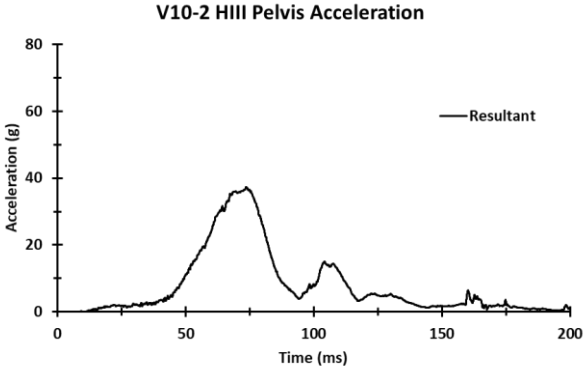

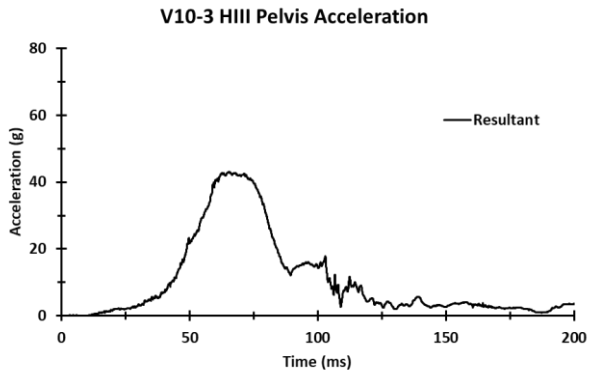
V10-3 HIII Pelvis Acceleration
Resultant
Acceleration (g)
Time (ms)
0
20
40
60
80
0
50
100
150
200

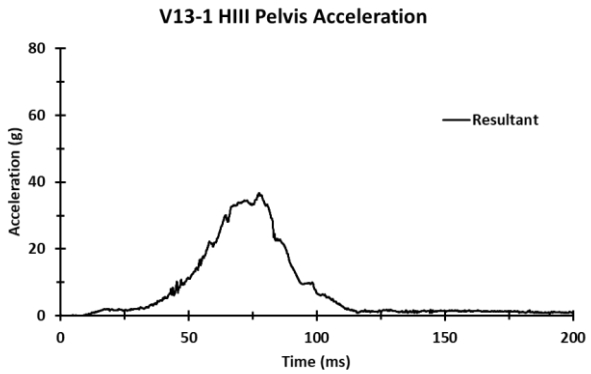
V13-1 HIII Pelvis Acceleration
Resultant
Acceleration (g)
Time (ms)
0
20
40
60
80
0
50
100
150
200

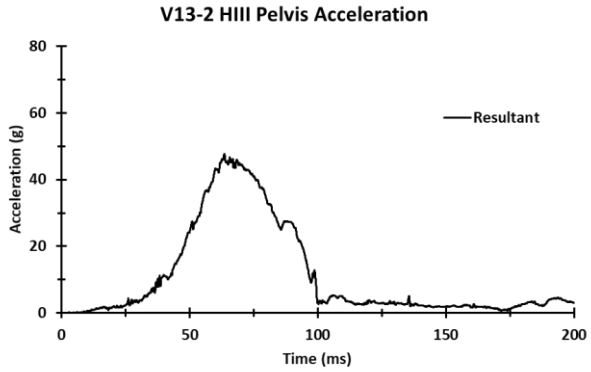
V13-2 HIII Pelvis Acceleration
Resultant
Acceleration (g)
Time (ms)
0
20
40
60
80
0
50
100
150
200

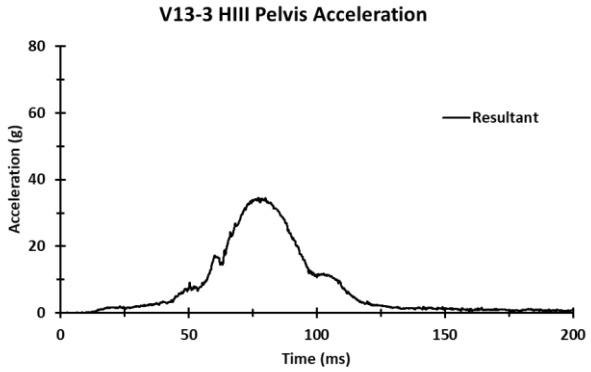
V13-3 HIII Pelvis Acceleration
Resultant
Acceleration (g)
Time (ms)
0
20
40
60
80
0
50
100
150
200

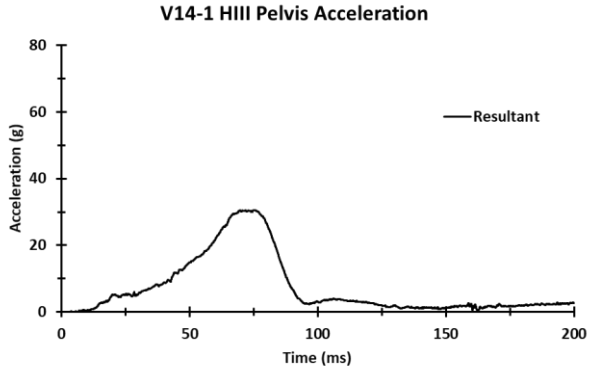
V14-1 HIII Pelvis Acceleration
Resultant
Acceleration (g)
Time (ms)
0
20
40
60
80
0
50
100
150
200

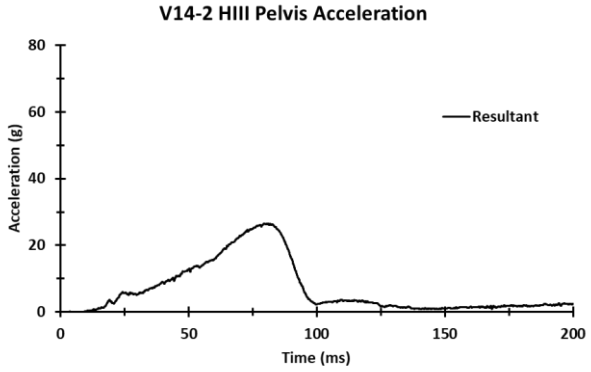
V14-2 HIII Pelvis Acceleration
Resultant
Acceleration (g)
Time (ms)
0
20
40
60
80
0
50
100
150
200

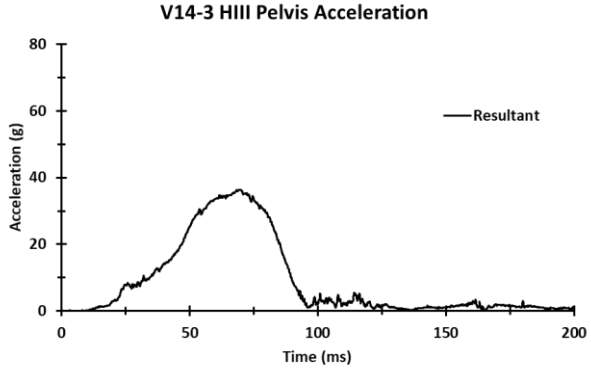
V14-3 HIII Pelvis Acceleration
Resultant
Acceleration (g)
Time (ms)
0
20
40
60
80
0
50
100
150
200

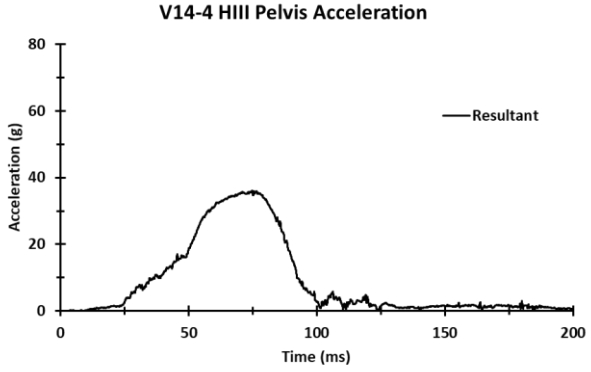
V14-4 HIII Pelvis Acceleration
Resultant
Acceleration (g)
Time (ms)
0
20
40
60
80
0
50
100
150
200

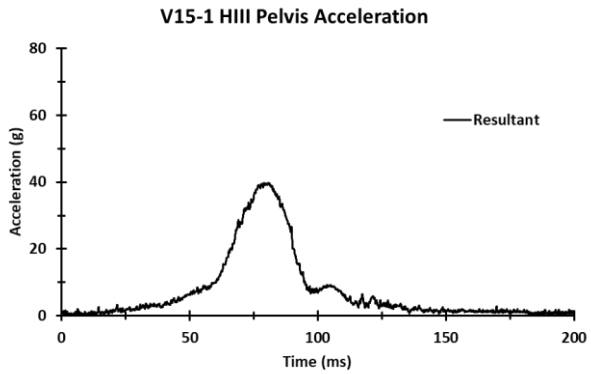
V15-1 HIII Pelvis Acceleration
Resultant
Acceleration (g)
Time (ms)
0
20
40
60
80
0
50
100
150
200

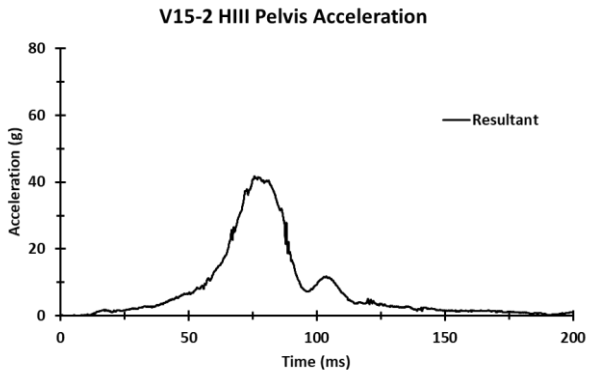
V15-2 HIII Pelvis Acceleration
Resultant
Acceleration (g)
Time (ms)
0
20
40
60
80
0
50
100
150
200

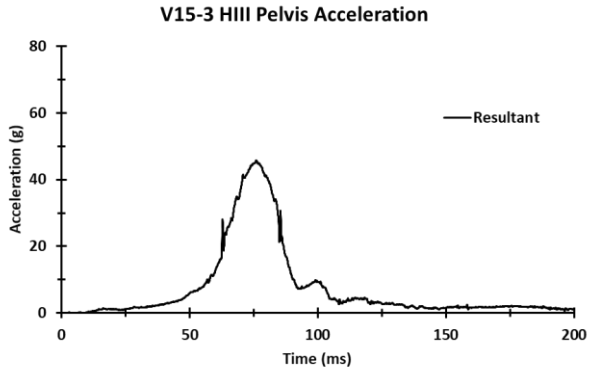
V15-3 HIII Pelvis Acceleration
Resultant
Acceleration (g)
Time (ms)
0
20
40
60
80
0
50
100
150
200

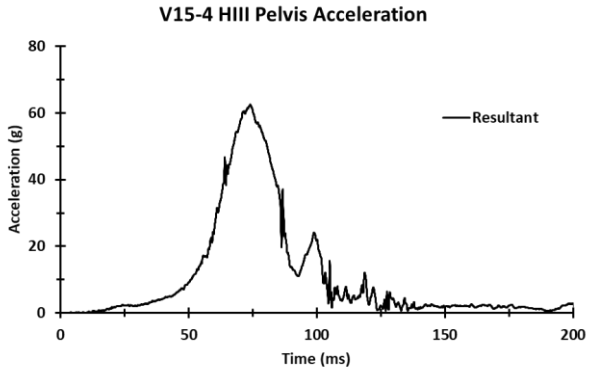
V15-4 HIII Pelvis Acceleration
Resultant
Acceleration (g)
Time (ms)
0
20
40
60
80
0
50
100
150
200

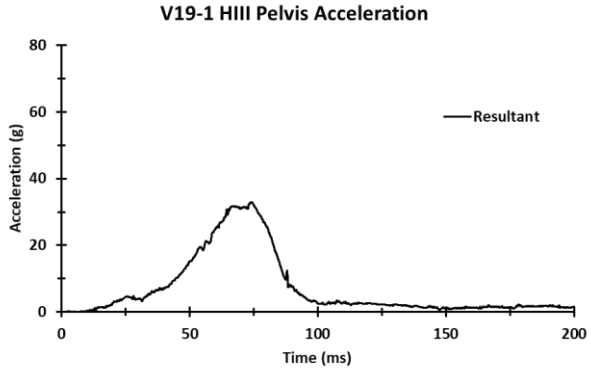
V19-1 HIII Pelvis Acceleration
Resultant
Acceleration (g)
Time (ms)
0
20
40
60
80
0
50
100
150
200

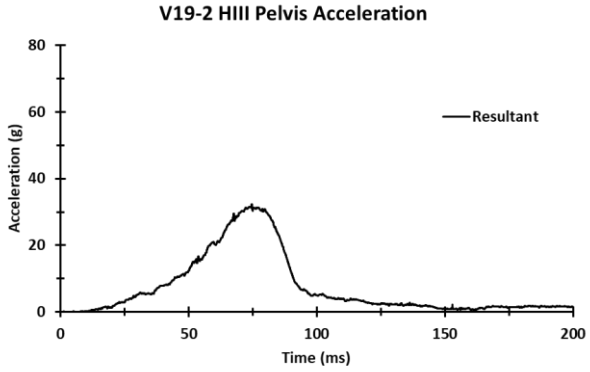
V19-2 HIII Pelvis Acceleration
Resultant
Acceleration (g)
Time (ms)
0
20
40
60
80
0
50
100
150
200

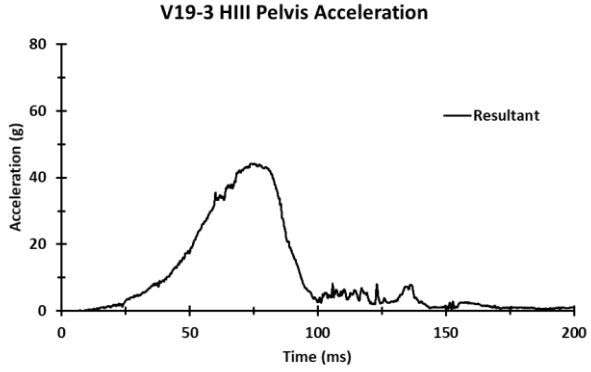
V19-3 HIII Pelvis Acceleration
Resultant
Acceleration (g)
Time (ms)
0
20
40
60
80
0
50
100
150
200

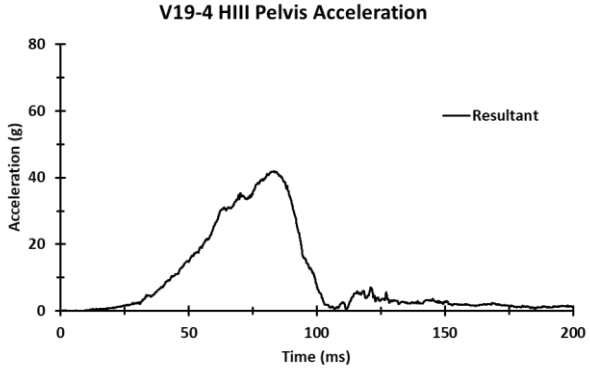
V19-4 HIII Pelvis Acceleration
Resultant
Acceleration (g)
Time (ms)
0
20
40
60
80
0
50
100
150
200

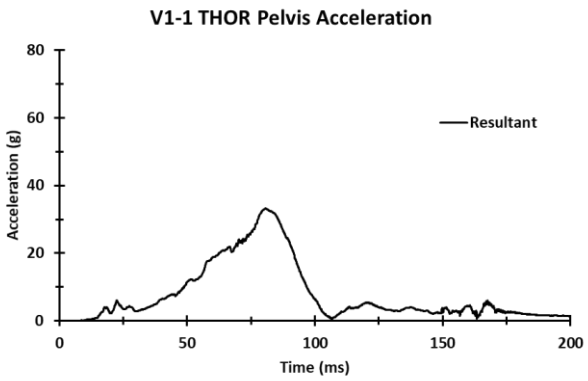
V1-1 THOR Pelvis Acceleration
Resultant
Acceleration (g)
Time (ms)
0
20
40
60
80
0
50
100
150
200

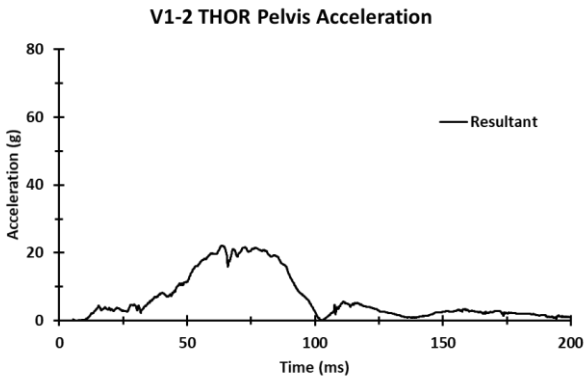
V1-2 THOR Pelvis Acceleration
Resultant
Acceleration (g)
Time (ms)
0
20
40
60
80
0
50
100
150
200

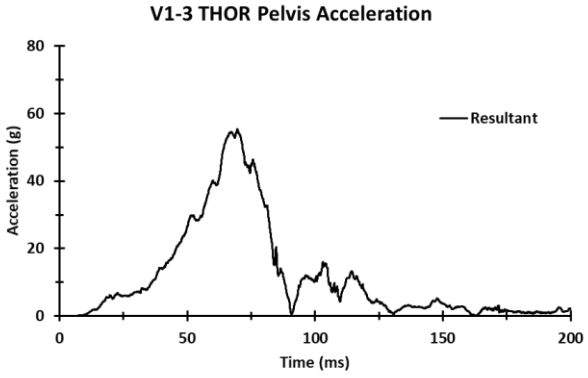
V1-3 THOR Pelvis Acceleration
Resultant
Acceleration (g)
Time (ms)
0
20
40
60
80
0
50
100
150
200

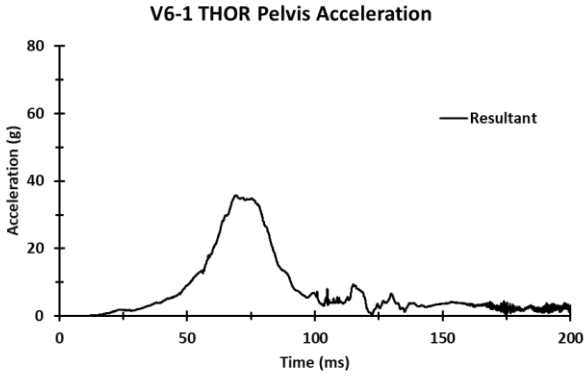
V6-1 THOR Pelvis Acceleration
Resultant
Acceleration (g)
Time (ms)
0
20
40
60
80
0
50
100
150
200

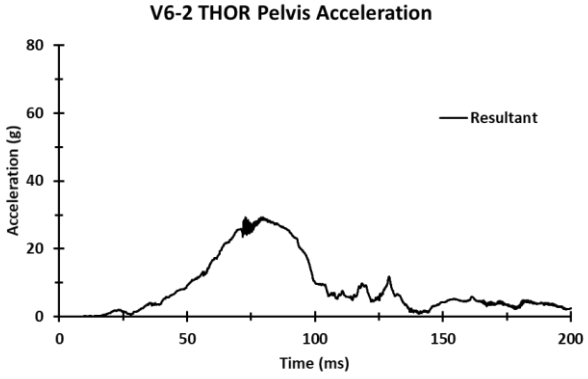
V6-2 THOR Pelvis Acceleration
Resultant
Acceleration (g)
Time (ms)
0
20
40
60
80
0
50
100
150
200

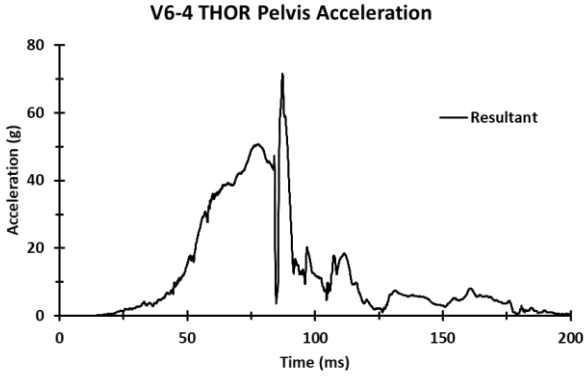
V6-4 THOR Pelvis Acceleration
Resultant
Acceleration (g)
Time (ms)
0
20
40
60
80
0
50
100
150
200

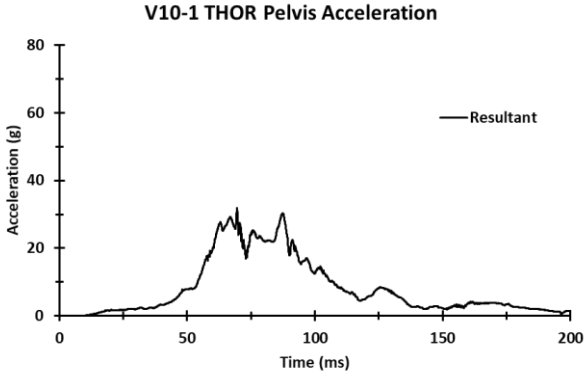
V10-1 THOR Pelvis Acceleration
Resultant
Acceleration (g)
Time (ms)
0
20
40
60
80
0
50
100
150
200

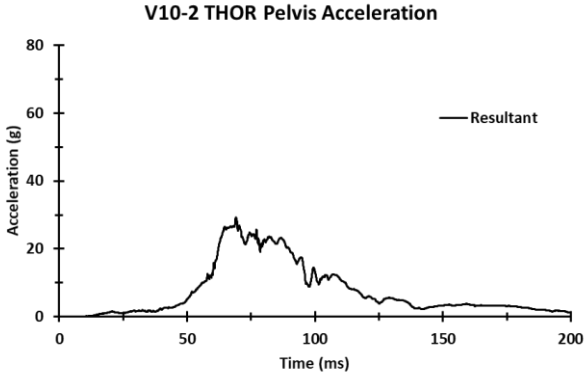
V10-2 THOR Pelvis Acceleration
Resultant
Acceleration (g)
Time (ms)
0
20
40
60
80
0
50
100
150
200

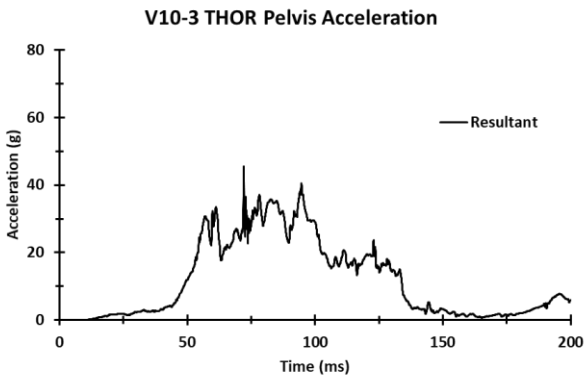
V10-3 THOR Pelvis Acceleration
Resultant
Acceleration (g)
Time (ms)
0
20
40
60
80
0
50
100
150
200

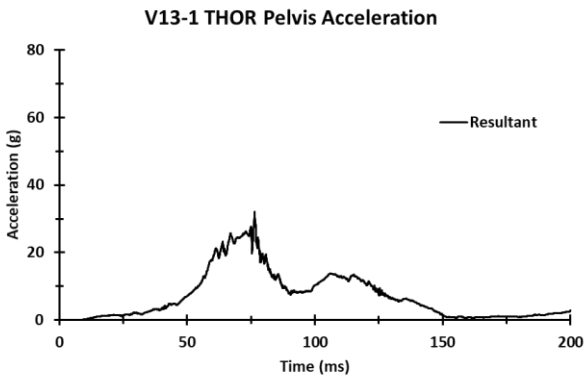
V13-1 THOR Pelvis Acceleration
Resultant
Acceleration (g)
Time (ms)
0
20
40
60
80
0
50
100
150
200

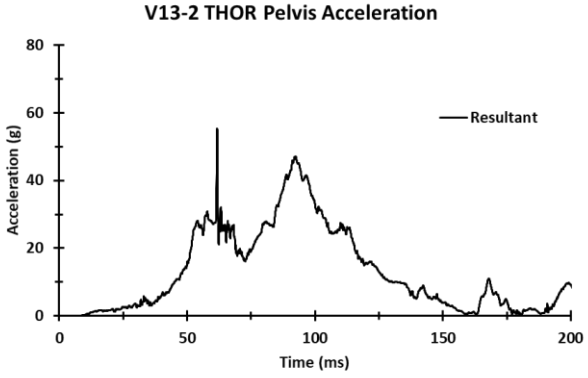
V13-2 THOR Pelvis Acceleration
Resultant
Acceleration (g)
Time (ms)
0
20
40
60
80
0
50
100
150
200

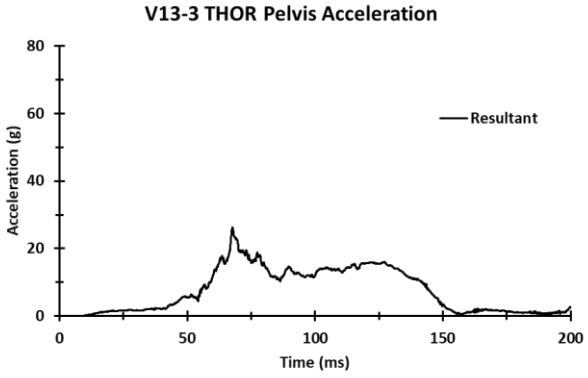
V13-3 THOR Pelvis Acceleration
Resultant
Acceleration (g)
Time (ms)
0
20
40
60
80
0
50
100
150
200

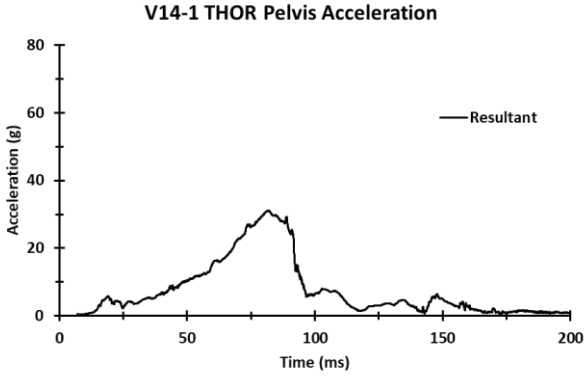
V14-1 THOR Pelvis Acceleration
Resultant
Acceleration (g)
Time (ms)
0
20
40
60
80
0
50
100
150
200

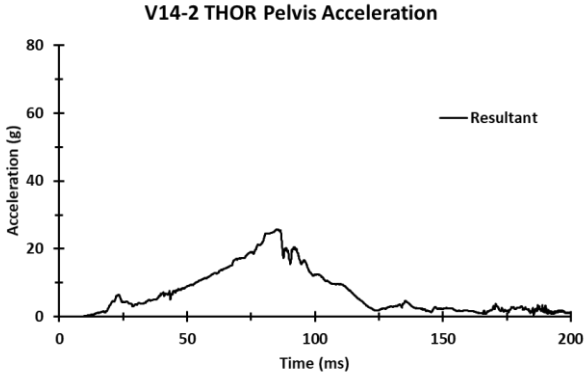
V14-2 THOR Pelvis Acceleration
Resultant
Acceleration (g)
Time (ms)
0
20
40
60
80
0
50
100
150
200

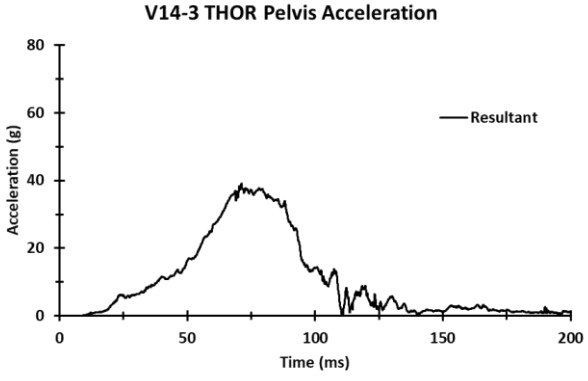
V14-3 THOR Pelvis Acceleration
Resultant
Acceleration (g)
Time (ms)
0
20
40
60
80
0
50
100
150
200

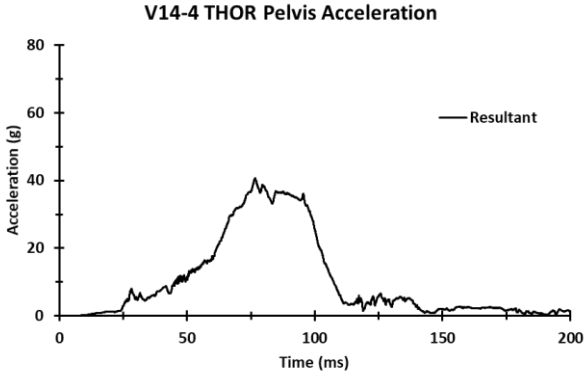
V14-4 THOR Pelvis Acceleration
Resultant
Acceleration (g)
Time (ms)
0
20
40
60
80
0
50
100
150
200

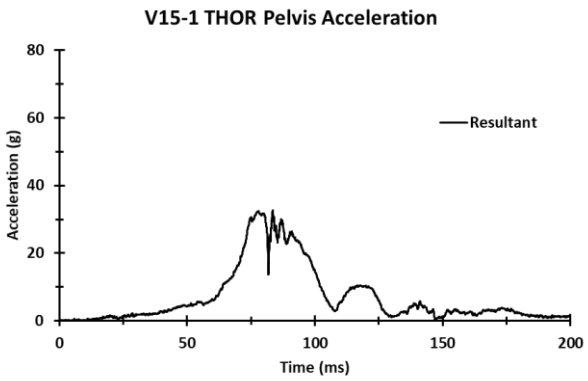
V15-1 THOR Pelvis Acceleration
Resultant
Acceleration (g)
Time (ms)
0
20
40
60
80
0
50
100
150
200

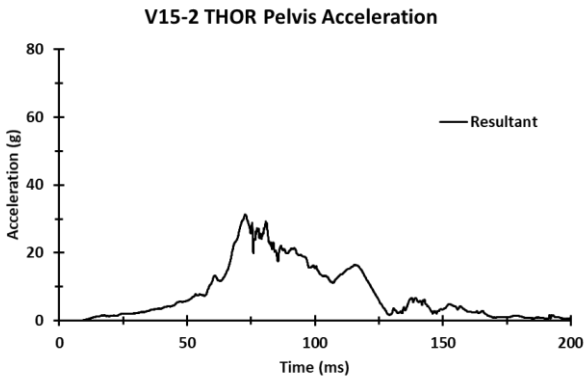
V15-2 THOR Pelvis Acceleration
Resultant
Acceleration (g)
Time (ms)
0
20
40
60
80
0
50
100
150
200

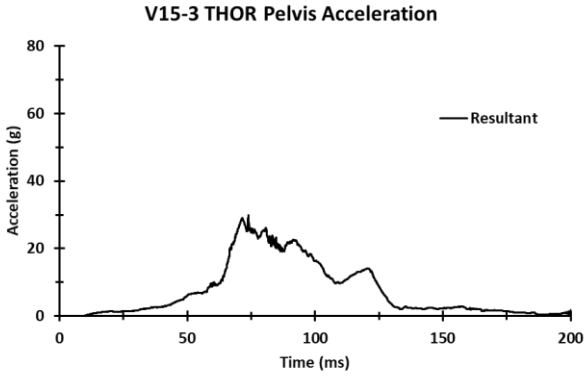
V15-3 THOR Pelvis Acceleration
Resultant
Acceleration (g)
Time (ms)
0
20
40
60
80
0
50
100
150
200

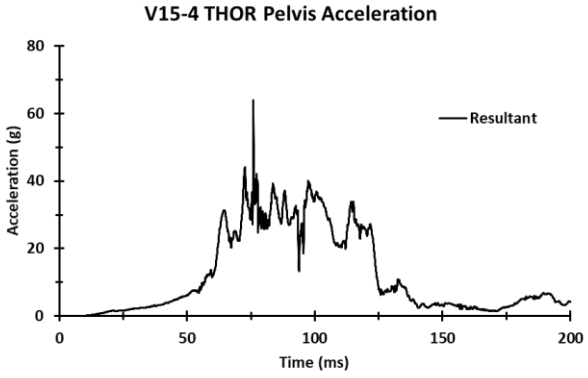
V15-4 THOR Pelvis Acceleration
Resultant
Acceleration (g)
Time (ms)
0
20
40
60
80
0
50
100
150
200

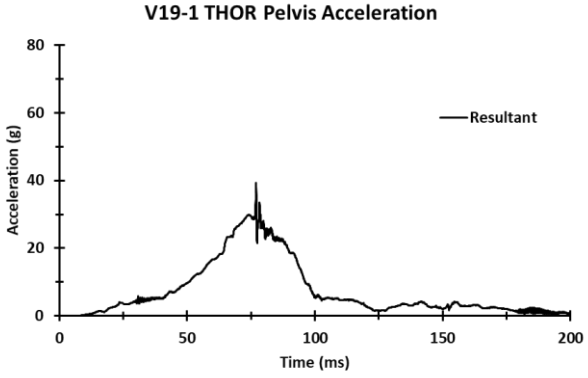
V19-1 THOR Pelvis Acceleration
Resultant
Acceleration (g)
Time (ms)
0
20
40
60
80
0
50
100
150
200

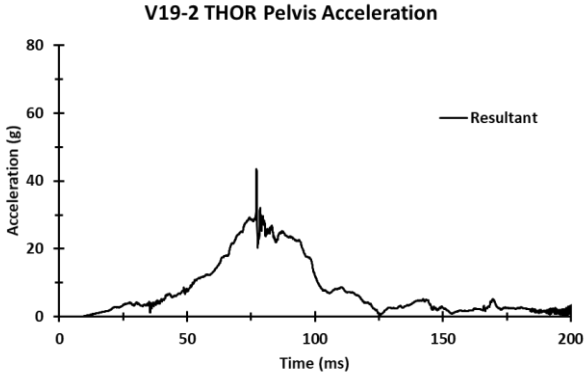
V19-2 THOR Pelvis Acceleration
Resultant
Acceleration (g)
Time (ms)
0
20
40
60
80
0
50
100
150
200

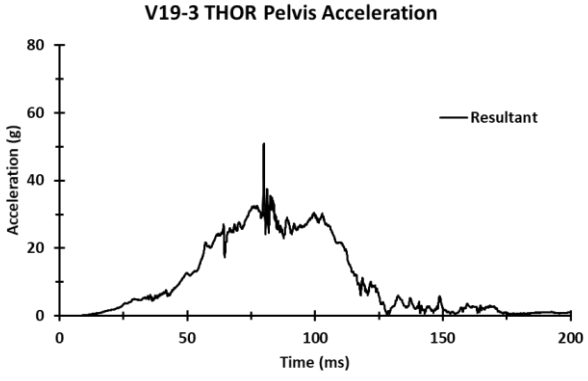
V19-3 THOR Pelvis Acceleration
Resultant
Acceleration (g)
Time (ms)
0
20
40
60
80
0
50
100
150
200

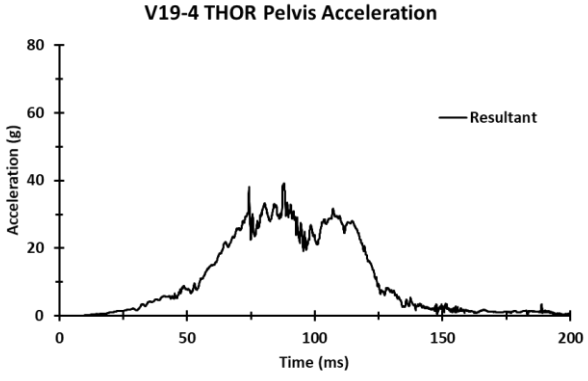
V19-4 THOR Pelvis Acceleration
Resultant
Acceleration (g)
Time (ms)
0
20
40
60
80
0
50
100
150
200

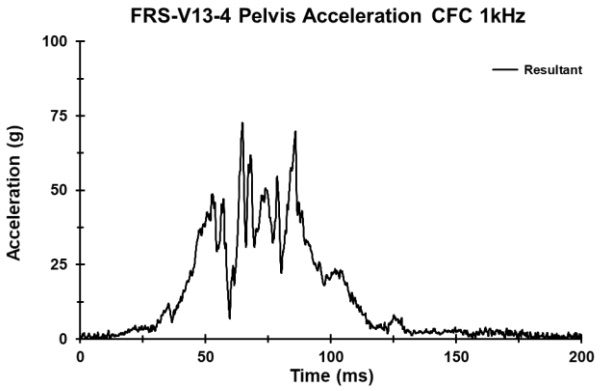
FRS-V13-4 Pelvis Acceleration CFC 1kHz
Resultant
Acceleration (g)
Time (ms)

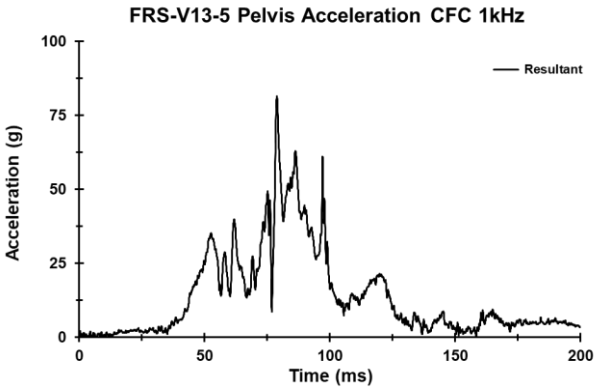
FRS-V13-5 Pelvis Acceleration CFC 1kHz
Resultant
Acceleration (g)
Time (ms)

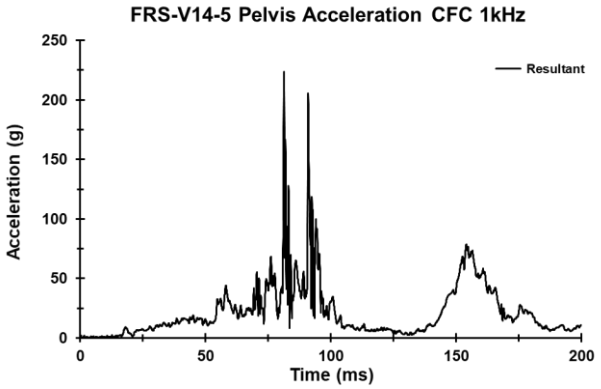
FRS-V14-5 Pelvis Acceleration CFC 1kHz
Resultant
Acceleration (g)
Time (ms)

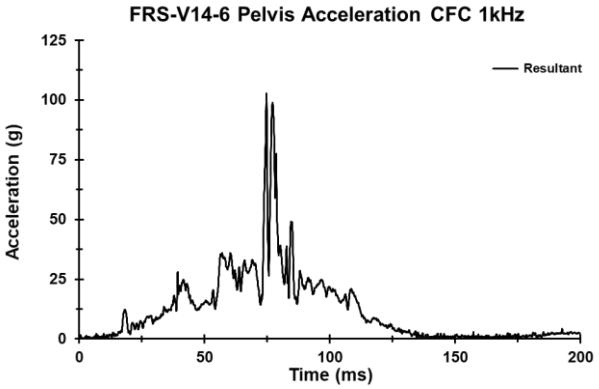
FRS-V14-6 Pelvis Acceleration CFC 1kHz
Resultant
Acceleration (g)
Time (ms)

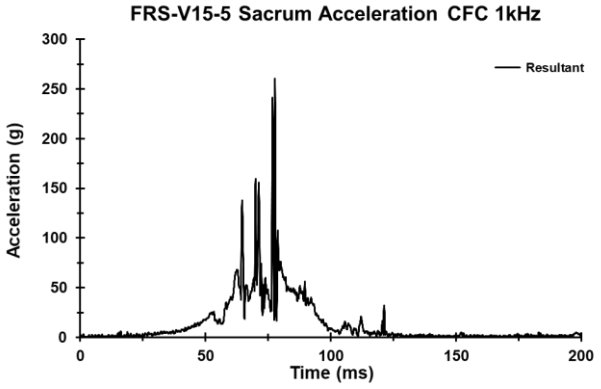
FRS-V15-5 Sacrum Acceleration CFC 1kHz
Resultant
Acceleration (g)
Time (ms)

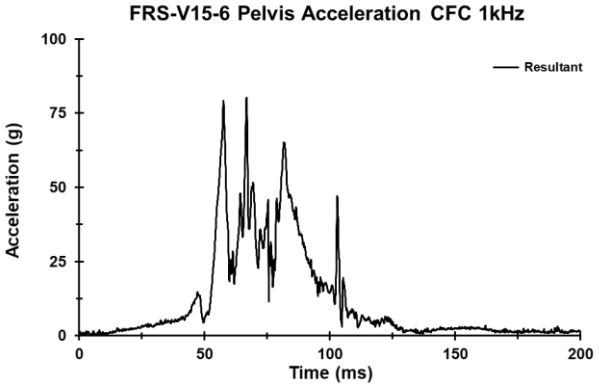
FRS-V15-6 Pelvis Acceleration CFC 1kHz
Resultant
Acceleration (g)
Time (ms)

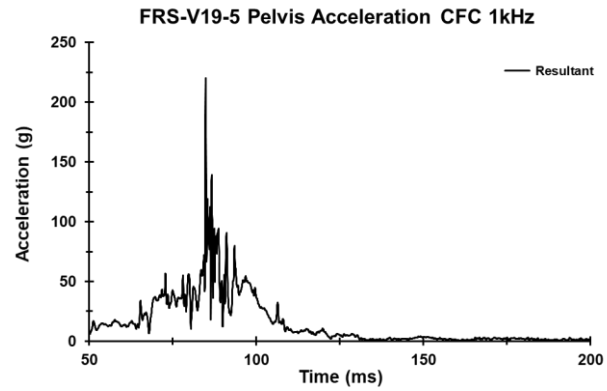
FRS-V19-5 Pelvis Acceleration CFC 1kHz
Resultant
Acceleration (g)
Time (ms)

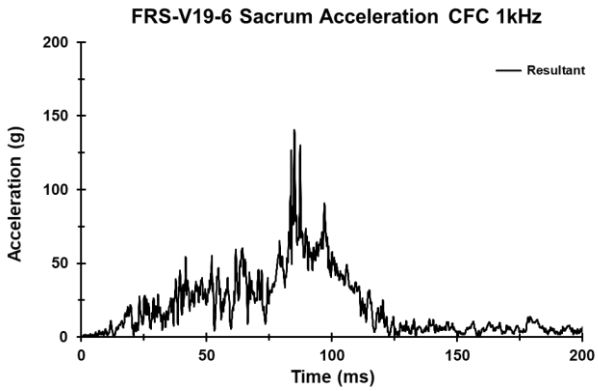
FRS-V19-6 Sacrum Acceleration CFC 1kHz
Resultant
Acceleration (g)
Time (ms)

Appendix H: Matched NCAP85 Pelvis X and Z-Direction Acceleration

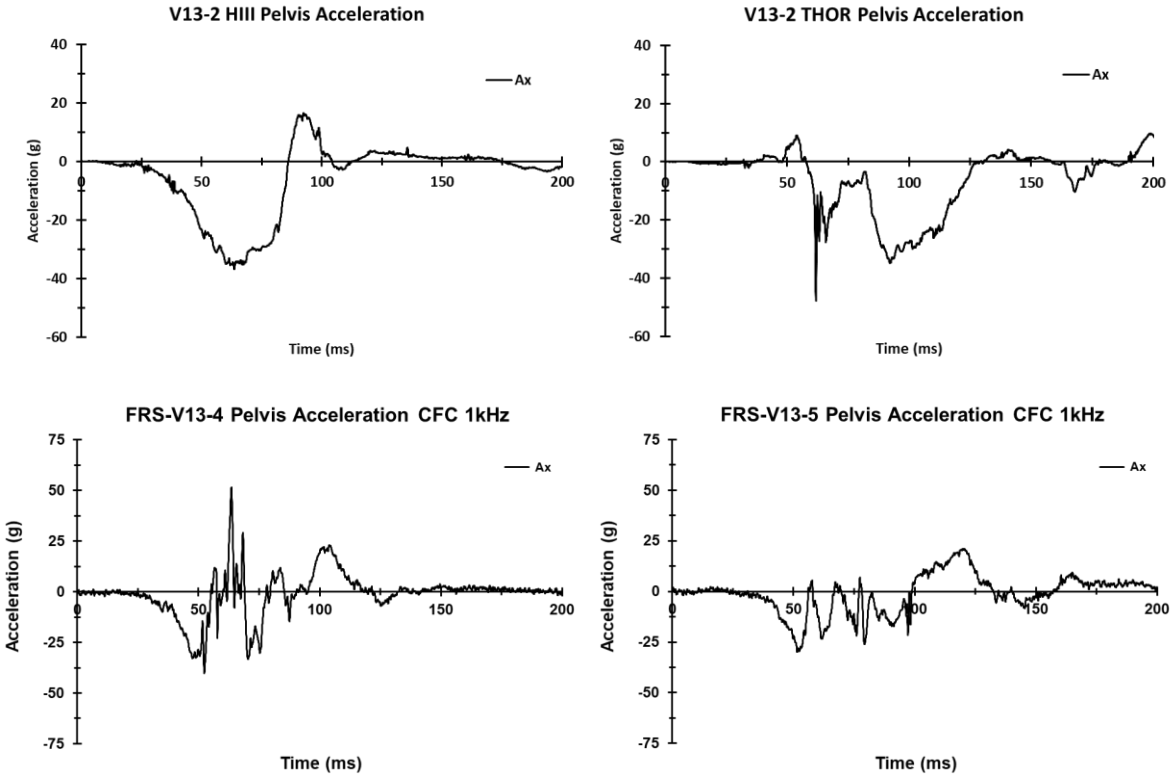

Figure 101. Pelvis X-direction acceleration for the HIII, THOR, and both PMHS in vehicle V13.

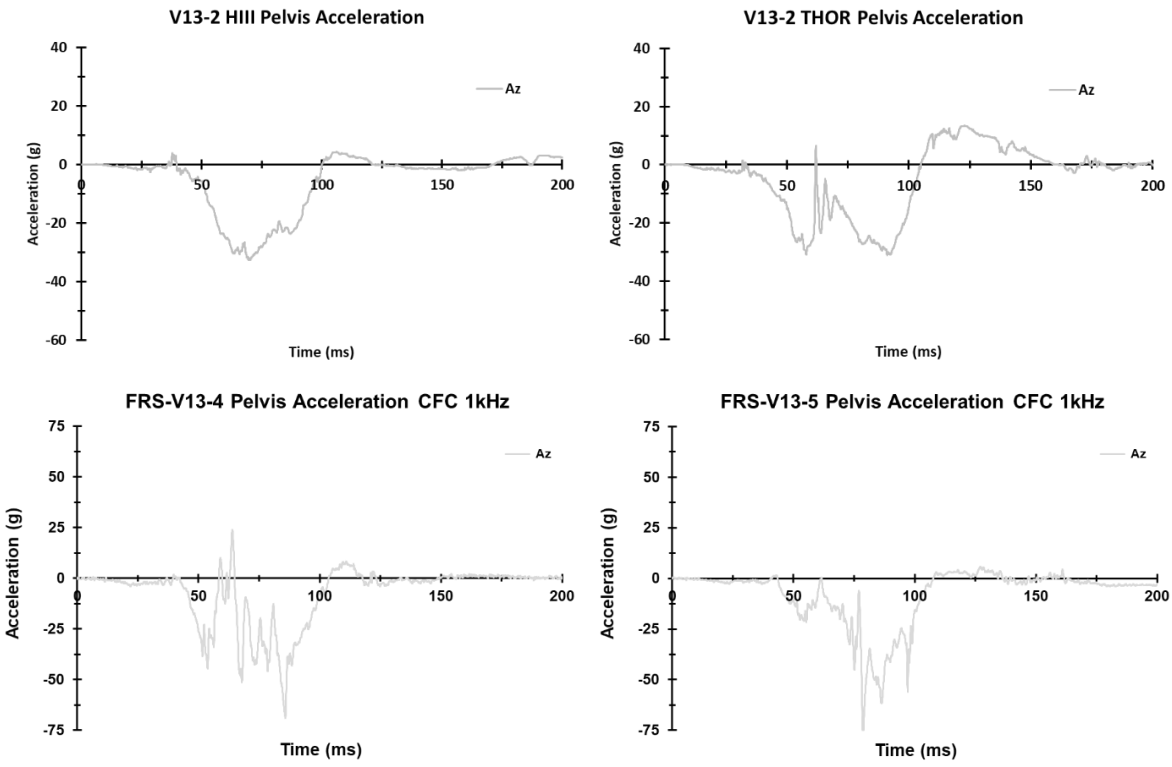

Figure 102. Pelvis Z-direction acceleration for the HIII, THOR, and both PMHS in vehicle V13.

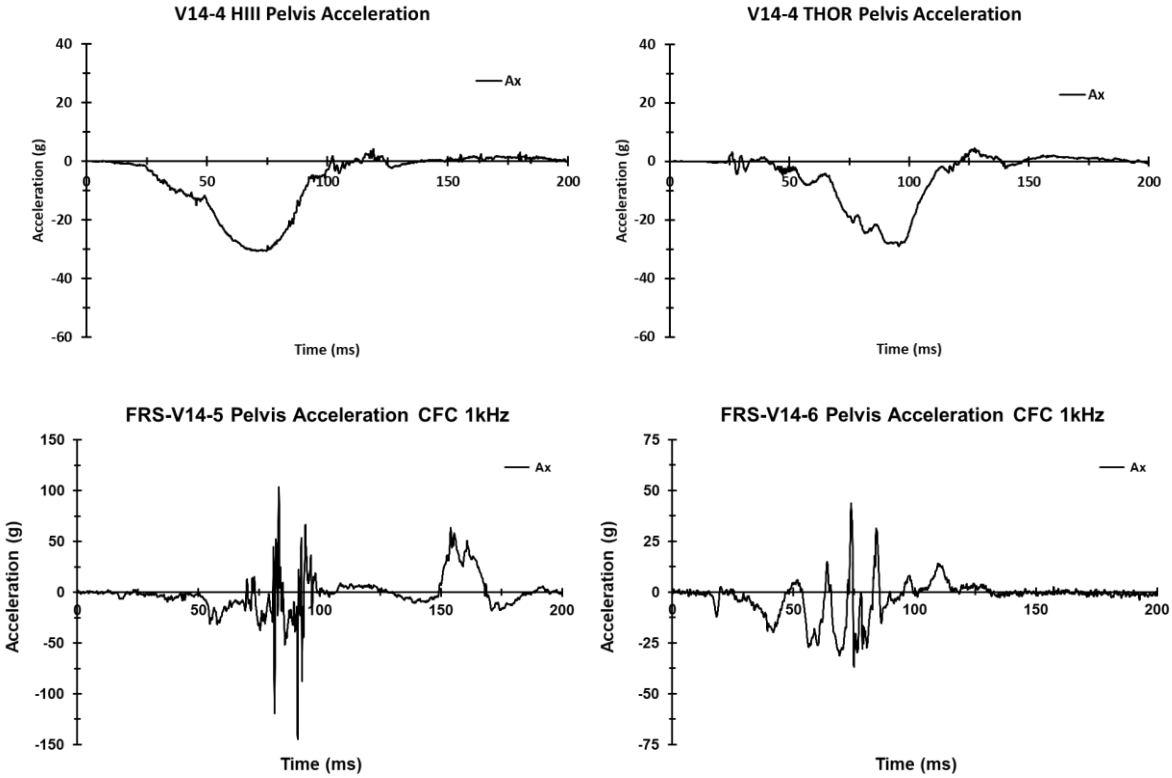

Figure 103. Pelvis X-direction acceleration for the HIII, THOR, and both PMHS in vehicle V14.

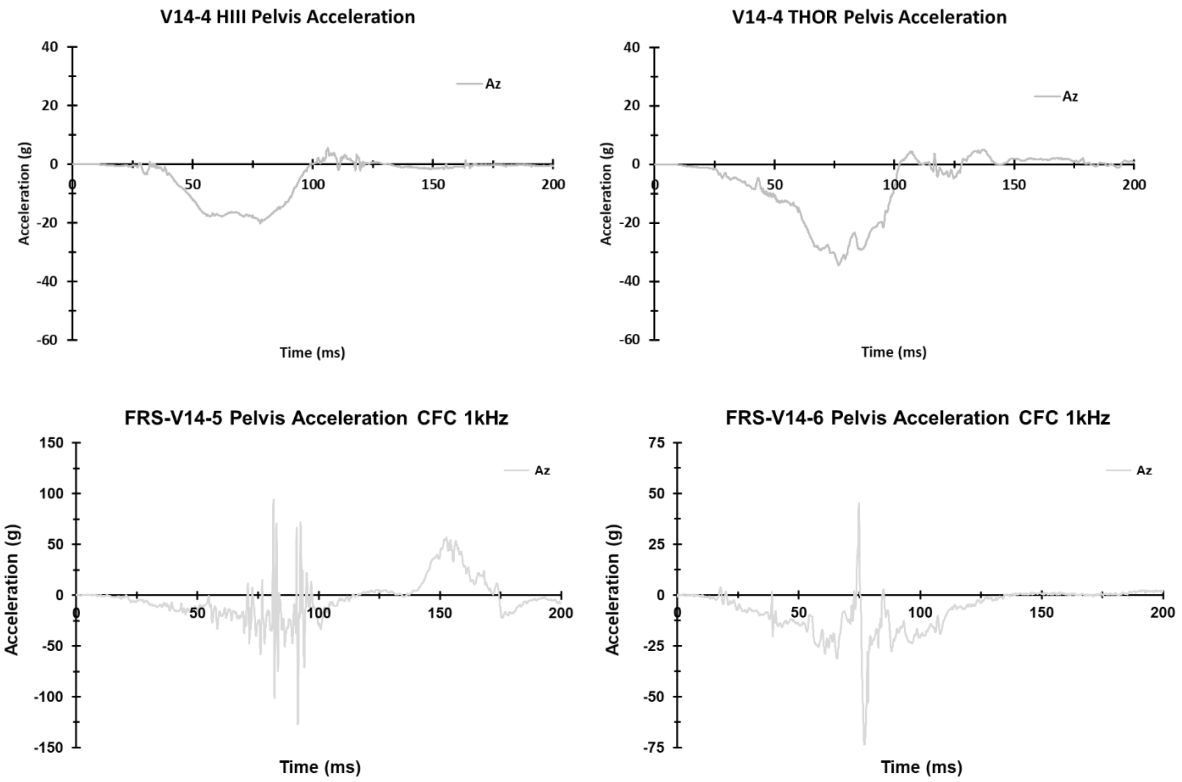

Figure 104. Pelvis Z-direction acceleration for the HIII, THOR, and both PMHS in vehicle V14.

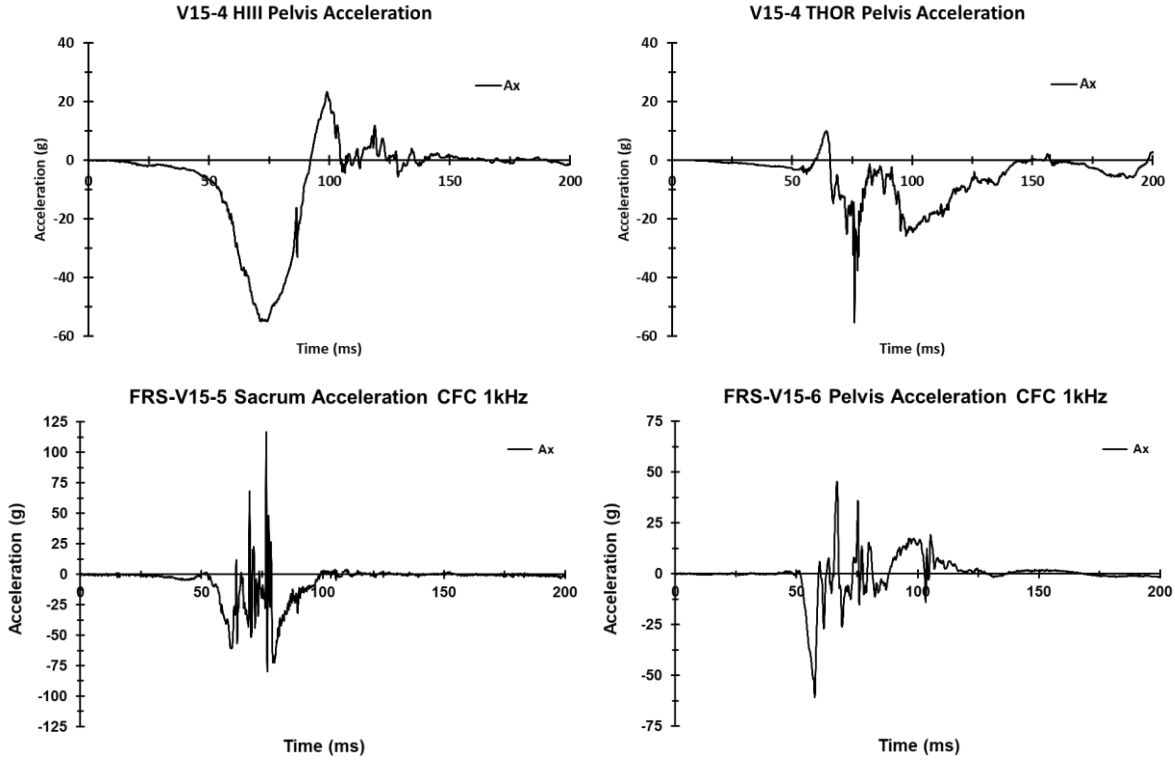

Figure 105. Pelvis X-direction acceleration for the HIII, THOR, and both PMHS in vehicle V15.

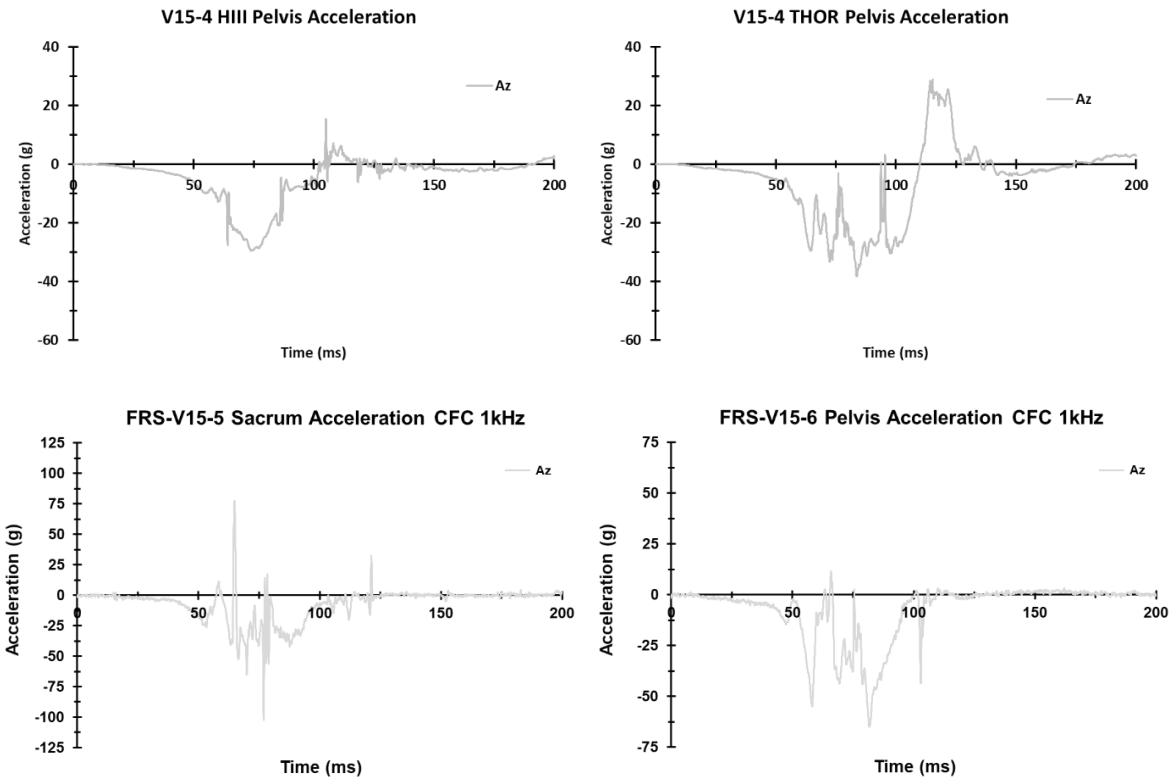

Figure 106. Pelvis Z-direction acceleration for the HIII, THOR, and both PMHS in vehicle V15.

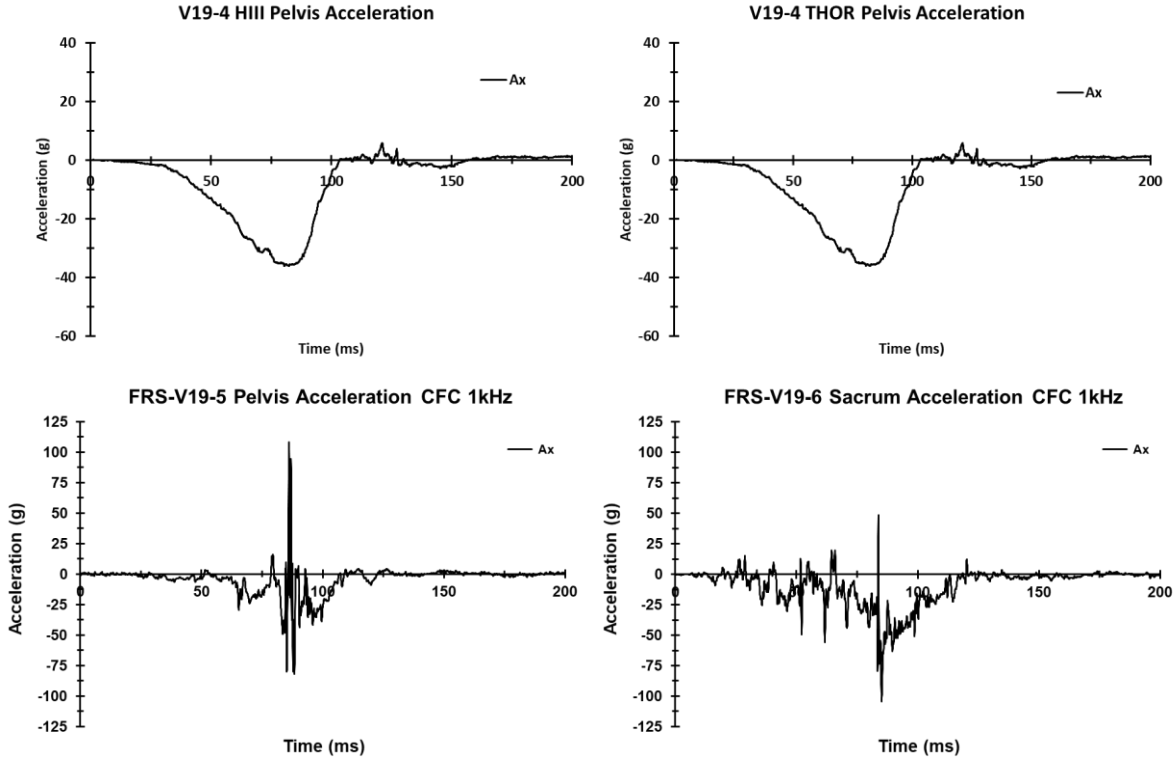

Figure 107. Pelvis X-direction acceleration for the HIII, THOR, and both PMHS in vehicle V19.

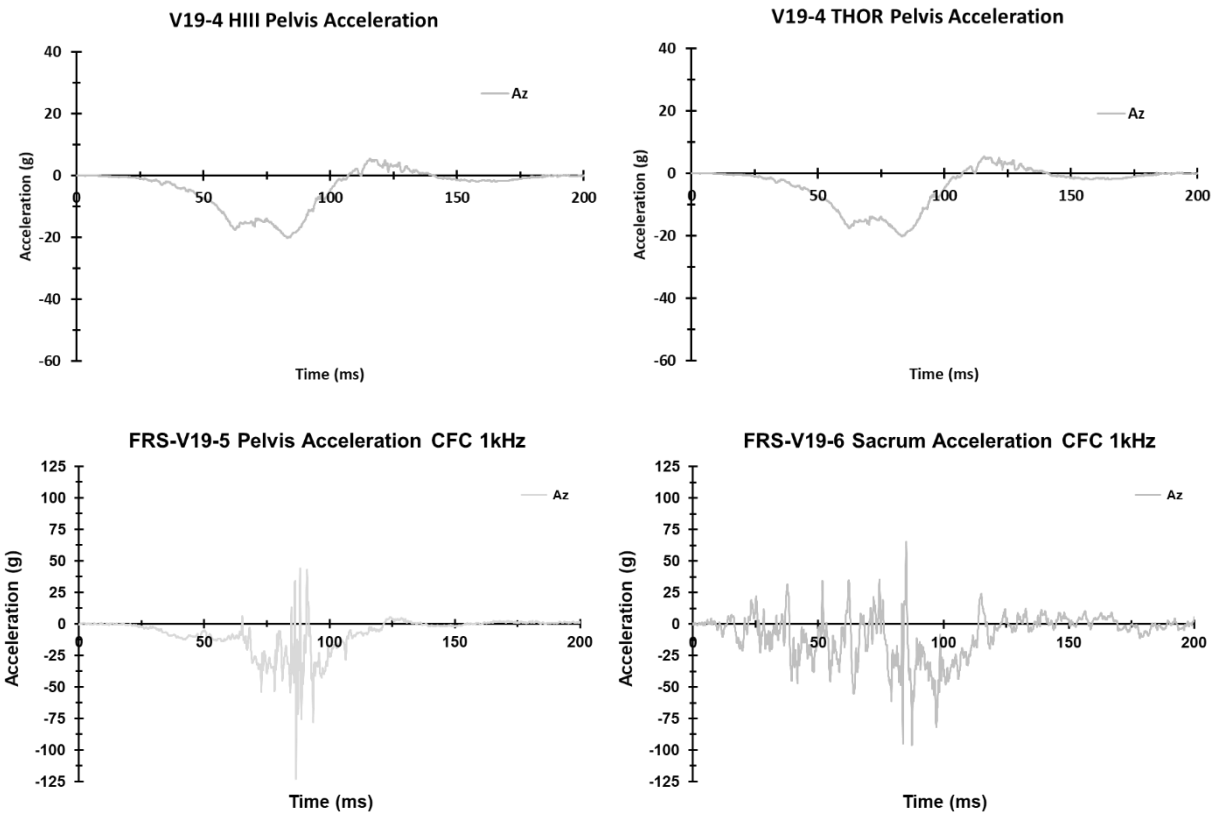

Figure 108. Pelvis Z-direction acceleration for the HIII, THOR, and both PMHS in vehicle V19.

Appendix I: THOR Submarining Table

Test	Post-Test Photos		High-Speed Video		ASIS Force/ Moment		Seat Belt Loads		ABISUP Pressures		Submarining	
	L	R	L	R	L	R	L	R	L	R	L	R
V1-1	N	N	N	Y	N	?	N	N	N	Y	N	Y
V1-2	?	?	N	Y	N	?	N	N	N	?	N	Y
V1-3	N	N	N	N	N	N	N	N	N	N	N	N
V6-1	N	N	N	N	?	N	?	N	N	N	N	N
V6-2	N	N	N	N	N	N	N	N	N	N	N	N
V6-4	?	?	N	N	N	N	N	N	N	N	N	N
V10-1	Y	N	Y	?	Y	Y	Y	Y	Y	Y	Y	Y
V10-2	Y	?	Y	?	Y	Y	Y	Y	Y	Y	Y	Y
V10-3	Y	?	Y	Y	Y	Y	?	Y	Y	Y	Y	Y
V13-1	Y	Y	Y	Y	Y	Y	Y	Y	Y	Y	Y	Y
V13-2	Y	Y	Y	Y	Y	Y	-----	?	Y	Y	Y	Y
V13-3	Y	Y	Y	Y	Y	Y	Y	Y	Y	Y	Y	Y
V14-1	N	N	N	N	N	N	?	N	N	N	N	N
V14-2	?	?	N	N	N	?	Y	N	N	N	N	N
V14-3	?	?	N	N	N	N	-----	N	N	N	N	N
V14-4	N	N	N	N	N	N	?	N	N	N	N	N
V15-1	?	?	N	Y	N	Y	N	N	----	----	N	Y
V15-2	?	Y	N	Y	N	Y	N	N	N	Y	N	Y
V15-3	N	Y	N	Y	N	Y	N	N	N	Y	N	Y
V15-4	Y	Y	Y	Y	Y	Y	?	N	Y	Y	Y	Y
V19-1	N	N	N	?	N	Y	?	?	N	?	N	Y
V19-2	N	?	N	?	N	Y	N	?	N	Y	N	Y
V19-3	Y	Y	Y	Y	Y	Y	Y	N	Y	Y	Y	Y
V19-4	Y	?	Y	Y	Y	Y	Y	N	Y	Y	Y	Y

Appendix J: Image Sequences from Matched NCAP85 Tests

Figure 109. Test V13-2, Submarining

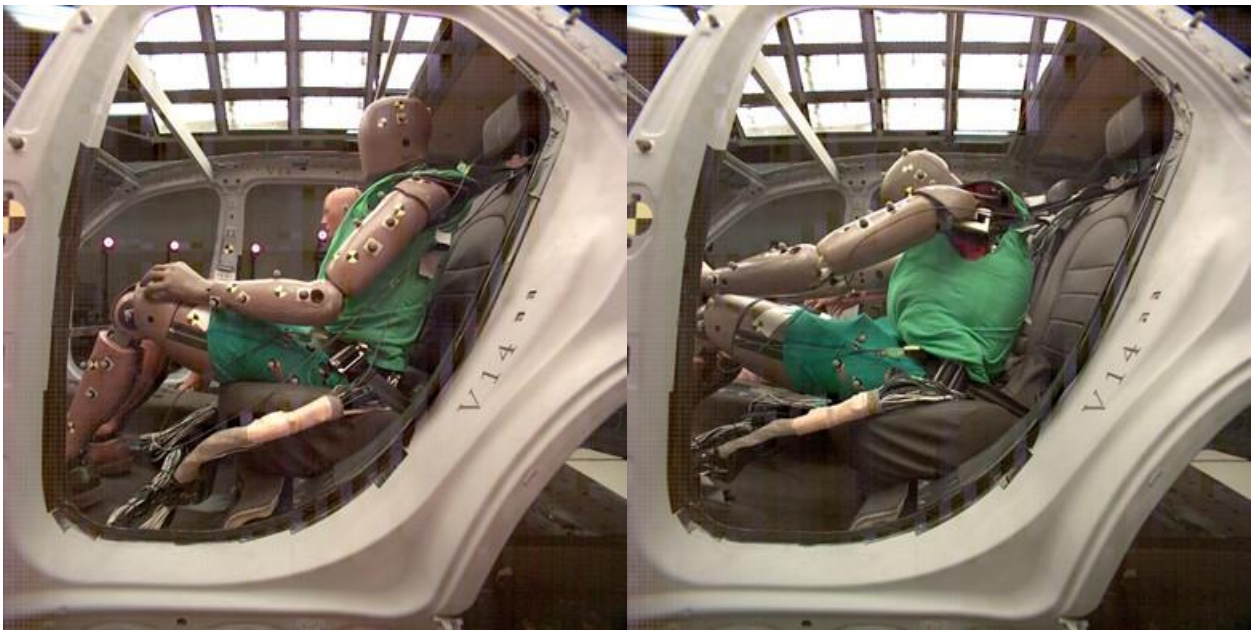

Figure 110. Test V14-4, No Submarining

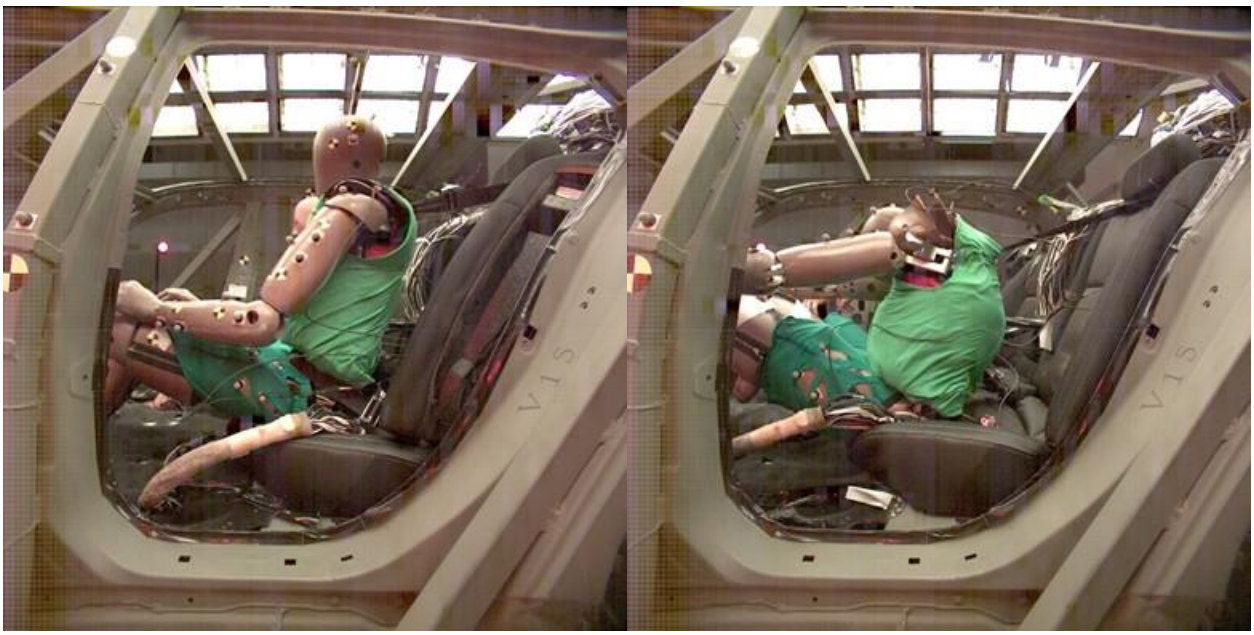

Figure 111. Test V15-4 Submarining

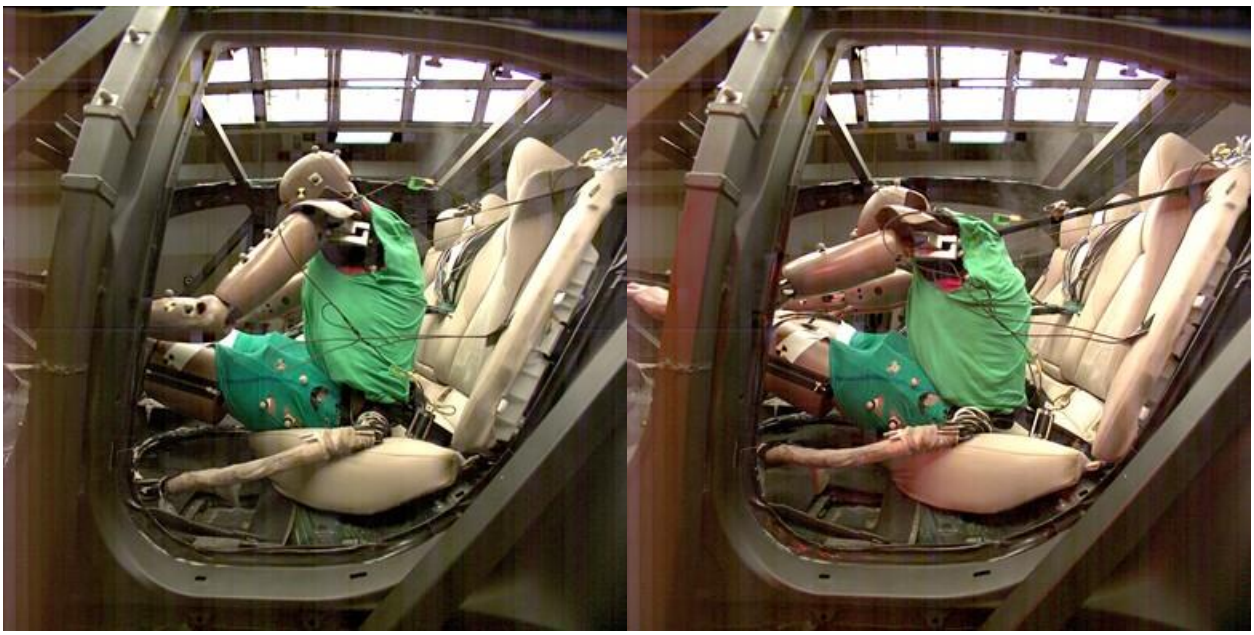
Figure 112. FRS-V19-4 Submarining

Figure 113. Test V13-4, Submarining

Figure 114. Test V13-5, Submarining

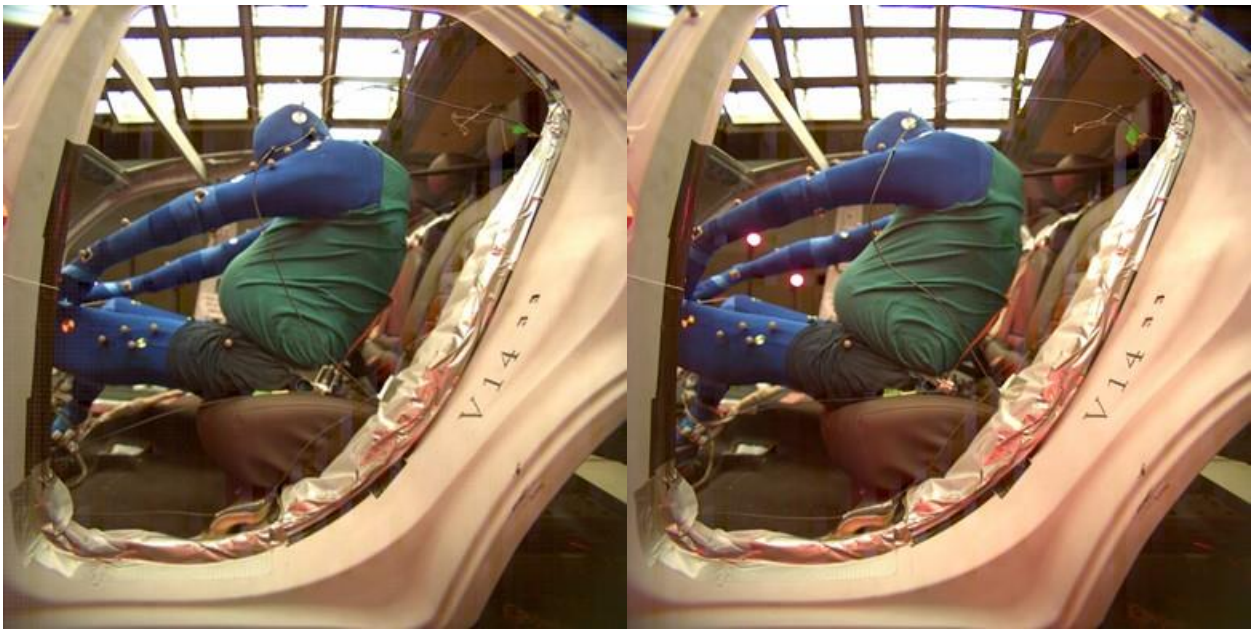

Figure 115. FRS-V14-5, pelvis fracture

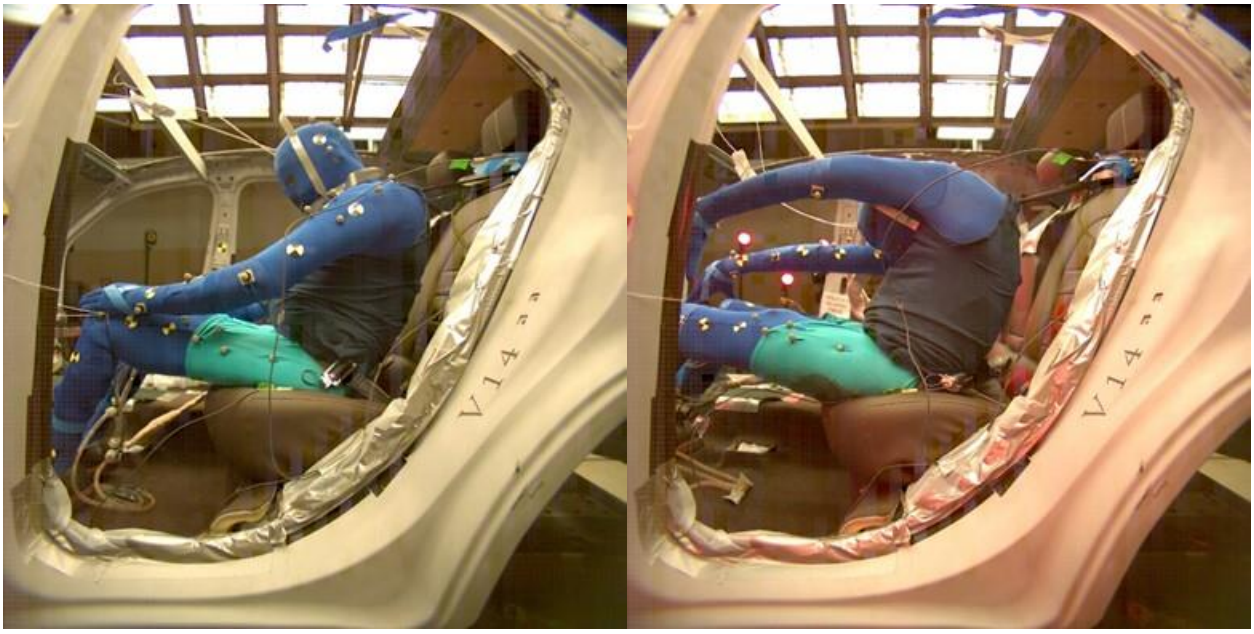

Figure 116. Test V14-6, Submarining

Figure 117. Test V15-5, pelvis fracture

Figure 118. Test V15-6, no pelvis fracture and no Submarining

Figure 119. Test V19-5, pelvis fracture

Figure 120. Test V19-6, No fracture and no Submarining

Appendix K: ATD Spine Loads

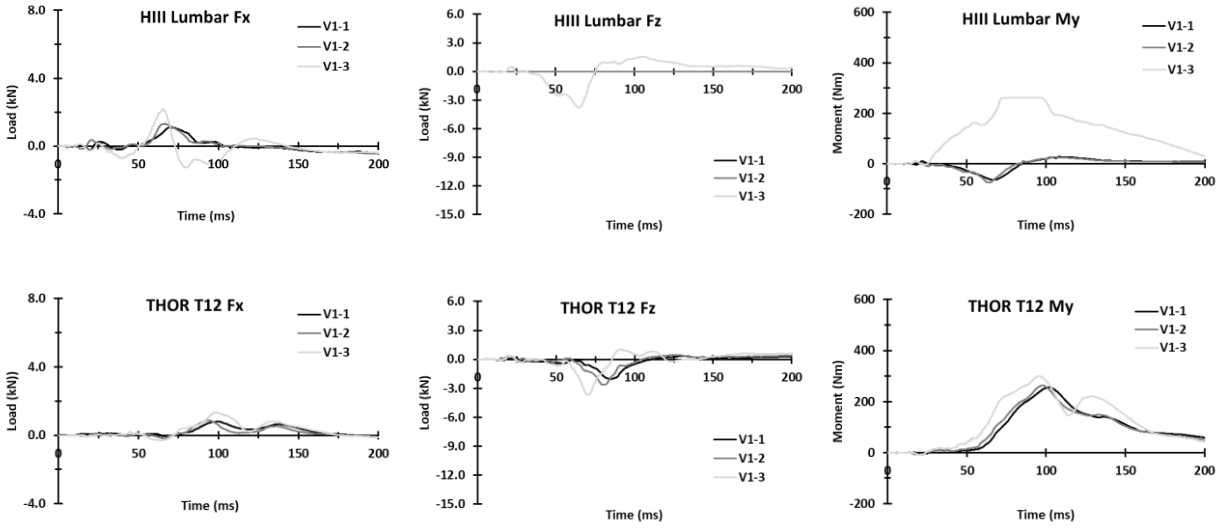

Figure 121. Spine loads for the HIII (top row) and THOR (bottom row) in vehicle V1

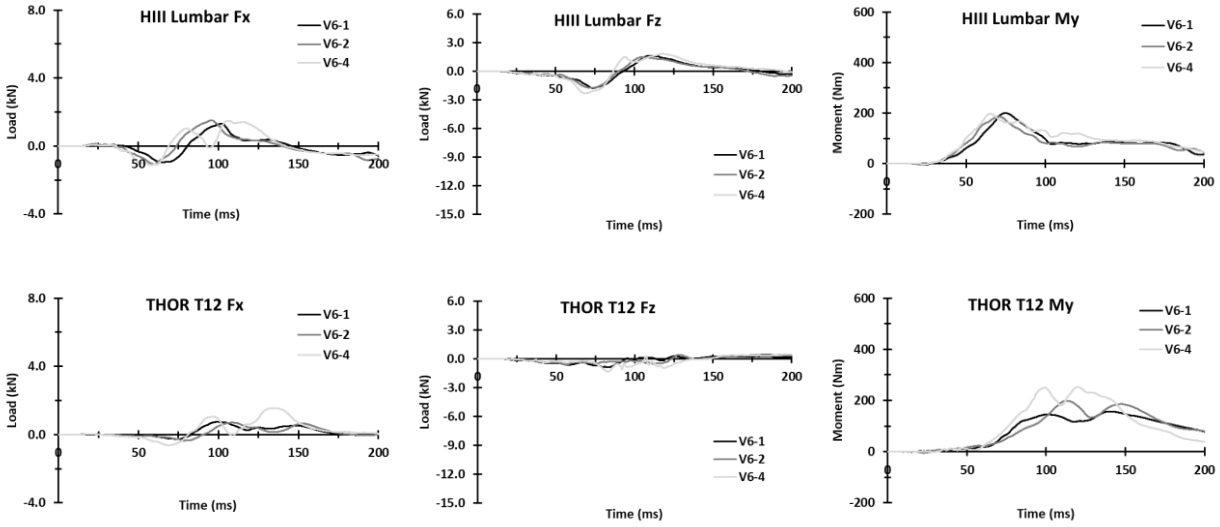

Figure 122. Spine loads for the HIII (top row) and THOR (bottom row) in vehicle V6

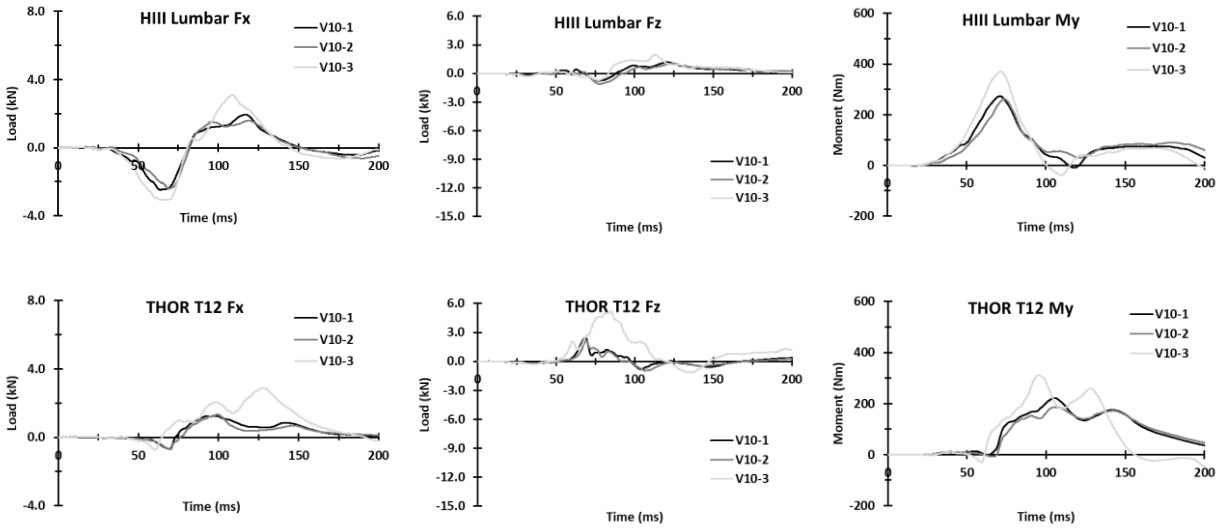

Figure 123. Spine loads for the HIII (top row) and THOR (bottom row) in vehicle V10

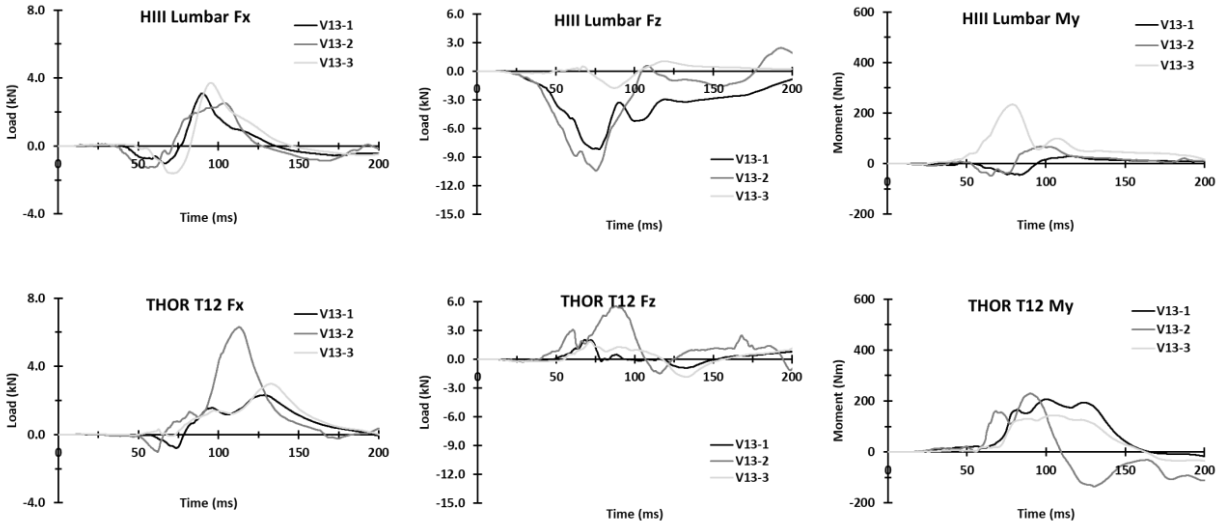

Figure 124. Spine loads for the HIII (top row) and THOR (bottom row) in vehicle V13

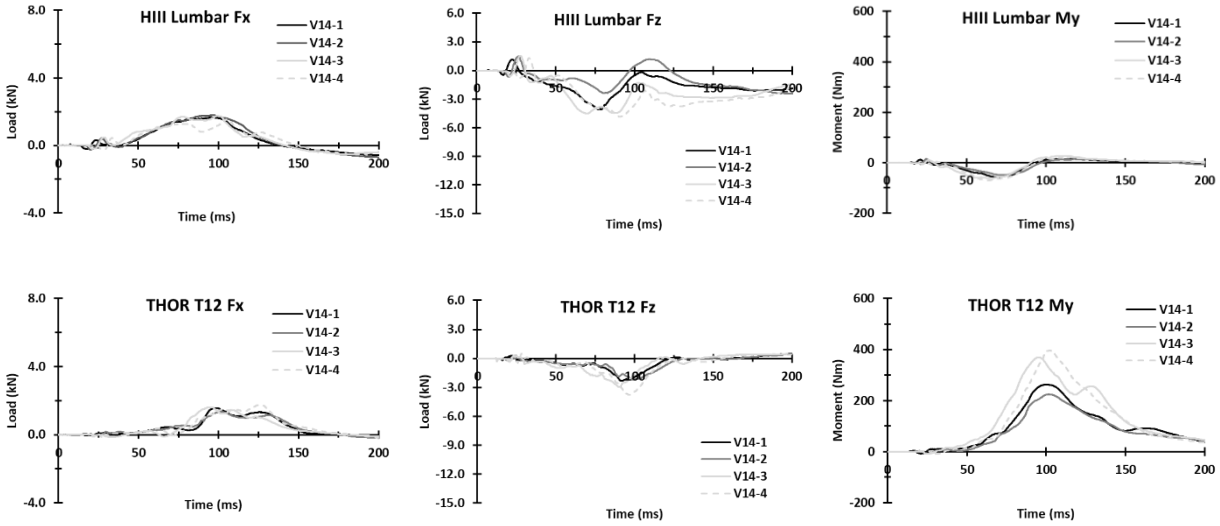

Figure 125. Spine loads for the HIII (top row) and THOR (bottom row) in vehicle V14

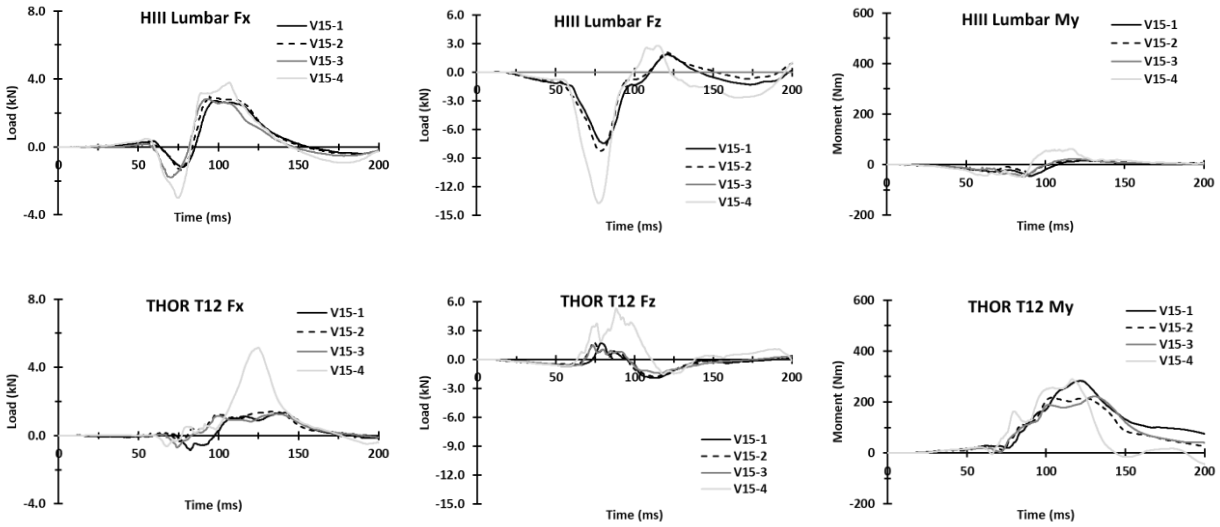

Figure 126. Spine loads for the HIII (top row) and THOR (bottom row) in vehicle V15

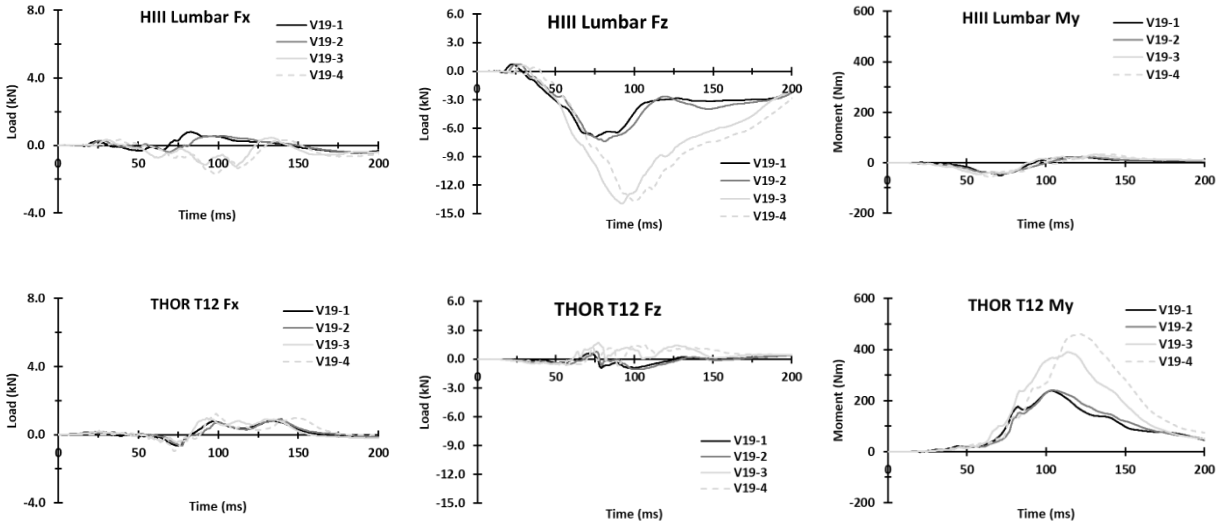

Figure 127. Spine loads for the HIII (top row) and THOR (bottom row) in vehicle V19

Appendix L: PMHS Abdominal Pressures

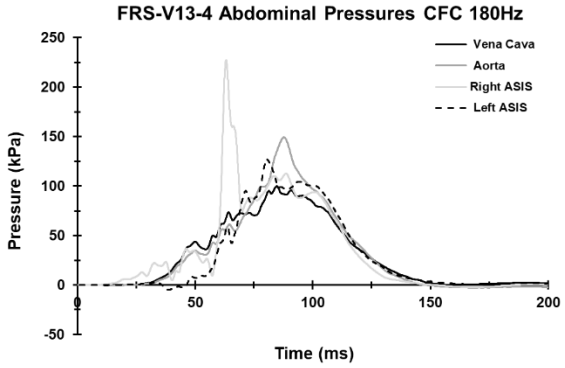

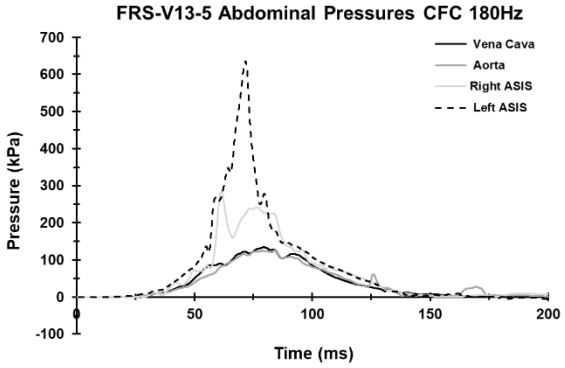

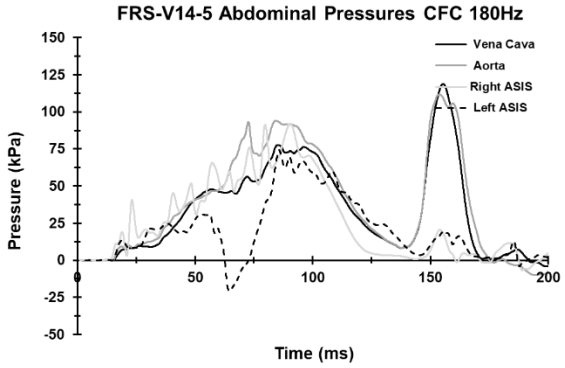

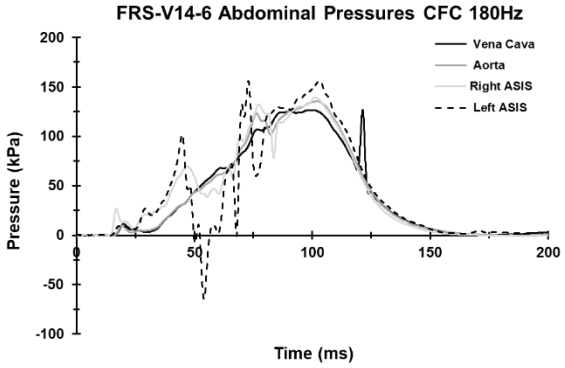

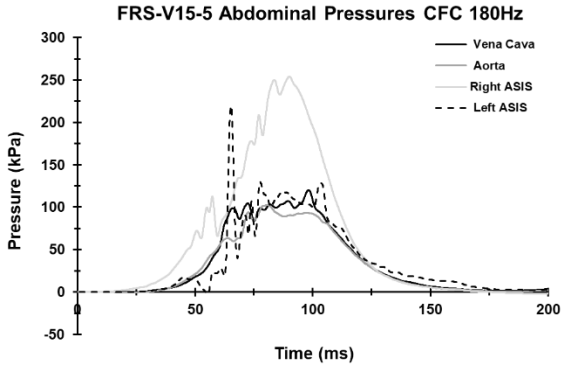

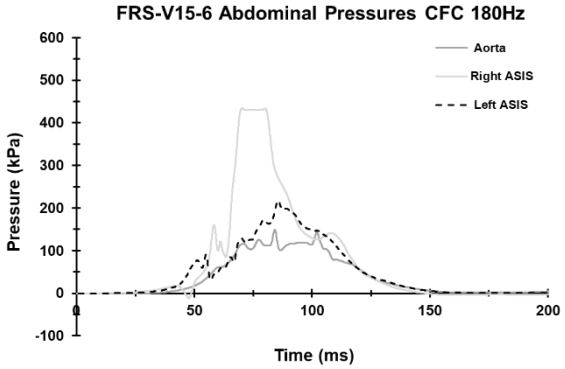

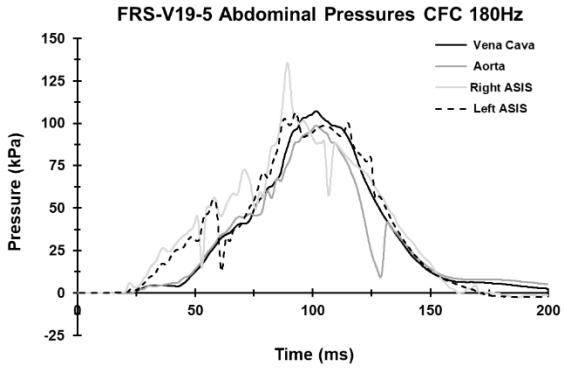

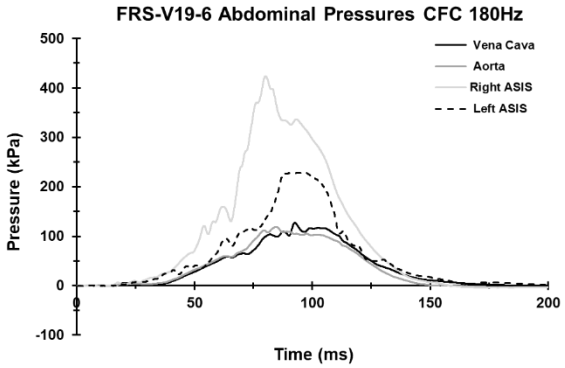

Appendix M: PMHS Belt Loads

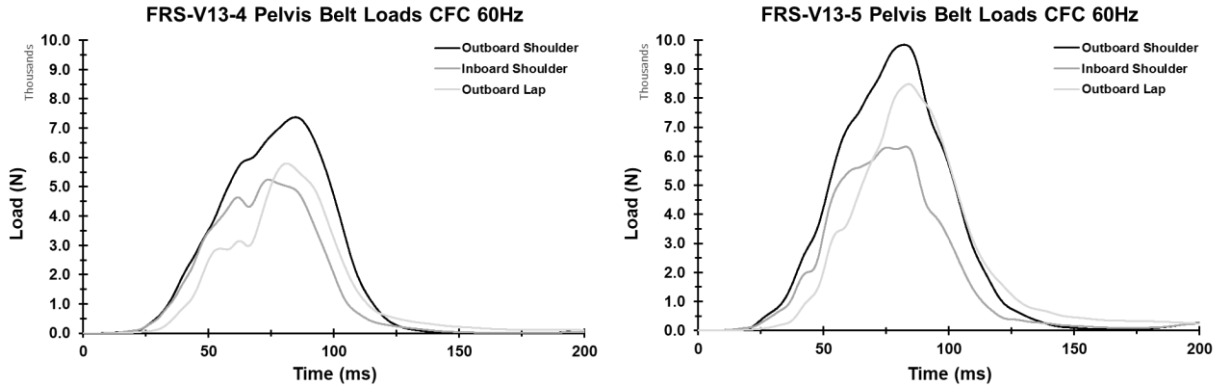

Figure 128. PMHS seat belt loads for vehicle V13

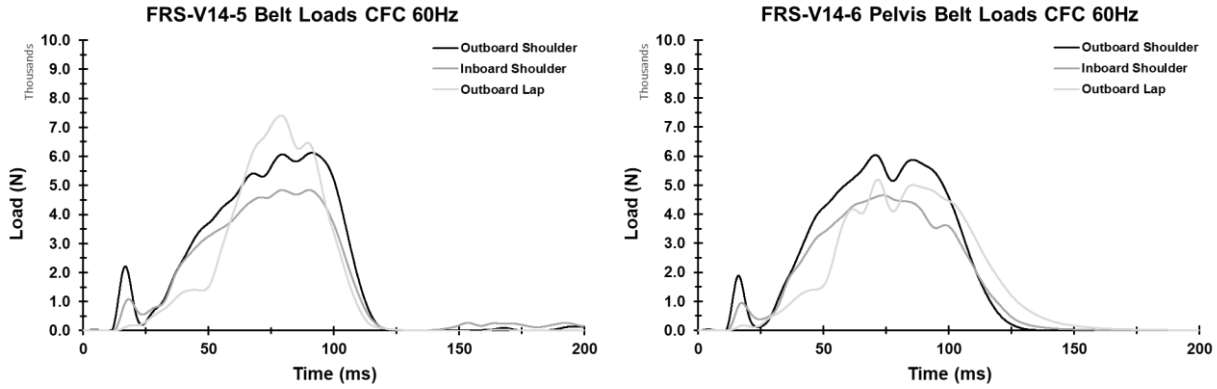

Figure 129. PMHS seat belt loads for vehicle V14

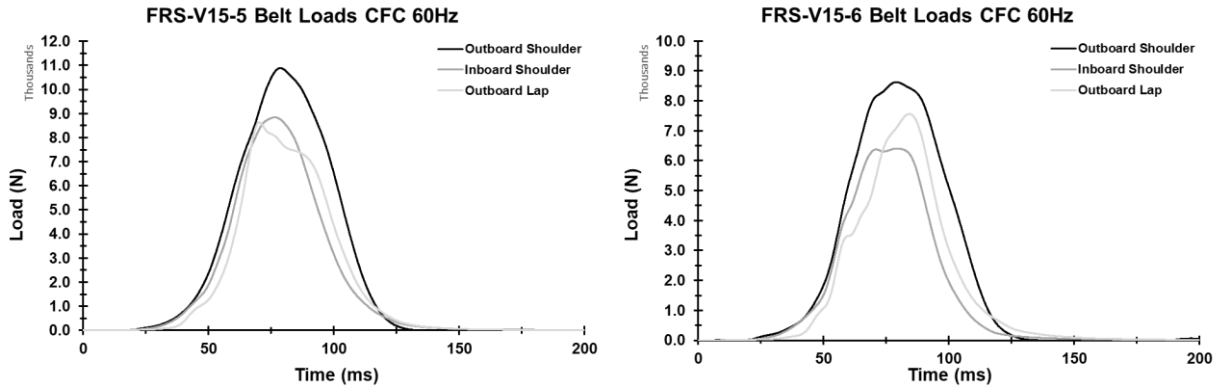

Figure 130. PMHS seat belt loads for vehicle V15

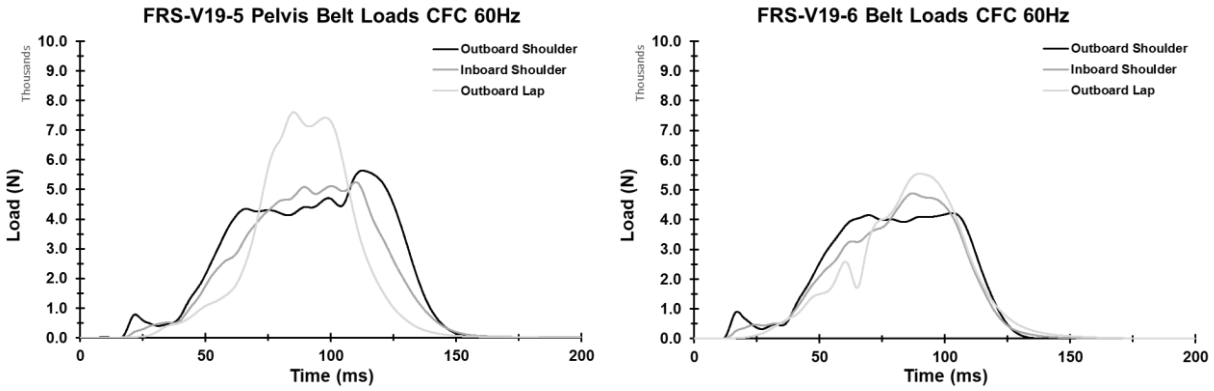

Figure 131. PMHS seat belt loads for vehicle V19

Appendix N: Autopsy Results

PMHS	Sex	Stature (cm)	Mass (kg)	Test	Submarining
SM129	M	178	63	V13-4	Yes
Region	Damage				
1. Peritoneum	• 12 cm wide, 10 cm long tear in the peritoneum to the right of the bifurcation of the abdominal aorta				
2. Mesentery and small intestine	• A. Tear in mesentery (8 cm long) and stretching of the small intestine (3 cm long) 234 cm from the ileocecal junction. (ileum) • B. Tear in mesentery (7 cm long) and transection of the small intestine 264 cm from the ileocecal junction. (ileum)				
3. Mesentery	• Button hole tear (3 cm long) 0.5 cm perpendicular to the intestine, 455 cm from the ileocecal junction (jejunum)				
4. Ileocecal Junction	• Partial tear (serous membrane), 9 cm long				
5. Sigmoid Colon	• Longitudinal tear through wall (3 cm long) about 25 cm from the anus. In the vicinity of the ala of the left pelvic bone				
6. Lumbar vertebrae	• A. Fracture of the tip of the right transverse process of L2 • B. Fracture of the tip of the left transverse process of L4 • C. Fracture of the right transverse process of L4				
7. Thorax	• A. Right rib Fx (24): 1,2,3,4,5,6,7,8,9,10 • B. Left rib Fx (23): 1,2,3,4,5,6,7,8,9,10 • C. Gladiolus Fx • D. Left clavicle Fx				

PMHS	Sex	Stature (cm)	Mass (kg)	Test	Submarining
SM155	M	168	85	V13-5	Yes
Region	Damage				
1. Liver	• A. Field of multiple surface compromise on the dorsolateral aspect of the diaphragmatic side, 6-to-10cm long, up to 2.5-cm deep • B. Triangular field of disruption/abrasion on the ventrolateral aspect of the diaphragmatic side, with 2 accompanying fractures (1.5 cm x 0.5-cm deep, and 3.0 cm x 1.5-cm deep) • C. Triangular field of disruption/abrasion on the lateral aspect of the visceral side, with an accompanying fracture (3.0 cm x 2.0-cm deep)				
2. Spleen	• A. Capsular tear on the dorsomedial aspect of the diaphragmatic side (3 x 1.5 cm) • B. Capsular tear on the ventromedial aspect of the visceral side (3 x 2cm)				
3. Small Intestine	• Complete transections, forming a segment from 142 cm to 266 cm from the ileocecal junction				
4. Mesentery and large intestine	• Mesentery tear to the root and colon “sleeve” (6 cm long) 99 cm from ileocecal junction				
5. Lumbar vertebrae	• A. L2: cranial and caudal ventral avulsion • B. Fracture of the right transverse processes of L1-L4 • B. Fracture of the left transverse processes of L1-L2				
6. Thorax	• A. Right rib Fx (23): 1,2,3,4,5,6,7,8,9 • B. Left rib Fx (23): 1,2,3,4,5,6,7,8,9,10 • C. Gladiolus Fx				

PMHS	Sex	Stature (cm)	Mass (kg)	Test	Submarining
SM156	M	188	89	V14-5	No
Region	Damage				
1. Liver	• Fracture on diaphragmatic surface (4.3 cm long, 1.5 cm deep) within 13 cm from the lateral edge of the visceral surface and 7.5 cm from the posterior edge of the visceral surface				
2. Mesentery	• Small mesenteric tear, 1.7-cm long				
3. Peritoneum	• Tear (6 cm long) at about the level of L5 vertebra				
4. Pelvis	• A. Fracture of the ala of the right ilium • B. Fracture of the ala of the left ilium				
5. Thorax	• A. Right rib Fx (14): 1,2,3,4,5,6,7,8 • B. Left rib Fx (8): 2,3,4,5,6,7 • C. Manubrium Fx				

PMHS	Sex	Stature (cm)	Mass (kg)	Test	Submarining
SM157	M	173	68	V14-6	Yes
Region	Damage				
1. Liver	• Superficial disruption 9.5 cm long on diaphragmatic surface, from 2 cm to 8.5 cm from the lateral margin and 5 cm to 2.5 cm from the dorsal margin				
2. Mesentery and small intestine	• A. Mesenteric tear starting 486 cm and ending 540 from the duodenum, having transverse/circumferential length of 17 cm • B. Contused/stretched ileum 271 cm from the ileocecal junction, with mesenteric tear having radial length of 8.5 cm				
3. Thorax	• A. Right rib Fx (14): 2,3,4,5,6,7,8,9,10 • B. Left rib Fx (3): 3,4,5				

PMHS	Sex	Stature (cm)	Mass (kg)	Test	Submarining
SM152	M	180	81	V15-5	No
Region	Damage				
1. Diaphragm	• A. Lacerations to pleural surface on the right side (multiple) • B. Minor lacerations to pleural surface on the left side (multiple)				
2. Liver	• A. Large laceration/fracture/puncture in diaphragmatic surface of right lobe. 9.5 cm long, 2.3 cm deep; 7.4 cm from anterior visceral margin • B. Fracture on dorsal diaphragmatic surface, 2.1-cm long, 0.8-cm deep; 16.6 cm from anterior visceral margin				
3. Small Intestine	• Ileum contusion 126 cm from ileocecal junction, 10-cm long				
4. Pelvis	• A. Fracture of the ala of the right ilium • B. Fracture of the ala of the left ilium • C. Separation of the sacroiliac joint on the left side				
5. Thorax	• A. Right rib Fx (30): 1,2,3,4,5,6,7,8,9,10 • B. Left rib Fx (10): 1,2,3,4,5,6,8 • C. Manubrium Fx • D. Left clavicle Fx				

PMHS	Sex	Stature (cm)	Mass (kg)	Test	Submarining
SM153	M	168	64	V15-6	No
Region	Damage				
1. Liver	• A. Multiple deep fractures of parenchyma on the ventrolateral diaphragmatic surface, some through to visceral surface at ventrolateral margin • B. Multiple superficial disruptions of the dorsolateral aspect of the diaphragmatic surface, 0.2-to-1.2-cm deep				
2. Mesentery	• A. Tear in mesentery, 106 cm from ileocecal junction, 14-cm long, 4-cm wide at small intestine • B. Tear in mesentery, 332 cm from ileocecal junction, 12-cm long (to the root) and 4.6 cm wide at small intestine • C. Tear in mesentery to root, 9.5 cm from rectum, 23 cm along the sigmoid colon				
3. Large Intestine	• Transection of the descending colon, 38 cm from the rectum				
4. Thorax	• A. Right rib Fx (15): 2,3,4,5,6,7,8,9 • B. Left rib Fx (2): 1,2 • C. Manubrium continuing to gladiolus Fx				

PMHS	Sex	Stature (cm)	Mass (kg)	Test	Submarining
SM154	M	178	89	V19-5	No
Region	Damage				
1. Pelvis	• A. Fracture of the ala of the right ilium • B. Fracture of the ala of the left ilium				
2. Thorax	• A. Right rib Fx (10): 2,3,4,5,6,7,8,9 • B. Left rib Fx (8): 2,3,4,7 • C. Gladiolus Fx				

PMHS	Sex	Stature (cm)	Mass (kg)	Test	Submarining
SM95	M	170	64	V19-6	No
Region	Damage				
1. Mesentery	• Tear (53-cm long) parallel to the longitudinal direction of the small intestine starting 239 cm and ending 292 cm from the ileocecal junction				
7. Thorax	• A. Right rib Fx (24): 2,3,4,5,6,7,8 • B. Left rib Fx (2): 2 • C. Gladiolus Fx				

Appendix O: Autopsy Photos

SM129 (FRS-V13-4)

Figure 132. Abdomen autopsy results for PMHS SM129

SM155 (FRS-V13-5)

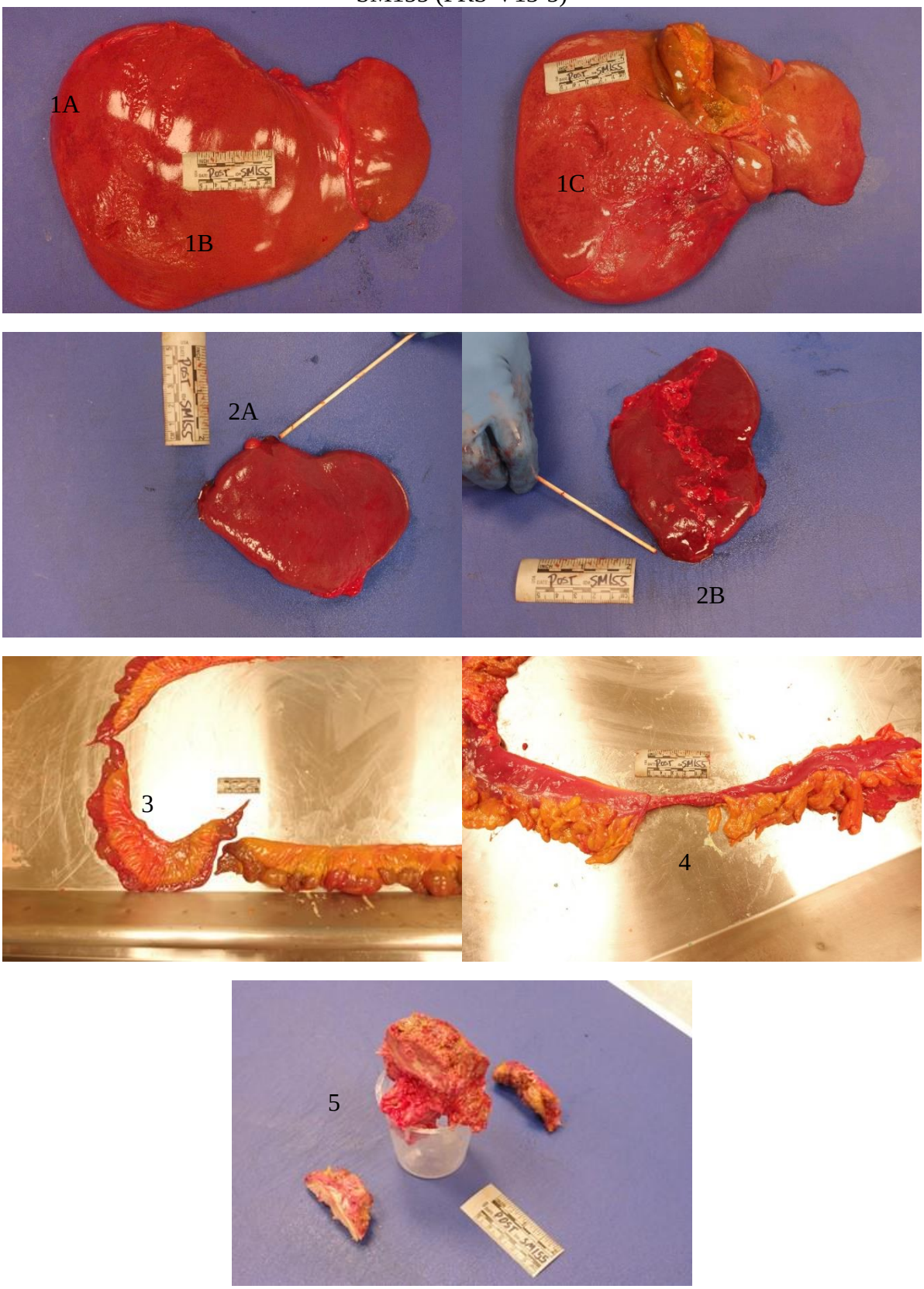

Figure 133. Abdomen autopsy results for PMHS SM155

SM156 (FRS-V14-5)

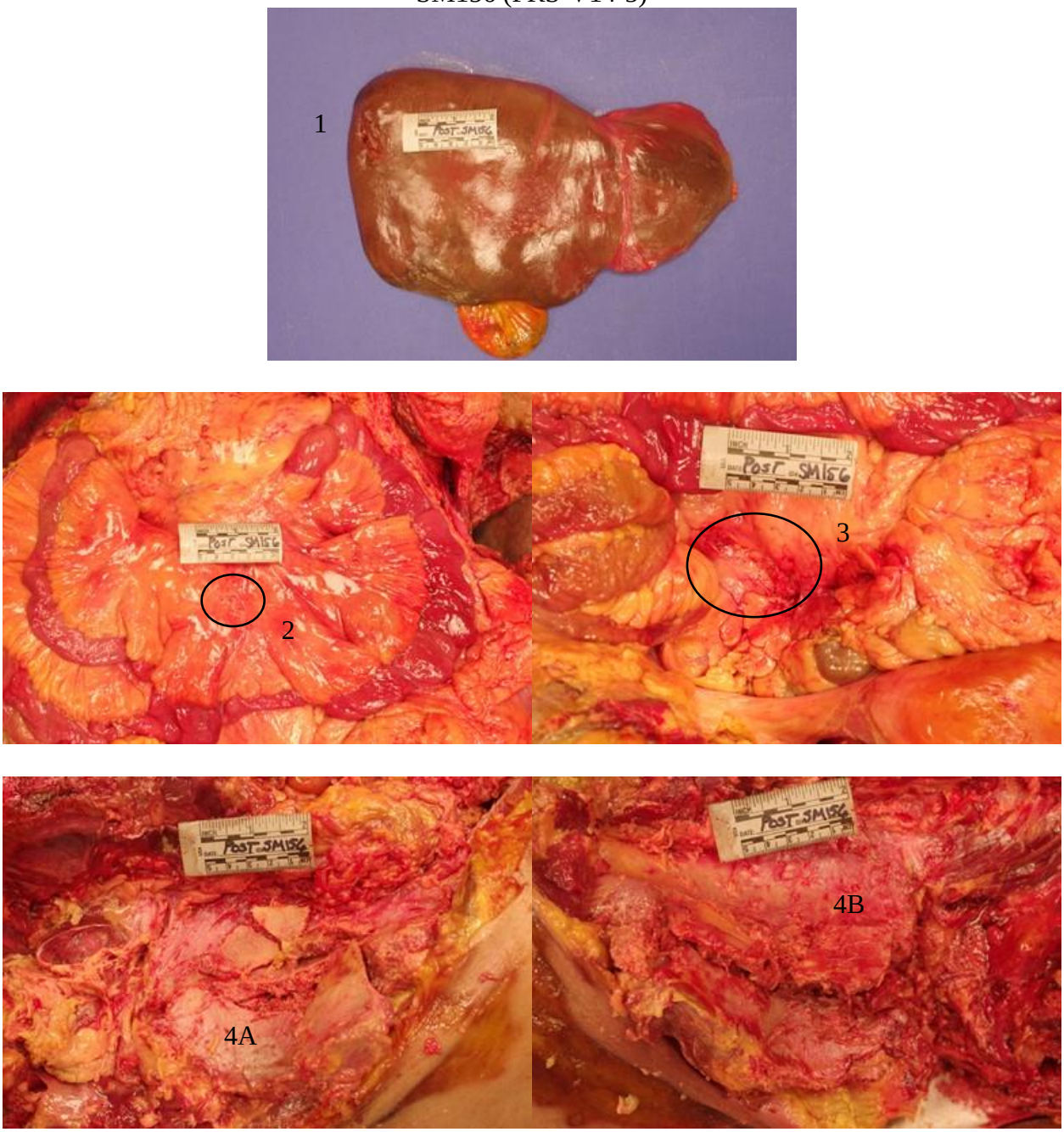

Figure 134. Abdomen autopsy results for PMHS SM156

SM157 (FRS-V14-6)

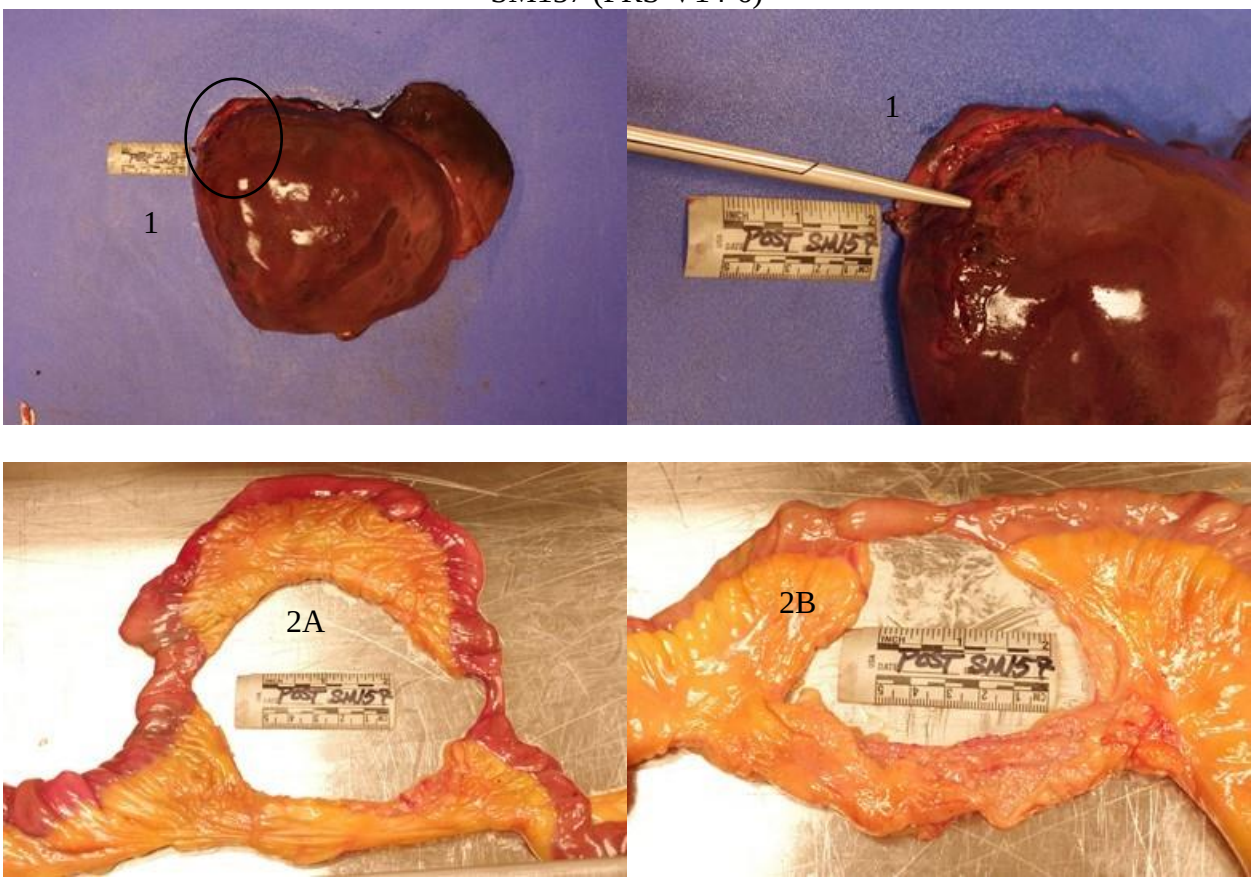

Figure 135. Abdomen autopsy results for PMHS SM157

SM152 (FRS-V15-5)

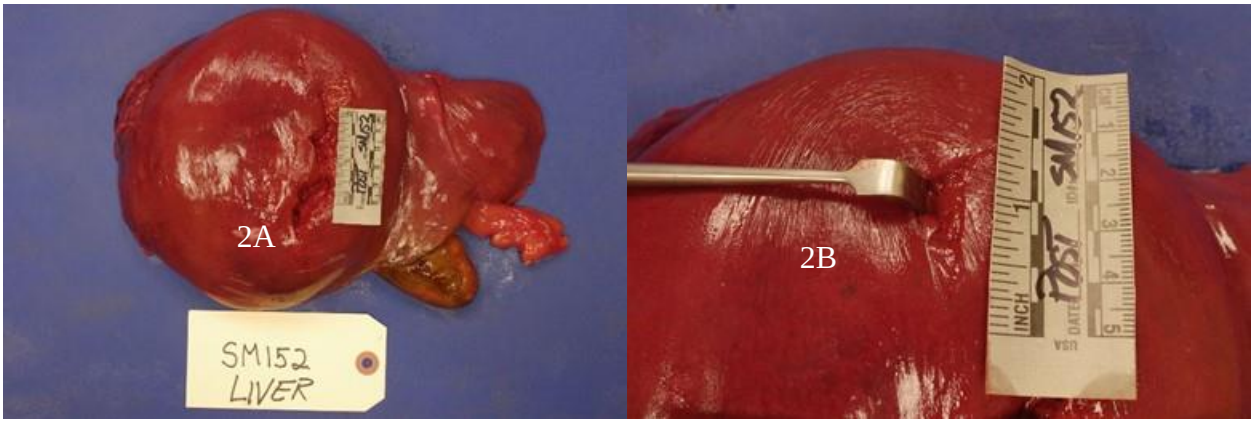

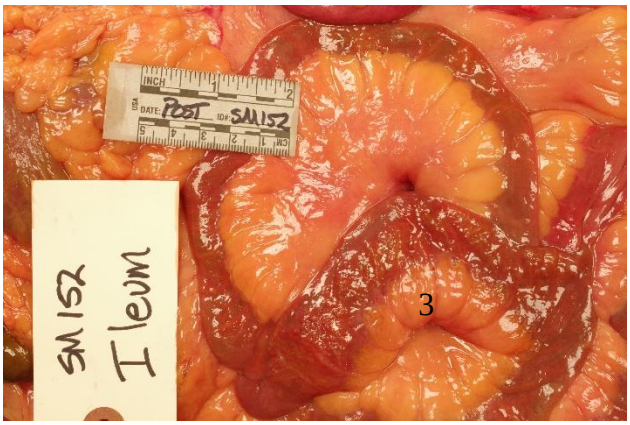

Figure 136. Abdomen autopsy results for PMHS SM152

SM153 (FRS-V15-6)

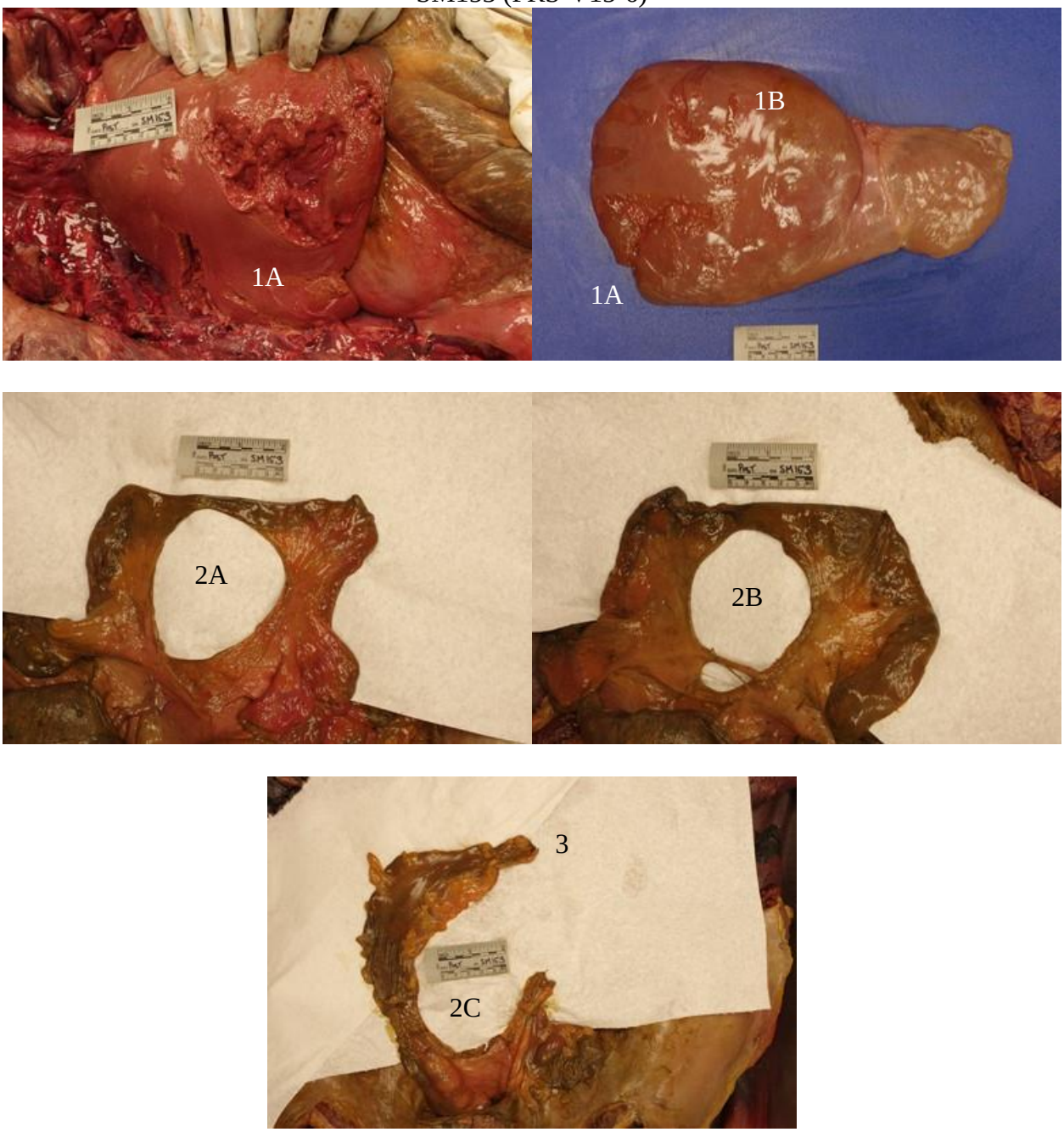

Figure 137. Abdomen autopsy results for PMHS SM153

SM154 (FRS-V19-5)

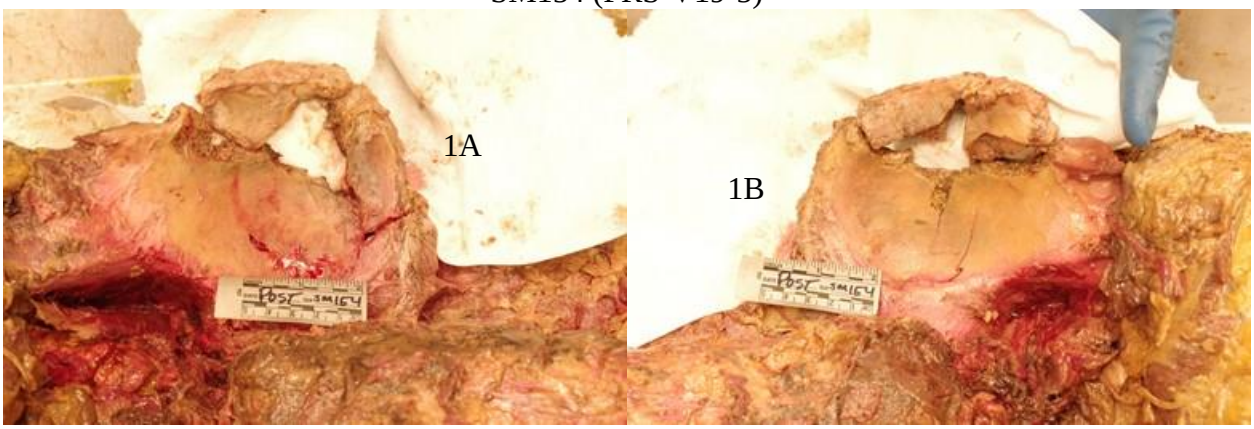

Figure 138. Abdomen autopsy results for PMHS SM154

SM95 (FRS-V19-6)

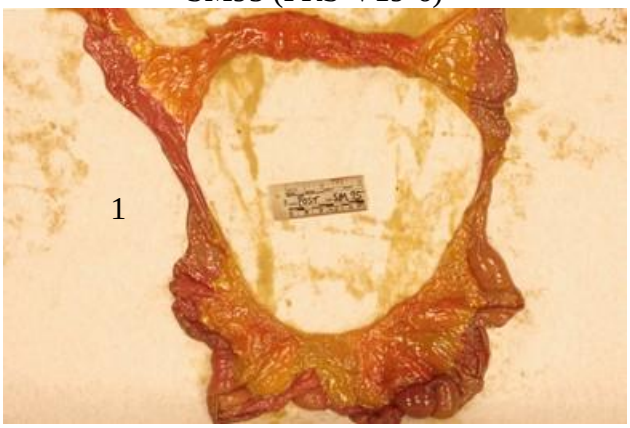

Figure 139. Abdomen autopsy results for PMHS SM95